INTERACTIONS BETWEEN SYNOPTIC-SCALE EDDIES AND THE LARGE-SCALE FLOW DURING THE LIFE CYCLES OF PERSISTENT FLOW ANOMALIES

by

Peter Paul Neilley

B.S., Meteorology, McGill University
(1982)
S.M., Meteorology, Massachusetts Institute of Technology
(1984)

Submitted to the Department of
Earth, Atmospheric and Planetary Sciences
in partial fulfillment of the requirements for the degree of

DOCTOR OF PHILOSOPHY
IN METEOROLOGY

at the

MASSACHUSETTS INSTITUTE OF TECHNOLOGY

June 19, 1990

Signature of Author _____
Center for Meteorology and Physical Oceanography
19 June 1990

Certified by _____
Randall M. Dole, Thesis Supervisor

Accepted by _____
Thomas H. Jordan, Department Chairman

INTERACTIONS BETWEEN SYNOPTIC-SCALE EDDIES AND THE LARGE-SCALE FLOW DURING THE LIFE CYCLES OF PERSISTENT ANOMALIES

by

PETER PAUL NEILLEY

Submitted to the Department of Earth, Atmospheric and Planetary Sciences
on June 19, 1990 in partial fulfillment of the requirements for the Degree of
Doctor of Philosophy in Meteorology

ABSTRACT

Recurrent large-scale persistent anomaly (PA) patterns are an important component of the total wintertime low-frequency variability of the atmosphere. In this study, we present a detailed examination of the interactions occurring between the large-scale flow and the synoptic-scale eddies during the life cycles of wintertime PAs over the northern Atlantic and Pacific Oceans. We focus on two fundamental questions: first, how does synoptic-scale eddy activity vary through the life cycles of positive and negative PAs, and second, how do changes in the eddies feedback and influence the evolution of the large-scale flow anomalies? In order to address these questions, composite analyses of eddy activity and feedbacks are constructed by averaging over all identified cases of both positive (blocking) and negative (zonal) PA's over each ocean, where the compositing is usually performed relative to either onset or breakdown times. In addition, a case study of an Atlantic positive PA event is also presented to illustrate synoptically the results obtained in the composite analyses.

Through the entire life cycles of the PAs, the maxima in eddy activity (i.e. storm tracks) closely follow but are somewhat downstream of the regions of large-scale 700mb baroclinicity The primary maxima are shifted well north of the climatological-mean storm track during the blocking cases and well to the south during the zonal cases. Anomalous eddy activity is generally stronger at upper levels than at the surface. At least 6 days prior to the onset of positive PAs in both regions, significantly enhanced eddy activity appears well upstream of the point where the block subsequently forms, and spreads eastward in time reaching the key region by the time of onset. This enhanced eddy activity is associated with anomalously strong downgradient eddy heat fluxes. About a week prior to decay, the upstream eddy activity anomalies begin to weaken. Eddy activity is suppressed within the blocked region throughout the life cycle of the PA. Results for negative PAs are broadly similar, but of opposite sign to the positive cases with the Pacific negative cases having the least anomalous eddy activity observed.

Extended Eliassen-Palm fluxes (or E-vectors) and a form of the quasi-geostrophic height tendency equation forced by anomalous eddy potential vorticity fluxes are used to diagnose the anomalous eddy feedbacks on the large-scale flow. During blocking, significant anomalous eddy anticyclonic forcing is found upstream (Atlantic cases) or near (Pacific cases) the block during all phases of the life cycles. The upper-level horizontal (barotropic) component is strongest during the mature phase suggesting that strong eddy vorticity forcing is playing a significant role in maintaining the block. The total eddy forcing is found to lead the development of both the positive and negative Atlantic cases by about five

days suggesting that, in these cases, forcing by synoptic-scale eddies may also play an important role in the development of the flow anomalies. The results for the Atlantic positive cases are somewhat reminiscent of some sudden stratospheric warming events. For the Pacific cases, no clear temporal differences are found between the large-scale flow and the eddy forcings although the forcing patterns are broadly similar to the corresponding patterns during the Atlantic cases. Again, the Pacific negative cases appear to have the least amount of anomalous eddy feedbacks. Results of experiments with a hemispheric barotropic model suggest that the observed composite bandpass eddy forcing can account for about one-half of the observed Atlantic developments.

The results indicate that significant changes in the synoptic-scale eddy activity occur throughout the life cycles of PA's. Anomalous feedbacks by the eddies on the large-scale flow appear important in the maintenance of the PAs, and may also be critical to the formation of some PAs, particularly the Atlantic cases. Although eddy characteristics in the Atlantic and Pacific cases are broadly similar, significant differences do exist, with the Pacific negative PAs showing the least evidence of significant eddy interactions. Overall, however, the results suggest that a correct representation of the interactions between the eddies and the large-scale flow is important in order to correctly simulate the complete life cycles of persistent anomalies.

Thesis supervisor: Dr. Randall M. Dole
Title: Associate Professor of Meteorology

TABLE OF CONTENTS

Acknowledgments

I wish to express my sincerest gratitude to my advisor, Dr. Randall Dole for his insightful, intellectual, inspirational and patient guidance throughout this research. He originally suggested studying the eddy activity changes during the life cycles of persistent anomalies. He has always unselfishly dedicated his time to aid all of his students research. His efforts have been impeccable and deserve considerable respect.

I also wish to thank my thesis committee members Dr. Kerry Emanuel, Dr. Alan Plumb and Dr. Paola Malanotte-Rizzoli for their guidance and suggestions. I would like to further thank Dr. Alan Plumb and Dr. Peter Stone for their well organized and insightful lectures on atmospheric dynamics. I have also benefited by many conversations with Dr. Brian Farrell of Harvard University.

Many of my fellow students at MIT have been a continuing source of friendship and inspiration. Rob Black, John Nielsen, Chris Davis, Josh Wurman, Brad Lyon, Micheal Morgan, Keith Groves, Randy Mackie and Steve Garner deserve considerable thanks for making the many years at MIT enriching and enjoyable. I also wish to acknowledge Phil Atkinson and the rest of the Alumni Pool lunchtime crowd for helping me stay in shape and relieve the stress of life as a graduate student.

Specific help on this thesis was provided by Rob Black in providing the hemispheric plotting code and the PA case date lists and by Micheal Morgan in providing the tropopause data used in Chapter 6. Dennis Joseph of the Data Support Group at NCAR was helpful during the construction of the NMC dataset. Dr. Steven Mullen of the Univ. of Michigan provided the code used to solve the three dimensional height tendencies. Several members of the EAPS staff deserve recognition for their efforts in supporting my research as well as

the entire operations of the department. Most notable in this regard are Jane McNabb, Eddie Nelson, Speed Geotis and Diana Speigel.

But most of all, I wish to thank my wife Lyn. Her love, encouragement, patience, dedication and unselfish commitment to both me and this work will forever be cherished. I express my deepest appreciation and love to her.

Financial support for this research was provided by NASA grant NAGS-927, and NSF grants ATM-8617132 and ATM-8820938.

This thesis is dedicated to my father, who would have been proud.

Chapter 1

Introduction

A major objective of the science of meteorology is to provide accurate weather forecasts to the public for periods as long as possible. Over the last several decades, considerable advances have been achieved in the accuracy of weather forecasts. Much of this improvement has been attributed to the use of various dynamical weather prediction models in preparing the forecasts. Today, skill in a 6 day forecast produced by such models equals the skill of an 3 day forecast made just a decade or so ago (Bengstsson, 1985). Some skill is now found in dynamical forecasts out to about 10 days (O'Lenic and Livezey, 1989; Roads, 1989), whereas 20 years ago useful forecasts were limited to about 3.5 days (Miyakoda *et al.*, 1972). Continued improvements in the treatment of physical process, numerical resolution, solution techniques, initialization schemes and databases will all likely lead to increased forecast model skill.

Approximately coincident with the current limit to numerical forecasting skill, is the transition from the synoptic-scale temporal regime to the low-frequency regime. Many studies (e.g. Hoskins *et al.*, 1983; Blackmon *et al.*, 1984a,b; Wallace, 1987) have shown that even though there is no clearly defined spectral gap, phenomena with temporal scales on the order of several days behave considerably different than those with characteristic time-scales greater than about a week. Several studies have shown that synoptic-scale phenomena tend to have meridionally elongated, westward-tilting baroclinic structures approximately steered by the 700 mb flow, while low-frequency phenomena typically have

larger, and more zonally elongated structures, slower phase speeds and more are more nearly equivalent barotropic. While the synoptic-scale waves are primarily responsible for the day-to-day variability in the weather, the low-frequency phenomena are associated with long term trends or weather regimes. Although both types of phenomena contribute significantly to the total winter transience of the extratropical troposphere, low-frequency variability (LFV) dominates synoptic-scale variability by a factor of about 3:1 (Blackmon, 1976). Despite its large contributions, there is considerable evidence that a major part of the inability of numerical models to forecast beyond about a week is due to an inadequate capability to correctly simulate the evolution of the low-frequency components of the atmosphere. Indeed, operational forecast models have relatively poor forecast skill during the onset of blocking (Tibaldi and Molteni, 1988; Tracton *et al.*, 1989) and recent evidence has been presented linking low frequency variations in model skill to the polarity of the Pacific-North American (PNA) teleconnection pattern (Palmer, 1988; Tracton *et al.*, 1989).

Since successful dynamical extended-range forecasting (DERF) will depend upon our ability to forecast the evolution of low-frequency phenomena, an understanding of the processes that determine the evolution of these phenomena should be useful in developing improved methods of long-range weather prediction. In particular, if there is a significant class of low-frequency phenomena that critically depends upon interactions with smaller-scale phenomena or other internal dynamical processes, then successful long-range weather forecasting of that class can only be achieved if the explicit details of the initial state are correctly initialized and simulated. The required accuracy of the details depends upon the specific dynamical processes operating. However, if low-frequency phenomena largely depend upon variations in the boundary conditions for their existence, then accurate long-range weather forecasting of large-scale atmospheric motions may be achieved by incorporating (and predicting) those boundary conditions and then correctly simulating the

atmospheric response. In this case, simulation of synoptic-scale phenomena may not be crucial and only the mean statistics of the synoptic-scales, rather than the details of the individual events, need be predicted in order to interpret the forecasts.

There is currently considerable debate over the relative importance that boundary variations and internal dynamics play in forcing low-frequency phenomena (see Wallace, 1987, for a review). One the one hand, many studies have shown the sensitivity of the extratropical atmosphere to various boundary conditions including snow cover and sea ice (Namias, 1978), soil moisture and vegetation (Shukla and Mintz, 1982; Mintz, 1984), local sea-surface temperature (SST) anomalies (e.g. Frankignoul, 1985) and tropical SST anomalies (e.g. Simmons, 1982; Weickmann *et. al.*, 1985). One the other hand, Simmons *et al.* (1983), Fredericksen (1982, 1983, 1986), Dole and Black (1990) and others have shown the importance of large-scale dynamics in forcing LFV, while Hoskins *et al.* (1983), Shutts (1986) and Mullen (1987) among many others have demonstrated the importance of nonlinear interactions with synoptic-scale eddies in forcing LFV.

In reality, the relative importance of the various processes may just differ in degree from case to case. Further, the role that each process plays can not always be separated into a set of linear responses from each mechanism. For example, forcing by transient eddies has been shown to be important in the maintenance of blocking (e.g. Illari, 1984). However in one case, Hoskins and Sardeshmukh (1987) showed that the circulations induced by strong tropical convection over SST anomalies played a crucial catalytic role in initially altering the transient forcing to allow the establishment of a block. They argued that only through the nonlinear interactions between the boundary forced circulation and the internally generated synoptic-scale eddies could the block have evolved.

Whatever the relative importance of the various mechanisms that contribute to the LFV of the atmosphere may be, understanding how changes in synoptic-scale eddy activity are related to low frequency circulation anomalies is itself, an important problem. This is self evident if the synoptic-scale eddies play a major role in forcing low-frequency phenomena. But even if not, understanding the relationships of synoptic-scale eddies to low-frequency phenomena is important because of the significant role the eddies play in determining the local weather. Both long-range weather prediction models and GCMs must (at least) parameterize the synoptic-scale eddies correctly in order to describe the time-mean weather conditions associated with the large-scale flow. Further, if the eddies are indeed important in determining the low-frequency evolution, then the models must also correctly simulate the entire life cycles of the eddies and their nonlinear interactions with the mean flow in order to produce accurate long-range weather forecasts.

The objective of this thesis is to document the observed interactions between synoptic-scale eddies and extratropical low-frequency phenomena. We focus on a major form of LFV, the wintertime, extratropical persistent anomalies as defined by Dole and Gordon (1983). We concentrate on determining the interactions that occur between synoptic-scale eddies and the larger-scale flow during the entire life cycles of persistent anomalies. An implicit motivation underlying this thesis is to contribute towards a better understanding of low-frequency phenomena, with the intent that such a contribution may eventually help improve the accuracy of long-range weather forecasting. As persistent anomalies generally grow and decay on time scales less than those normally associated with changes in the large-scale boundary conditions, internal dynamics are likely to play a crucial role in their evolution (Dole, 1989). Here, we investigate the role of synoptic-scale eddies in forcing persistent anomalous flows. This addresses the issue of the potential

model and data requirements necessary to achieve successful extended-range predictability of large-scale persistent flow anomalies.

The problem we address is inherently nonlinear (i.e. changes in the large-scale flow may alter the synoptic-scale eddy behavior which in turn may modify the large-scale flow). We will find it useful to approach this general problem as two separate parts by asking, What are the changes in synoptic-scale eddy activity during the life cycles of persistent anomalies and, how do the eddies feedback and influence the anomalous large-scale flow?

Our specific objectives are:

- To *quantitatively* and *objectively* determine the *changes* in synoptic-scale eddy activity during the entire life-cycles of persistent anomalies.
- To analyze the *anomalous* feedbacks by the synoptic-scale eddies during the life cycles of persistent anomalies.
- To determine if the approximate *response* to the anomalous eddy forcing appears to reproduce the large-scale flow anomalies.
- To generalize previous blocking studies to *both* positive (blocking) and negative (zonal) persistent anomalies.

The remainder of this thesis is structured as follows. Chapter 2 provides a background and overview of previous relevant research. In Chapter 3, the data sets and basic procedures are described. Chapter 4 describes results of quantitative analyses of the changes in eddy behavior during the life cycles of persistent anomalies. Chapter 5 describes diagnostic analyses that are aimed at determining the role of synoptic-scale forcing during the life-cycles of persistent anomalies.

Chapter 6 presents a detailed case study of one of the PA events to further illustrate the composite results of the previous chapters. The final chapter provides a summary, discussion and interpretation of the major results.

Chapter 2

Observations and Theories of Persistent Anomalies

2.1 Introduction

Dole and collaborators (Dole and Gordon,1982; Dole, 1984, 1986a, 1986b, 1989; Dole and Black, 1990) have used the phrase "persistent anomaly" to identify and describe the characteristics of large and long-lived anomalies in the extratropical 500 mb flow field. In this thesis we will also use the terminology "persistent anomaly" to refer to the persistent flow patterns identified by Dole or to similar structures obtained using the same methodology. Locally, the positive persistent anomaly cases are often associated with blocking while the negative persistent anomaly cases are generally associated with intense zonal flows. Persistent anomalies (PAs) are an important part of the total low-frequency variability of the atmosphere and have considerable influence on the local weather conditions. A complete understanding of these phenomena is important in understanding the dynamics of low frequency phenomena in general, and may also aid in the improvement of medium and long-range weather predictions. The remainder of this chapter is devoted to reviewing previous observational and theoretical studies of PAs. During this review, we will focus primarily on studies concerning the relationships between PAs and variations in synoptic-scale eddy activity.

2.2 Observations of Persistent Anomalies.

Dole and Gordon (1983, hereafter DG) studied the geographical distribution of wintertime PAs over the Northern Hemisphere. They defined a local, latitude-scaled temporal height anomaly Z_θ by

$$Z_\theta = \frac{\sin 45°}{\sin \theta} \cdot Z'$$

where Z' is the deviation of the 500 mb geopotential heights from its long-term seasonal trend and θ is latitude. Thus Z_θ is a streamfunction-like quantity that better describes horizontal Rossby wave propagation on a sphere than does the unscaled geopotential height field (Hoskins *et al.*,1977). As illustrated in Fig. 2.1, DG defined a persistent anomaly event of duration D days whenever Z_θ exceeds a threshold of M for at least T consecutive days.

DG were interested in obtaining a method for objectively identifying persistent phenomena that generalized approaches used in previous blocking studies. They concentrated particularly on phenomena that persisted for durations longer than the time scales normally associated with synoptic-scale variability. Fig. 2.2 shows the geographical distribution of the PA events they found using M=±100m and T=10 days in a lowpass-filtered (Blackmon, 1976) 14-winter season 500 mb dataset. They found that positive and negative PA events have nearly identical frequencies and distributions, with PAs occurring most frequently in three primary ("key") regions: over the eastern North Atlantic Ocean (ATL), the eastern North Pacific Ocean (PAC) and over the Northern Soviet Union (NSU). These key regions are coincident with the locations of maxima in intraseasonal low-frequency variability identified by Blackmon (1976). Later work by Dole (1986a) showed that the PA cases he identified represented particularly strong realizations of the dominant patterns of the low-frequency variability of the atmosphere.

DG studied the characteristics of events over a wide range of values for M and T. They found that the results for values of M=±100 m and T=10 days were typical of a wide range of values, and that these choices provided a reasonable number of cases (on the order of one of each sign per season) in the key regions for further study. Throughout the rest of

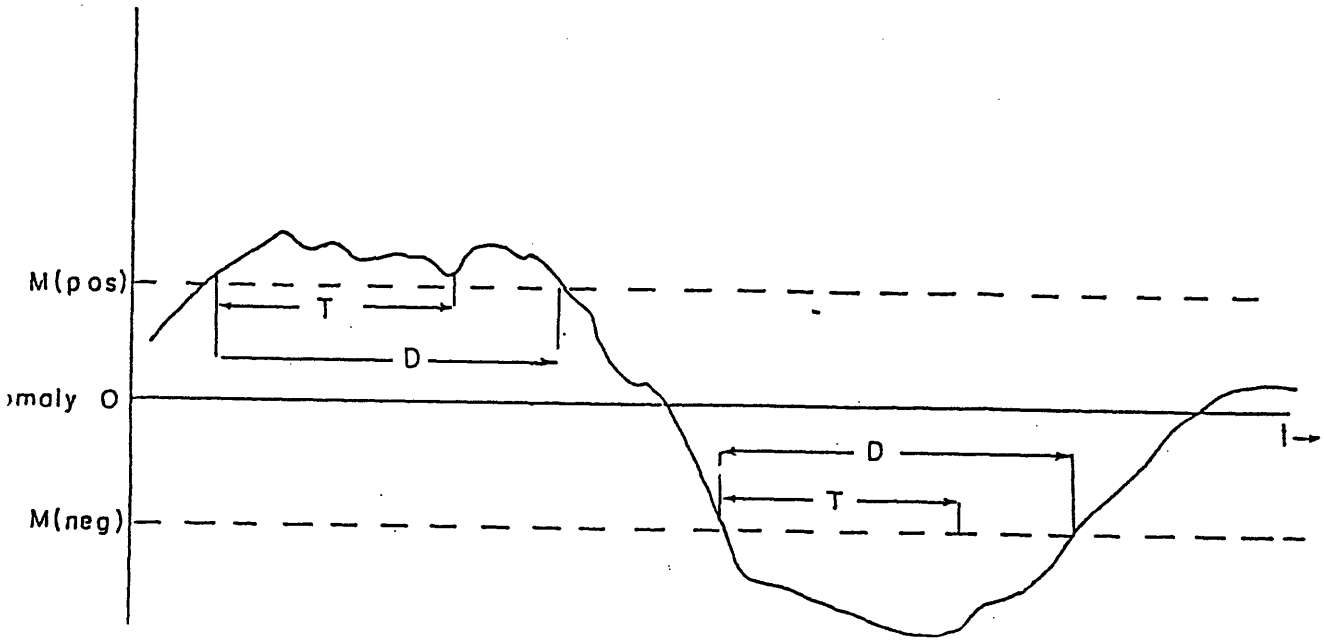

Fig. 2.1. Illustrative example of the technique used to define a persistent anomaly. An event of duration D is said to occur whenever the local anomaly exceeds M (positive or negative) for at least T consecutive days. From Dole and Gorden (1982).

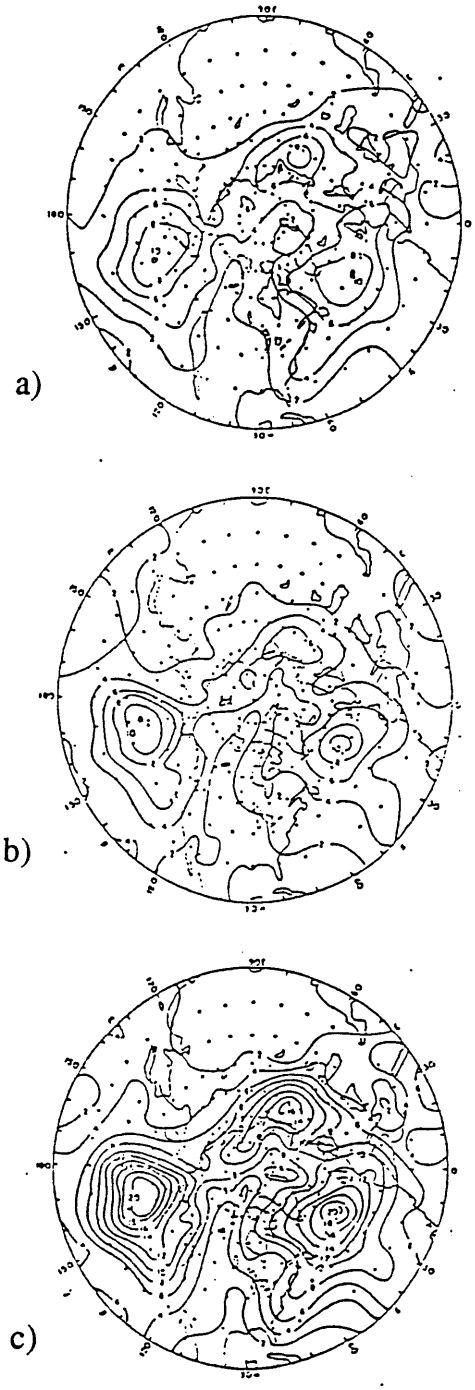

Fig. 2.2. Distribution of wintertime 500mb persistent anomaly events with a) M= +100m, T=10 days, b) M=-100m, T=10 days and c) the sum of the the two distributions. From Dole (1982).

this thesis, we will focus on PA events defined using these ±100 m and 10 day criteria applied to lowpass filtered 500 mb data.

Dole (1986a, hereafter D86a) examined the mature, composite-mean structure of PAs. He restricted himself to those events identified in the key regions. Figs. 2.3 and 2.4 respectively show his composite 500 mb geopotential heights and anomalies for both Atlantic and Pacific cases. D86a found that the composite-anomaly patterns of the positive and negative cases over each region could be broadly described as opposite phases of the same basic pattern. However, the full field composites were characterized by considerably different structures. Near the key points, the positive cases were often associated with blocking patterns (Rex, 1950a) while the negative cases were characterized by abnormally intense zonal flow. Apart from these primary features, significant anomalies are often found downstream of the key regions. The complete patterns consisting of both the primary and downstream anomalies resemble strong realizations of the major teleconnection patterns identified by Wallace and Gutzler (1981). Specifically, the Pacific pattern is similar to Wallace and Gutzler's Pacific-North American (PNA) teleconnection pattern while the Atlantic pattern resembles their Eastern Atlantic (EA) pattern.

D86a found that PAs are generally a large-scale phenomena (primarily composed of zonal wave numbers less than 5) with the patterns typically being characterized by a single major anomaly center with a few associated downstream anomaly centers. D86a also found large, deep thermal anomalies in the troposphere during mature PAs that were nearly in phase with the geopotential anomalies, that is, the PA patterns had approximately "equivalent barotropic" structures. Synoptically, the Atlantic and Pacific cases were associated respectively, with significant changes in the surface position and intensity of the Icelandic and Aleutian lows. D86a also showed that the positive and negative cases in a given region were associated with pronounced differences in their distributions of synoptic-scale variability.

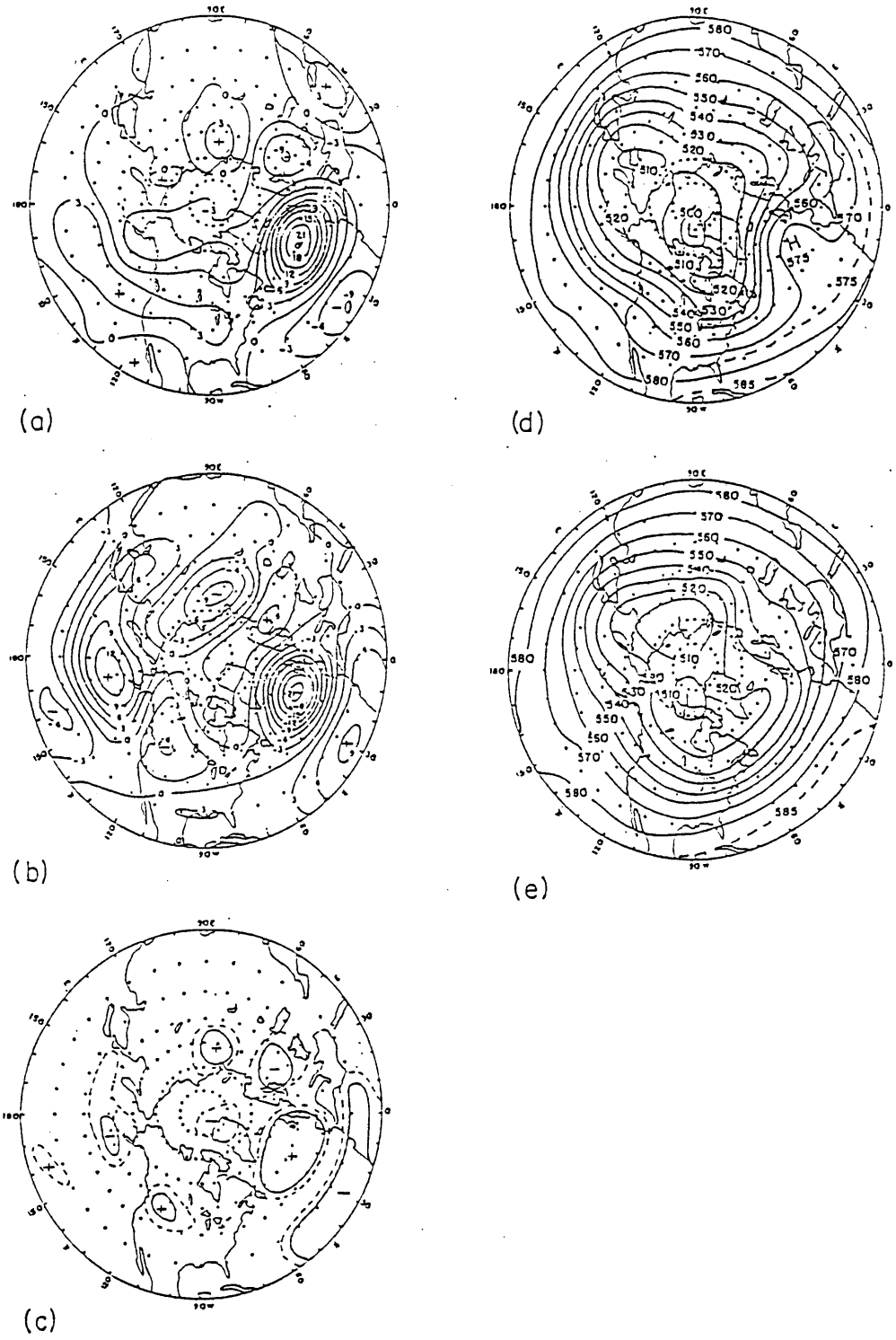

Fig. 2.3. Case mean composite 500mb anomalies for a) Atl. pos. PAs, b) Atl neg. PAs, c) 95% and 99% significance of the differences between a and b, d) the full Atl. pos. geopotential heights and e) the full Atl. neg. geopotential heights.

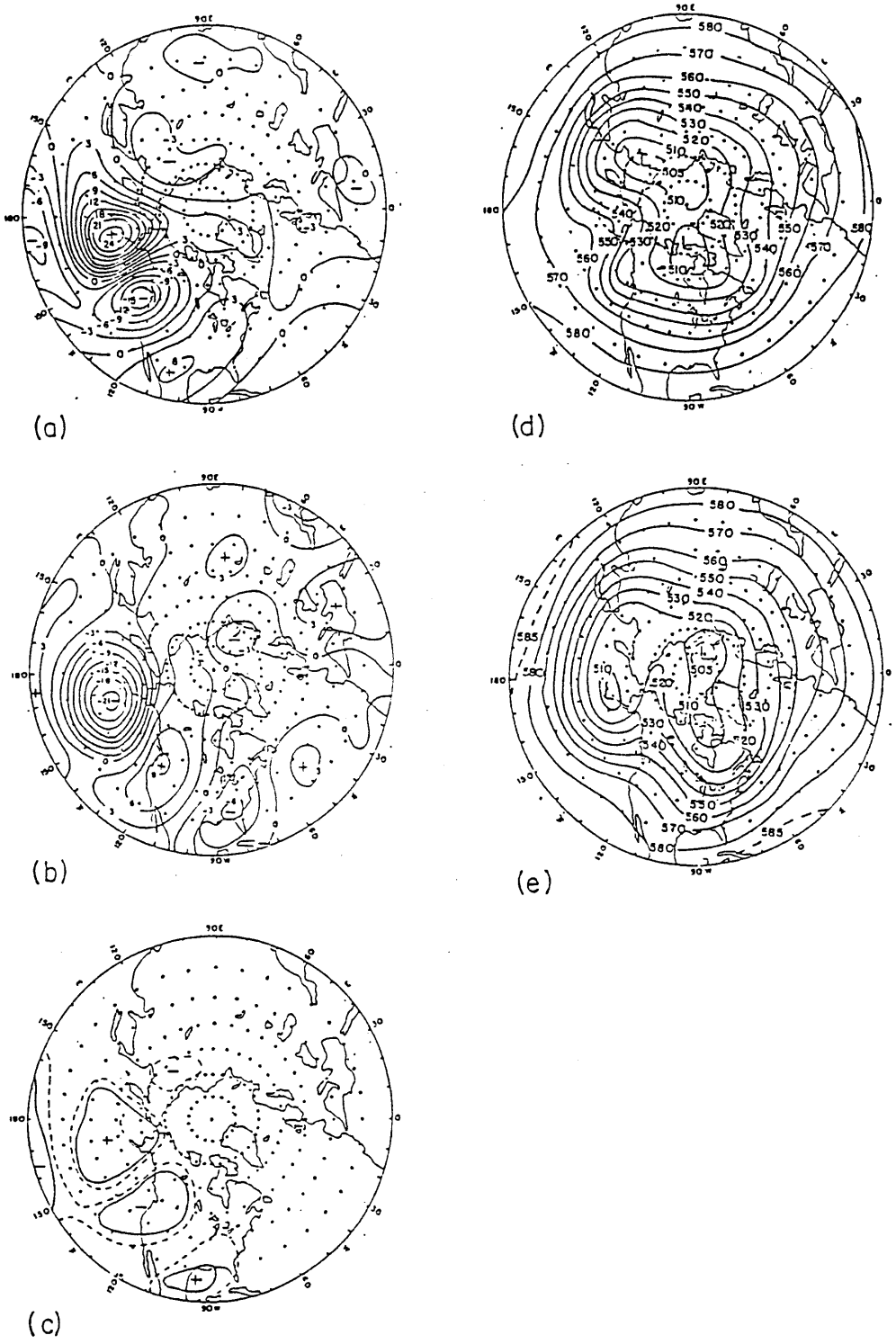

Fig. 2.4. As in Fig 2.3 except for Pacific positive and negative PA composites.

The life cycles of PAs were discussed in a series of papers by Dole (1986b, 1989) and Dole and Black (1990). Here we summarize the major results. These studies have shown that the structural symmetry between positive and negative PAs generally exists throughout the life cycles of the PAs. This suggests that opposite phases of a similar mechanism(s) may be forcing the large-scale flow. Over each of the key points, little evidence of an atmospheric precursor to the development of the PA is found until just a few days prior to onset. Development of the primary anomaly is then relatively rapid, usually occurring in about a week. Following the development of the primary anomaly, downstream anomaly centers often develop within several days in a manner similar to that described by Petterssen (1956). This downstream development resembles barotropic energy dispersion from a localized vorticity source on a sphere (Hoskins *et al.*, 1977) and is most prominent during the Pacific cases. During the Pacific negative cases, the first downstream ridge is often strong enough itself to be considered as a block. Fully developed, the mature PA patterns show little or no systematic phase propagation. Breakdown of the anomaly patterns tends to be as rapid as onset. Up until just prior to breakdown, the anomaly patterns are similar to those found just after onset.

Despite the fact that no systematic onset precursor is found at the key points, precursors often do exist elsewhere. For example, about 4 days prior to the onset of Atlantic cases, an unusually strong northward extension of the subtropical ridge often occurs just west of North Africa and over the Mediterrarean Sea. In time, this ridge retrogrades and builds northwestward, eventually forming the primary anomaly at the key point. In general, stronger (weaker) than normal diffluence is found across the Atlantic Ocean between 20N and 50N during the onset of positive (negative) Atlantic PAs which may have important implications concerning the interactions with synoptic-scale eddies (Shutts, 1983), as will be discussed later. During the PAC cases, similar precursors are found. However, in these cases, there is more evidence of an upstream precursor,

particularly prior to the negative PAC cases. In these cases a significant pool of cold air exists in eastern Asia prior to development, associated with an anomalously strong subtropical jet that extends from the Himalayas eastward through the South China Sea.

2.3 Relationships between Blocking and Persistent Anomalies

A principal objective of the work by Dole (1982) was to generalize blocking research to the analysis of persistent anomalies. This was motivated in part by a lack of consistency in the definition of blocking in previous studies as well as the overwhelming emphasis in prior work on blocking flows, with little observational or theoretical work on anomalies of the opposite sign. This discrepancy still exists today, although it has been somewhat alleviated by recent work by Dole and others. The bias in studying positive anomaly events has perhaps been due to the fact that, unlike negative PA patterns, the blocking patterns represent a considerable departure from pure zonal flow, and thus may seem to represent a more obvious problem to study.

Reviews of early blocking research can be found in Dole (1982) and Shutts (1983), and a broad overview of relatively current research on blocking is given in the text, *Anomalous Atmospheric Flows and Blocking* (1986). Since we will often draw comparisons between our PA results and results obtained in previous blocking studies, it is useful to provide a brief overview of blocking and its relationship to PAs.

Blocking has been defined by a number of different criteria (see Dole,1982 for a review of methodologies). Despite this, there are several features common to nearly all blocks that have allowed a generalized description of blocking to emerge. In general, blocking consists of a quasi-stationary, persistent, warm and unusually strong anticyclone or ridge. A fundamental concept underscoring the definition of a blocking flow is that the

associated large-scale flow pattern tends to divert or "block" transient synoptic-scale systems far from their normal paths (Petterssen, 1956). During blocking, synoptic-scale storms are usually steered well to the north and/or to the south of the blocking anticyclone. However, this fundamental characteristic of blocking has never been fully exploited in defining blocking cases. Since much of the precipitation and general day-to-day variability in the weather of mid-latitudes is associated with transient synoptic-scale systems, blocking flows can often lead to relatively long periods of abnormal weather conditions[1] (e.g. Green, 1977). Thus the understanding of blocking represents not only a challenging problem for researchers, but also one that has important practical implications.

The major differences between the various methods for defining blocking cases lie in the degree to which various structural or temporal features are emphasized. For example, Rex (1950a) emphasizes the persistence of a large-scale split in the upper-level westerlies, White and Clark (1975) stressed the degree of 700 mb meridional flow, while Lejenas and Doos (1987) identify blocking whenever there is a mid-latitude upper-level easterly flow. Criteria which emphasize the split or diffluent nature of the mean flow tend to define cases which have a warm anticyclone to the north of a cold cyclone while criteria emphasizing the meridional aspects of the flow often do not have as strong a southern cold low (Sumner, 1954). These latter blocking configurations are often refered to as "omega" blocks.

Despite these differences, given the same data, most different blocking definitions yield a broadly similar set of cases. This is because most of the blocking definitions implicitly require that the magnitude of mean flow aspect ratio, (|v/u|), to be large (or infinite) over a broad region at upper-levels. However, a priori we expect that such criteria will tend to select more cases in regions where the climatological-mean flow already

[1] Of course, the large thermal and flow anomalies directly associated with the block may also significantly influence the local weather.

exhibits a large value of this ratio. Such regions would be north of the mean zonal jet[1] and at longitudes where the climatological-mean zonal flow is relatively weak. Indeed, Rex's (1950b) climatological study of blocking shows a greater tendency for blocks to form in these regions. Thus, although there may be dynamical reasons why large flow anomalies preferentially form in these regions, blocking climatologies can not necessarily be used to support them.

From the above discussion, it is unclear whether blocks represent the largest deviations from the climatological mean flow found in the atmosphere or whether they are merely one of the more obvious. Persistent anomaly studies, on the other hand, focus specifically on cases exhibiting the largest and most persistent deviations in the flow field from its climatological-mean values. It is perhaps surprising then, that the composite-mean structure of positive PAs (Figs. 2.3 and 2.4) exhibit most of the features attributed to more traditionally-defined blocking episodes, including a split flow, upper level easterlies and a warm anticyclone throughout the troposphere. Some blocking cases, however, are relatively transient, occasionally lasting for only a few days (e.g. Sumner, 1954). Thus, while most positive PA cases are associated with blocking, not all blocking cases would be considered persistent anomalies. With regard to their distributions, persistent anomalies tend to occur somewhat further south and closer the the mean jet than do blocks. They also tend to occur further west, particularly over the Atlantic. In general, Atlantic positive PAs tend to resemble traditional blocking structures more than their counterparts over the Pacific. This is at least partly because the Atlantic key point lies close to a ridge in the stationary waves, whereas the Pacific key points lies on an inflection point between a stationary ridge and trough. Thus Atlantic PAs tend to have exaggerated meridional flows and are therefore more likely to be associated synoptically with blocking.

---

[1]Anticyclones to the south of the jet are associated with a stronger then normal mid-latitude zonal flow and are thus not considered a blocked flow. However, cases with a cyclone south of the jet are indeed associated with a weaker than normal westerly jet, but these cases are usually considered as "cut-off lows" (Bell and Bosart, 1990) and will be discussed later in the text.

The structural differences between blocks and positive PAs becomes somewhat more pronounced when examining the associated potential vorticity (PV) fields. Fig 2.5 shows Ertel's PV[1] on the 320K surface during both a mature positive PA case and a traditional blocking case. The PV structure in the persistent anomaly case is characterized by an open-wave structure with the main PV gradient pushed well to the north of its mean position. One the other hand, the blocking PV field consists of a more convoluted structure, with closed (or nearly closed) off low PV pool north of the main PV gradient. These structural differences highlight the fact that traditionally defined blocking cases tend to form away from large meridional PV gradients, whereas PAs tend to occur within or at least closer to them. The open-wave PV structure of positive PAs may have significant dynamical implications as to the applicability to persistent anomalies of certain nonlinear structure theories (i.e. modons and coherent structures) that require isolated PV pools (McWilliams, 1980). It may also indicate the reason why there is an apparent quasi-linearity in the signed structures of PAs (Dole, 1986a). Therefore, in the future, a closed low PV contour to the north of the mean PV gradient may be a more suitable alternative objective criteria for defining blocking .

To some degree, the inverse phase of blocking may be regarded as the so-called "cut-off low" (Bell and Bosart, 1989). This terminology has been used frequently by synopticians to describe upper-level, isolated and usually equivalent-barotropic cold-core cyclones. Although closed circulation centers form most often to the north of the mean jet, a closed low to the south of the main jet is usually referred to as "cut-off" (Glossary of Meteorology, 1955). Since these features are usually well removed from the jet, they tend to be relatively slow moving and are often long lived. They have a similar (but weaker) relationship to negative persistent anomalies as blocking does to positive persistent anomalies. Cut-off lows are perhaps best characterized by closed PV or geopotential

[1] See Hoskins *et al.*, 1985 for a comprehensive discussion on the use of potential vorticity charts.

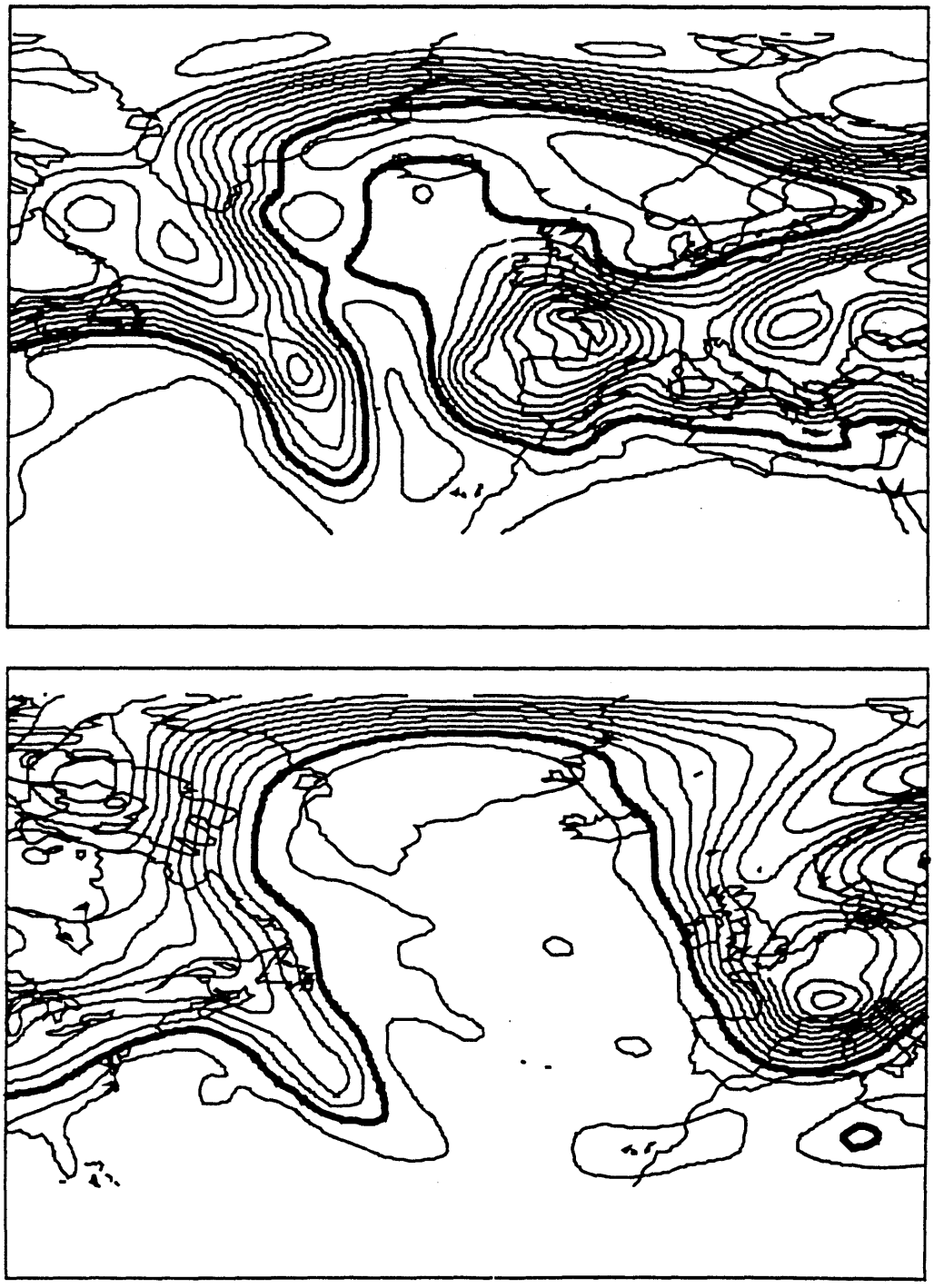

Fig. 2.5. Distribution of Ertel's potential vorticity on the 320K isentrope for a) a typical Atlantic blocking case and b) a typical Atlantic persistent anomaly case. The contour interval .5 PVUs and the 1.5 PVU contour is highlighted. One PVU is equal to 1×10^{-6} K m^2 s^{-1} kg^{-1}.

contours located south of the main jet, whereas the primary anomalies during negative PA cases tends to remain north of the main jet. Cut-off lows also appear to be major flow perturbations. However, like blocks, it is not clear to what extent they represent the largest and most persistent flow anomalies, nor what their contributionn is to the total low-frequency variability of the atmosphere.

2.4 Synoptic-Scale Eddies and Persistent Anomalies.

A significant motivation for studying blocking is to gain insight into the causes of the major weather anomalies that frequently occur during blocking (e.g. Green, 1977). An important part of the anomalous weather during blocking is apparently related to the diverted paths of the synoptic-scale disturbances. Thus, most observational blocking studies have discussed to some extent the effect of blocking on the synoptic-scales. Since positive persistent anomalies are usually associated with blocking, we will draw upon the body of research on the relationships between synoptic-scale eddies and blocks in discussing the effects that persistent large-scale flow anomalies may have on the behavior of synoptic-scale eddies.

Changes in eddy[1] activity associated with blocking have traditionally been presented in one of two ways. The first is somewhat subjective and was typically employed in most early blocking studies (e.g. Bergren *et al.*,1949; Petterssen,1956). These studies usually showed either a sequence of maps or a composite map of the paths of low pressure centers or frontal positions during blocking episodes. For example, Fig. 2.6 from Petterssen (1956) shows the analyzed positions of surface fronts during two consecutive 10-day periods prior to and during a major European blocking event. Prior to the onset of

[1] Here, and throughout this thesis, an unqualified use of "eddy" implies synoptic-scale disturbances whose temporal and horizontal scales are on the order of a few days and a few thousand kilometers respectively.

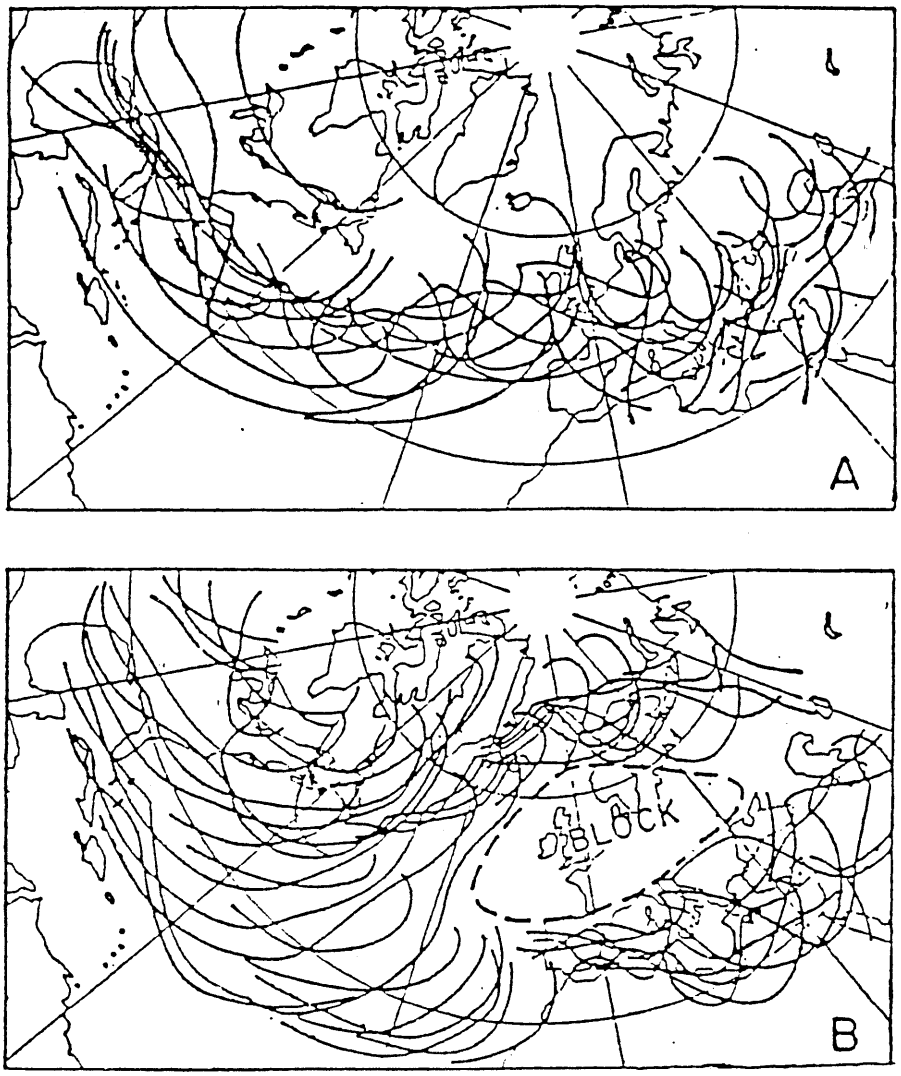

Fig. 2.6. Frontal trough positions during two week periods that a) preceeds the formation of a block and b) during a blocking episode. Reproduced from Petterssen (1956).

blocking, disturbances can be seen to migrate eastward in a relatively narrow band from North America across the Atlantic and into Europe. In stark contrast, disturbances during the blocking event are forced well to the north or well to the south of the blocking surface high. Upstream from the block, the frontal troughs appear to slow and to meridionally elongate before splitting into two branches which subsequently propagate around either side of the block. The point where the frontal troughs become nearly stationary was referred to as a "shock front" by Rex (1950a).

The second, more objective method for describing observed eddy activity changes during blocks (and other low-frequency phenomena) has been to analyze the variance in the bandpass-filtered (usually retaining periods between 2.5 and 6 days) geopotential heights. The climatological mean distribution of this variance (Blackmon, 1976) exhibits several mid-latitude local maxima that tend to be elongated in the mean flow direction. These maxima are often referred to as "storm tracks", although no explicit dependence on the paths of individual disturbances is contained in the analyses. Nonetheless, comparison between the distributions of bandpass variance and the actual paths of cyclones and anticyclones (Petterssen, 1956; Klein, 1957) indicates that maxima in bandpass variance generally correspond well with the concentrated regions of the storm tracks. To the extent that this is true, then changes in the position and distribution of the bandpass variance maxima during low-frequency events can then be associated with corresponding shifts in the storm tracks. We will confirm this point later in the thesis.

Dole (1982) found significant differences in the storm tracks during the mature phase of positive and negative PAs. Fig 2.7 shows his distribution of variability in the bandpass-filtered 500mb geopotential heights during both Atlantic and Pacific PAs. During the Atlantic positive PA cases, the principal Atlantic storm track extends from North America northeastward towards Iceland and then eastward into Scandinavia. In contrast, during the negative PA events, the principal storm track is zonally oriented extending eastward from

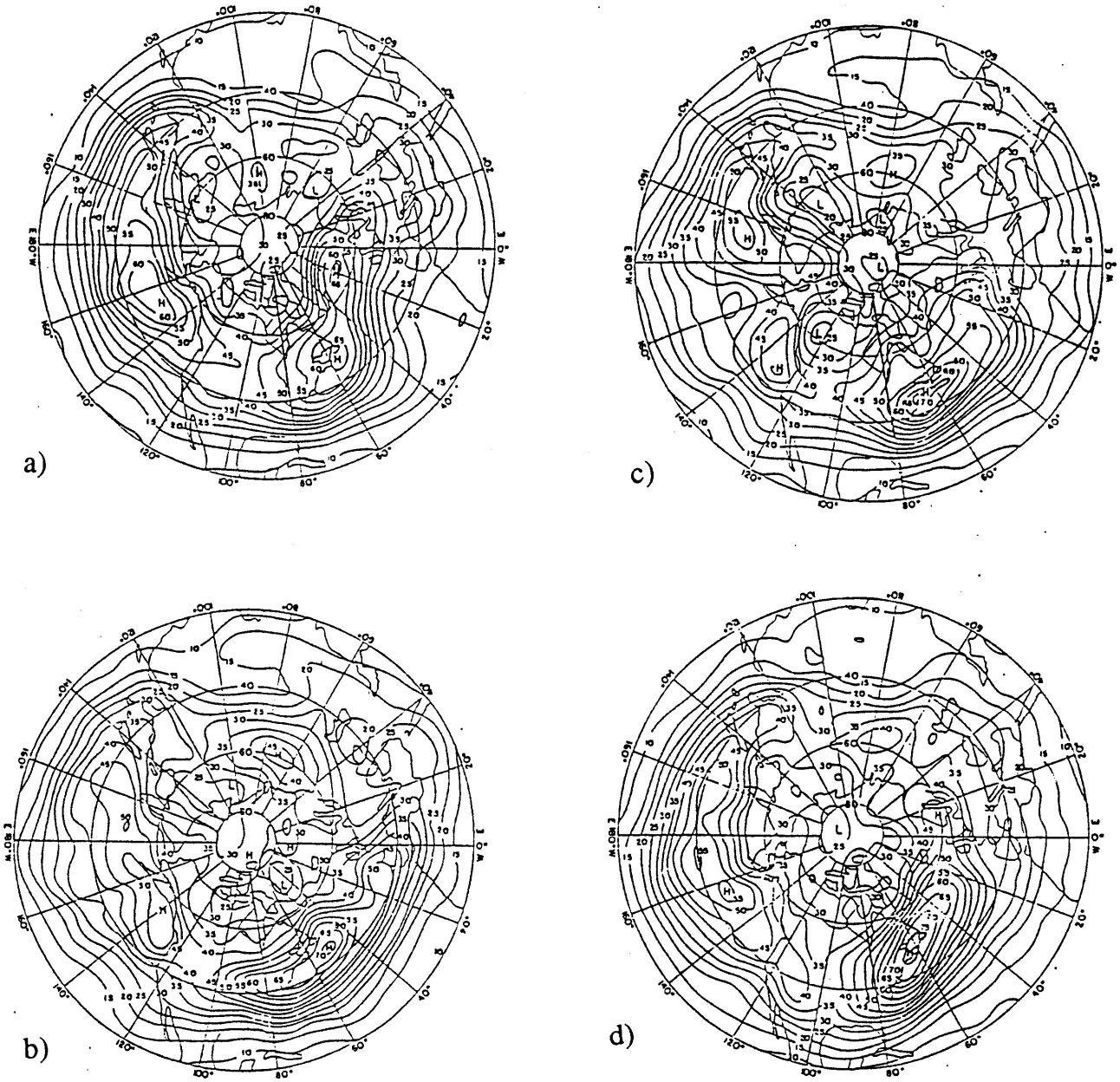

Fig. 2.7. Composite-mean distributions of 500mb bandpass geopotential height variance (m)during a) Atl. pos. b) Atl. neg. c) Pac. pos. and d) Pac. neg. persistent anomalies. Reproduced from Dole (1982).

North America to central Europe. Similar changes in the storm tracks are evident in the Pacific cases. Overall, the storm paths and the mean jets tend to parallel each other, consistent with a simple model in which the eddies develop in regions of strong baroclinicity and are advected downstream by the large-scale flow. Mullen (1987) found that the storm tracks during mature Atlantic and Pacific positive PAs in both the real atmosphere and a GCM modeled atmosphere were similar to Dole's results. Robertson and Metz (1989) found that in a simple GCM model, large shifts in the regions of synoptic-scale baroclinic growth occurred when the model was linearized about basic states resembling the major teleconnection patterns. In a somewhat different study, Lau (1988) found that the leading EOFs[1] of the 500 mb heights associated with anomalies in the monthly-mean variance of synoptic-scale disturbances tend to resemble the primary teleconnection patterns (Wallace and Gutzler, 1981). Similarly, Anderson and Gyakum (1989) found the leading rotated EOFs in the 500 mb flow associated with variations in a cyclone density function also resembled many of the more prominent teleconnection patterns.

In a very recent study, Nakamura and Wallace (1990) defined an "envelope" function that describes the slow evolution in the local amplitude of the synoptic-scale eddy activity. They formed composite anomalies of this envelope function during various phases in the life cycles of several low-frequency teleconnection patterns. Focusing on the Alaska blocking pattern, they found that significant eddy activity anomalies form a "sandwich" pattern about the key region. During the blocked or positive (negative) phase of the large-scale pattern, positive (negative) anomalies are found to the north and to the south of key point and negative (positive) anomalies are found near the key point. Further, they found that positive (negative) eddy activity anomalies occur just upstream of the key

[1] EOF (emperical orthogonal functions) methods for decomposing analyzed atmospheric fields was described by Lorenz (1956).

point during the onset of the positive phase. During the decay of the large-scale pattern, similar eddy activity anomalies, but of opposite sign, were also found.

Several other techniques have been used to diagnose eddy activity changes during blocking and other prominent low-frequency events. However, the goal in many of these studies was to deduce the role that the synoptic-scales may play in forcing the larger-scale circulation. A discussion of these results is reserved for later in this chapter. For now, we note that although there have been several studies identifying the synoptic-scale changes during various low-frequency phenomena, the degree and significance of changes that occur during the life cycles of persistent anomalies remains to be determined.

2.5 Theories for Persistent Anomalies.

In this and the next section we summarize the major theoretical work aimed at explaining persistent anomalies. Although not all of this work was necessarily intended to account for the observed PA patterns, certain aspects of the results are directly relevant to this problem. In this section, we concentrate on theories other than those related to forcing by synoptic-scale eddies, reserving a more comprehensive discussion of that subject matter until the next section. As persistent anomalies contribute a significant part of the total low-frequency variability of the atmosphere, and as the positive PA cases are often associated with blocking, we will draw heavily upon theoretical work on these two areas. Here we provide the reader with a general overview of the relevant research. More comprehensive discussions can be found in *Dynamics of Low Frequency Phenomena in the Atmosphere* (1987).

Any complete theory for persistent anomalies must of course explain all of the observed characteristics of PAs. Probably the most important characteristics to explain

however, are the distribution, magnitudes, structures, growth and decay, and symmetric nature of the phenomena. Lindzen (1986) has discussed the persistence characteristics of PAs, and argues that the observed durations can be accounted for by the temporal characteristics of ultralong Rossby waves. Although we have emphasized the symmetry between the two phases of PAs, considerable asymmetries do exist, particularly in the full field. There are also differences between PAs in different regions as well as between individual cases. Therefore, although it would be somewhat pleasing to have one generalized theory to explain all types PAs, this is not necessarily warranted. Indeed, several theories correctly account for some of the variability associated with PAs with the relative importance of the different mechanisms varying from case to case.

Theories for PAs can broadly be placed in two categories: either a free response or an anomalously forced wave response. Here a free response implies that there are no significant changes in the sources of potential vorticity necessary for the development, although such changes may have been important in establishing the initial conditions upon which the response evolves. Thus in this context, a free response may contain some degree of forcing. However, a change in this forcing must not be critical to the evolution and may only be second order.

Instability or growth of planetary waves at the expense of the basic state is one type of free response theory. Fredericksen (1983) calculated the unstable modes in a 2-level quasi-geostrophic model linearized about the climatological mean flow. He envisioned the blocking initiation process in two stages: an initial large-scale mixed baroclinic-barotropic instability stage followed by stationary barotropic growth stage. Barotropic instability (Simmons *et al.*, 1983) and barotropic growth (Farrell, 1989) theories have also had success in reproducing some of the characteristics of PAs. Observational evidence (Dole and Black, 1990) suggests that both baroclinic and barotropic extraction of energy from the climatological-mean state on a large-scale are likely to play a important role in the

development of negative PAs over the North Pacific, with the baroclinic conversions dominating the early stages of development.

Coherent structures or modons (McWilliams, 1980; Malguzzi and Malanotte-Rizzoli, 1984, 1985; Malanotte-Rizzoli and Malguzzi, 1987; Verkley, 1990) have also been shown to resemble some mature blocking structures. They are localized, nonlinear, stationary solutions of the potential vorticity equation, that can freely evolve from an initial condition consisting of a suitable refractive index distribution. They are characterized by internal and external flow regions having separate functional relationships between the potential vorticity and the non-divergent flow. They have usually been applied to mature blocking flows although recent generalizations (Haines and Rizzoli, 1990) have also shown a possible relevance to strongly zonal flows. Modons share many structural and temporal characteristics with atmospheric blocking and thus appear to be sufficient prototypes for its study. However, as noted earlier, PAs are usually not characterized by isolated PV structures and thus the relevance of modon theory to at least some PAs may be limited.

Multiple equilibria theories (Charney and DeVore, 1979; Charney and Straus, 1980; Charney *et al.*, 1981) hypothesize that the atmosphere can exist in more than one state of equilibrium with its boundary conditions. The equilibrium states they found in a simple barotropic model resembled high (blocking) and low (zonal) index regimes (Namias, 1950). It was speculated that certain persistent flow patterns such as blocking may be close to a particular quasi-equilibria. Depending upon the stability of each state, the transition to and persistence within each state may be relatively rapid or long and may project strongly on the LFV of the atmosphere. It was also speculated that synoptic-scale eddies may play a role in the transition between various quasi-equilibria states. This has been verified in some simple modelling studies (e.g. Rienhold and Pierrehumbert, 1981). Early observational evidence for the existence of multiple states (e.g. White (1980) and DG) was

limited, although more recent analyses (Benzi *et al.*, 1986; Hansen, 1986; Sutera, 1986) have found some evidence for certain preferred states of the planetary waves.

Changes in the amplitude and propagation characteristics of the stationary waves associated with mean flow variations has been proposed as a mechanism for the excitation of PAs. Here the mechanism is not related to a change in the forcing per se, but rather to a change in the response of modes excited by stationary sources. Nigam and Lindzen (1989) and DaSilva (1989) have studied how the amplitudes and phases of the stationary waves depend on changes in the mean-zonal flow. Relatively large geopotential height changes in the troposphere (even larger in the stratosphere) are often found to develop in their models on time scales similar to observed PAs, although DaSilva (1989) found much less sensitivity in a baroclinic model than in a barotropic model response. Recent calculations of the flux of stationary wave activity (Plumb, 1985) by Black (1990) suggests that the source for Pacific negative PA wave energy is over the central Pacific, and is apparently not directly tied to any major topographic features such as the Himalayas. Since the dominant stationary wave forcing is from topography (Jacqmin and Lindzen, 1985) there is some doubt then, as to whether the Pacific negative cases can be directly explained by changes in the stationary wave response to topographic forcing caused by mean zonal wind variations.

Other theories of anomalous forced waves include that by Kalnay-Rivas and Merkine (1981) who show how changes in topographic forcing can lead to blocking in a barotropic model. In addition, White and Clark (1975) argued that baroclinic instability of planetary-scale waves in the presence of sensible heating from extratropical sea-surface thermal anomalies might lead to blocking. Many theories have suggested that diabatic heating from the tropics could be important in forcing low-frequency variability in mid-latitudes. Webster (1981), Hoskins and Karoly (1981), Karoly and Hoskins (1982), Simmons (1982), Weickmann *et al.* (1985) and Navarra (1990) are examples of investigations as to

the extratropical response to tropical heating. However, numerical investigations have had only limited success in producing significant extratropical response to tropical heating. Lindzen (1986) notes that as the sophistication of the models increases, the mid-latitude response to tropical heating anomalies tends to decrease. Further, Plumb (1985) found little observational evidence for the forcing of the stationary waves from tropical sources (although his quasi-geostrophic framework precluded his ability to infer the effects of divergent circulations). Even if tropical heating does not play a direct role in forcing intraseasonal mid-latitude planetary waves, it may still have an indirect effect on the midlatitudes by modifying the mean flow and thus making it more or less likely that a PA will develop within a given season. It might also indirectly effect mid-latitude LFV by modifying the mid-latitude transients, as suggested by Held *et al.* (1989) which could force anomalous planetary waves through their Reynold's stresses. Therefore, although tropical flow and heating variations may not have a major role in the energetics of extratropical low frequency variability, tropical variability may still sill have significant influence in establishing the basic state upon which extratropical waves grow and propagate.

2.6 Forcing of Persistent Anomalies by Synoptic-Scales

The potential role of synoptic-scale transient disturbances in forcing large-scale flow anomalies has been a topic of considerable recent interest. Since synoptic-scale systems represent an internal response to the mean flow that do not directly require any nonconservative external forcing, their impacts on the larger-scale flow may be regarded as a free response as outlined earlier. However, the equations for the mean large-scale flow are often written is such a way so that the interactions between the transients and the mean flow are contained in a single forcing term (e.g. Plumb, 1986) that is related to the eddy flux of potential vorticity. It is through this interaction that synoptic-scale disturbances are

regarded as a potential source term for the the larger-scale flow. Further, variations in synoptic-scale eddy activity can cause large-scale variations is diabatic heating patterns which may also force changes in the large-scale flow.

Early blocking investigations (Bergren *et al.*, 1949; Rex 1950a) noted the likely importance of synoptic-scale systems (particularly cyclones) in development of the blocking patterns. For example, in describing such processes during the onset of a wintertime blocking event over Western Europe, Berggren *et al.* (1949) stated:

> Each trough, as it deepened and slowed down over the central part of the Atlantic, gave birth to a strong southerly current on its eastern side through which the preceding trough was cut off and partially filled. These intermittent warm currents gradually broadened the initially quite narrow anticyclonic ridge until ... a large, warm anticyclone extended along 60°N from Scandinavia to Greenland....

and that

> The [eddy] processes described above were repeated a total of four times during the eight day period [of development].

They pictured blocking as not only affecting the paths of synoptic-scale disturbances, but also that the disturbances were crucial to the formation of the block. They argued that the block was formed by the successive exchange and accumulation of warm and cold parcels of air across the mean meridional thermal gradient caused by several incident cyclones. Colucci (1985) presented a case of blocking development in which this destruction of the thermal gradients (and thus a weakening of the upper-level westerlies) and the establishment of a block was accomplished by an unusually rapid cyclone development or "bomb" (Sanders and Gyakum, 1980). Crum and Stevens (1988) reached a similar conclusion using PV analyses.

Shutts (1983) describes a method in which barotropic transient eddies in a diffluent mean flow can give up their energy to the mean flow. In his conceptual model, the eddies slow and becomes meridionally elongated in the diffluent region upstream of a block. This elongation is associated with a cascade of potential enstrophy to smaller scales. Since the smaller scale eddies are more prone to diffusion, the enstrophy cascade is thus associated with an increased eddy dissipation. It can be shown using the potential enstrophy equation (see Shutts' Eq. 2) that this dissipation should be accompanied by an eddy potential vorticity flux down the mean PV gradient[1]. Since large-scale diffluence is associated with a downstream weakening of the mean PV gradient (assuming the $\bar{q}$ and $\bar{\psi}$ contours are nearly parallel), eddies incident on the diffluent region are thus acting to force the large-scale flow anomalies. Shutts went on to numerically confirm his ideas with a barotropic model. Haines and Marshall (1987) have also shown in a barotropic model how this type of forcing can lead to the growth from a weakly diffluent mean flow into modon-like blocking structure. The mechanism is also consistent with the calculations of Hansen and Sutera (1984) who showed that during blocking episodes there is a net upscale transfer of energy associated with the dissipation of eddy enstrophy.

Farrell (1989) suggests an alternative mechanism for eddy forcing of the large-scale flow that does not rely upon eddy diffusion. Rather, he suggests that the blocking flow may be formed by the far field inversion of several suitably structured eddy PV anomalies that have become compressed (to distances less than their individual radii of influence) in the weak flow region downstream of the diffluence. During such a process, there would still be an upscale eddy energy cascade but a downscale eddy potential enstrophy cascade.

There have been many studies on the role of synoptic-scale eddies in the maintenance of blocks. Green (1977) postulated that eddy fluxes may have maintained the

---

[1] This requires an assumption that there is not net divergence of the term that represents a correlation between the eddy velocity and eddy enstrophy, which is $O(\varepsilon^3)$.

European block of July 1976 against dissipation. Austin (1980) tested Green's hypothesis with a simple quasi-geostropic model and concluded that eddy forcing of the large-scale flow must occur one-quarter wavelength upstream to balance the downstream advection of the large-scale anomaly by the mean flow. Hansen and Chen (1982), Hoskins *et al.* (1983), Illari and Marshall (1983), Illari (1984), Dole (1986a), Shutts (1986), Trenberth (1986), Mullen (1986,1987), Holopainen and Fortelius (1987) and others have all used various diagnostic techniques to demonstrate the positive role of feedbacks by the transients in the *maintenance* of blocking patterns. In general, these studies have found that anomalous eddy anticyclonic vorticity forcing occurs upstream of the block, intermediate between the phase relationships suggested by Green or Austin, implying that both advection and dissipation are important in the time-mean balances of mature blocking events. Pierrehumbert (1986), Egger *et al.* (1986), Haines and Marshall (1987), Mullen (1987) and Malanotte-Rizzoli and Malguzzi (1987) among others have all reached similar conclusions using analytic or numerical models. In a more general sense, Gall *et al.* (1979), MacVean (1985), Young and Villere (1985) and Ebisuzaki (1986) have found that the growth of planetary-scale waves in enhanced by non-linear interactions with synoptic-scale disturbances.

Despite the plethora of evidence in the above studies, many questions remain as to the role synoptic-scale eddies play in forcing anomalous persistent flows. For example, studies that focused on the Atlantic blocking generally found anticyclonic eddy forcing upstream of the block over the central North Atlantic Ocean. However, this is precisely a region where Lau and Holopainen (1984) found a wintertime mean anticyclonic forcing by synoptic-scale transients. Thus it is not clear to what extent the eddy forcing is anomalous during these events, nor what relationships the anomalous portion of the eddy forcing has to the large-scale flow anomaly. The problem is further clouded because many studies have focused on transients of all time scales, thus combining the effects of possible

transience associated with the large-scale flow in the analyses. Further, quantitative descriptions of the roles of eddies during the onset on PAs has been limited to a few case studies of relatively intense blocking situations (e.g. Colucci. 1987; Crum and Stevens, 1988; Tsou and Smith, 1990). This is despite the fact that several qualitative descriptions, such as those by Berggren *et al.* (1949) discussed earlier, have stressed the role of the synoptic-scales in the initiation of the block. It is also unclear how the blocking case studies pertain more generally to the onset of PAs, particularly to the negative phase of the anomalies. It is also unclear whether or not synoptic-scale eddies are important in the breakdown of PAs. These are among the main questions we wish to address.

2.7 Summary

Persistent anomalies are defined as large-scale flow anomalies that persist for periods longer than those normally associated with synoptic-scale variability. In the Northern Hemisphere, PAs occur most frequently over the eastern North Atlantic and eastern North Pacific Oceans downstream of the major storm tracks. They occur in two phases: the positive phase being associated locally with blocking, and the negative phase associated with abnormally intense zonal flows. They develop and decay relatively rapidly, usually in less than a week and typically persist for two to three week periods. They generally have large thermal anomalies that are nearly in phase with the flow anomalies, yielding overall, nearly equivalent-barotropic structures. They have an important influence on the distribution of synoptic-scale disturbances and thus can lead to prolonged abnormal weather conditions over large regions. Several theories have been put forth to explain persistent anomalies, including forcing by synoptic-scale eddies, but as of yet no single theory has been widely accepted as an explanation of PAs. As there is some degree of case-to-case variability in PAs, a single theory may not be sufficient.

The remainder of this thesis is devoted to studying the interactions between synoptic-scale eddies and persistent anomalies. We will approach this problem in two parts: First, how does the large-scale flow effect the synoptic-scale eddies during the life cycles of persistent anomalies? And second, how do the eddies feedback and effect the large-scale anomaly? These questions are specifically addressed in chapters 4 and 5 respectively.

Chapter 3

General Procedures and Analyses

3.1 Introduction

In this chapter we briefly discuss the data, procedures and certain geopotential height analyses that are referenced throughout the remainder of this thesis. Data and procedures that are specific to one particular set of analyses are described in the appropriate section. Here we will discuss the construction of the primary dataset, the major filtering schemes, the selection of persistent anomaly cases, and our compositing techniques. We will also present the composite-mean geopotential height analyses, as these are referenced through the remainder of the thesis. In these analyses, we will focus primarily on the 300 mb geopotential heights, thus extending the 500 mb and 1000 mb analyses provided by Dole (1982, 1986a,b, 1989).

3.2 Construction of the primary dataset.

Our primary dataset is derived from the National Meteorological Center's (NMC) final analyses over the Northern Hemisphere. Dey (1989) gives a very thorough overview of the history of the NMC analyses. In summary, the final NMC analyses are twice-daily (0000 and 1200 UTC) mandatory pressure level[1] analyses of geopotential height, temperature, winds and relative humidity as well as several diagnosed quantities such as vertical motion and vorticity. The analyses are constructed from all available surface,

[1] The pressure levels used are (in mb) 1000, 850, 700, 500, 400, 300, 250, 200, 150, 100, 70, 50, 30, 10, 5, 1 and 0.1.

radiosonde, aircraft and satellite observations (see Dey for typical distributions of these observations) received at NMC during approximately the first 6 hours following the synoptic analysis time (Petersen and Stackpole, 1989). The observations are objectively fitted to a fixed-distance octagonal grid covering a north-polar stereographic projection of the Northern Hemisphere north of about 18N with a grid point spacing of approximately 320 km.

Both the database and the objective analyses scheme used to produce the NMC analyses have undergone considerable changes over the period of study (see Dey, 1989). Trenberth and Olson (1988) discuss the quality of the NMC analyses focusing on occasional "bad" analyses and systematic errors in the grids. As we focus on persistent anomalies and the anomalous aspects of eddy interactions in this thesis, many of these systematic errors are removed by the diagnostic techniques. However, since there may still be problems with the quality of the NMC dataset and particularly its use for higher order analyses, we have employed variations in diagnostic techniques, statistical significance tests and synoptic reasoning to help ensure the robustness of our results.

A majority of the NMC gridded analyses have been archived on the Mass Storage System at the National Center for Atmospheric Research (NCAR). The NCAR archives consist of most of the analyses from mid-1962 to the present, although the archives of certain quantities (e.g. 500 mb geopotential height) start considerable earlier. The stratospheric grids (above 100 mb) are available only after 1970.

Our dataset is a transformed version of the NCAR archives of geopotential heights, temperature and winds covering the period from 01 December 1962 through 31 December 1987. We use a 16-point Bessel scheme (Jenne, 1970) to horizontally interpolate the NMC analyses to a 2 degree latitude by 5 degree longitude cylindrical equidistant projection covering the Northern Hemisphere from 20N to the pole. In general, data on this grid is

simpler to use in diagnostic analyses than data on the NMC octagonal grid. The 2 x 5 degree grid spacing was explicitly chosen to match a similar dataset obtained from NASA-Goddard that was used for early development and testing of diagnostic routines. The choice is sufficient for the construction of the permanent dataset, as it provides a square grid near 65N, not far from the latitude of maximum LFV. Further, it provides a typical mid-latitude grid spacing of about 300 km, consistent with the original NMC grid spacing and suitable for diagnosis of the synoptic and larger-scale phenomena of primary concern to this thesis. It also appears to be consistent with the "typical" observational network density presented by Dey (1989), even over the oceans.

Grids that did not pass simple data quality checks similar to those used by Trenberth and Olson (1988) were not included in the transformed grid set. These bad grids, as well as grids that were otherwise missing from the NCAR archives, were reconstructed in one of several ways. First, if the heights and/or temperatures were missing for a particular level at any time, they were replaced by grids computed by integrating the hydrostatic equation (assuming a log-pressure thermal profile) both upward and downward from the neighboring levels and averaging the two results. The 100 mb missing grids were similarly replaced although in this case, the atmosphere was assumed isothermal from the 150 mb level if the temperature grid was missing. Grids that could not be replaced by this vertical interpolation scheme were replaced using a linear temporal interpolation from the nearest available times. All missing wind grids were replaced by their geostrophic values regardless of the source of the geopotential height grid.

Subjective analyses of grids reconstructed by the two interpolation methods during times when the original grid was available indicate that the vertical interpolation scheme was far superior in reproducing the missing data and thus an attempt to apply it was made first. In general, less than 4% of the grids were reconstructed, of which about 25% were vertically reconstructed. Several exceptions to this are noted: First, the 250 mb and 400 mb

grids prior to May 1965 were not available, the vast majority of which were replaced using the vertical interpolation scheme. No attempt has been made to replace the stratospheric grids that were unavailable prior to 1971. Only about 5% of the 1000 mb temperature grids were available. In general, they were replaced with vertically extrapolated grids using the 1000 mb heights and 850 mb heights and temperatures and assuming hydrostatic balance. These grids may therefore be subject to considerable error, especially over land where the surface is close to 1000 mb and where considerable variability in the low-level thermal structure (such as during nocturnal inversions) often occur. Nonetheless, for studies of vertically integrated thermal budgets, the methodology used to reconstruct the 1000 mb temperatures may be sufficient.

The majority of temporally interpolated grids were constructed from 12h neighbors. The longest span of temporally interpolated grids is 44.5 days starting April 1, 1963 during which all grids were missing from the NCAR archives. There is only one period during any of the cases studied in this thesis in which the temporal interpolation is longer than 1.5 days. This period (7 days long) occurred at the end of a relatively long (42 days) event and therefore the interpolation scheme did not play a role in deciding whether or not an event occurred (see Sec. 3.4). However, it may have affected the determination of the last day of the event. Nonetheless, subjective inspection of composite analyses formed during the breakdown phase showed no appreciable differences when this case was or was not included in the composites.

3.3 Filtering techniques

Filtering is used extensively throughout this thesis. It serves two basic purposes: first, it provides a means by which anomalies from the climatological mean can be defined and second, it allows the separation of synoptic-scale and low-frequency components in the

data time series. This latter separation is the basis of a majority of our calculations, and thus considerable care is taken to demonstrate the robustness of the results to various filtering schemes. Here will will describe the major filtering techniques used. A discussion of alternative filters and results from their use is contained in Appendix B.

Through this thesis, the mean annual cycle of a variable is defined at each grid point as the climatological mean plus the first four annual harmonics in a Fourier decomposition of the 26 year time series. In most of these decompositions, a vast majority of the variance is contained in the first harmonic. Thus the results are basically insensitive the number of harmonics (beyond 1) retained in the annual cycle. Anomalies at each grid point and at each time are defined as departures from this annual cycle.

The principal filter used in this thesis to isolate the synoptic-scale disturbances is the bandpass temporal filter described by Blackmon (1976)[1]. This filter retains fluctuations whose periods are approximately 2.5 to 6 days. It is a 31-point filter designed to act on 12-hour data and has relatively sharp frequency bounds. The characteristics of atmospheric fluctuations retained by this filter have been described widely, most notably in Blackmon (1976) and Blackmon *et al.* (1977, 1984a,b). The differences between the Blackmon bandpass filter and various other synoptic-scale temporal filters are discussed by Wallace *et al.* (1988). They show that the typical characteristics of fluctuations retained by the various filters are not sensitive to the explicit filtering scheme used. They also show that waves retained by such filters generally have baroclinic structures with mean wavelengths between 3000 km and 5000 km.

Fig. 3.1 shows the winter-mean geographical distribution of the RMS variance of bandpass filtered 500 mb geopotential heights. This shows that the major bandpass

---

[1] In this paper, Blackmon actually named the filter a "medium-pass" filter but later (Blackmon *et al.*, 1977) changed its name to the now familiar "bandpass" filter.

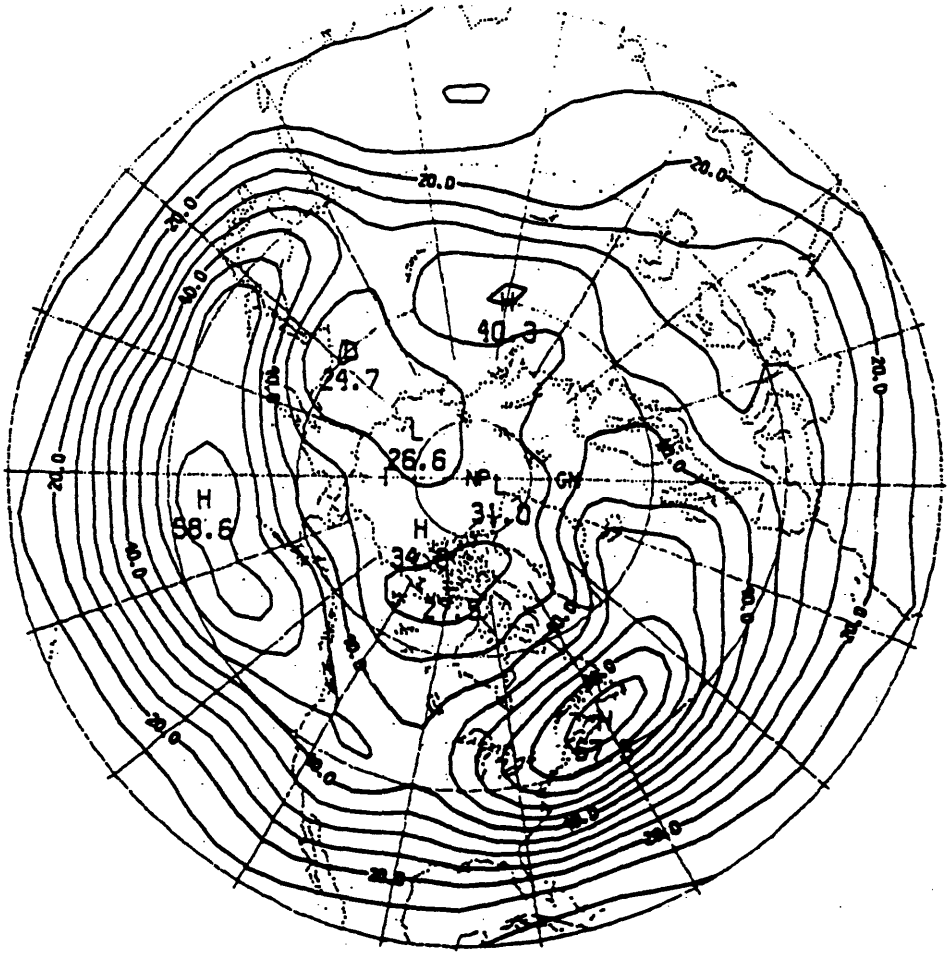

Fig 3.1. Winter-mean bandpass variance of the 500mb geopotential heights (m). Reproduced from Blackmon (1976).

variance maxima are found in two generally zonally elongated bands, one extending zonally across the central North Pacific and another located just east of the Canadian Maritimes. These maxima are often referred to as "storm tracks", and broadly coincide with maxima in the distributions of cyclone and anticyclone occurrences (Pettersen, 1956; Klein 1957; Whitteker and Horn, 1977). The bandpass variance method for identifying the variability in synoptic-scale activity has the advantage over the cyclone/anticyclone distribution method in that it is objective, quantitative, easily applied to upper-levels (since no closed contour feature recognition is required) and accounts for the intensities and sizes[1] of the systems. Further, its distribution is not effected by climatological-mean pressure gradients, as are the tracks of cyclone and anticyclones (Wallace *et al.*, 1988). Its primary disadvantages are that no direct inference to the storm paths can be made, it does not discriminate between cyclones and anticyclones (although the difference is often dynamically unimportant) and that it may not represent systems in the same way as subjective synoptic analyses. Also, the length scales that characterize the mean bandpass variance distributions are not necessarily the same scales that characterize the track lengths of individual storms. In general, the individual tracks of surface disturbances are about half to two-thirds the scales associated with climatological distributions of bandpass variance. Nielsen (1990) has shown that the lengths of tracks for small-scale high-frequency cyclones are considerably less.

Eddies retained by bandpass (or similar) filters tend to be meridionally elongated and eastward propagating with typical phase speeds of around 15 ms^{-1}. Blackmon *et al.* (1984b) show that bandpass eddies tend to be steered by the 700 mb flow. It has been argued that the meridionally elongated characteristic of bandpass eddies is an artifact of the

---

[1] Analyses of surface disturbance tracks contains information on the positions of the centers of the disturbances but no information on the sizes of the disturbances. However, bandpass variance analyses implicitly contain information on the sizes of the disturbances since many grid points about the circulation centers are effected upon passage of each disturbance.

filtering scheme and does not represent the true shapes of synoptic-scale systems. However dynamically, we expect synoptic-scale disturbances to be meridionally elongated if the radius of deformation is less than the length scale of the baroclinic zones, a commonly observed condition. Indeed several studies (e.g. Simmons and Hoskins, 1976,1978; Fredricksen, 1979, 1982) have shown that the horizontal structures of unstable synoptic-scale eddies in a spherical model are indeed meridionally elongated. Further, the results of selecting synoptic-scale eddies based upon a spatial filter indicate (Appendix B) that the eddies tend to be meridionally elongated.

Therefore, without any otherwise convincing argument, we consider diagnosed eddy shapes as representative. This has particular significance in the eddy mean-flow interaction problem. For example, if the Shutts (1983) mechanism is of primary importance, then for diffluent mean flows, only meridionally elongated eddies that propagate into the diffluent region will have an initial positive feedback onto the large-scale flow. Zonally elongated eddies would initially tend to become more isotropic and less prone to dissipation and thus, to have decreasing rates of down gradient PV fluxes. Depending upon the scale of the diffluent mean flows and the initial eddy configuration, little or no eddy feedback may occur. However, Farrell (1989) shows that zonally elongated eddies can linearly grow and expand their scale in a diffluent mean flow, and speculates that this may be the fundamental blocking mechanism. Thus, the shapes of incident eddies can be important in ascertaining the potential role of eddy-mean flow interactions.

We have also often made use of Blackmon's (1976) lowpass filter, most notably during the identification of the persistent anomaly cases. This filter retains periods longer than about 10 days, and provides a suitable gap between eddies captured by the 2.5-6 day bandpass filter. As noted earlier, although there is no spectral gap providing a clear separation, considerable differences are evident in the mean behavior of eddies retained in each frequency band (see Wallace, 1987 for a detailed review). Throughout, we will

generally focus on the lowpass evolution of the PAs and their relationships to the bandpass eddies. However, the lowpass filtering is usually not explicitly applied, but rather is a by-product of the compositing procedures as discussed in Sec. 3.5.

3.3 Case Selection and Compositing Techniques

We have taken Dole's (1986a) list of wintertime persistent anomaly cases and have extended it to include cases occurring in the 10 winters subsequent to his dataset. We have followed his methodology for identifying cases of persistent anomalies, except that our anomalies are defined as departures from the climatological-mean annual cycle, rather than from a quadratic fit to the wintertime mean data (Dole only had seasonal data). As in Dole (1982), a PA case is identified whenever the lowpass filtered 500 mb scaled height anomalies exceed either ±100m for at least 10 consecutive days at the key point. No attempt has been made to define new "key" points with the extended dataset.

We have focused on cases that occur at the Atlantic (50N 25W) and Pacific (46N 170W) key points[1]. These two points lie near the center of the major PA regions (Dole and Gordon, 1983), as well as near the most prominent regions of low-frequency variability (Blackmon, 1976). Extension of these analyses to the Northern Soviet Union cases as well as to other forms of low-frequency variability is left for future studies. Updated case dates for the Atlantic and Pacific events are listed in Appendix A. One each of an Atlantic positive and a Pacific negative case were subjectively combined from two cases that were separated by only one day. This subjective combination provides clearer results during onset and breakdown phases of the events, in accord with the main objectives of this thesis.

---

[1] Actually Dole defined (45N, 170W) as the key point in his 5x5 degree data set. We have chosen the next closest point in our 2x5 degree data set as the key point for this study.

On average, in a given region, slightly less than one case of each type (positive or negative) occurs per season, although there is considerable annual variability. Case durations are highly varied, ranging between 10 and 56 days, with a mean duration of about 17 days (see Appendix A).

Throughout, we will focus on composite results for both positive and negative cases in each key region. Compositing combined with statistical significance testing allows the systematic (coherent) and reproducible aspects of the persistent anomalies to be more readily ascertained. It is particularly useful during the relatively rapid onset and breakdown periods, where in individual cases it is often difficult to distinguish which part of the flow is associated with the large-scale evolution and which part is associated with transient eddies. This is because compositing acts as an implicit smoothing filter that tends to eliminate incoherent case-to-case variations (i.e. those related to random phases in either space or time). As our analysis will show, the bulk of the synoptic-scale variability is associated with fluctuations that are incoherent in this sense.

Our composite analyses are constructed as follows. First, the averaging is done over all cases relative to a specific day during the life cycles of the individual cases. Composites are usually performed relative to day 0 of either the onset or breakdown of the event. Day 0 of onset (breakdown) refers to the first day that the magnitude of the lowpass 500 mb anomaly exceeds (falls below) the +100 m (-100 m) criteria at the key point. This technique insures that all of the cases are in an identical phase in their evolutions. Although phase propagation alone can account for the local growth of the PAs at the key points, Dole (1989) indicates that significant amplification and decay does indeed occur during onset and breakdown in the individual cases. Composites relative to the mid-point in the life cycle of each case do not guarantee that all cases will be in similar phases of their life cycles, since there is a wide range in case durations. Thus compositing relative to the midpoint in the life

cycle can yield misleading results about the evolution of PA events (Dole, 1989; Nakamura and Wallace, 1990).

In addition, for some analyses, temporal averages of the composites are constructed over several days during similar phases of the life cycles. This additional averaging is useful for displaying second moment statistics that tend to have relatively large spatial and temporal variability. The periods for this additional averaging are identified as: *Prior* (days -10 to 0 of onset), *Onset* (days -5 to +5 of onset), *Case* (day 0 of onset to day 0 of breakdown), *Break* (days -5 to +5 of breakdown) and *After* (days 0 to +10 of breakdown). These periods are chosen so that all the days within each period will likely have relatively similar evolution characteristics.

The student t-test (Brooks and Carruthers, 1953) is used to estimate the statistical significance of the composite anomalies. Unless otherwise stated, these tests are based on the null hypothesis that the composite-mean anomalies are not different from zero. The sampled variance is used as an approximation to the true variance in these tests and the number of degrees of freedom is assumed equal to the number of cases minus one. For some fields, significance tests based on the differences between positive and negative PA composites are also performed. This alternative test was used by Dole (1982) and is based on the observation that there are strong symmetries between results obtained for the positive and negative cases of PAs (i.e. similar patterns but with opposite sign). Note that the first test is considerably more stringent.

3.5 Composite Analyses of Persistent Anomalies.

In this section we present the evolution of the composite-mean geopotential height fields during the life cycles of persistent anomalies. For two reasons we focus on the 300

mb geopotential heights. First, the life cycles at 1000 mb and at 500 mb have previously been documented by Dole (1986b, 1989) and Dole and Black (1990) for a smaller set of cases. The basic results of these analyses were discussed in Sec. 2.5. Composite 500 mb and 1000 mb height analyses (not shown) using the updated list of cases are essentially identical to those described by Dole. Therefore the 300 mb analyses extend the earlier results. Second, during many of the eddy diagnostic calculations, we concentrate on results obtained for 300 mb level data. This level is chosen as it is near the level of maximum geopotential height variance of both PAs and synoptic-scale eddies.

Fig. 3.2 shows the composite-mean 300 mb geopotential heights at 3 day intervals between days -9 and +6 during the onset of Atlantic positive persistent anomaly events. Corresponding composite anomalies are displayed in Fig 3.3. Prior to about day -6, there are no major statistically significant anomalies evident in the composites (not shown). However, a weak positive anomaly corresponding to an extension of the subtropical ridge is located southeast of the key region just west of Europe and North Africa. By day -6, composite anomaly values in this region are significantly greater than zero at the 95% confidence level. This anomaly then amplifies and propagates northwestward, eventually becoming the primary anomaly at the key region. By day +6, the primary anomaly is fully developed, with its structure at that time resembling the structure of the composite time-averaged anomaly pattern. Although there are no closed contours in the full composites at day +6, the 930 dam maxima just south of the key point implies an easterly geostrophic flow to its south. Analyses from other levels (not shown) indicate that easterly winds exist throughout the troposphere during the mature Atlantic positive PA cases consistent with their association with blocking. To the south, a weak but highly significant negative height anomaly becomes established over the subtropical Atlantic by day 0. This anomaly center, combined with the primary positive anomaly to the north, leads to an anomalous upper level easterly flow and stronger than normal diffluence across the Atlantic.

Also apparent in the analyses is the development of a significant downstream negative anomaly over Eastern Europe and the Middle East. This development is lagged by about 3 days from the development of the primary anomaly. Other small and weak downstream anomaly centers develop subsequently over the Northern Soviet Union and over China, although the significance of these anomalies is rather low.

The Atlantic positive developments at 300 mb are qualitatively very similar to the 500 mb developments described by Dole (1989). The statistical significance of the 300 mb anomalies (not shown) tends to be equal to or even greater than the significance reported by Dole. These relationships also hold true for the other PAs studied. Therefore, for the other types, we will present the 300 mb results (as they will often be referenced later in this thesis) with only limited discussion. Interested readers are referred to section 2.5 and to references therein for a more comprehensive discussion of the developments.

Figs. 3.4 through 3.9 show respectively the 300 mb composite geopotential heights and the corresponding anomalies for the Atlantic negative, Pacific positive and Pacific negative cases. The developments of the Atlantic negative cases are broadly similar to the Atlantic positive developments, but with opposite sign. The mature Pacific positive flow patterns exhibit less of a blocking structure in the full field than the corresponding mature Atlantic patterns. This is at least partly because the Atlantic key point lies near a maximum in the climatological stationary waves, while the Pacific key point lies on a node in the stationary wave pattern. Thus, even though the Atlantic and Pacific composite anomalies are nearly equal in magnitude, the Atlantic cases tend to have more meridional structure and thus appear synoptically to be more like a conventional block. Nonetheless, the Pacific cases still have significant anomalous easterly flow throughout the troposphere and stronger than normal diffluence across the western Pacific, which is manifested by a split upper-level westerly flow. At the surface, the Pacific positive cases are characterized by a strong "blocking" anticyclone which replaces the normal Aleutian low (Dole, 1986a).

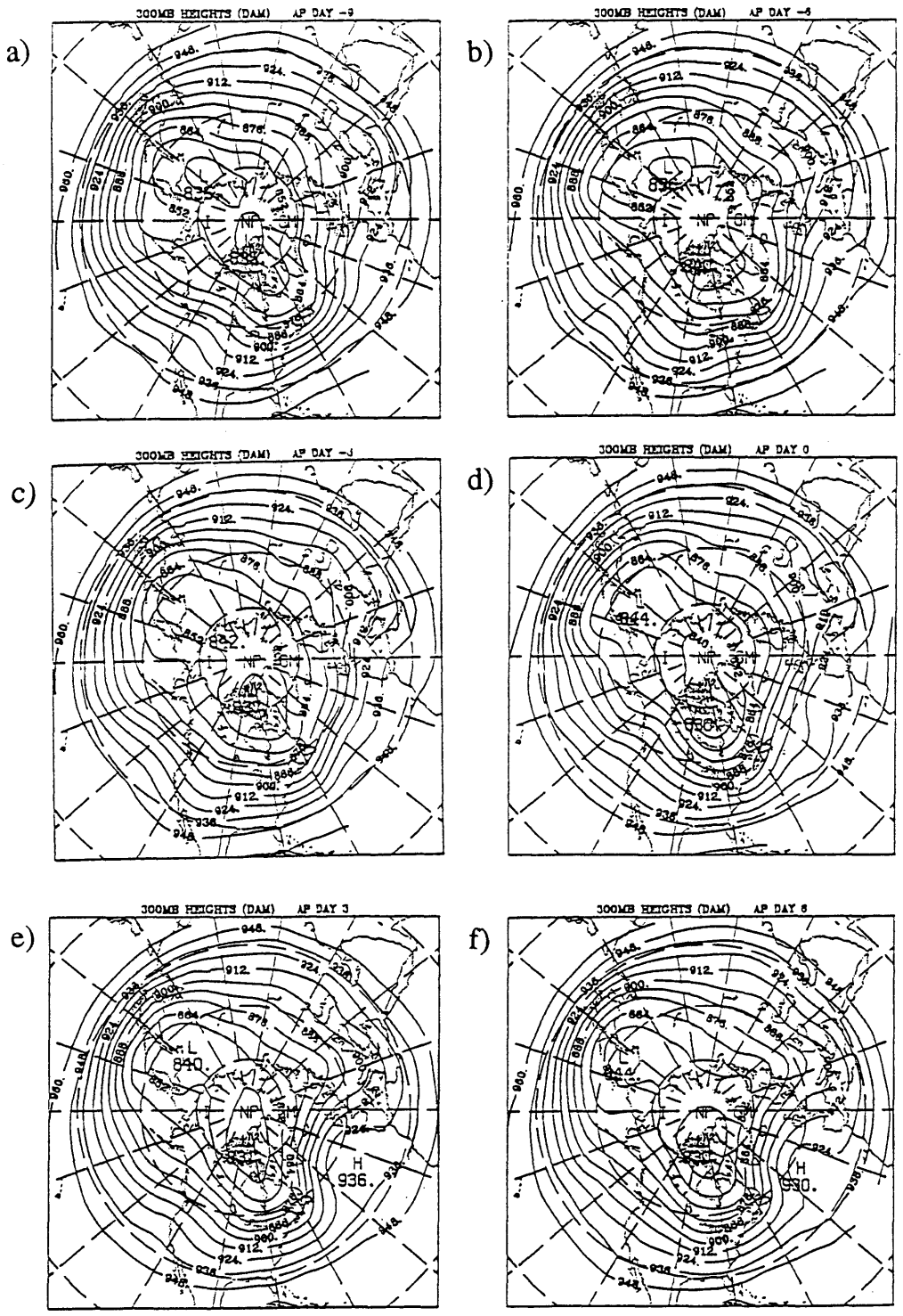

Fig. 3.2. Composite-mean 300 mb geopotential heights (dam) for days a) -9, b) -6, c) -3, d) 0, e) +3 and f) +6 during the onset of the Atlantic positive PA cases.

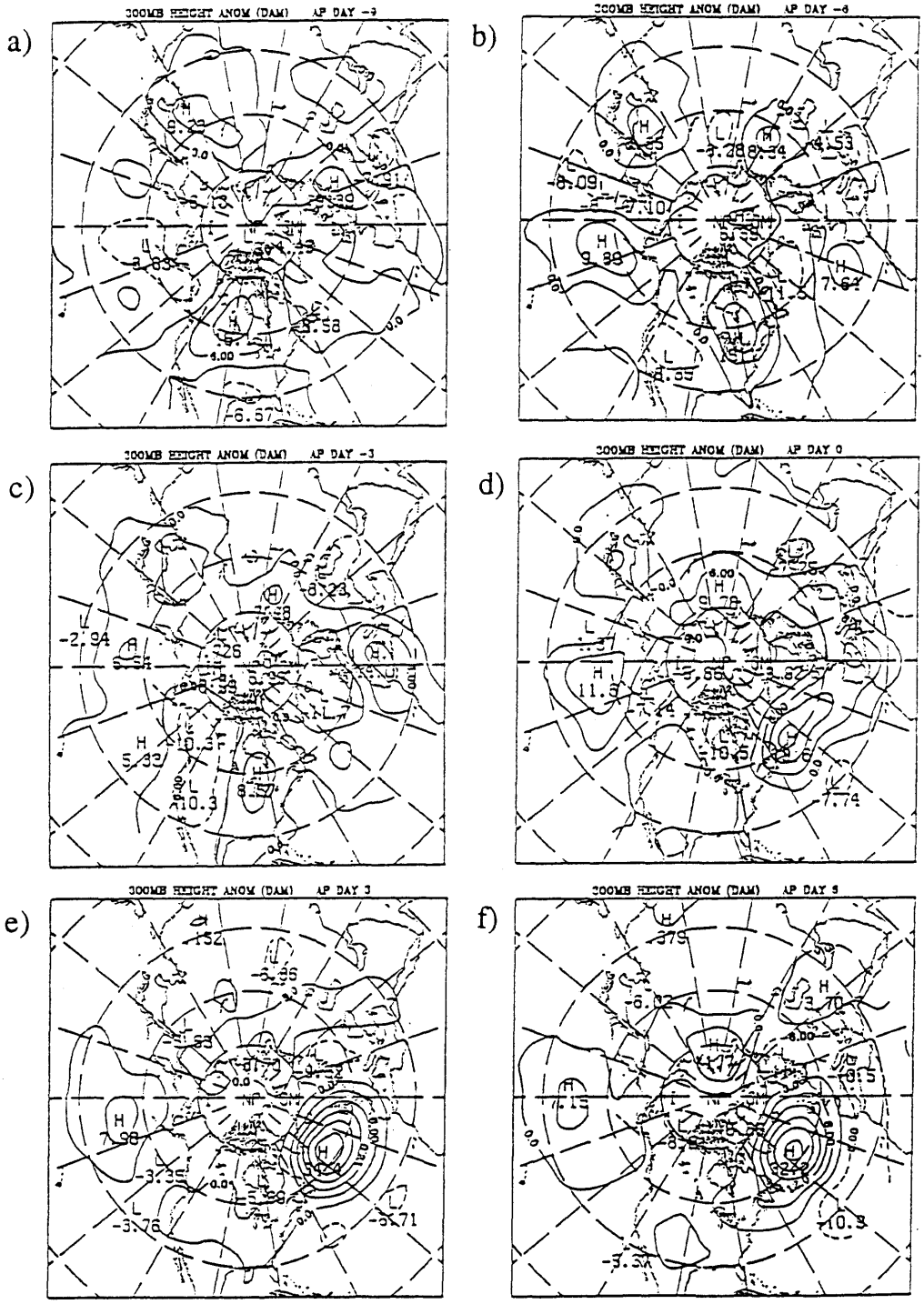

Fig. 3.3. Composite-mean 300 mb geopotential height anomalies (dam) for days a) -9, b) -6, c) -3, d) 0, e) +3 and f) +6 during the onset of Atlantic positive PA cases.

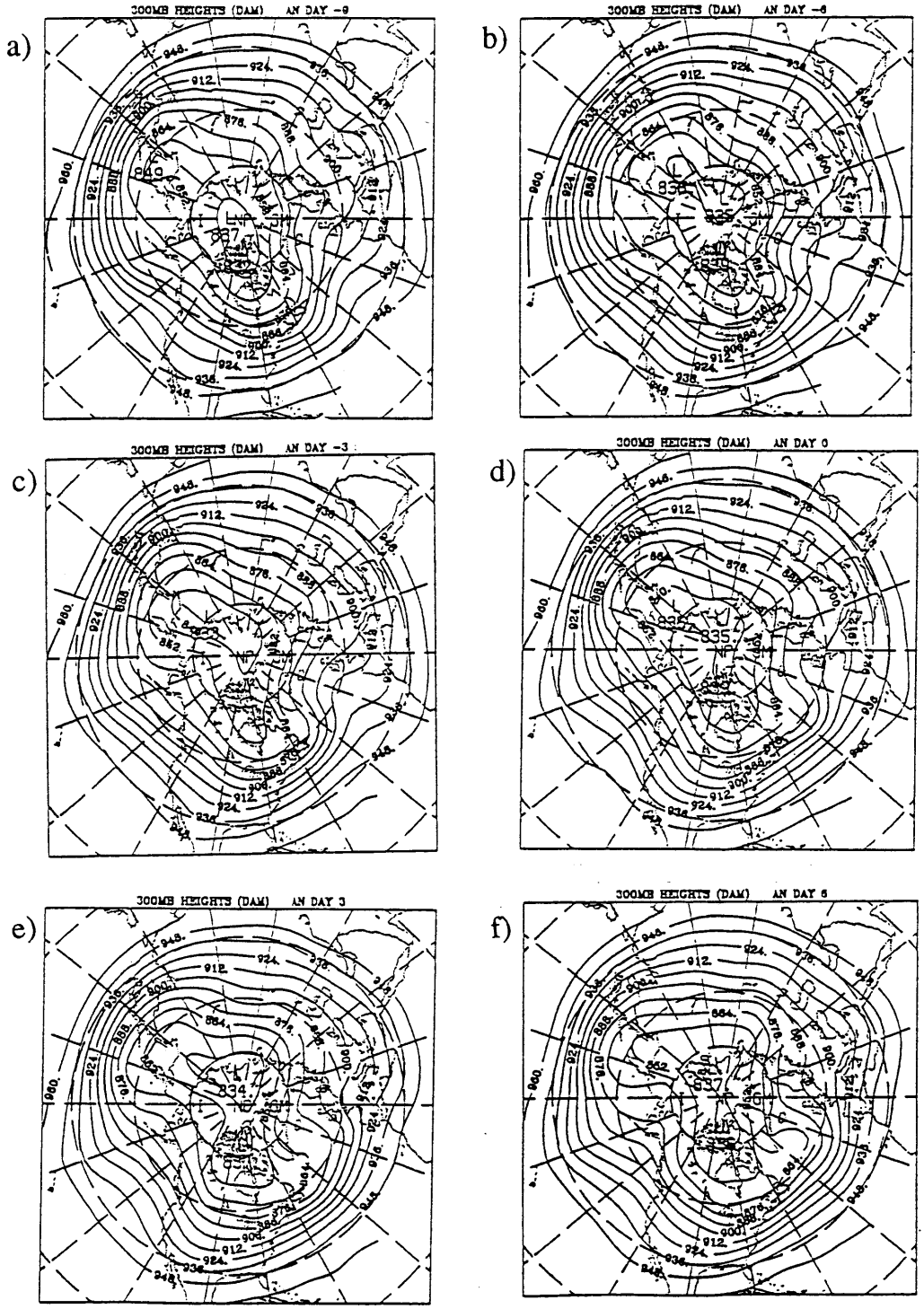

Fig. 3.4. Composite-mean 300 mb geopotential heights (dam) for days a) -9, b) -6, c) -3, d) 0, e) +3 and f) +6 during the onset of the Atlantic negative PA cases.

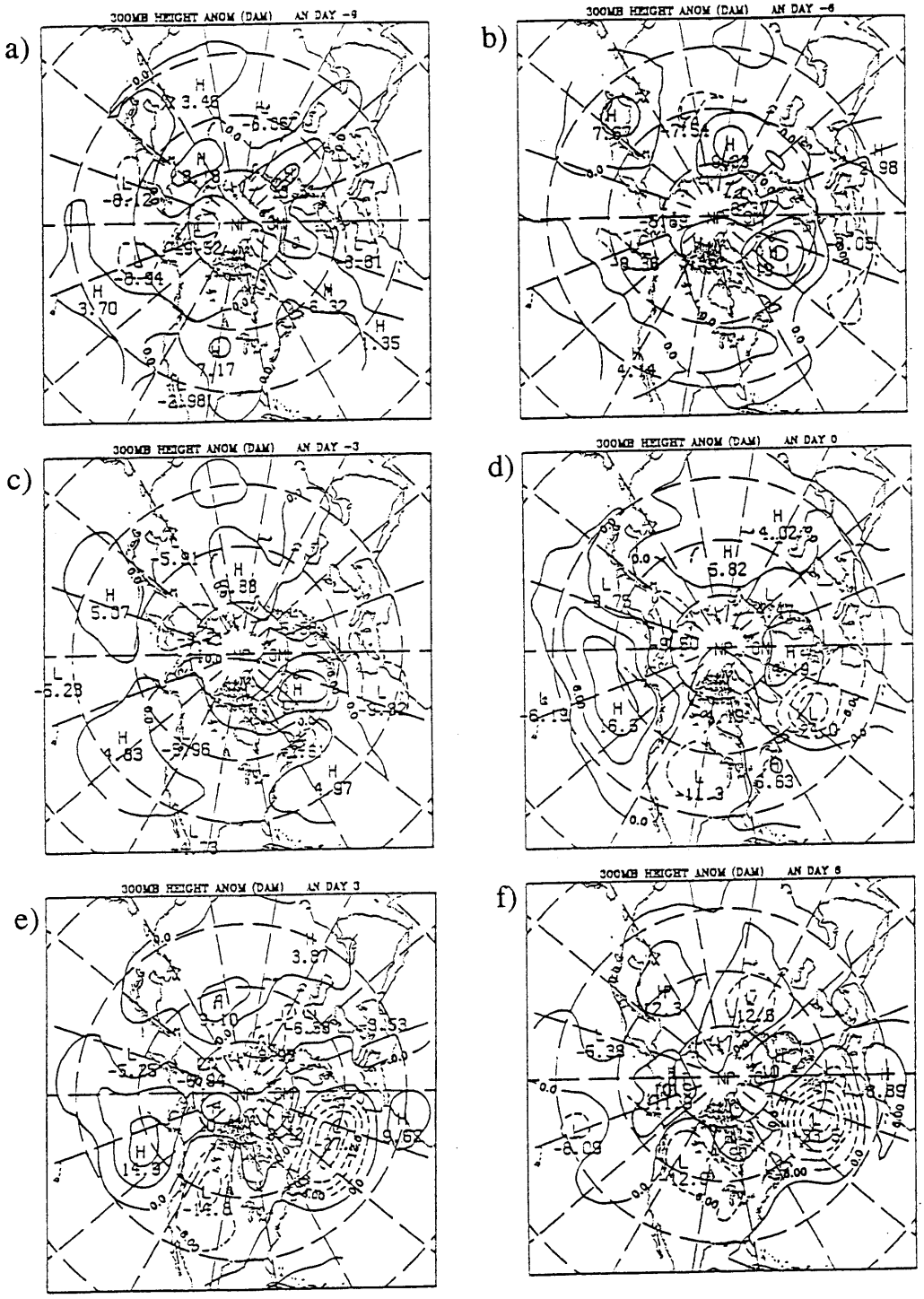

Fig. 3.5. Composite-mean 300 mb geopotential height anomalies (dam) for days a) -9, b) -6, c) -3, d) 0, e) +3 and f) +6 during the onset of Atlantic negative PA cases.

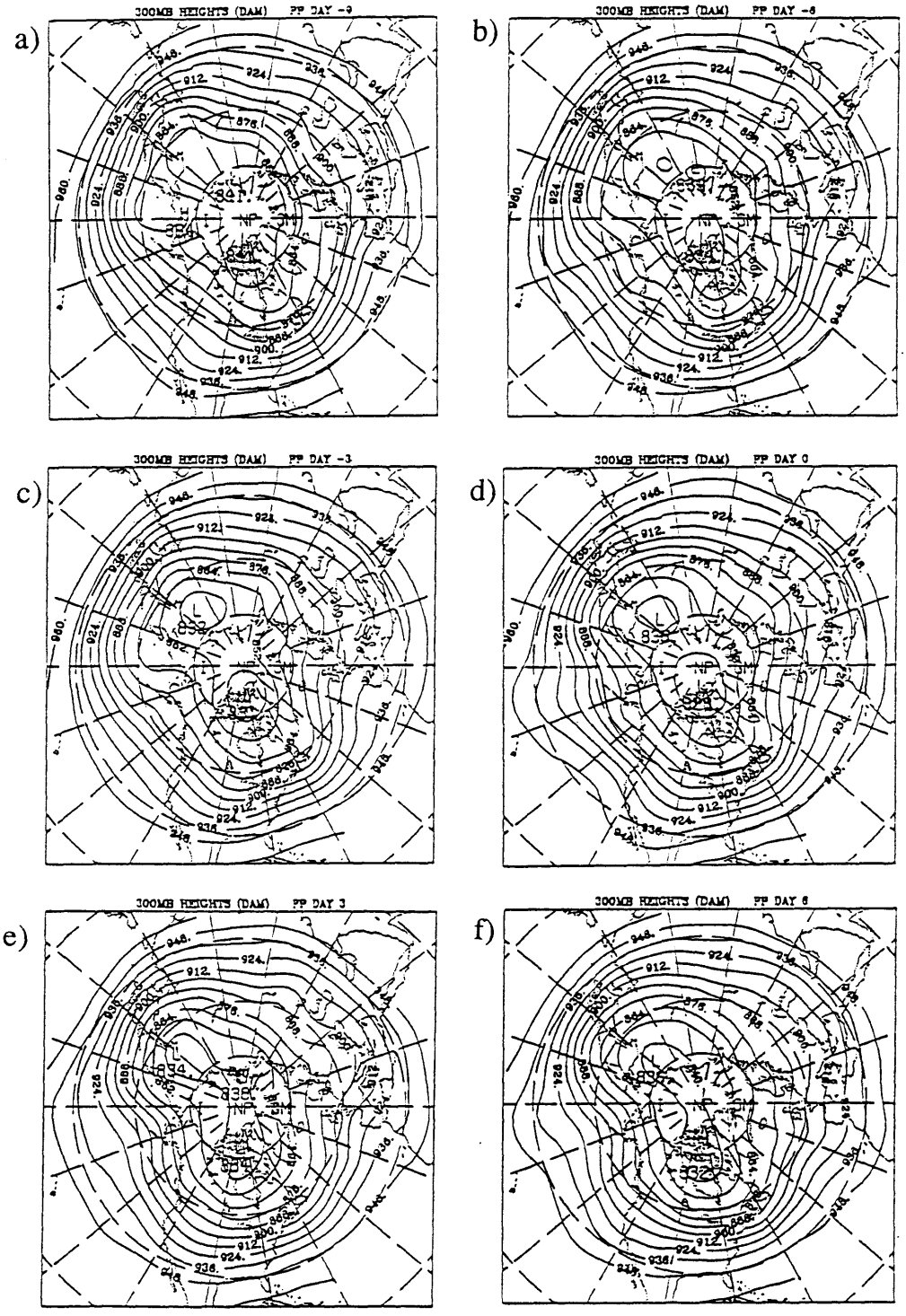

Fig. 3.6. Composite-mean 300 mb geopotential heights (dam) for days a) -9, b) -6, c) -3, d) 0, e) +3 and f) +6 during the onset of the Pacific positive PA cases.

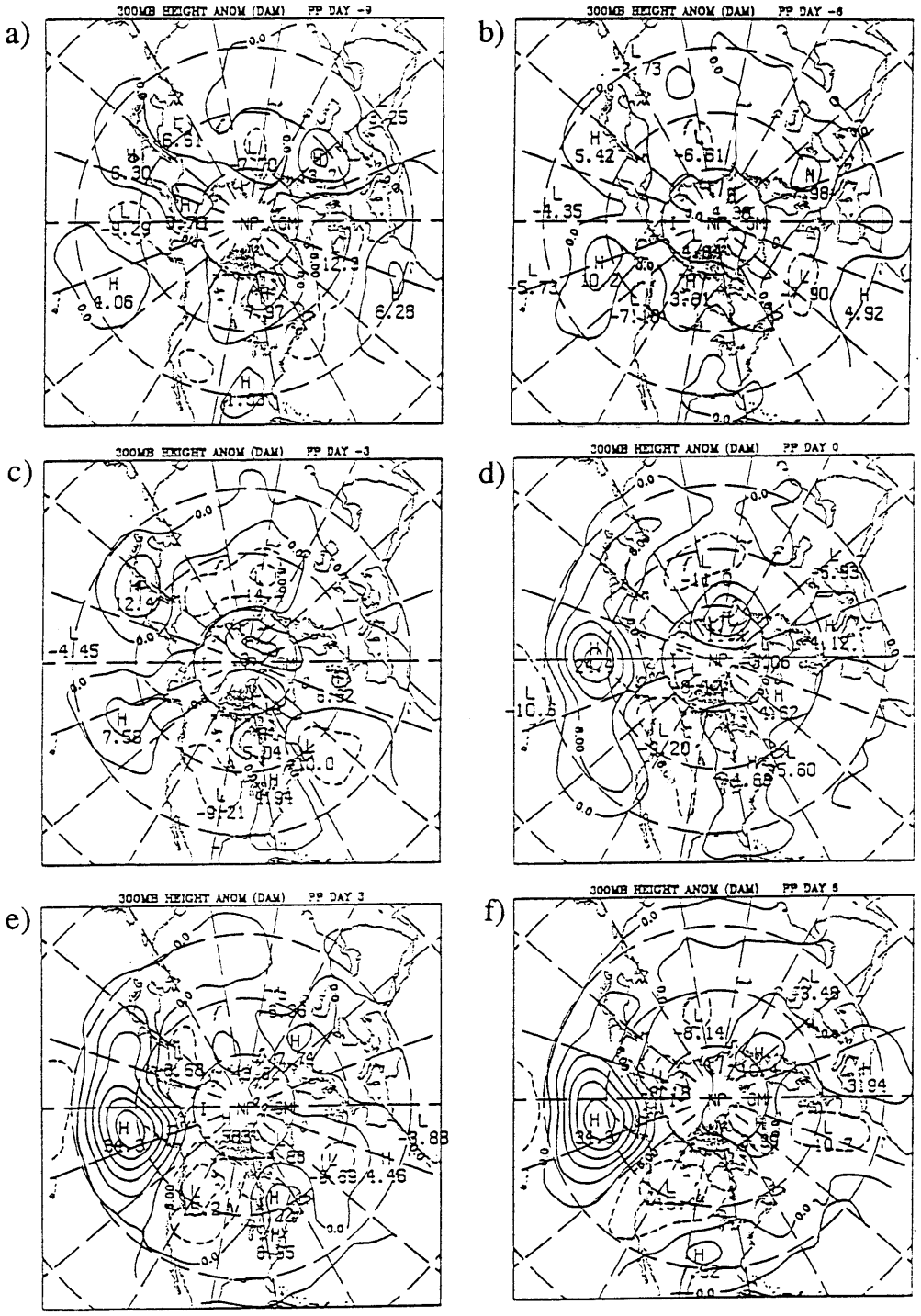

Fig. 3.7. Composite-mean 300 mb geopotential height anomalies (dam) for days a) -9, b) -6, c) -3, d) 0, e) +3 and f) +6 during the onset of Pacific positive PA cases.

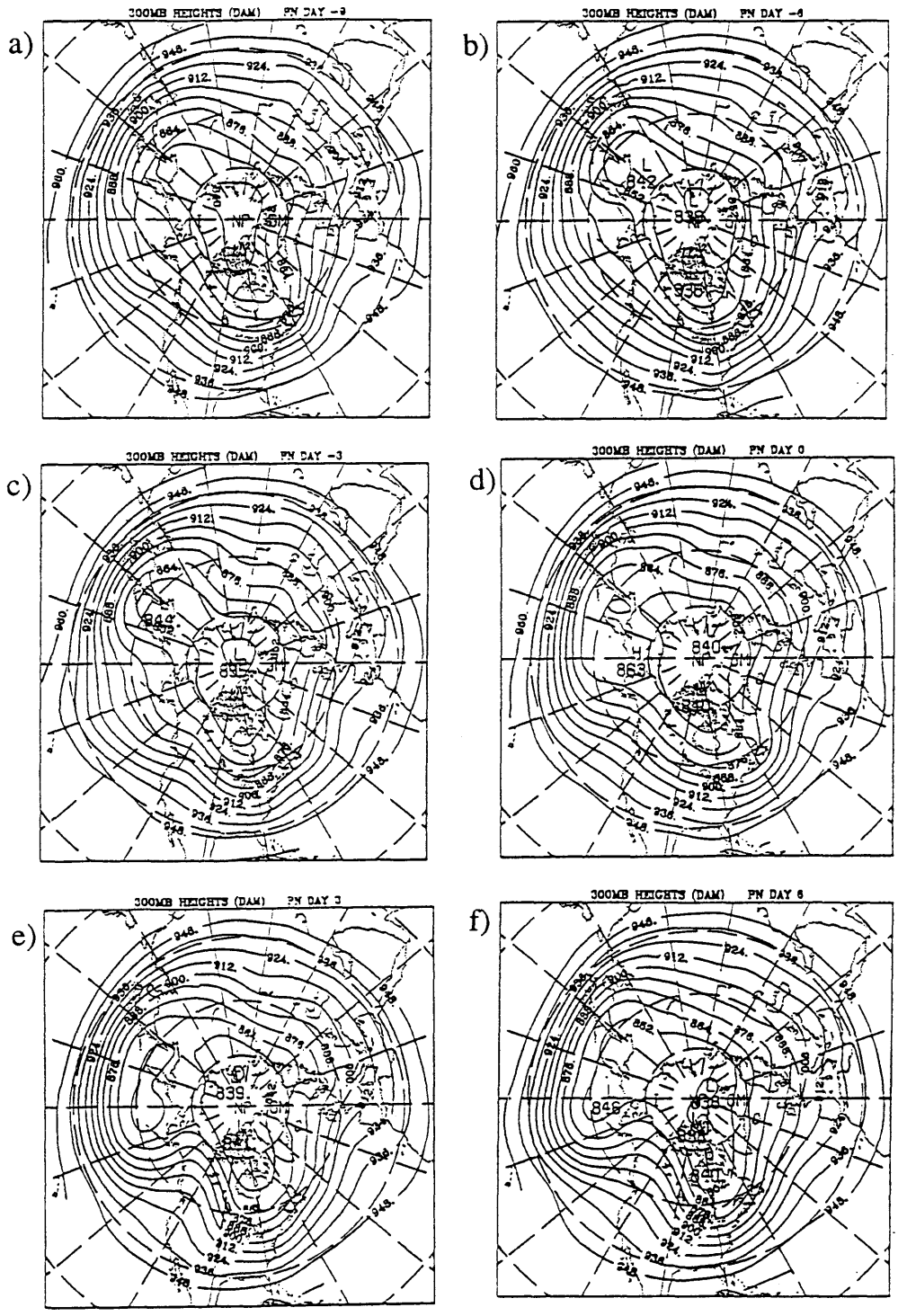

Fig. 3.8. Composite-mean 300 mb geopotential heights (dam) for days a) -9, b) -6, c) -3, d) 0, e) +3 and f) +6 during the onset of the Pacific negative PA cases.

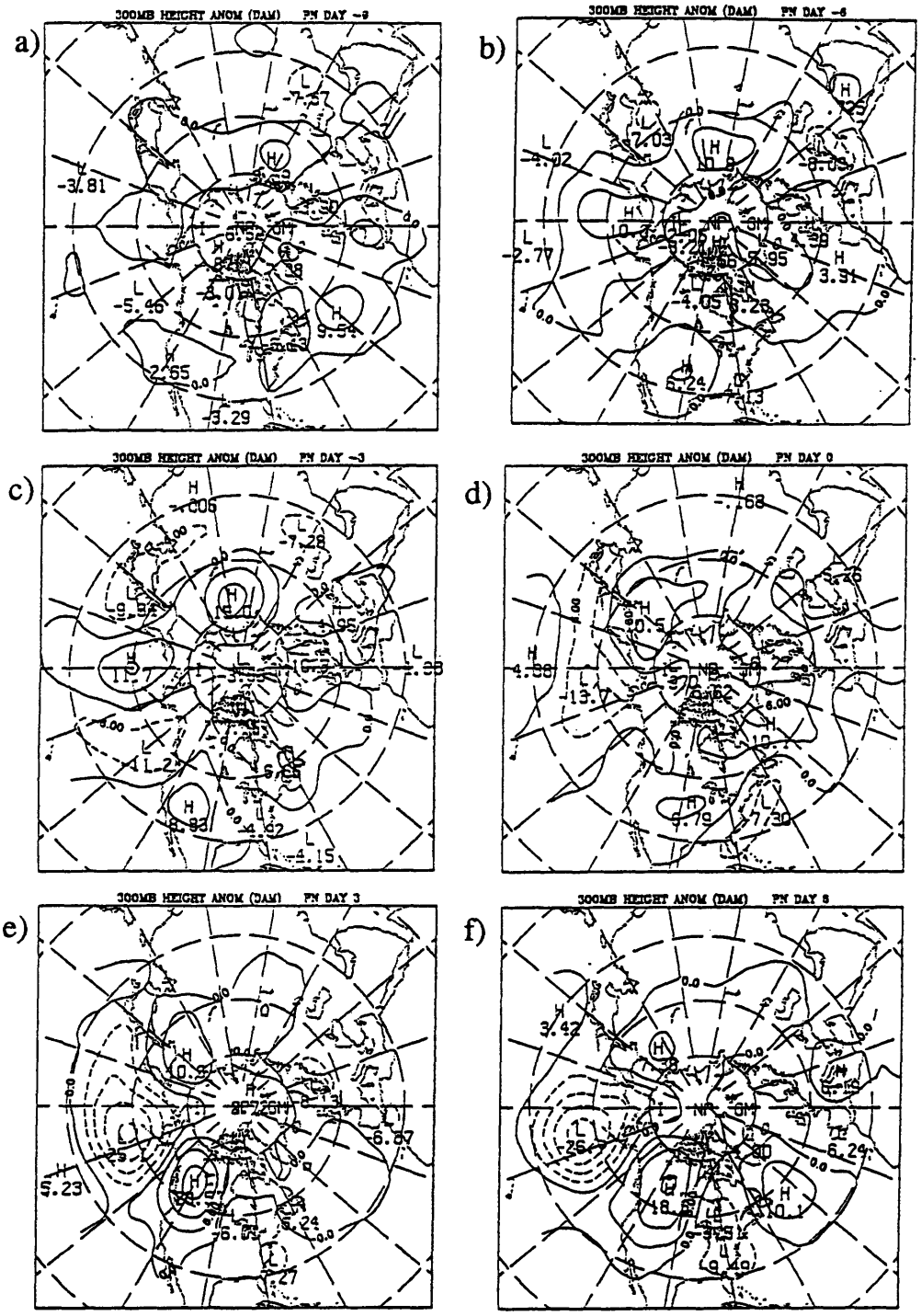

Fig. 3.9. Composite-mean 300 mb geopotential height anomalies (dam) for days a) -9, b) -6, c) -3, d) 0, e) +3 and f) +6 during the onset of Pacific negative PA cases.

Both the positive and negative Pacific cases have a considerably stronger downstream wavetrain pattern than is evident in the Atlantic composites. In particular, the Pacific negative cases have a strong ridge along the western North America, which in itself might be considered a block. By 6 days after the development of the primary anomaly center, a strong full latitude trough over eastern North America is also associated with these negative cases.

The breakdown sequences of the 300 mb anomaly patterns are presented in Figs. 3.10 through 3.13 for each of the PA types. Again, the breakdowns of the 300 mb composite anomalies strongly resemble the breakdowns at 500 mb discussed by Dole (1986b, 1989). Breakdowns are relatively rapid, usually occurring within a week. There appears to be no clear systematic precursor to the breakdown, with the primary anomalies just prior to breakdown resembling the anomalies observed just after onset. During breakdown, the primary anomaly centers often propagate toward the northwest as they rapidly weaken.

Composite anomaly evolutions formed using the lowpass filtered geopotential heights strongly resemble the unfiltered evolutions. Fig 3.14 shows the differences between the unfiltered and lowpass filtered 300 mb composite height anomalies at day +3 during onset of each of the PA types. In general, the variance in these difference maps is only a small percentage of the total variance in the unfiltered plots, and the statistical significance (not shown) of the difference fields is quite low. This implies that a major part of the temporal variability in periods less than 10 days is not phase locked (i.e. is not coherent) in time relative to the development of the PA. Indeed, the coherent part of the bandpass eddies contribute only about 20%-25% of the total bandpass variance during the development of PAs. Therefore most of the upper-level synoptic-scale disturbances during the development of the PA patterns are randomly distributed in time and space relative to the phase of the PA development. However, Dole and Black (1990) have identified a

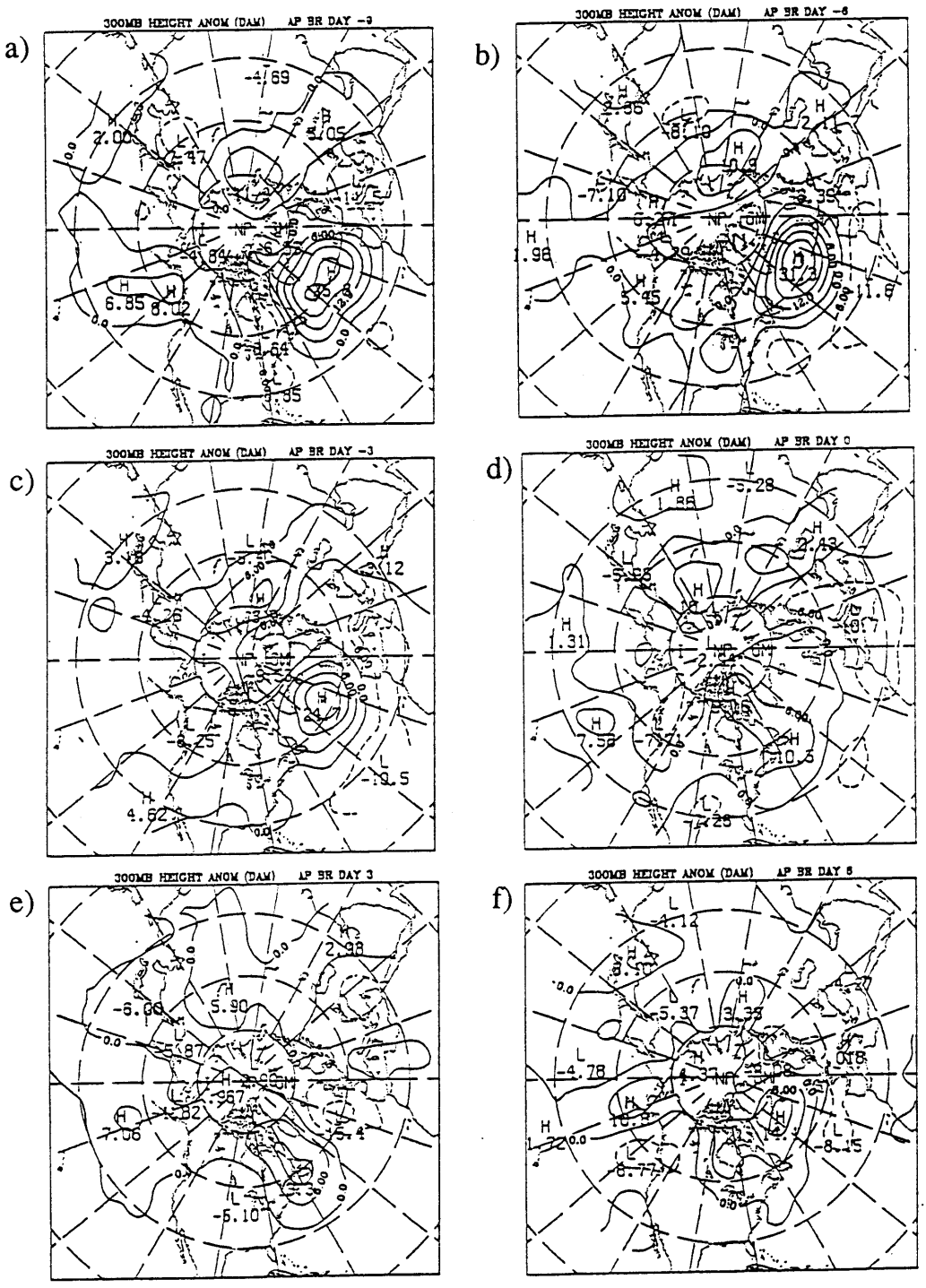

Fig. 3.10. Composite-mean 300mb geopotential height anomalies (dam) for days a) -9, b) -6, c) -3, d) 0, e) +3 and f) +6 during the breakdown of Atlantic positive PA cases.

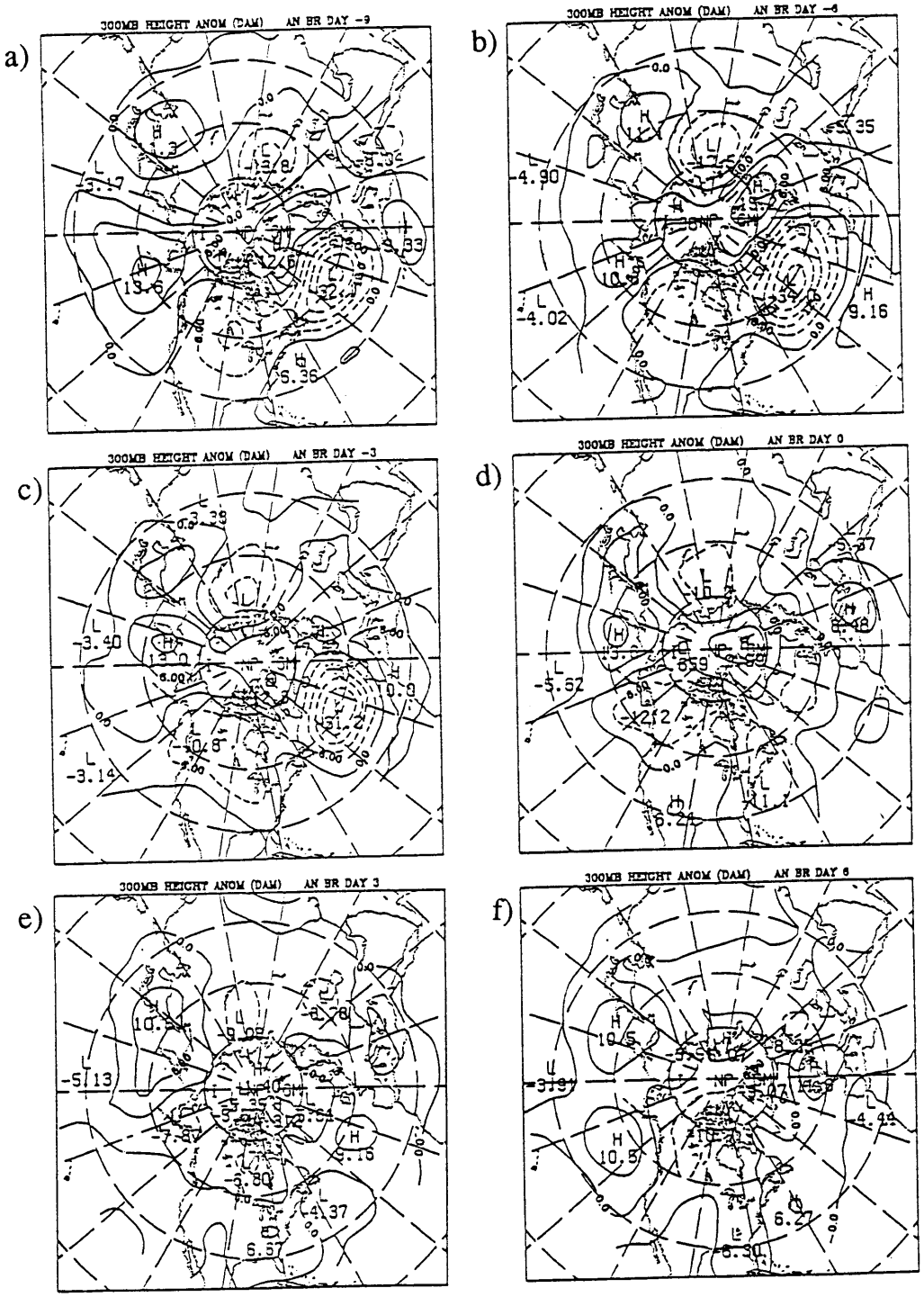

Fig. 3.11. Composite-mean 300mb geopotential height anomalies (dam) for days a) -9, b) -6, c) -3, d) 0, e) +3 and f) +6 during the breakdown of Atlantic negative PA cases.

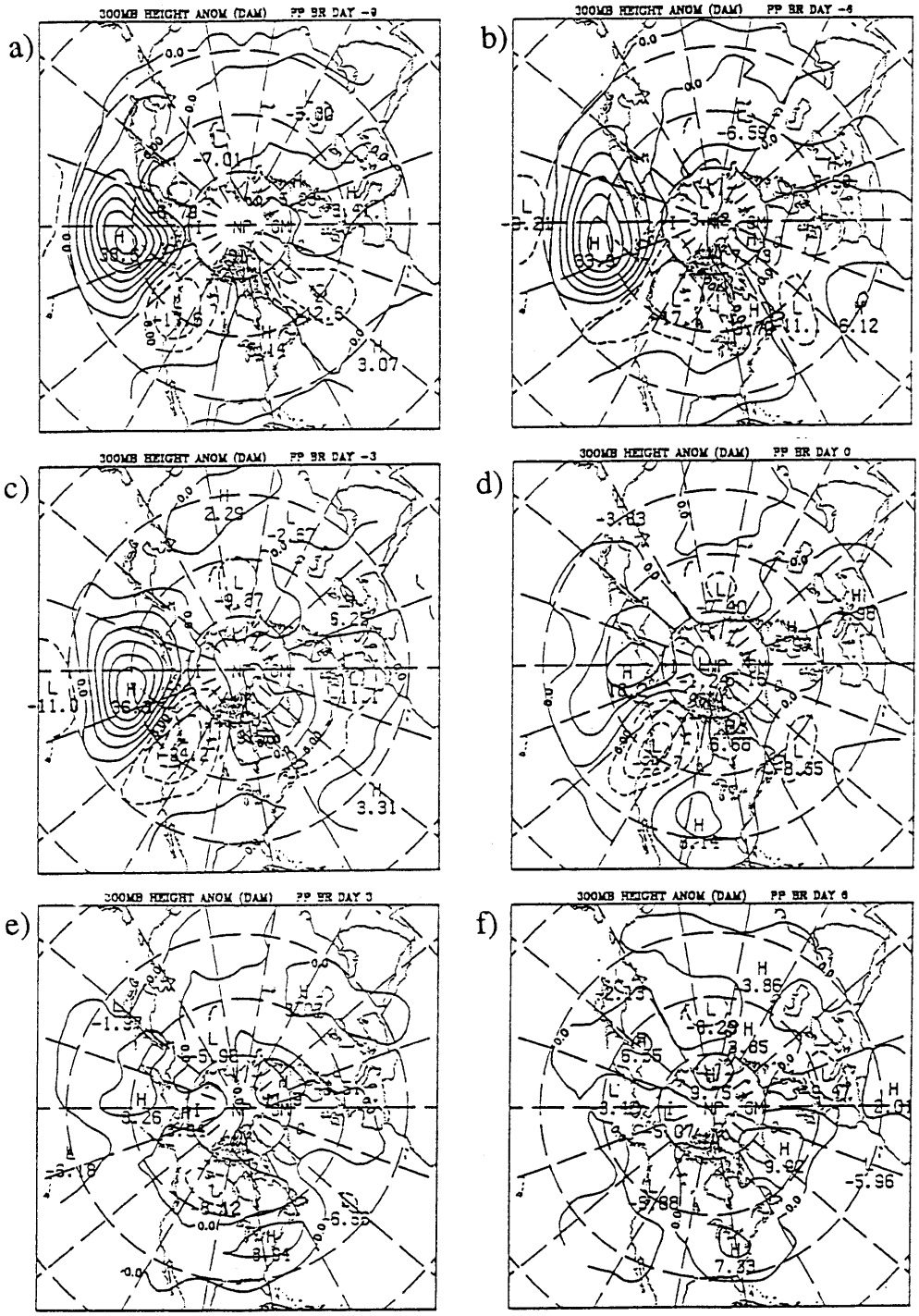

Fig. 3.12. Composite-mean 300mb geopotential height anomalies (dam) for days a) -9, b) -6, c) -3, d) 0, e) +3 and f) +6 during the breakdown of Pacific positive PA cases.

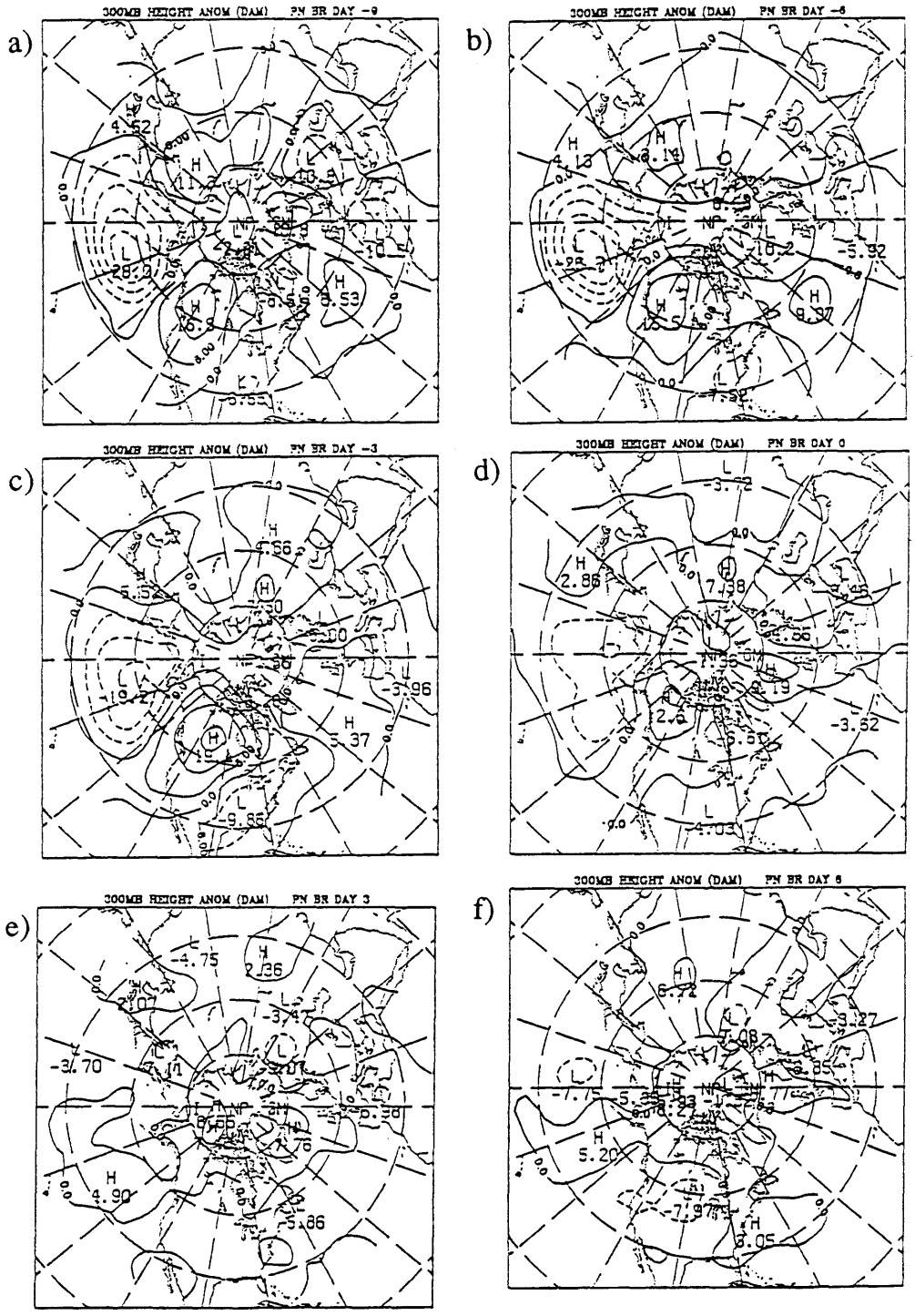

Fig. 3.13. Composite-mean 300mb geopotential height anomalies (dam) for days a) -9, b) -6, c) -3, d) 0, e) +3 and f) +6 during the breakdown of Pacific negative PA cases.

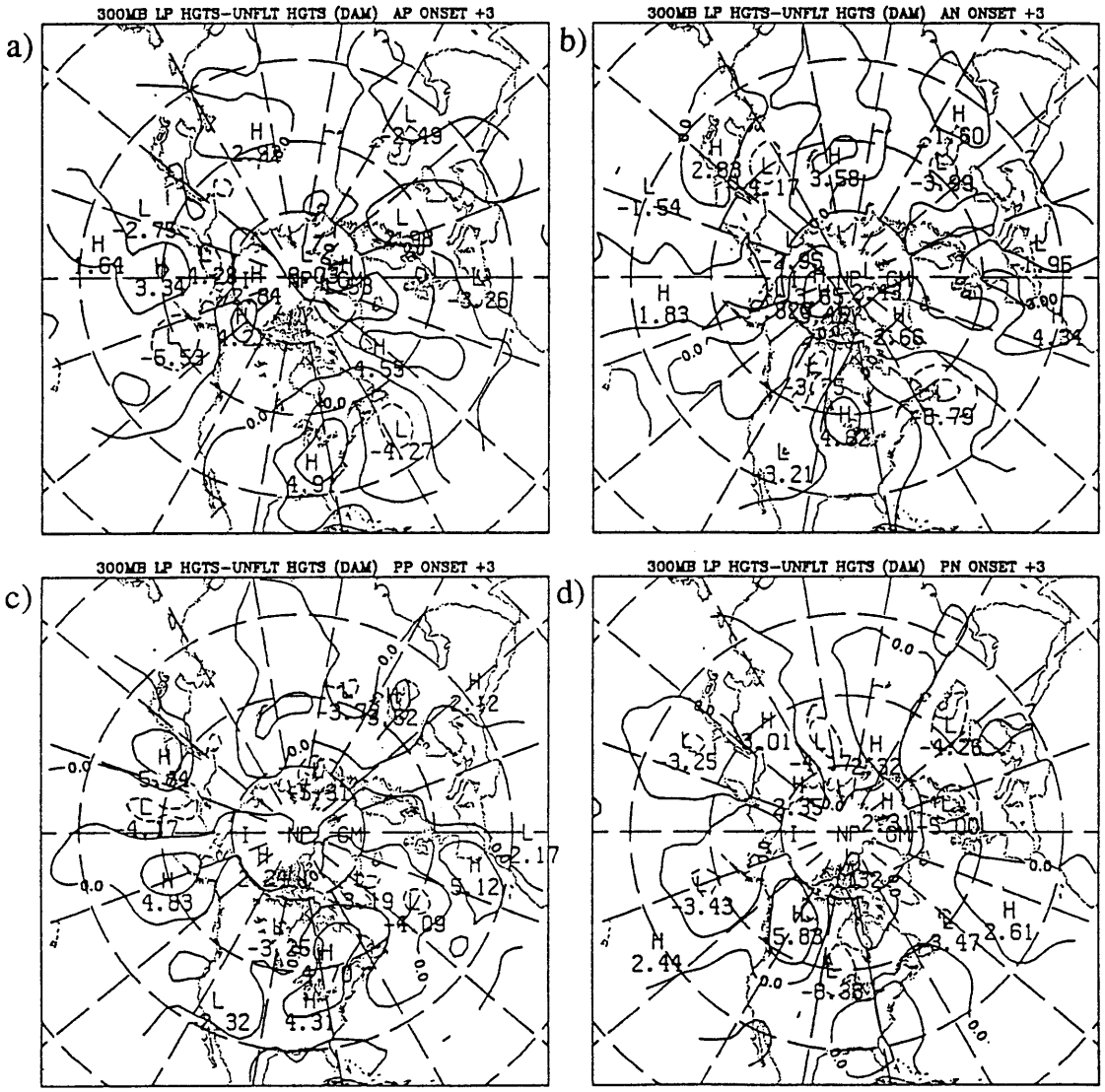

Fig. 3.14 Composite difference between the 300 mb lowpass filtered geopotential heights and the unfiltered heights (dam) for day +3 during the onset of the a) Atl. pos. b) Atl. neg. c) Pac. pos. and d) Pac. neg. PA cases.

weak coherent synoptic-scale eddy during the development of Pacific negative PAs that appears to be significant to the subsequent large-scale developments.

Of course, significant changes in the large-scale flow occur during the life cycles of the geopotential height anomalies. In the positive cases, the flow anomalies consist of weaker than normal zonal flow at midlatitudes and stronger than normal zonal flow at high latitudes in the vicinity of and to the north of the key points. An opposite pattern occurs during the negative cases. Associated with the development of the positive anomalies is an anomalous increase in the large-scale diffluence over the western oceans. The anomalous diffluence develops near the ends of the climatological mean storm tracks. As discussed in Sec. 2.6, eddies impinging on a diffluent large-scale flow may be systematically deformed with the changing eddy fluxes leading to a net forcing of the mean flow. Thus associated with the PA developments, we might also anticipate changes in eddy feedbacks onto the large-scale flow. Since in the climatological sense, there is mean diffluence downstream of the climatological mean storm tracks (Shutts, 1983), we may expect that there would be an increase (decrease) in the climatological eddy feedbacks onto the large-scale flow associated with positive (negative) persistent anomalies.

However, because PAs do not form in phase with the stationary waves, and since the principal cyclogenesis regions may also be modified by the existence of the PAs, the problem becomes considerably more complicated. Further, the eddy feedback process is not likely linearly related to the amplitude of the large-scale flow anomaly. For instance, assuming Shutts (1983) mechanism is indeed operational in these cases, it is possible that the climatological-mean diffluence already extracts all available eddy energy; thus an increase in the diffluence may not yield a stronger eddy feedback. Clearly, the problem requires more observational investigation. These and other issues will be addressed in the next two chapters.

Chapter 4

Variations in Eddy Activity

4.1 Introduction

In this chapter, results are presented of diagnostic analyses of the systematic changes in eddy activity that occur during the life cycles of persistent anomalies. The phrase "eddy activity" will be used here to refer to some local measure related to the amplitude of the synoptic-scale eddies. The total and anomalous aspects of eddy activity are ascertained using a variety of techniques. Although this chapter is primarily a descriptive and phenomenological discussion of the diagnosed eddy activity variations, we will also briefly discuss some of the mechanisms that may account for the observed changes.

4.2 Procedure.

The winter-mean distribution of bandpass 500 mb geopotential height variance was presented in Fig. 3.1. This analysis was produced by computing the bandpass fields for all available winter seasons and then computing the mean[1] and RMS variability from the filtered dataset at each point. In order to determine the local eddy amplitude for phenomena whose characteristic time-scales are considerably less than a season, we follow a similar methodology but limit the period over which we compute the variability. Specifically, we compute a variability statistic (**VSTAT**) as

$$\mathbf{VSTAT} = \{ \frac{1}{N} \sum^{N} (P_i' - \overline{P}')^2 \}^{1/2}$$

[1] Over a sufficiently long time, the mean of a bandpass quantity approaches zero.

where P_i' are the instantaneous values of the eddy field of interest and $\bar{P}$ is the mean over the N samples. Since our primary dataset is available twice per day, an M day VSTAT calculation implies that the number of samples (N) is 2M + 1. The specific choice of M should be such that it is longer than the characteristic time scale associated with P' field but shorter than the period associated with the large-scale, low-frequency phenomena. The first requirement ensures that the VSTAT function contains contributions from several eddies rather than the instantaneous values of a single eddy. The second requirement ensures the applicability of the function for the purposes of analyzing the evolution of the large-scale phenomena. For persistent anomalies, this latter time scale is about a month (Dole, 1989, Fig 1.). If a bandpass filtered quantity (whose mean period is about 3 or 4 days) is used for P', then a suitable choice for M is 10 days. The VSTAT function is then a slowly varying function describing the slow evolution of the local bandpass eddy activity during persistent anomalies. The periods retained by a 10-day VSTAT function will be similar to those retained by Blackmon's (1976) lowpass filter, thereby facilitating the comparisons with the composite evolution maps (which are essentially lowpass filtered) as presented in Chapter 3.

The VSTAT technique is essentially similar to the envelope function technique used very recently by Nakamura and Wallace (1990) to study variations in eddy activity associated with the principal teleconnection patterns. The periods retained by their function is considerably shorter (about 6 days) and thus the instantaneous values of their function are more sensitive to contributions from individual eddies. However, once ensemble-averaged over many similar cases, the results should be quite similar to those obtained using the VSTAT technique. The VSTAT and envelope function techniques were conceived and developed independently.

A typical time series of bandpass 300 mb geopotential heights along with its associated VSTAT function (the "300 mb VSTATs") for a point just south of the Atlantic key region is shown in Fig. 4.1. The corresponding full and lowpass filtered 300 mb heights are also shown for comparison. A positive PA event occurs during the mid-January to mid-Febuary period in this figure. During this event, the geopotential heights are anomalously high and, correspondingly, there is relatively weak high frequency variability compared to the neighboring periods. This reduced high frequency variability implies relatively weak bandpass filtered height fluctuations, and thus the period is characterized by relatively low values of VSTAT. In contrast, the early winter and early spring periods in this year are characterized by considerably larger high frequency variability, and thus relatively high values of VSTAT. The 1000 mb bandpass geopotential height VSTATS (the "1000 mb VSTATs") during the same period (not shown) show a qualitatively similar pattern, with relatively low VSTAT values during the positive PA event and relatively high VSTAT values during the neighboring periods. Similar VSTAT results using a highpass synoptic-scale filter (periods 0-6 days) are essentially identical, as the characteristics of the very high-frequency fluctuations (0-2.5 days) are quite similar to the bandpass characteristics. Synoptically, the high VSTAT regimes are characterized by frequent passages of intense synoptic-scale eddies, with the weather dominated by the circulations associated with those eddies. Conversely, during the low VSTAT regimes, synoptic-scale eddy activity is relatively weak, and the weather tends to be dominated by the thermal and flow anomalies associated with the larger-scale circulation.

Fig. 4.2 shows the geographical distribution of the mean mid-winter 300 mb VSTATs, along with the root mean-square (RMS) variability and the relative variability (RMS/mean) of the VSTATS. The winter-mean VSTAT amplitude shown here (Fig 4.2a) is computed from the sum of the first four fourier harmonics in the seasonal cycle evaluated on 15 January. Its distribution is essentially identical to that of the winter-mean 300 mb

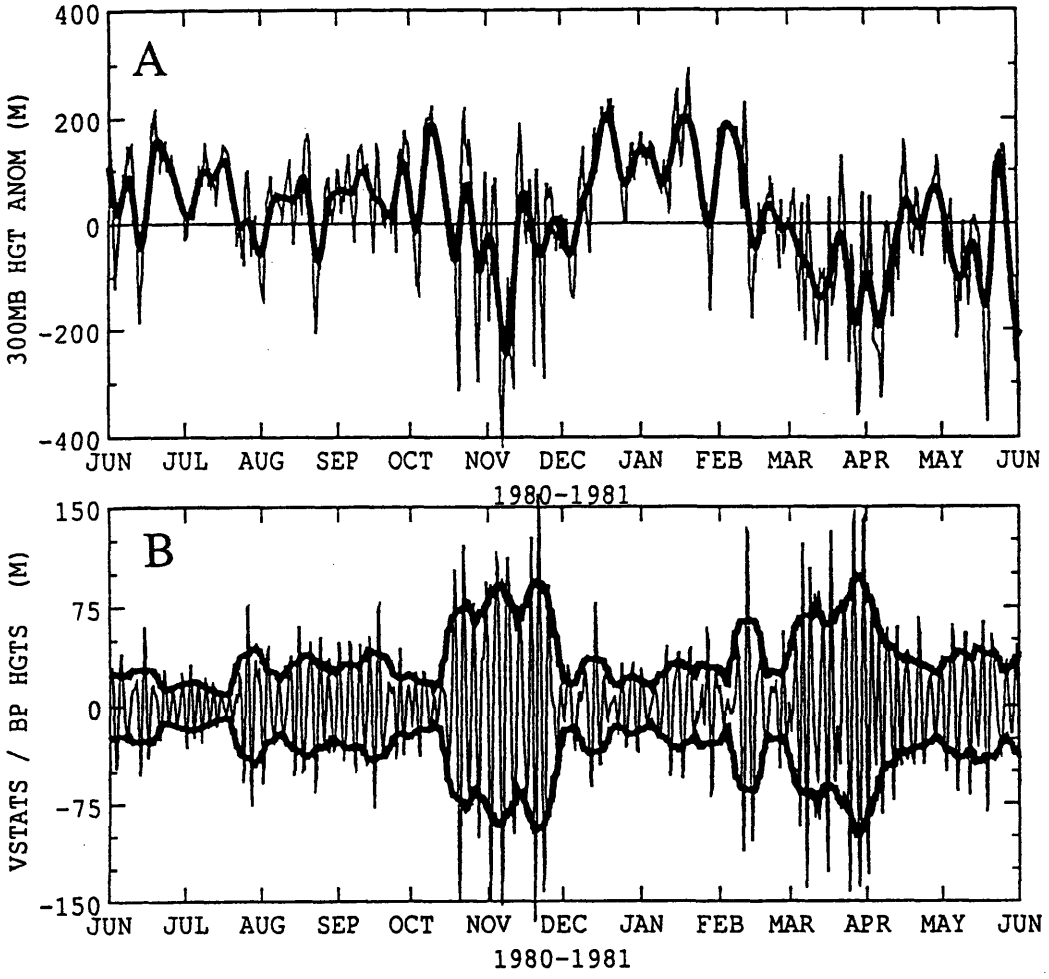

Fig. 4.1. Time series at 40N 25W of the a) 300 mb geopotential heights (thin) and lowpass filtered heights (thick) and b) bandpass filtered 300 mb heights (thin) and the corresponding 10-day VSTATs (thick). The negative VSTAT curve is also drawn to demonstrate the envelope nature of the VSTAT function.

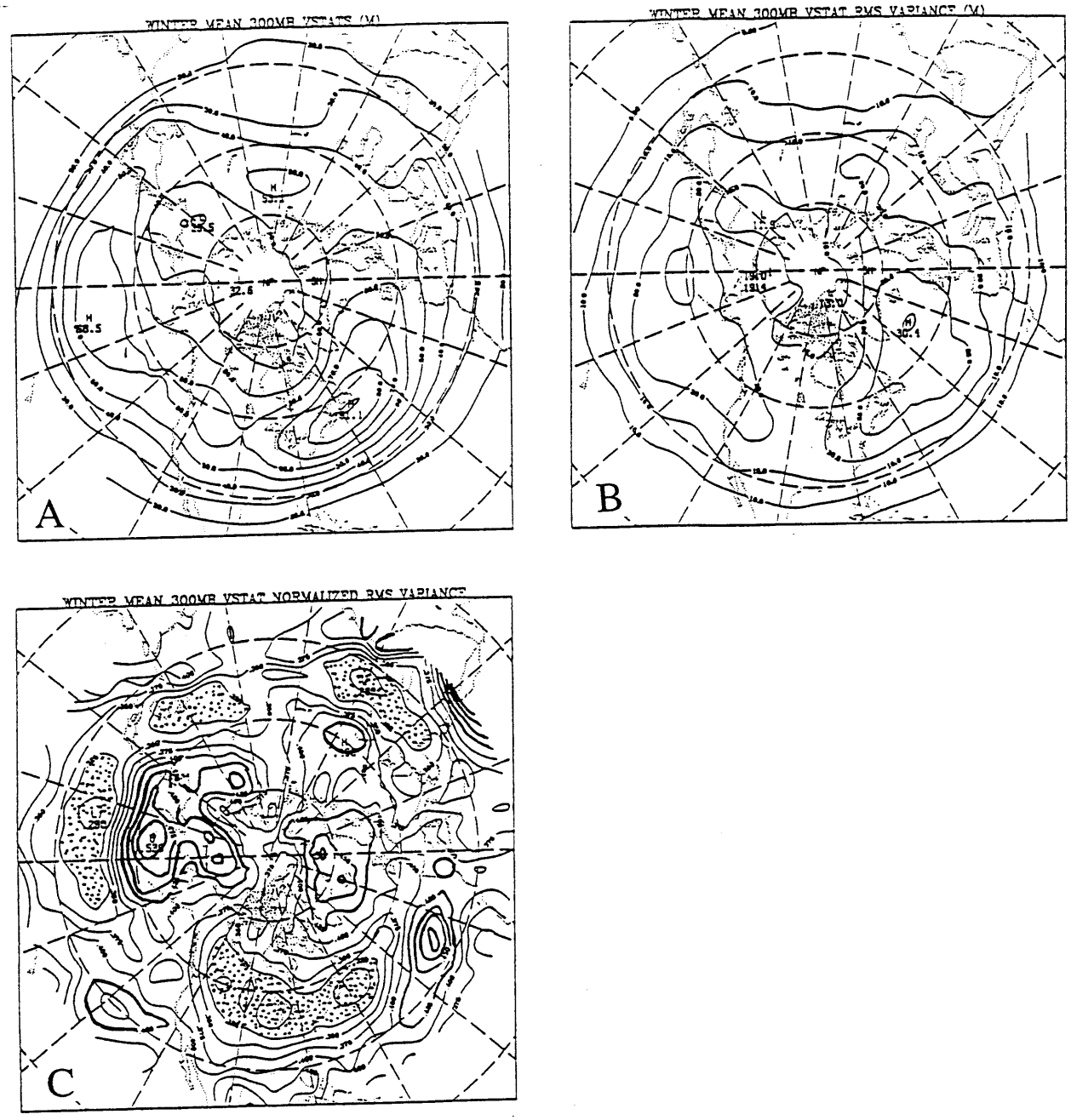

Fig. 4.2. a) Winter-mean distribution of 300 mb VSTATs (m). b) The RMS variability of winter 300mb VSTATs. c) The relative variability (variability / mean) of the 300 mb VSTATs. Regions with relative variability less the .325 are stipled while regions greater than .425 are contoured with thick lines.

height bandpass RMS variability. The mean 300 mb VSTAT distribution also qualitatively resembles Blackmon's (1976) winter-mean 500 mb bandpass distribution, with the peak magnitudes increasing from 67m to 91m (~35%) a ratio about equal to that of the square root of the densities at the two levels. Elongated regions of local maxima in the VSTATs are associated with the storm tracks, identical to the relationship noted for the mean bandpass variance.

The distribution of the mean RMS variability of the 300 mb bandpass VSTATs (Fig 4.2b) is intermediate between that of the mean bandpass and lowpass RMS distributions (Blackmon, 1976). The maxima in VSTAT variance are collocated with the low frequency centers of action. However the variance pattern still retains much of the zonally elongated structure that characterizes the mean bandpass RMS distribution. The relative VSTAT variance (Fig. 4.3c) indicates that the principal storm tracks are relatively stable features of the winter climatology, while regions north, south and downstream of the storm tracks are relatively more variable. Such a pattern would result, for example, if the regions of synoptic-scale eddy growth were relatively stationary (in space and time) but that the tracks of mature disturbances were governed by a variable large-scale flow.

Histograms of observed 300 mb VSTATs at several points (including two within the storm tracks) are shown in Fig 4.3. The distributions are nearly Gaussian, with only modest positive skewness. Some positive skewness should be expected, since VSTAT is a positive definite function whose mean is only two or three times the standard deviation. Thus, the skewness tends to increase as the distribution mean decreases. Because of the skewness, statistical significance tests of positive VSTAT anomalies may have a somewhat exaggerated significance attached to them, while negative anomalies may have a somewhat lessened significance. However in practice, the composite VSTAT anomalies and their significance tend to be symmetric about zero suggesting that weak skewness is not effecting the results in any substantial way.

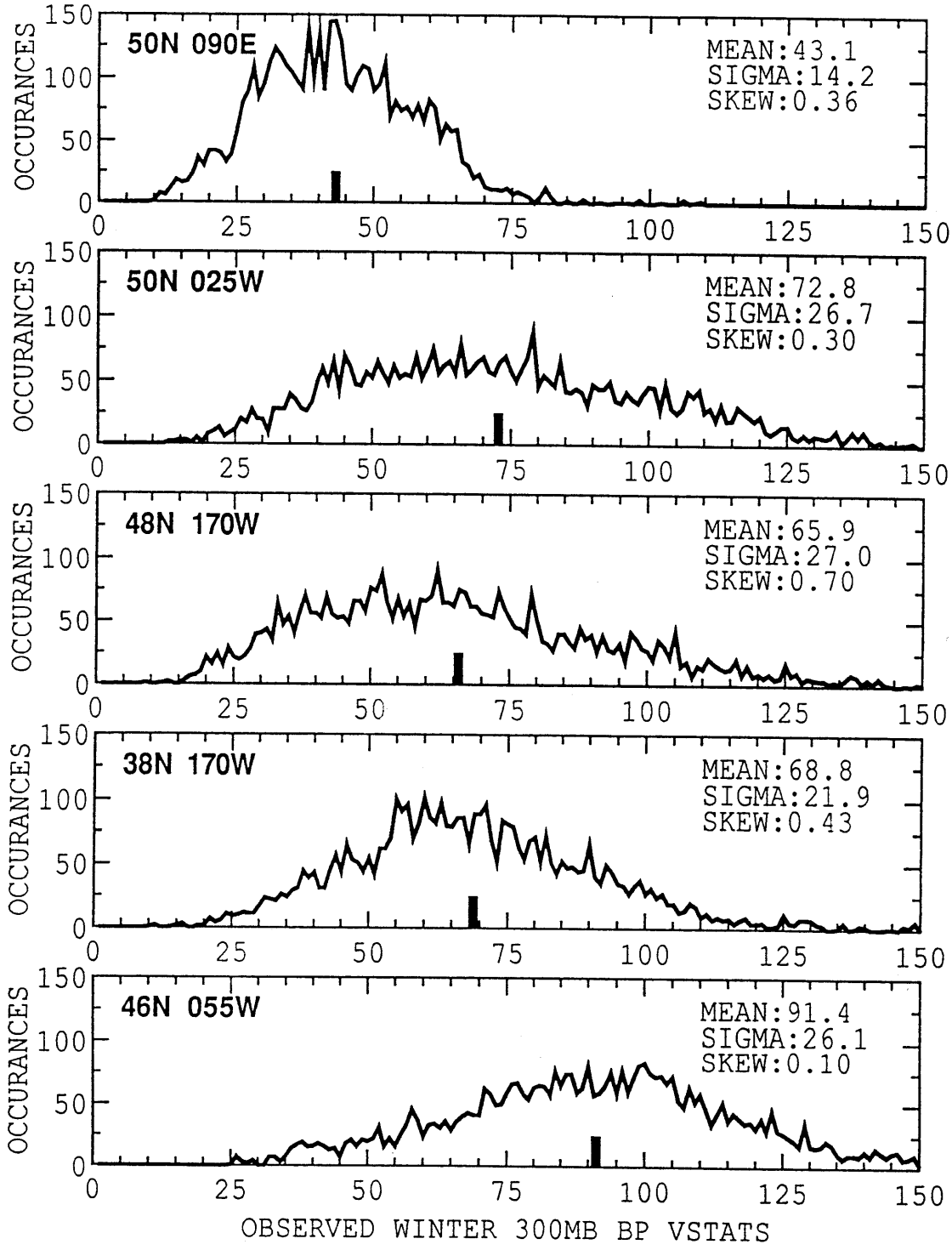

Fig. 4.3. Histograms of 300 mb VSTAT occurrences. The positions for each histogram is indicated in the top left. The mean, standard deviation and distribution skewness are indicated in the upper right of each plot. The last two plots are for points near the centers of the Pacific and Atlantic storm tracks respectively.

4.3 Changes in Eddy Activity during Mature PAs.

We now turn our attention to the distribution of VSTATs during the mature phase of persistent anomalies. Fig 4.4 presents the composites of the 300 mb VSTATs, the corresponding composite anomalies and the statistical significance of the anomalies at day +6 during the onset of each phase of the Atlantic and Pacific cases. As was shown in Chapter 3, day +6 is close to the time of maximum height anomaly amplitude at the key point, with the case mean composite height structure very similar to the day +6 structure. These relationships also apply to VSTAT composites.

During mature Atlantic positive PAs, the Atlantic storm track is shifted well to the north of its climatological mean position, with the primary axis of maximum activity extending from near Newfoundland northeast to Iceland and then eastward into Scandinavia. The corresponding composite anomalies for this time show a nearly north-south aligned anomaly dipole in eddy activity just offset from the key point. Enhanced eddy activity occurs north to the of the key point, with reduced eddy activity at and to the south of the key point. These eddy activity anomalies closely correspond with the large-scale zonal wind anomalies associated with the composite 300 mb height anomalies (Fig. 3.3). The peak VSTAT anomalies of about +/-25m represent approximately 50% of the local winter-mean values and are about equal to one standard deviation. The corresponding statistical significance shows that a majority of the anomalies in this dipole structure are characterized by significance values exceeding 95%. Indeed all of the Atlantic positive cases exhibit some degree of this VSTAT dipole anomaly structure.

There is some indication of an enhanced storm track well to the south and west of the key point, as has been reported in other blocking studies (e.g. Pettersen, 1956). However,

since our data region cuts off at 20N, much of this southern storm track (if any) is not detected. The relatively weak values of these southern VSTAT anomalies are partially due to the VSTATs being constructed from geopotential heights. If the VSTATs were scaled by the Coriolis parameter so as to be more representative of velocity or vorticity variations, then the relative importance of the southern anomalies would be somewhat enhanced. Also since traditional blocking patterns usually occur further north than positive PAs, blocking patterns also tend to have a stronger mean flow and synoptic-scale eddy activity to their south.

Associated with the mature Atlantic positive PAs, there is a weak but extensive region of enhanced eddy activity upstream of the key region. Most of the region over North America and the North Pacific Ocean is characterized by enhanced eddy activity. Over the Pacific, there is a relatively weak dipole VSTAT anomaly structure similar to the major dipole over the Atlantic. The Pacific dipole is associated with the weak geopotential height anomalies that occur at that time over the key region. Downstream of the key region, there is enhanced eddy activity that appears as an eastward extension of the Atlantic storm track well into eastern Europe. The statistical significance of these remote VSTAT anomalies is generally low; however, their large regional extent and temporal continuity (discussed later) suggests that there may be greater significance to the anomaly *patterns* than the *point-by-point* significance tests indicate. This issue will be discussed further in Sec. 4.5.

During the onset of the Atlantic negative cases the principal Atlantic storm track runs west to east from the Great Lakes eastward through southern Europe. The VSTAT anomaly pattern is essentially identical to the mature Atlantic positive cases but with opposite sign. The primary feature is a highly significant north-south aligned anomaly dipole about the key point with suppressed activity to the north and enhanced activity to the south. Most of the region upstream of key region over North America and the Pacific is

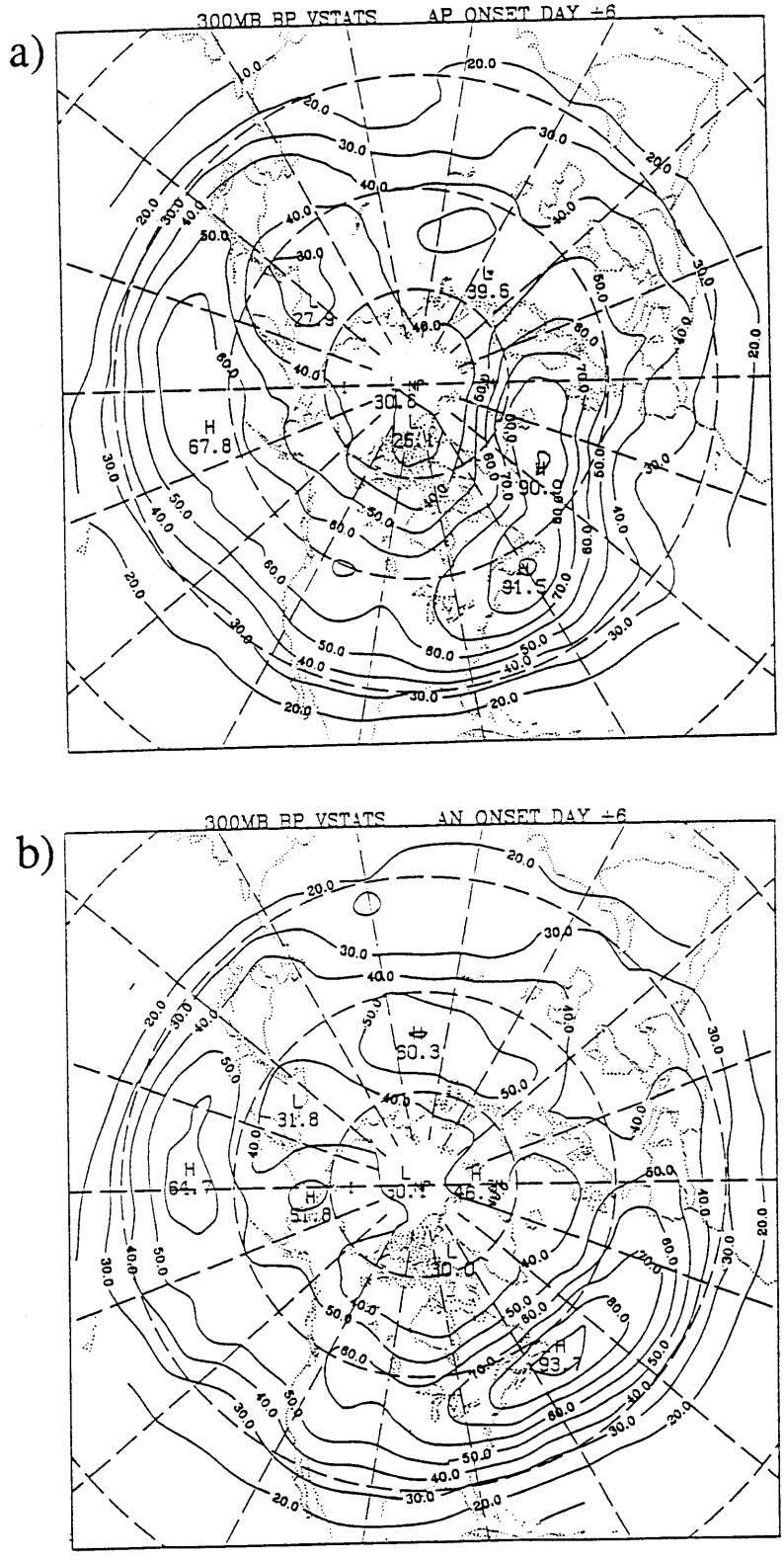

Fig. 4.4. Composite-mean 300 mb VSTATs (m) for day +6 during a) Atlantic positive and b) Atlantic negative PA events.

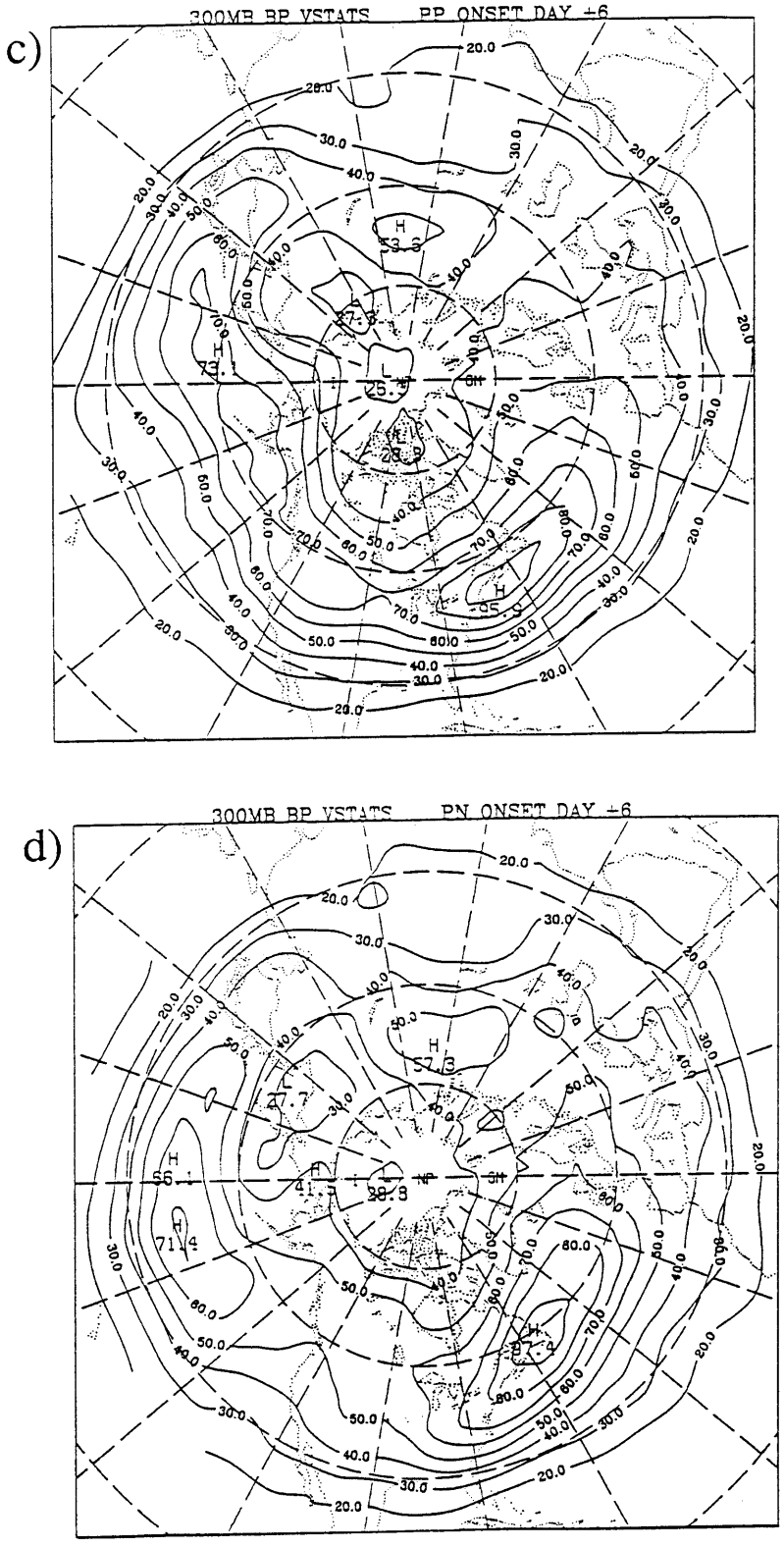

Fig. 4.4 (cont.) Composite-mean 300 mb VSTATs (m) for day +6 during c) Pacific positive and d) Pacific negative PA events.

e)

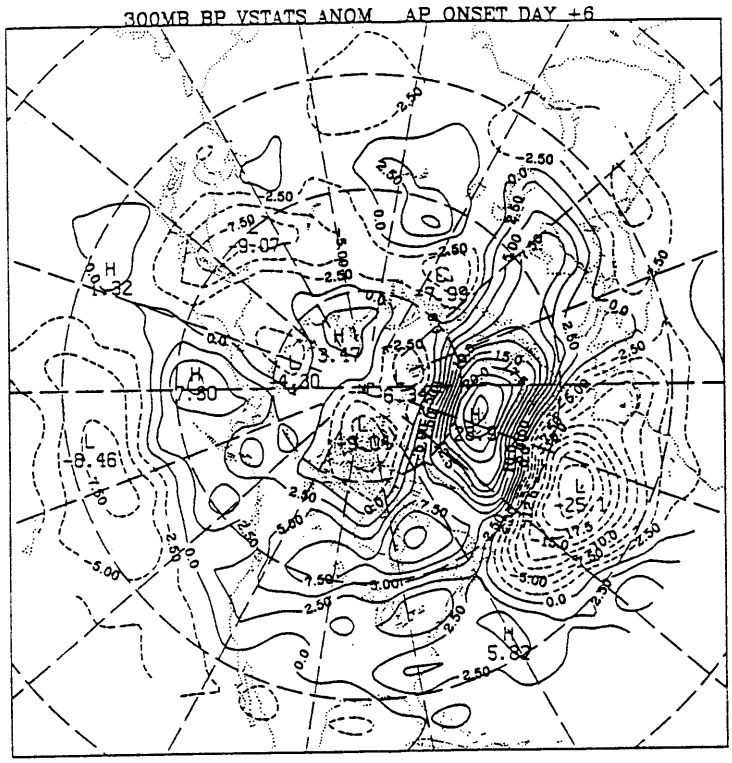

f)

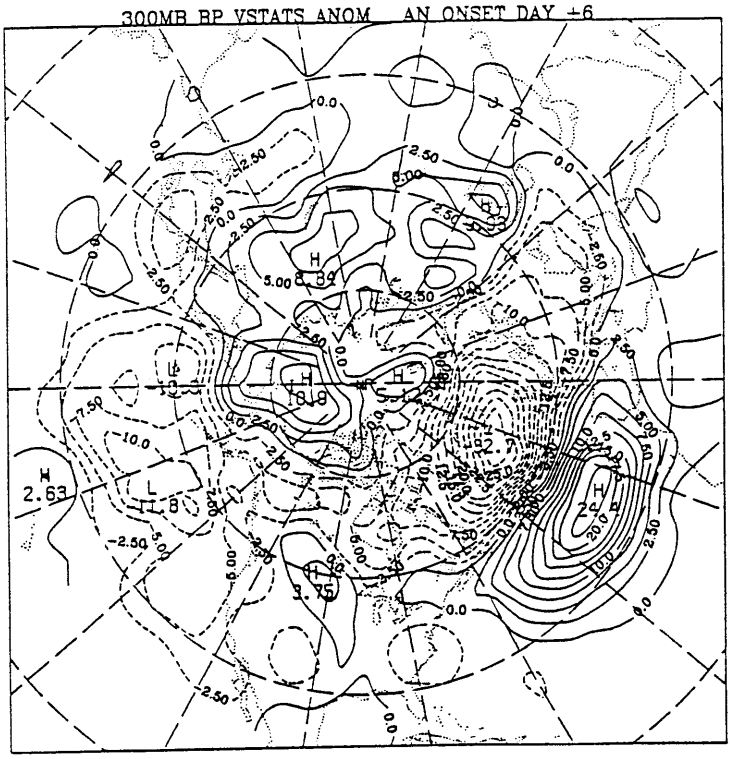

Fig 4.4 (cont.). Composite-mean 300 mb VSTAT anomalies (m) for day +6 during e) Atlantic positive and f) Atlantic negative PA events.

g)

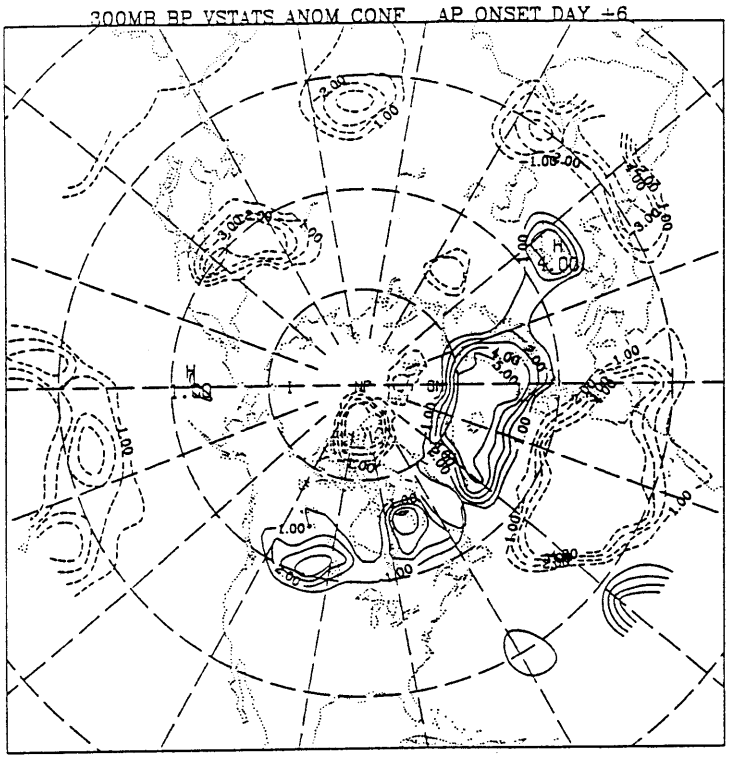

h)

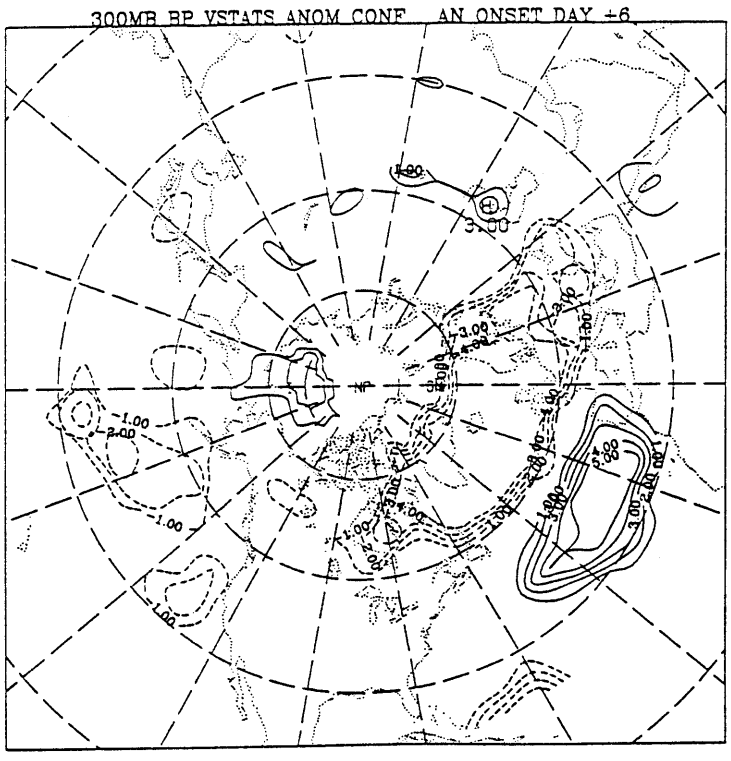

Fig 4.4 (cont.) Statistical significance of the composite-mean 300 mb VSTAT anomalies (m) for day +6 during g) Atlantic positive and h) Atlantic negative PA events. Contours are drawn for the 90, 95, 97.5, 99 and 99.5 confidence levels. Regions having corresponding negative anomalies are dashed.

i)

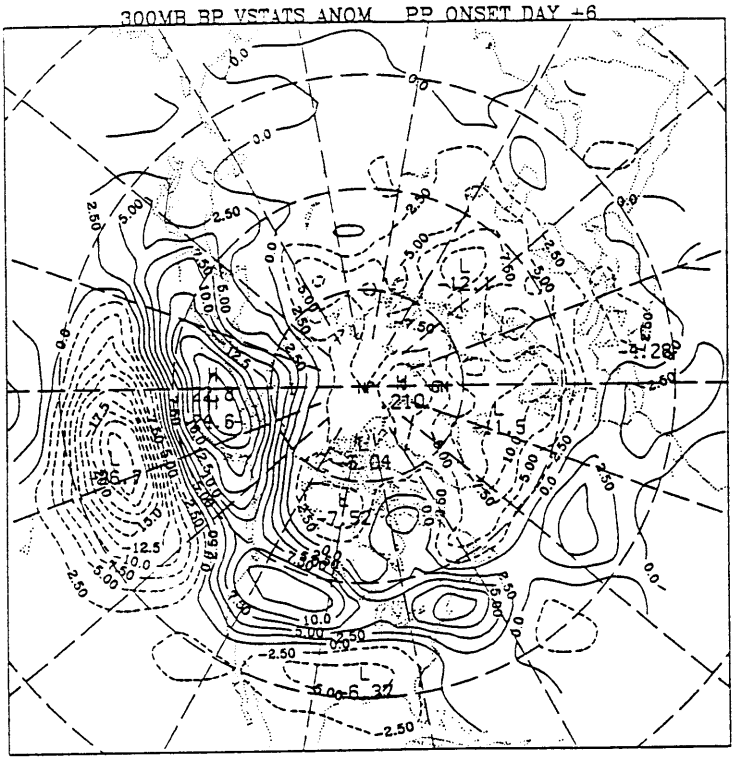

j)

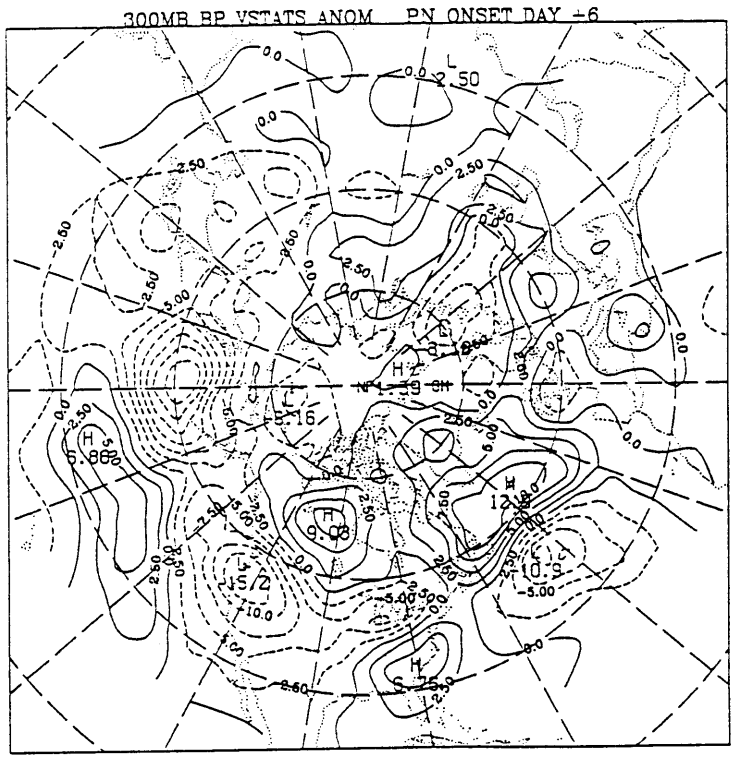

Fig 4.4 (cont.). Composite-mean 300 mb VSTAT anomalies (m) for day +6 during i) Pacific positive and j) Pacific negative PA events.

k)

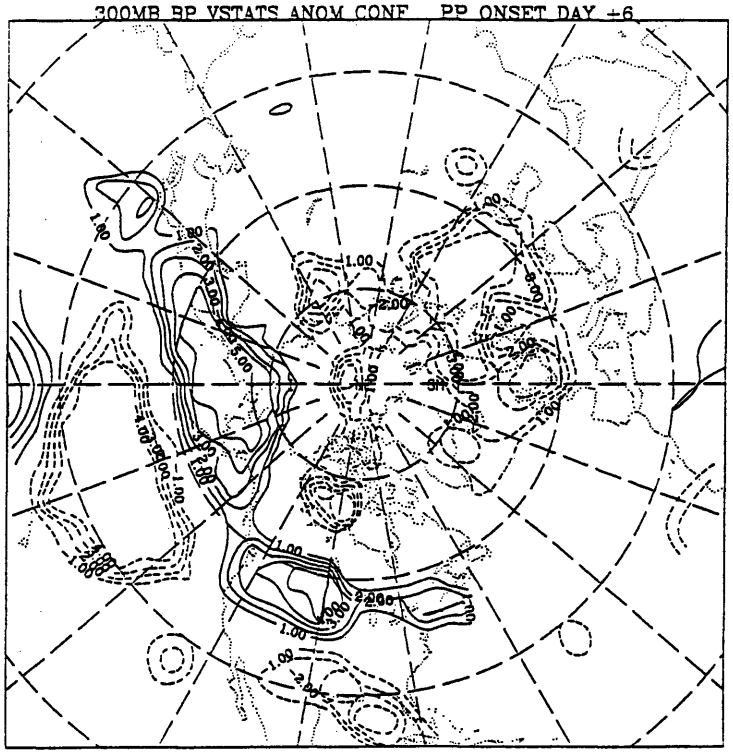

l)

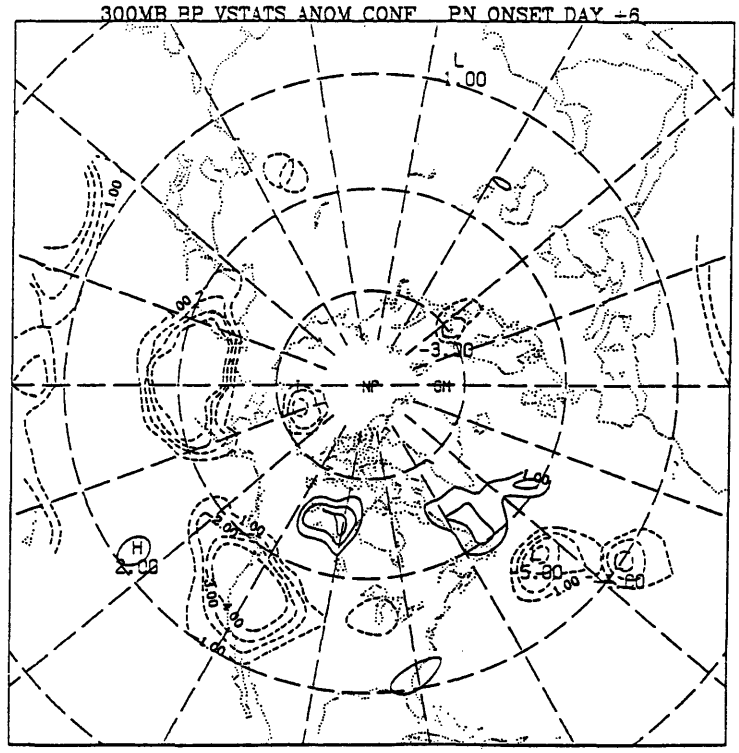

Fig 4.4 (cont.) Statistical significance of the composite-mean 300 mb VSTAT anomalies (m) for day +6 during k) Pacific positive and l) Pacific negative PA events. Contours are drawn for the 90, 95, 97.5, 99 and 99.5 confidence levels. Regions having corresponding negative anomalies are dashed.

characterized by suppressed eddy activity. Suppressed eddy activity is also found downstream of the key region.

During both the positive and negative Pacific cases, the VSTAT patterns are broadly similar to the corresponding patterns for the Atlantic cases. The principal Pacific storm track is deflected well to the north of its climatological mean position during the Pacific positive cases, and well to the south during the Pacific negative cases. The corresponding VSTAT anomaly dipoles in these cases takes on a slight southeast to northwest tilt. Of the four PA types considered, the Pacific negative cases show the least anomalous eddy activity near the key region. The Pacific negative cases also show the least symmetry in the relative magnitudes of the VSTAT anomaly dipole extrema, with the southern eddy activity enhancement considerably less than the corresponding eddy activity reduction to the north.

The geographic extent of the upstream VSTAT anomalies during the Pacific cases is confined to eastern Asia and the western Pacific. This is a considerably smaller domain than observed during the Atlantic cases. However, downstream of the Pacific key region there is considerably more anomalous eddy activity than is observed downstream in the Atlantic cases. This corresponds to the greater extent of downstream large-scale geopotential height anomalies observed during the Pacific cases. There is a significant reduction in eddy activity over the Pacific-Northwest region of the U.S. during the Pacific negative cases, which is associated synoptically with the strong blocking-like ridge that develops over that region. During the Pacific negative cases, the Atlantic western storm track becomes more meridionally oriented on the eastern side of the anomalous deep large-scale trough that develops in central and eastern North America. During these cases the Gulf coast and southeastern seaboard of North America become active cyclogenesis regions, with cyclones moving up along the eastern seaboard. During the mature Pacific

positive cases, the Atlantic storm track becomes more zonal, running from over the Pacific Northwest eastward over the Atlantic.

The results of similar analyses of the 1000 mb bandpass VSTATs are shown in Fig. 4.5. In general, these near surface analyses are quite similar to the 300 mb VSTAT analyses. The primary feature of the anomaly maps is a highly significant dipole structure near the key region that is north-south aligned during the Atlantic cases and southeast-northwest aligned in the Pacific cases. For both regions, the principal storm track is pushed north of its climatological mean position during the positive cases and south during the negative cases. Eddy activity anomalies with the same sign as the primary geopotential height anomaly are found upstream of the key region. The magnitudes of the 1000 mb VSTATS anomalies are about half of those observed at 300 mb; however when normalized by the climatological mean bandpass variance, the relative anomalies at the two levels are approximately equal. The Pacific negative composites again show the weakest anomalous eddy activity near the key region, although again display significant anomalies further downstream.

There are some structural differences in the eddy activity between the 300 mb and 1000 mb levels. First, relative to its 300 mb position, the location of the primary 1000 mb VSTAT anomaly dipole is shifted northward along the axis of the dipole such that the minimum (maximum) in the eddy activity anomalies now lies closer to the key point. The significance of the 1000 mb VSTAT anomalies is somewhat weaker than the corresponding 300 mb anomalies indicating a weaker anomaly to variance ratio. This may be due to the fact that the local structures of the surface disturbances are more likely to be influenced by inhomogeneities in the underlying surface, and thus contributions of upper-level flow changes to the total surface variability may be relatively smaller.

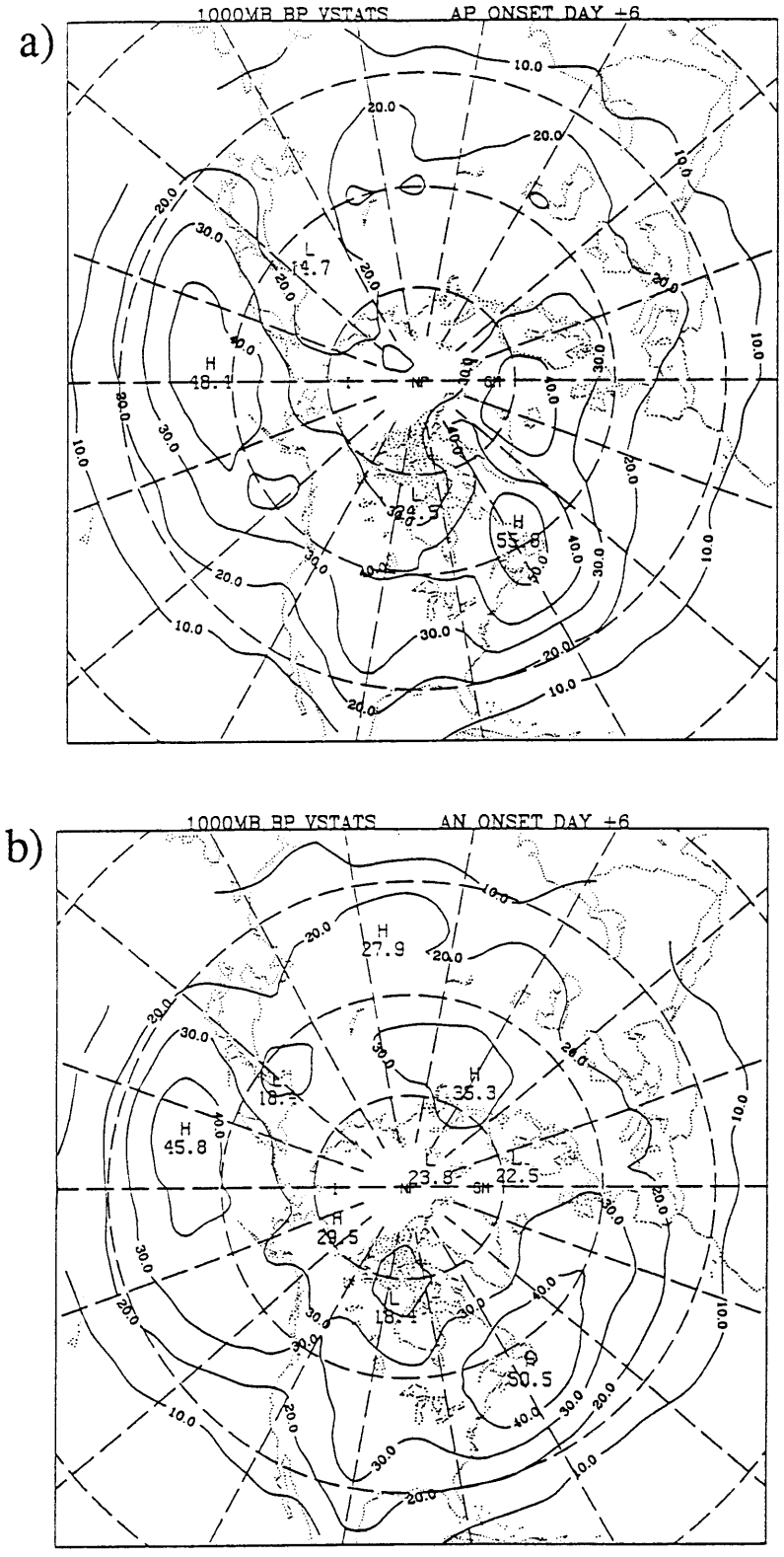

Fig. 4.5. Composite-mean 1000 mb VSTATs (m) for day +6 during a) Atlantic positive and b) Atlantic negative PA events.

c)

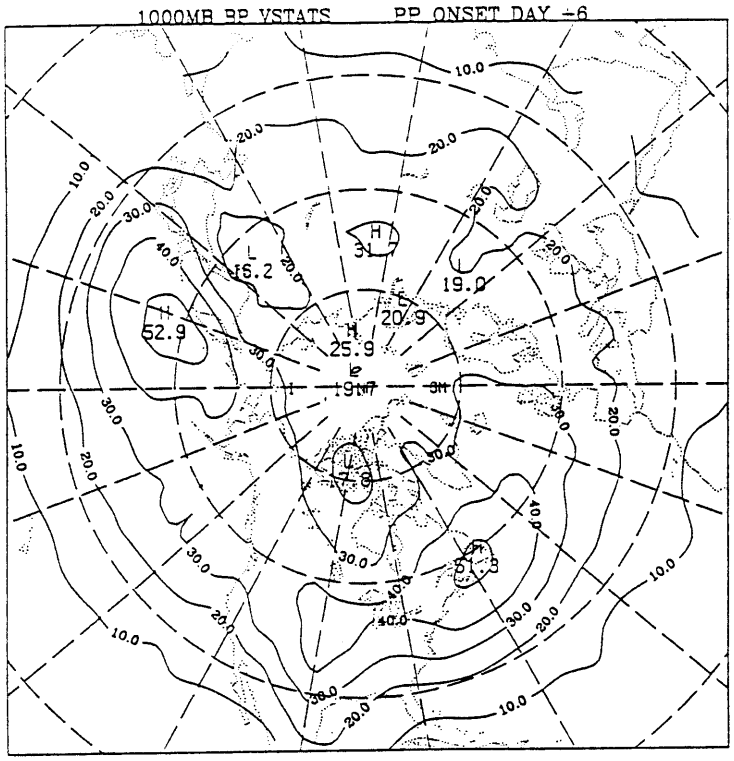

d)

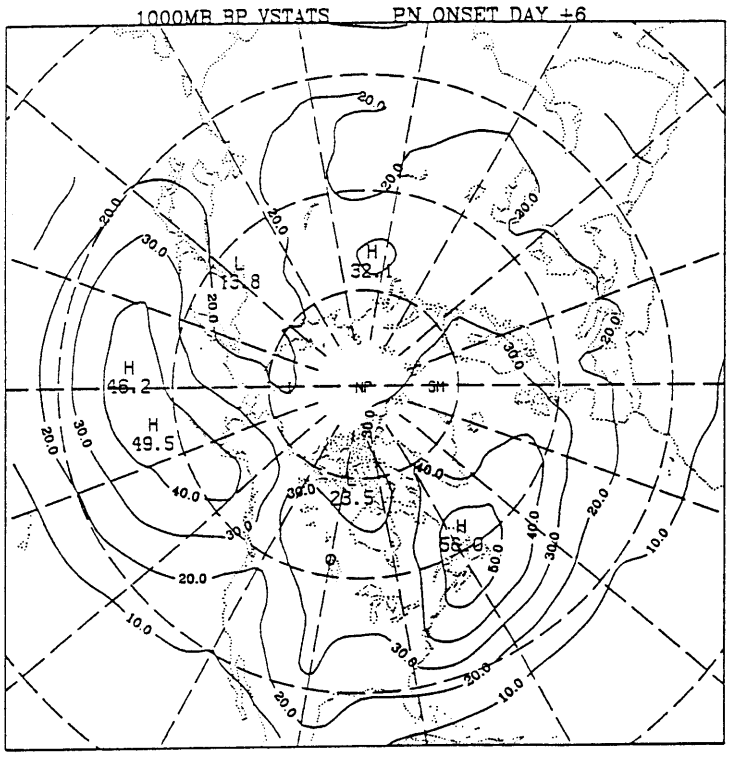

Fig. 4.5 (cont.) Composite-mean 1000 mb VSTATs (m) for day +6 during c) Pacific positive and d) Pacific negative PA events.

e)

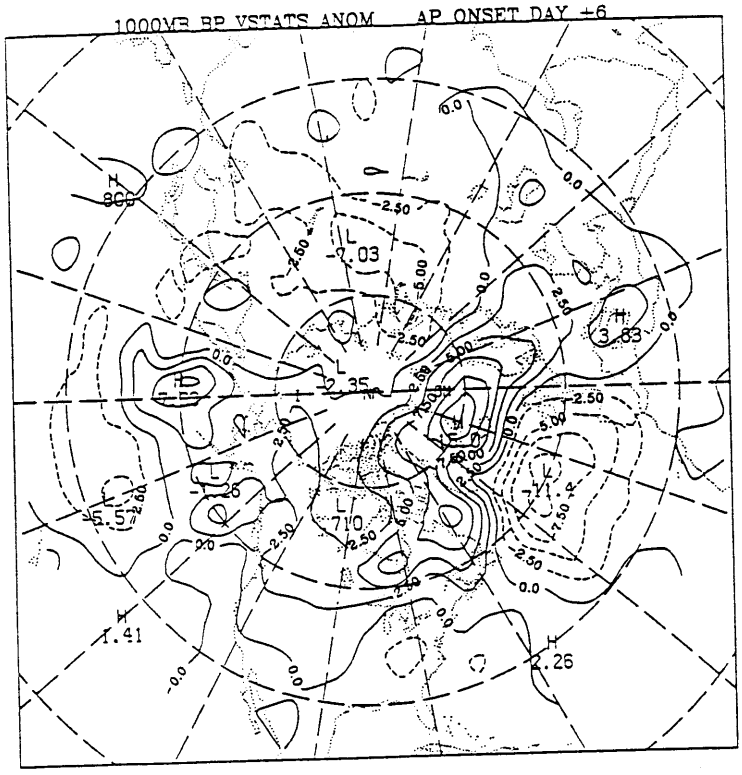

f)

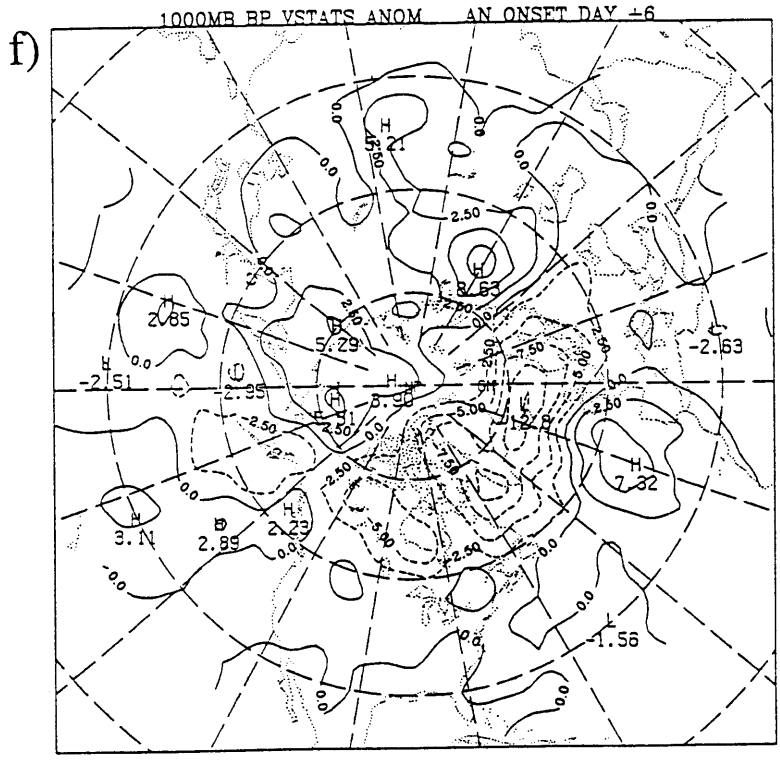

Fig 4.5 (cont.). Composite-mean 1000 mb VSTAT anomalies (m) for day +6 during e) Atlantic positive and f) Atlantic negative PA events.

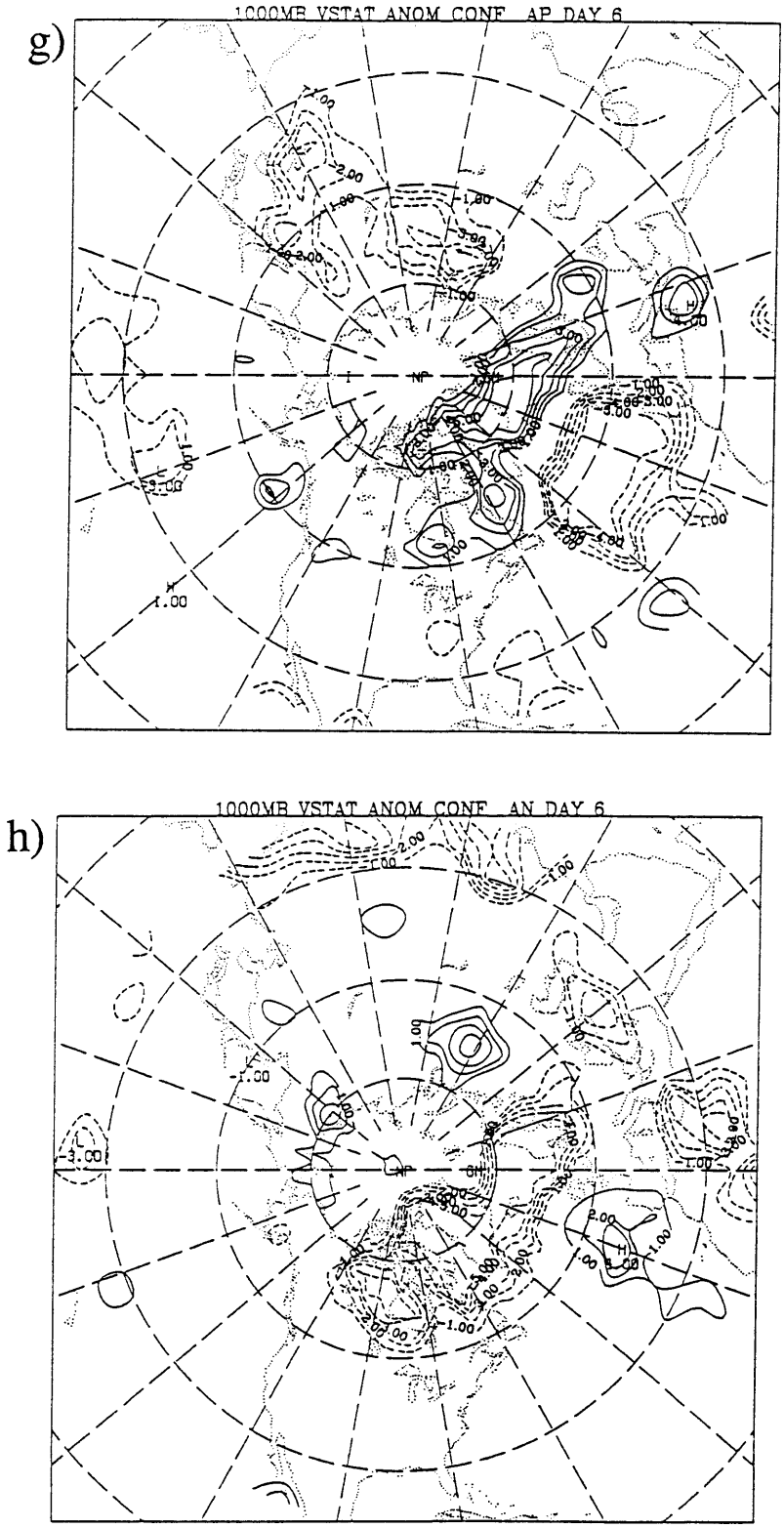

Fig 4.5 (cont.) Statistical significance of the composite-mean 1000 mb VSTAT anomalies (m) for day +6 during g) Atlantic positive and h) Atlantic negative PA events. Contours are drawn for the 90, 95, 97.5, 99 and 99.5 confidence levels. Regions having corresponding negative anomalies are dashed.

i)

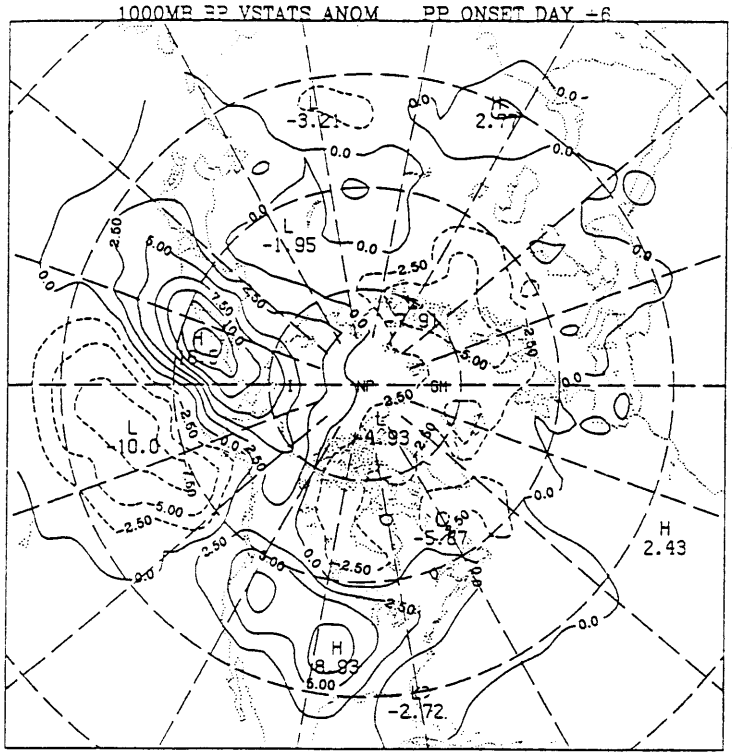

j)

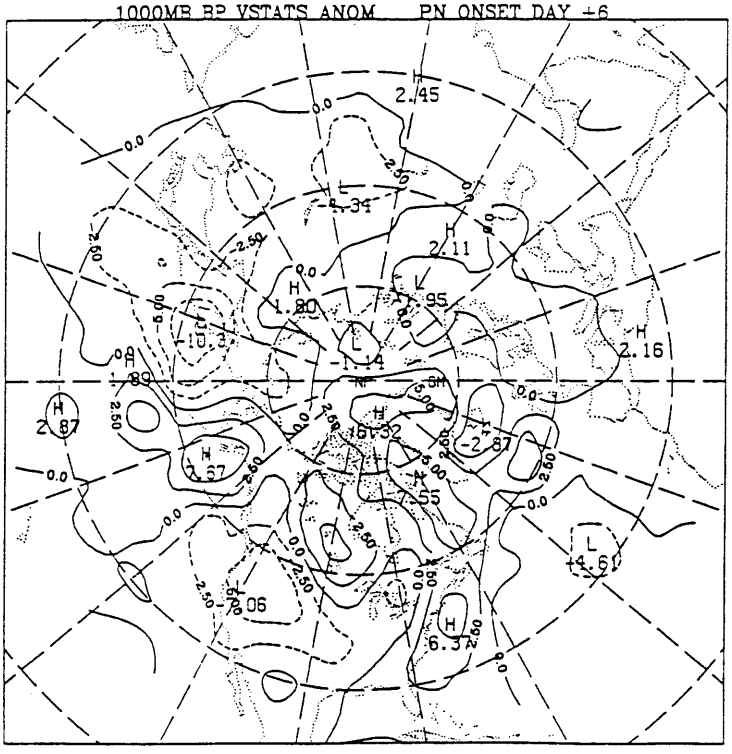

Fig 4.5 (cont.). Composite-mean 1000 mb VSTAT anomalies (m) for day +6 during i) Pacific positive and j) Pacific negative PA events.

k)

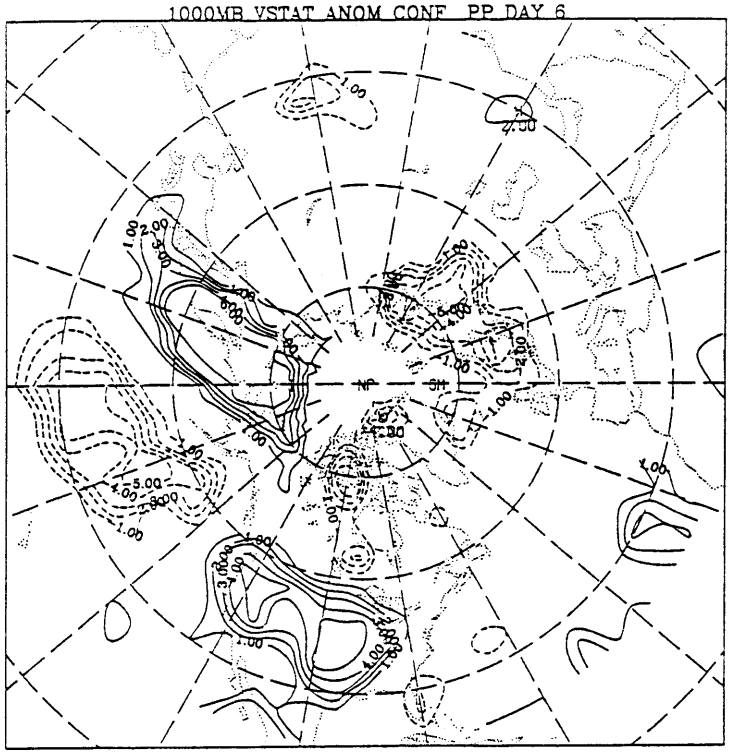

l)

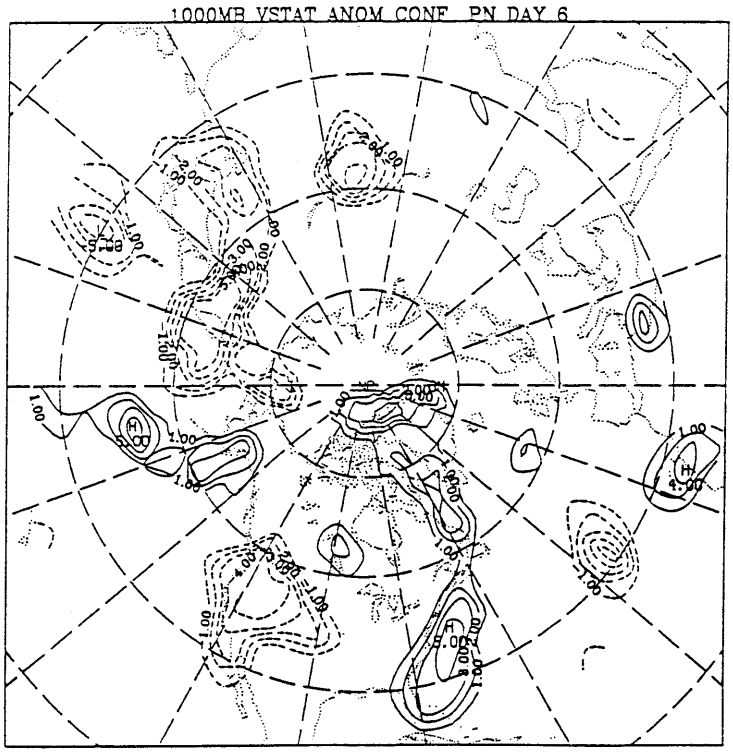

Fig 4.5 (cont.) Statistical significance of the composite-mean 1000 mb VSTAT anomalies (m) for day +6 during k) Pacific positive and l) Pacific negative PA events. Contours are drawn for the 90, 95, 97.5, 99 and 99.5 confidence levels. Regions having corresponding negative anomalies are dashed.

To help interpret the VSTAT results, Fig. 4.6 shows the analyzed tracks of a random subset of surface cyclones[1] that originated during the mature phase of the Atlantic events. During the Atlantic positive PA cases, the principal Atlantic cyclone track runs northeast just off the U.S. coast, turns northward through the Canadian Maritimes and then splits around either side of Greenland. The total void of cyclones over Greenland is probably due to a reduction to sea-level problem associated with the very cold surface air over the relatively high terrain. The cyclone track that passes east of Greenland turns eastward over Iceland and then into Scandinvania, while the western branch continues to curve to the west. The region in and near the key point is nearly void of any cyclone tracks. To the south of the key point there is a weak and erratic track that, according to the VSTAT analyses, does not represent any enhanced eddy activity. These storm tracks qualitatively correlate very well with the regions of maximum 1000 mb VSTATs and are basically aligned parallel to the upper-level flow.

In strong contrast, the principal storm track associated with the Atlantic negative PA cases, consists of a single west-to-east orientated track across the Atlantic that passes directly through the key point. The regions about 10 degrees to the north or to the south are nearly void of any cyclone tracks. The principal storm track again qualitatively correlates very well with the storm tracks deduced from the 1000 mb VSTATs, and again is approximately parallel to the mean upper-level flow. Near the key point, many of the individual storm tracks briefly curve northward before ending. This is partly due to the fact that the cyclones are propagating into a region of strong mean surface pressure gradient associated with the very strong Icelandic low that characterizes these negative PA events. As the cyclones propagate into the strong mean gradient, there is a tendency to analyze their

[1] These tracks were obtained from a tape of all NMC analyzed cyclone tracks that passed through the region 120E through 0E during the period 1-Jan 1965 through 31-Dec-1975. A detailed description of a dataset that differs only by the period covered can be found in Gyakum et. al. (1989). Here we display only a subset of the tracks to present a clearer figure.

positions north of their own circulation centers (Wallace *et al.* 1988). This effect is not as apparent in the positive cases, because the mean surface gradient is relatively much weaker, with the climatological mean Icelandic low replaced by a surface blocking high.

The surface cyclone tracks accompanying mature Pacific PA events are shown in Fig. 4.7. Again the principal storm tracks during the two phases of the PAs appear as nearly mutually exclusive tracks that generally follow the associated upper-level flow. The cyclones either propagate around the key point (blocking PAs) or through the key point (zonal PAs). There are considerable differences in the downstream cyclone track behavior in the Pacific cases, particularly along the Pacific Northwest coast, where the strong downstream ridge that accompanies Pacific negative cases appears to strongly "block" the approaching synoptic-scale cyclones.

4.4 Changes in Eddy Activity during the Life Cycles of PAs

In this section, we describe how synoptic-scale eddy activity varies during the life cycles of the PAs. We will focus primarily on the 300 mb VSTAT[1] anomalies, as results of the previous section show that these anomalies are strongly correlated with the eddy activity anomalies near the surface. The discussion will mainly be limited to documenting the eddy activity anomalies; the significance of the anomalies will be addressed in Sec. 4.5. Here we will focus the discussion mainly on the features considered significant. Although the results for each of the PA types will be presented, we will focus on the Atlantic cases. The Atlantic and Pacific PA eddy results are broadly similar during the entire PA life cycles, as was also seen in the mature PA analyses. Thus the discussion of the Pacific results will mainly address the differences with the Atlantic results.

---

[1] Unless specifically stated otherwise, the 300mb bandpass geopotential height VSTATs will be referred to as just the VSTATs for brevity.

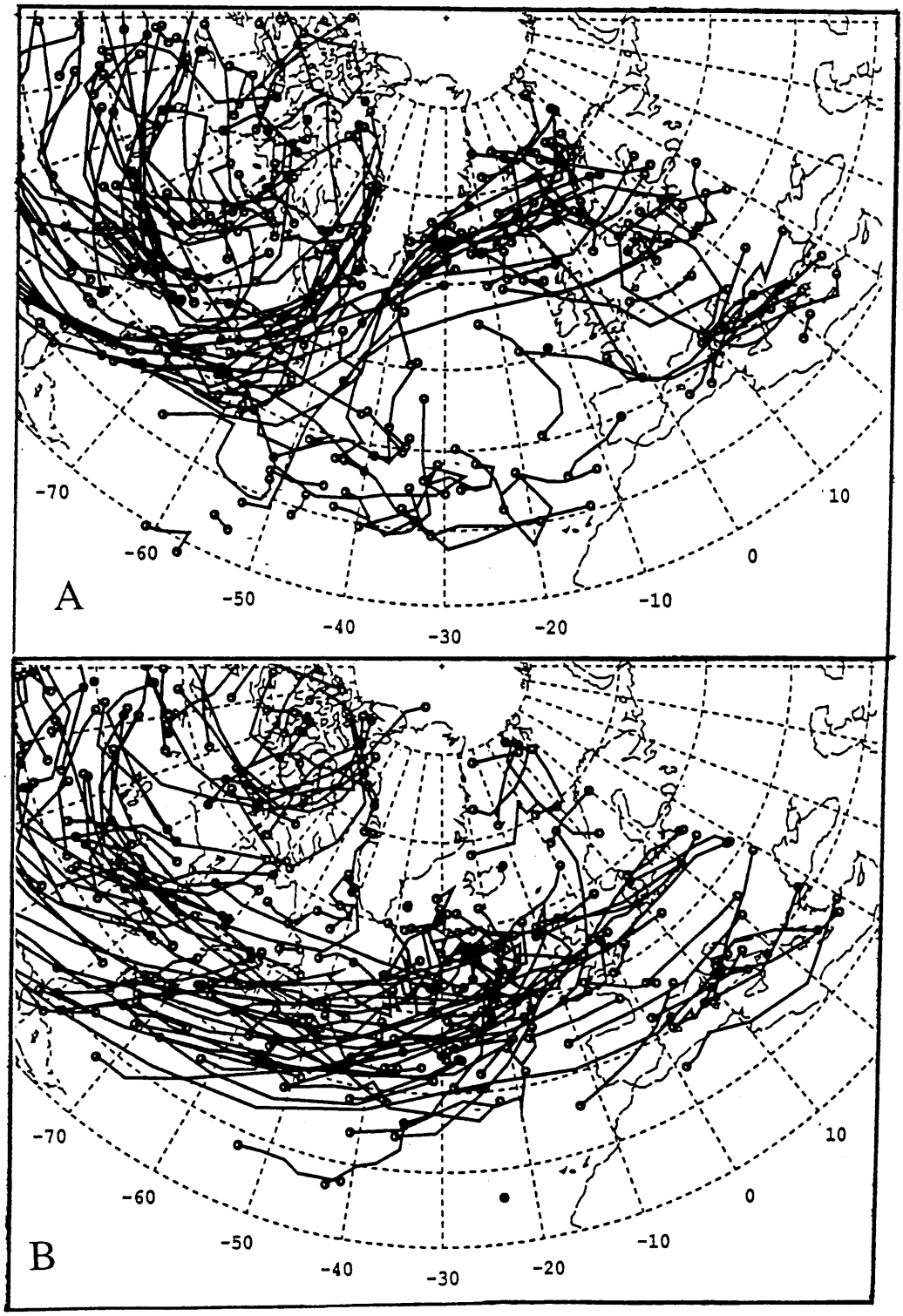

Fig 4.6. Random subset of the NMC analyzed surface cyclone tracks during mature a) Atlantic positive and b) Atlantic negative persistent anomaly events.

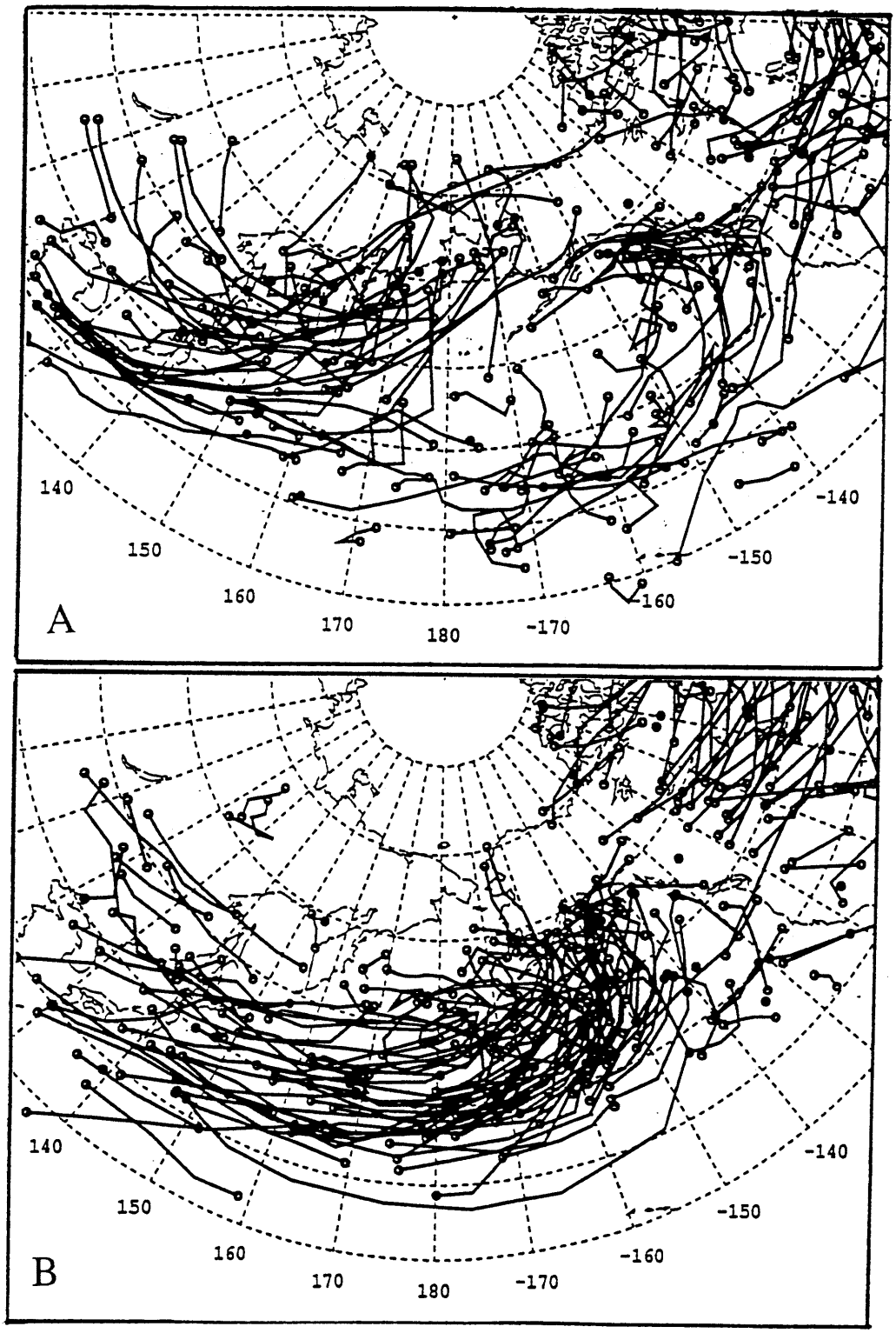

Fig. 4.7. Random subset of the NMC analyzed surface cyclone tracks during mature a) Pacific positive and b) Pacific negative persistent anomaly events.

Fig 4.8 shows the 300 mb composite VSTAT anomalies at three day intervals between days -6 and +3 of onset of the Atlantic positive cases. One of the most striking features of this set of maps is the overall positive anomaly bias throughout the period. This implies that both before and during the onset of Atlantic positive PAs, there is considerable enhancement of synoptic-scale eddy activity over much of the hemisphere. At day -6, this enhancement is most noticeable in a broad mid-latitude belt extending from the east Asian coast eastward through the central Atlantic region. At this time, there is a weak VSTAT anomaly dipole in the far eastern Atlantic. This feature is collocated with the weak subtropical ridge that first begins to appear in the geopotential height composites at that time (Fig. 3.3). The entire Asian continent is also characterized by weakly enhanced eddy activity. Between days -6 and +3 we see that the main belt of positive upstream VSTAT anomalies progresses slowly eastward with the largest of these anomalies reaching the western Atlantic by day 0, just as the large-scale flow anomalies are undergoing their most rapid growth. Also during this time, the anomaly dipole over the eastern Atlantic grows slowly while retrogressing, similar to the development of the large-scale flow. By day +3, the overall pattern strongly resembles the fully mature pattern. The main VSTAT anomaly dipole near the key point becomes the most dominant feature of the maps, with the upstream anomalies having merged with the positive part of the primary dipole into a continuous anomalous storm track.

It appears, then, that the evolution of the eddy anomalies associated with mature Atlantic positive PAs follows two distinct courses. First, there is a broad, zonally elongated packet of eastward-propagating enhanced eddy activity over the Pacific and western North America that appears before and separate from any large-scale flow anomaly and whose leading edge reaches the upstream side of the developing PA just as it is undergoing its period of most rapid growth. Initially, these upstream eddy activity anomalies are primarily related to upper-level disturbances as the 1000 mb VSTAT

anomalies (not shown) at the early times are relatively weak. Second, there is the development of the primary anomaly dipole associated with the pronounced northward shift in the storm tracks associated with the development of the large-scale flow. This anomaly VSTAT dipole is initially biased towards the sign of the large-scale flow anomaly associated with the overall in eddy activity anomalies .

The development of the VSTAT anomalies during the onset of negative PAs over the Atlantic is shown in Fig. 4.9. This shows that during the development, the VSTAT anomaly pattern undergoes a similar evolution as the Atlantic positive cases but with opposite sign. Before and during the large-scale development, there is a negative bias in the upstream eddy activity. These negative anomalies are most notable in a broad region over Canada and the Pacific at days -6 and -3. The primary eddy activity dipole near the key region appears to develop separately from the upstream anomalies and is roughly in phase with the large-scale flow development (Fig. 3.5). By day +3, the broad region of upstream negative anomalies has merged with negative half of the VSTAT anomaly dipole anomaly. The development of the positive (southern) half of the primary dipole lags the negative half by about three days consistent with the overall reduction in eddy activity. However, unlike the Atlantic positive cases, these Atlantic negative cases do not appear to have a clearly defined eastward propagating packet of anomalous eddy activity.

The symmetry of the changes in the eddy activity that occur well prior to the onset of Atlantic PAs is highlighted in Fig 4.10. Here the differences (positive minus negative) in the VSTATs at day -6 of onset is shown. With the exception of a few small regions, the entire map is characterized by positive VSTAT differences. The differences are often close to one standard deviation (see Figs. 4.2 or 4.3) of the climatological distributions. Therefore, there appears to be an eddy activity precursor to the development of Atlantic PAs in terms of a nearly hemispheric-wide change in the level of synoptic-scale eddy activity.

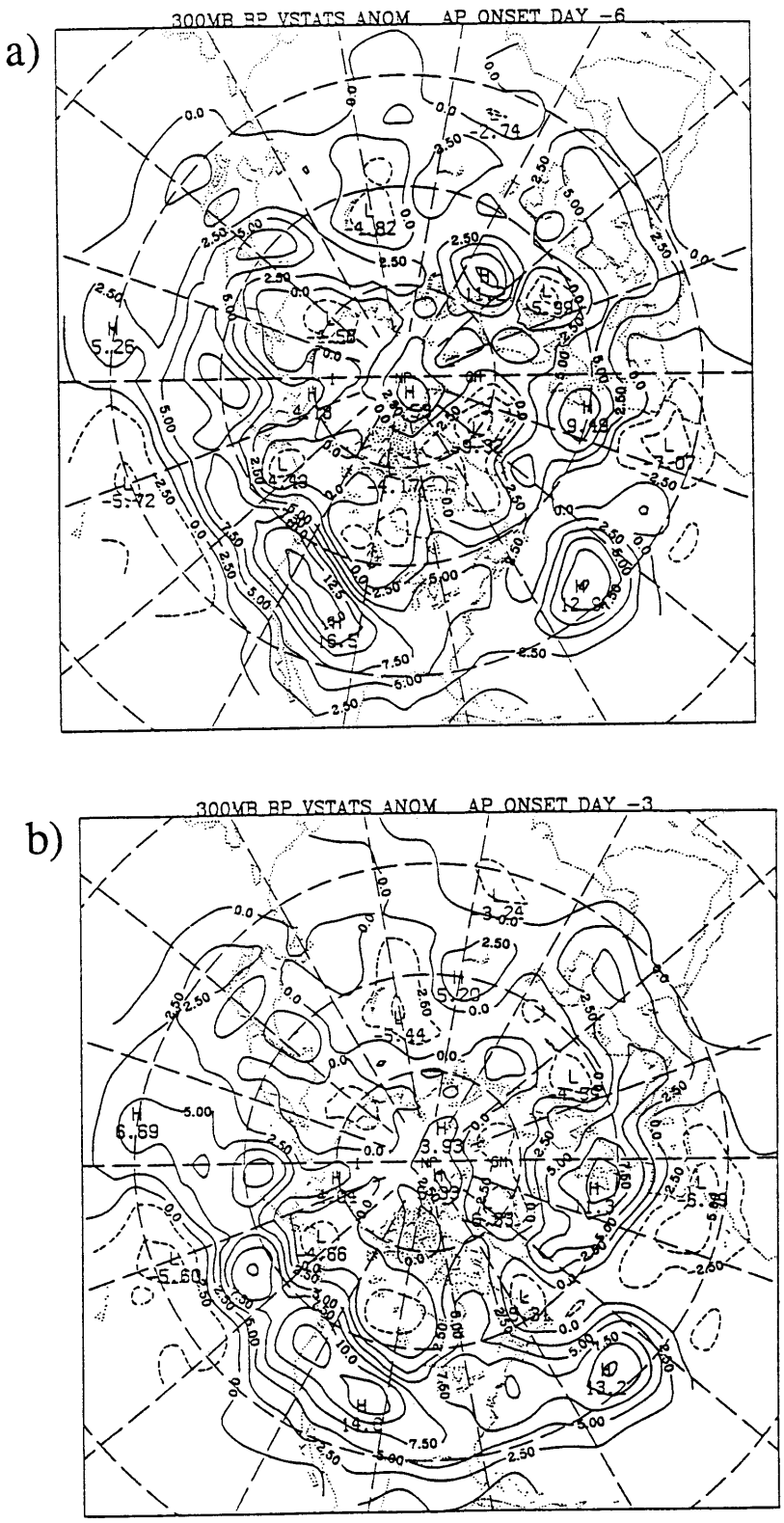

Fig. 4.8. Composite anomalies of the 300 mb VSTATs (m) for days a) -6 and b) -3 during the onset of Atlantic positive persistent anomaly cases.

c)

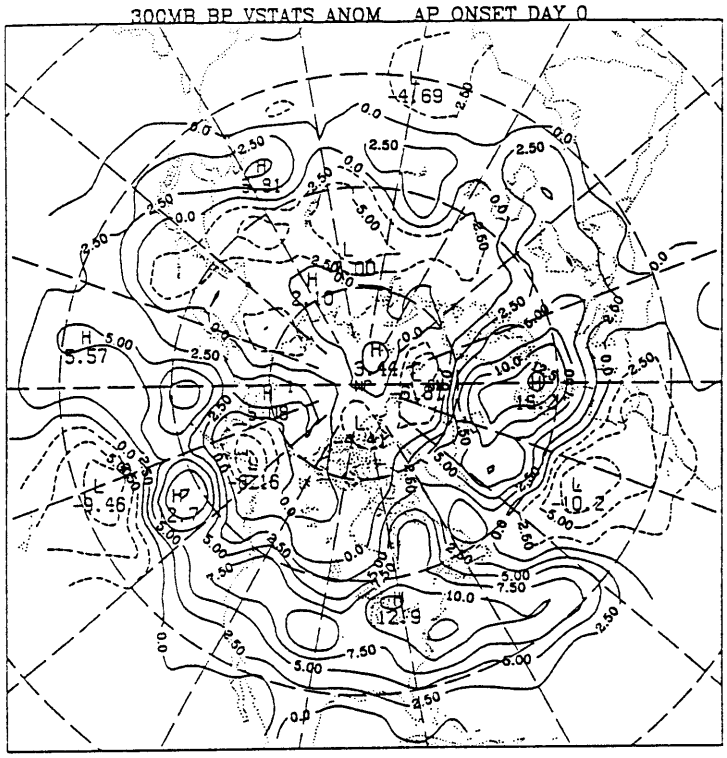

d)

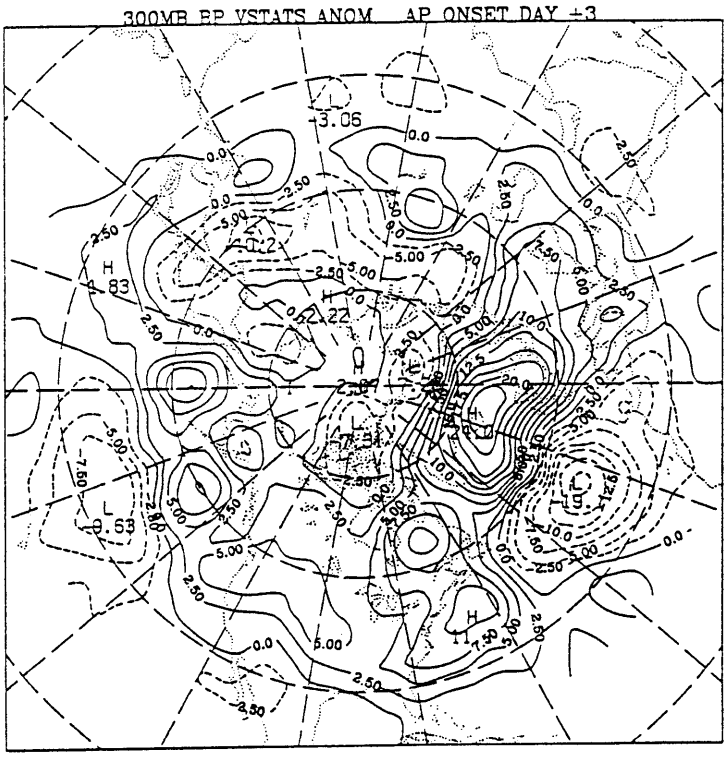

Fig. 4.8 (cont). Composite anomalies of the 300 mb VSTATs (m) for days c) 0 and d) +3 during the onset of Atlantic positive persistent anomaly cases.

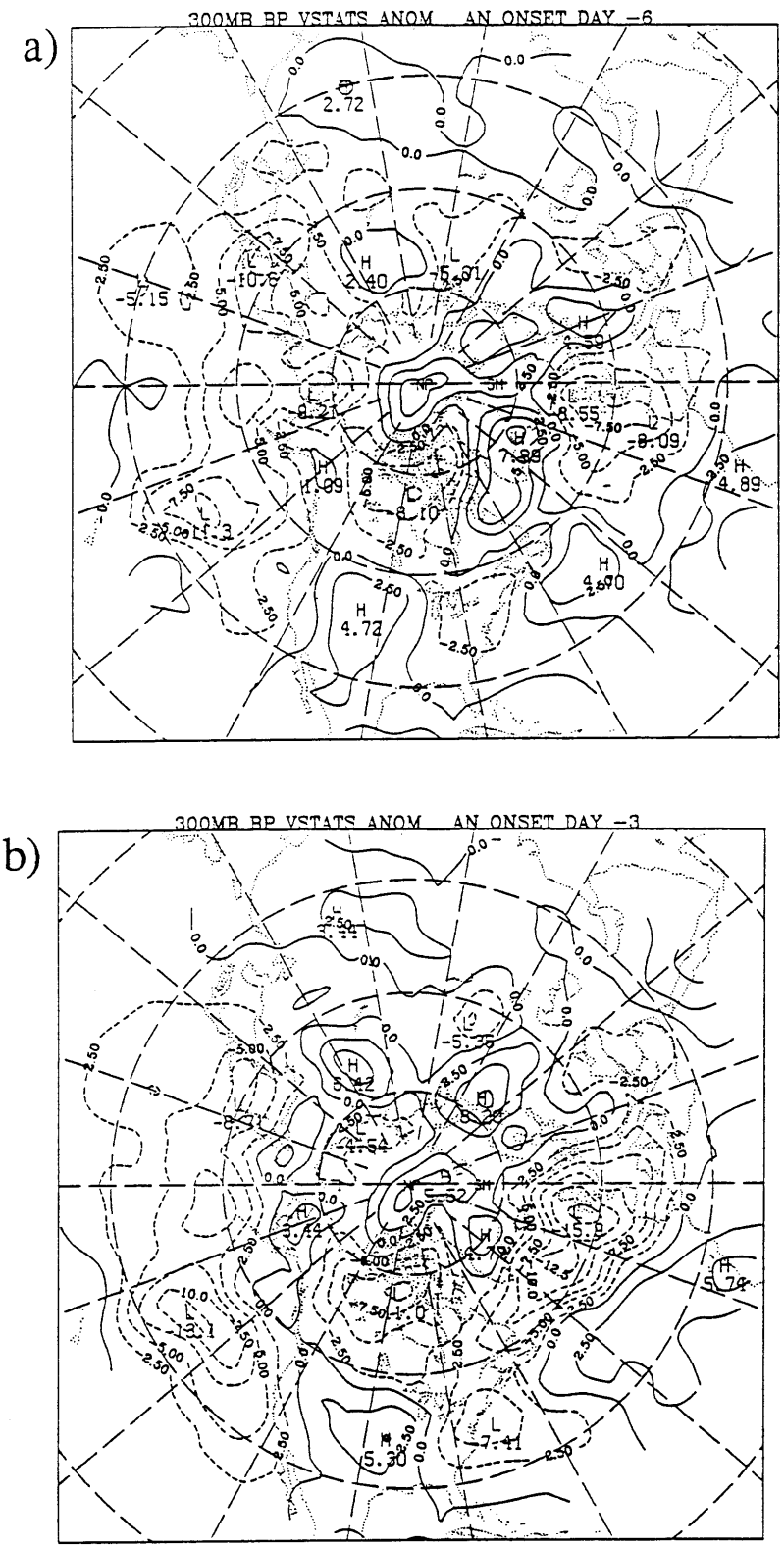

Fig. 4.9. Composite anomalies of the 300 mb VSTATs (m) for days a) -6 and b) -3 during the onset of Atlantic negative persistent anomaly cases.

c)

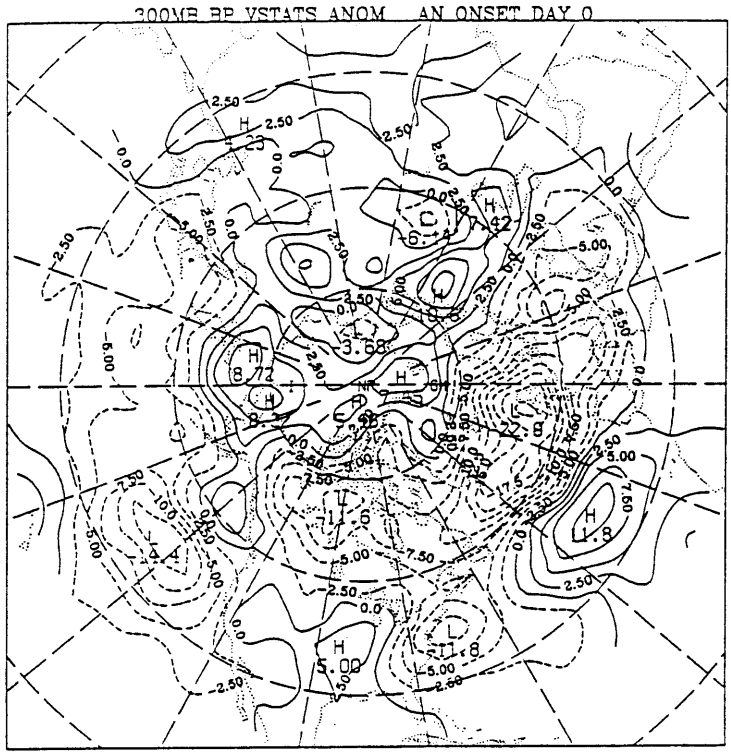

d)

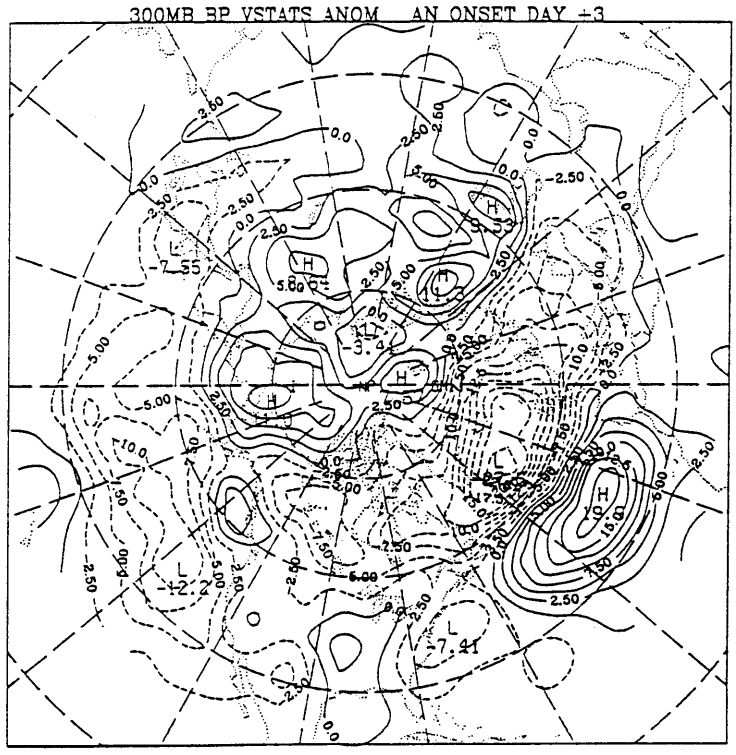

Fig. 4.9 (cont). Composite anomalies of the 300 mb VSTATs (m) for days c) 0 and d) +3 during the onset of Atlantic negative persistent anomaly cases.

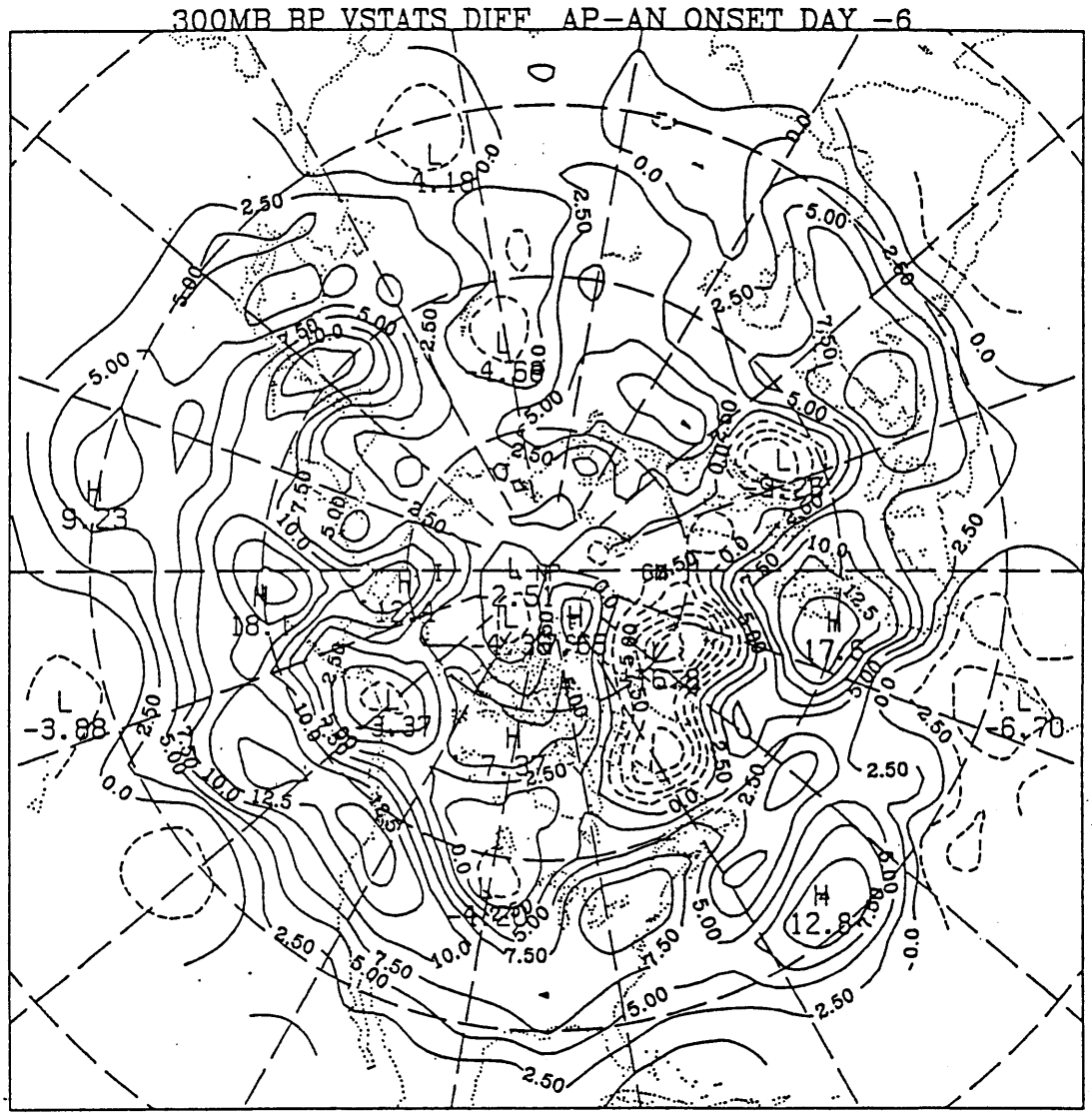

Fig. 4.10. Composite difference between the 300 mb VSTATs (m) at day -6 during the onset of Atlantic positive and negative PA cases.

Similar analyses of eddy activity anomalies during the onset of Pacific positive and negative PAs are shown in Figs. 4.11 and 4.12 respectively. (Corresponding large-scale flow development analyses were shown in Figs 3.7 and 3.9.) In general, the Pacific developments are broadly similar to their counterparts over the Atlantic. The development phase is characterized by broad regions of eddy activity anomalies upstream of the key region having the same sign as the developing PA. The main region of upstream eddy activity anomalies at day -6 is smaller than observed during the Atlantic cases and is generally confined to the Asian continent. In addition, there is the development of the primary VSTAT anomaly dipole associated with the amplification of the large-scale flow anomalies. Again the development of the positive half of this dipole during the negative events lags its positive counterpart by several days. The overall magnitude of the VSTAT anomalies throughout the development of the Pacific negative cases is the weakest of the four PA cases studied.

Changes in eddy activity that accompany the breakdown of the Atlantic positive PA events are shown in Fig 4.13. Here the composite VSTAT anomalies at 3 day intervals between days -6 and +3 of breakdown are shown. At day -6 of breakdown, the large-scale flow is essentially similar to that observed at day +6 of onset (Fig 3.11). The VSTAT anomaly patterns at this time are also broadly similar to the patterns observed at day +6 of onset with a large north-south oriented dipole dominating the pattern. However, the broad region of enhanced eddy activity that characterizes the onset and mature phase of the PA has weakened considerably, so that there is no longer an obvious sign of the hemispheric-mean VSTAT anomalies. This weakening in most notable over the central Pacific and eastern North America regions, where enhanced eddy activity has been replaced by suppressed activity. As the large-scale breakdown continues, the upstream negative anomalies increase, so that by day 0, most of the North Pacific basin is characterized by

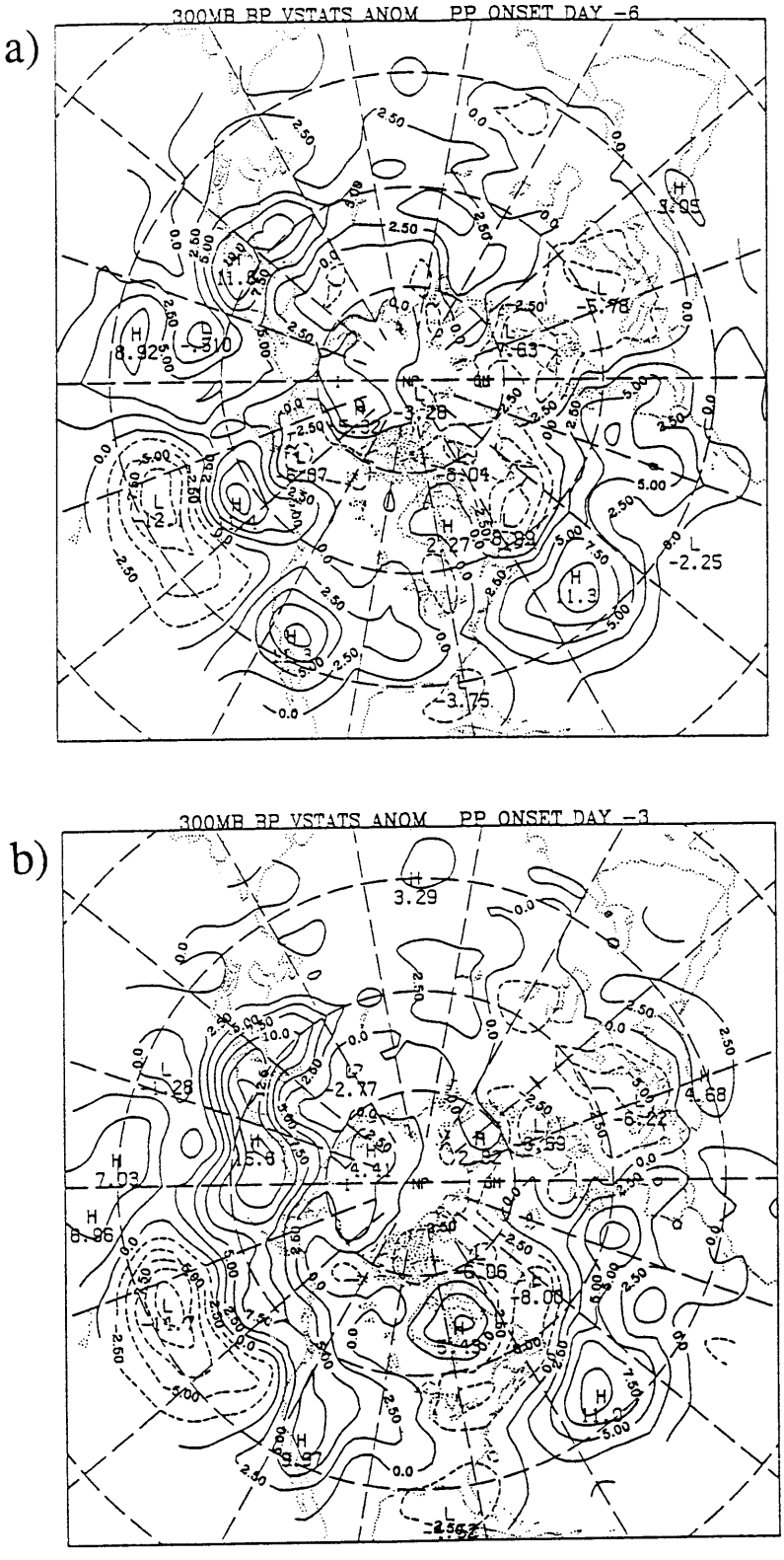

Fig. 4.11. Composite anomalies of the 300 mb VSTATs (m) for days a) -6 and b) -3 during the onset of Pacific positive persistent anomaly cases.

c)

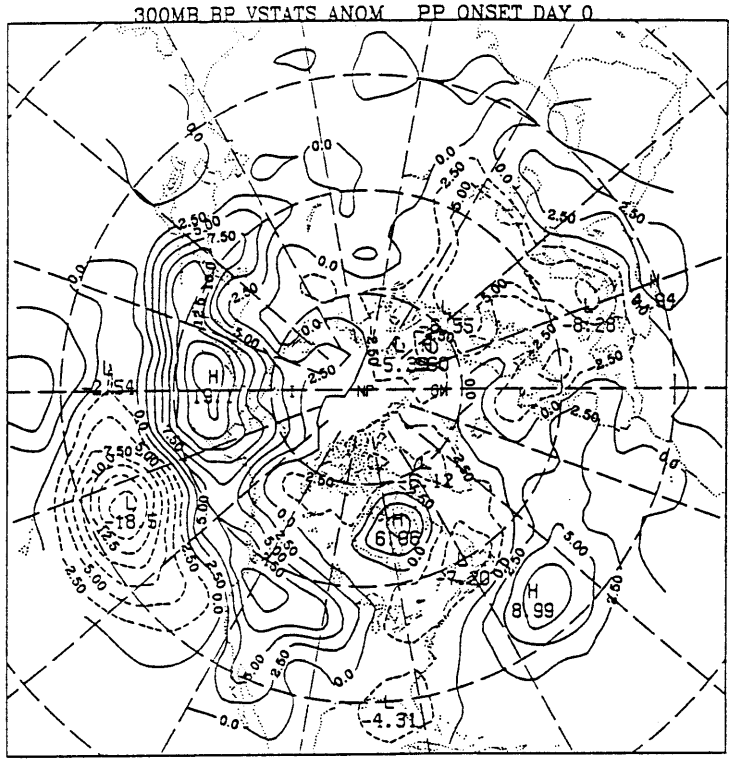

d)

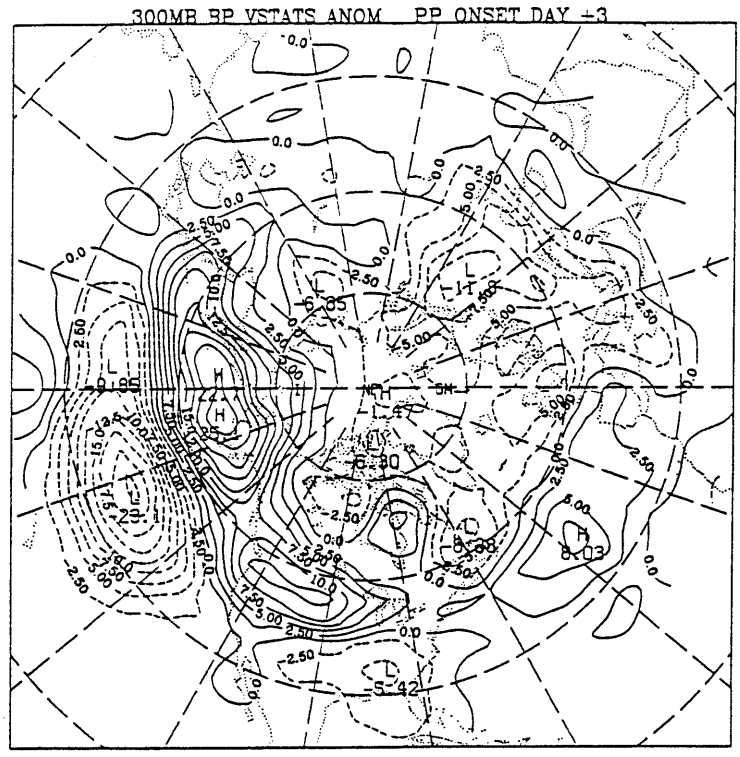

Fig. 4.11 (cont). Composite anomalies of the 300 mb VSTATs (m) for days c) 0 and d) +3 during the onset of Pacific positive persistent anomaly cases.

a)

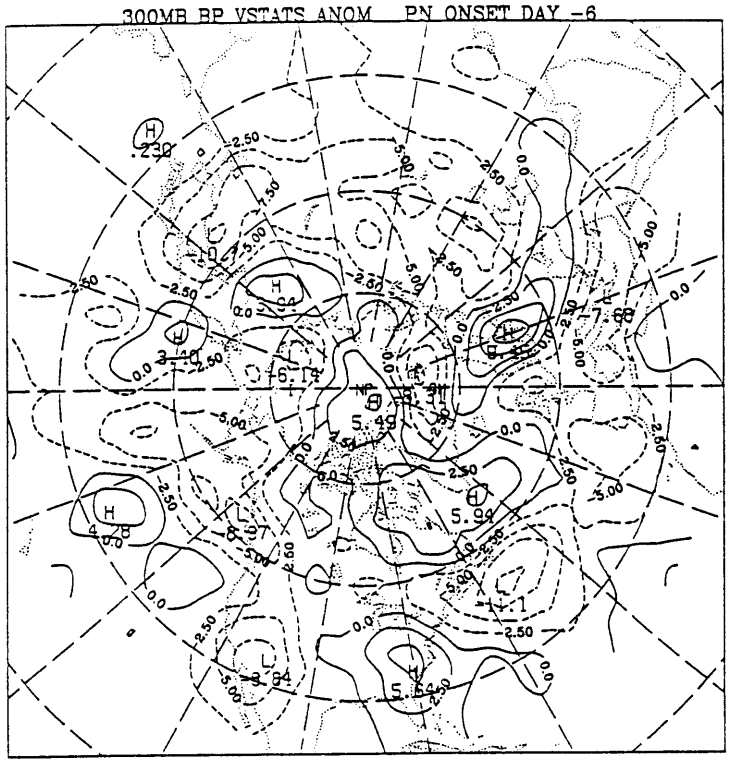

b)

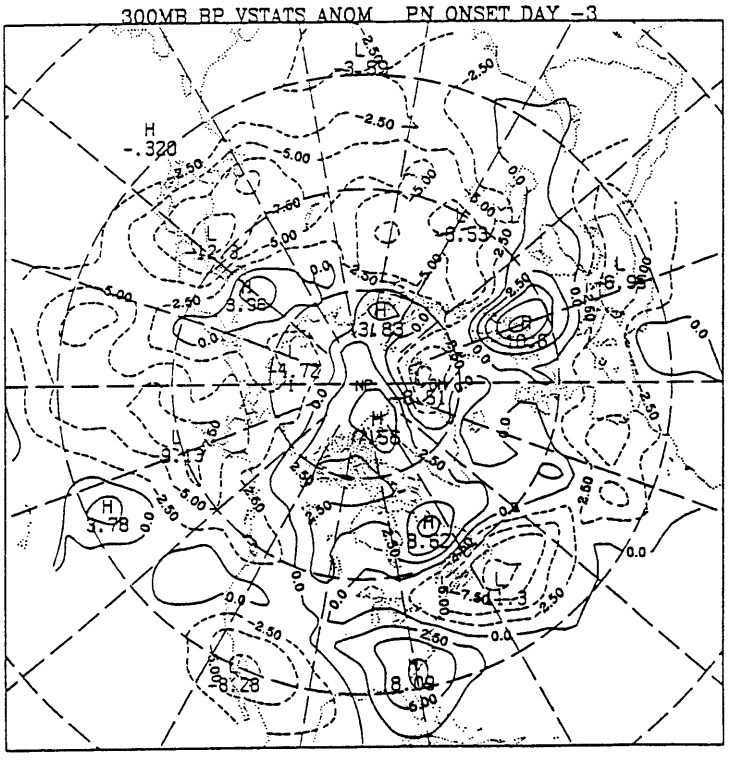

Fig. 4.12. Composite anomalies of the 300 mb VSTATs (m) for days a) -6 and b) -3 during the onset of Pacific negative persistent anomaly cases.

c)

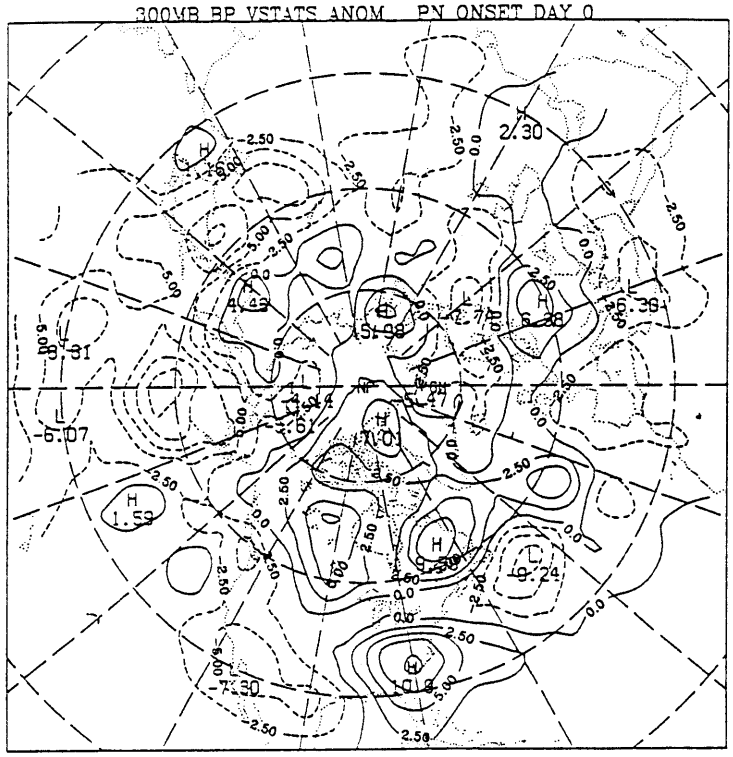

d)

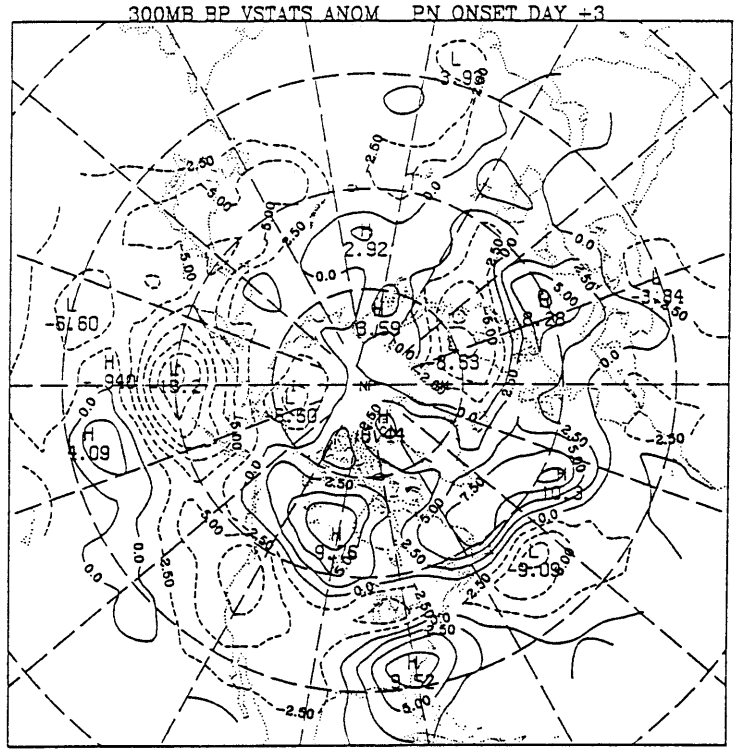

Fig. 4.12 (cont). Composite anomalies of the 300 mb VSTATs (m) for days c) 0 and d) +3 during the onset of Pacific negative persistent anomaly cases.

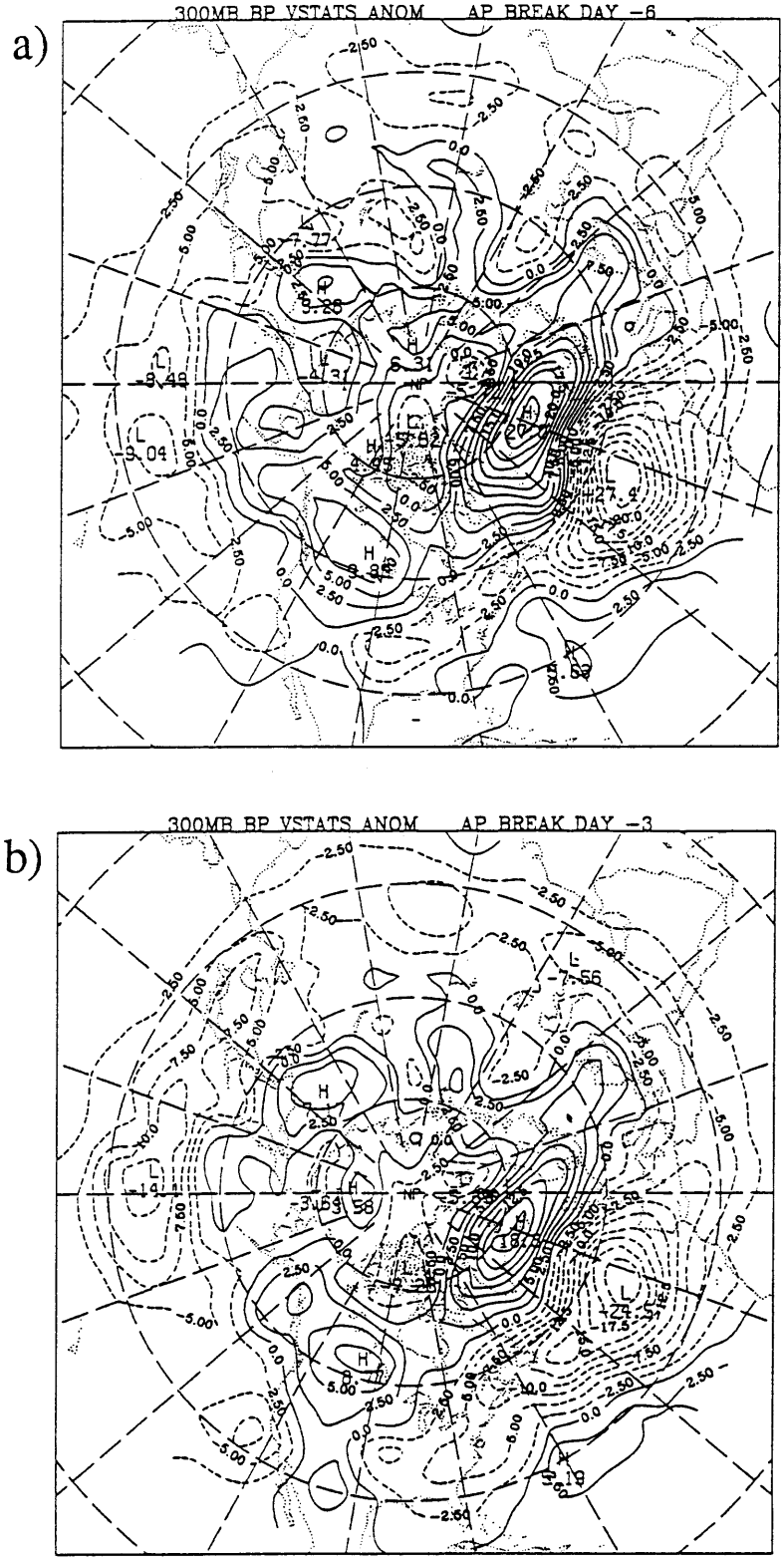

Fig. 4.13. Composite anomalies of the 300 mb VSTATs (m) for days a) -6 and b) -3 during the breakdown of Atlantic positive persistent anomaly cases.

c)

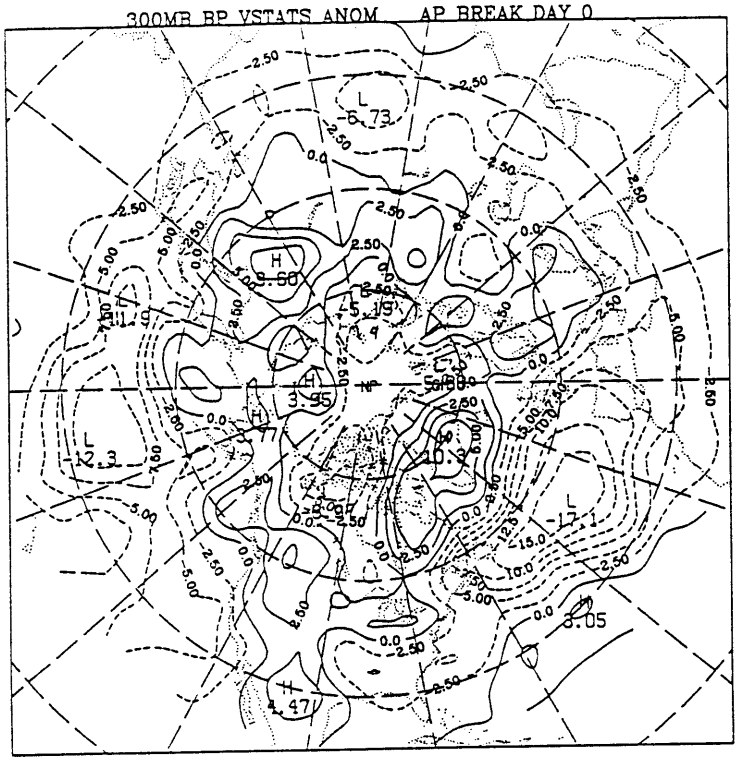

d)

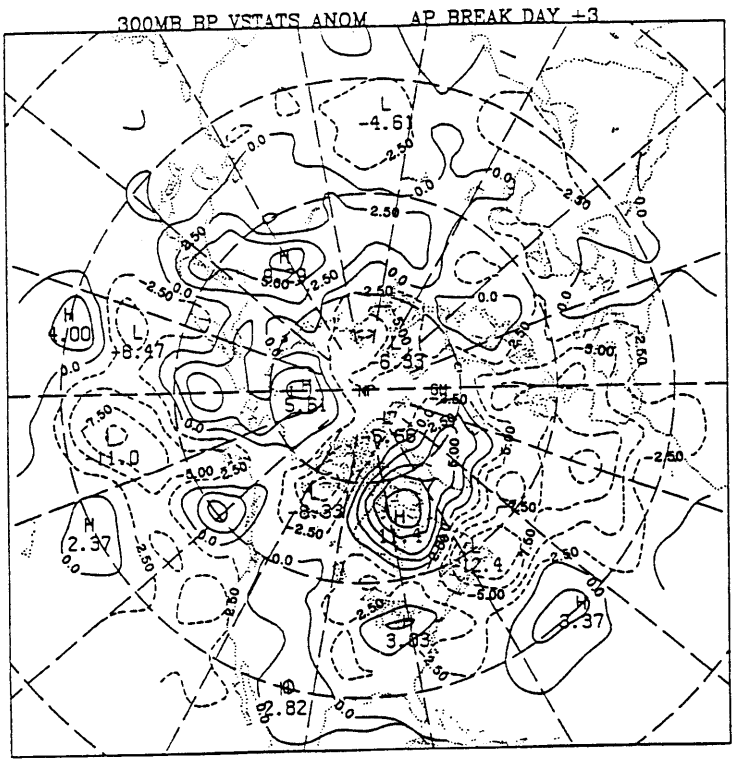

Fig. 4.13 (cont). Composite anomalies of the 300 mb VSTATs (m) for days c) 0 and d) +3 during the breakdown of Atlantic positive persistent anomaly cases.

weaker than normal eddy activity. Between days -3 and +3, the primary VSTAT anomaly dipole weakens considerably and retrogresses westward toward Canada.

The changes in the character of the synoptic-scale eddy activity during the onset and breakdown phases of the large-scale flow is further illustrated in Fig 4.14. This shows the differences in the VSTATs between these two phases (breakdown minus onset) of the Atlantic positive cases. The map is characterized by negative differences in and upstream of the key region, including a majority of both the North Atlantic and North Pacific oceans. This implies that relative to the onset of positive Atlantic PAs, the breakdown phase consists of a general reduction of eddy activity, most notably in the upstream storm tracks.

If enhancement of the upstream eddy activity is important for the development of blocks, as has been suggested (e.g. Haines and Marshall, 1987), then a reduction and reversal in the anomalous eddy activity may be important in its breakdown. The observed reduction and reversal of sign of the observed VSTAT anomalies over eastern North America during the breakdown of the Atlantic positive PAs would be consistent with that hypothesis. This upstream eddy activity reduction first appears as a westward expansion rather than a propagation of the suppressed half of the primary VSTAT anomaly dipole. Since the primary anomaly dipole appears to be directly related to the large-scale PA flow pattern, the large-scale flow may also be the cause for the westward expansion of suppressed activity. Thus the PA itself, may be indirectly responsible for its own demise as it weakens the eddy source needed to maintain itself against dissipation (Green, 1977) and advection (Austin, 1980).

The sequence of anomalous VSTATs during the breakdown (days -6 to +3) of the Atlantic negative cases is shown in Fig 4.15. As during onset, the changes in eddy activity during breakdown of the Atlantic negative cases are symmetric with those observed in the positive cases. The upstream reduction in eddy activity that characterized the onset period,

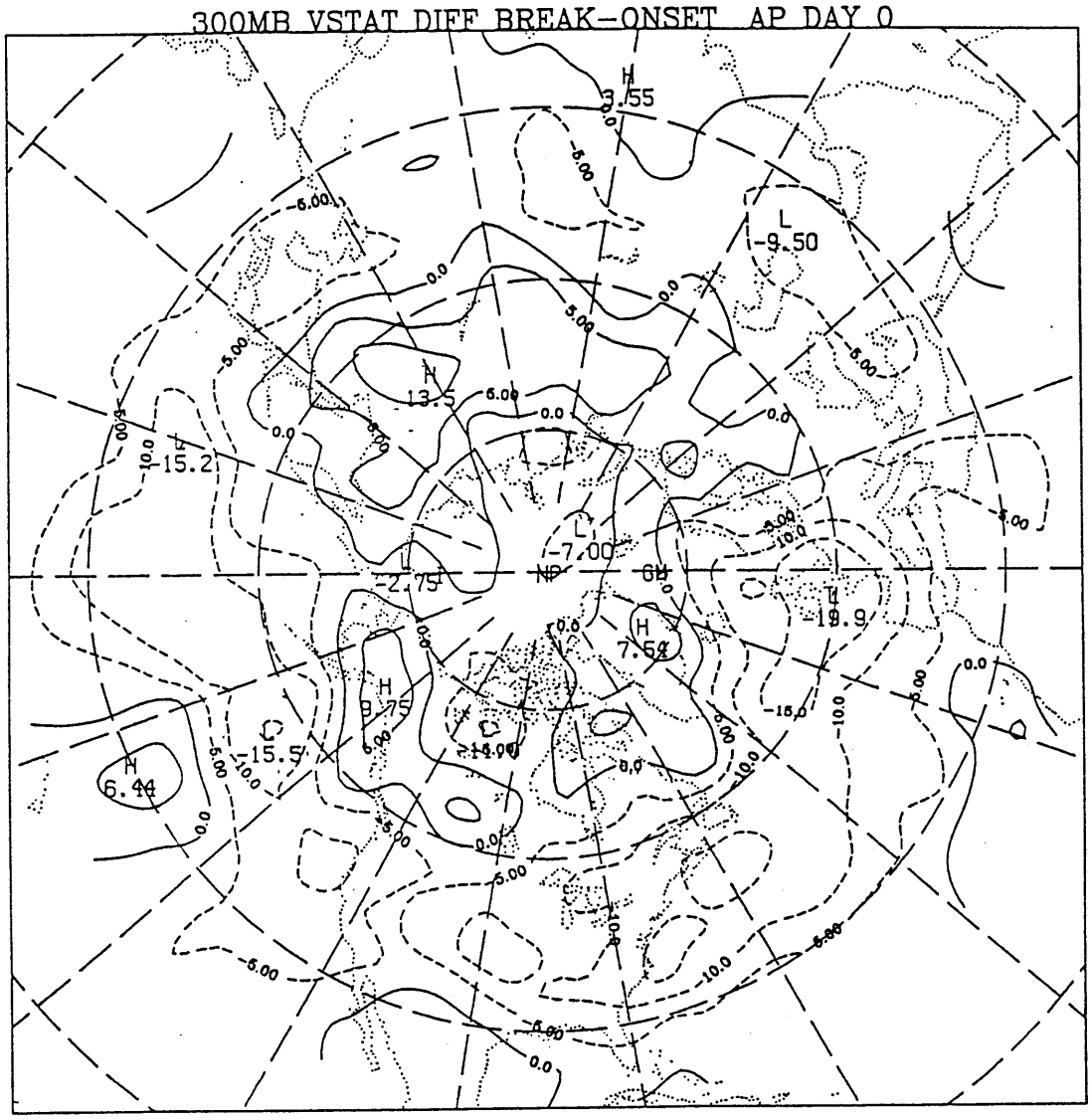

Fig. 4.14. Difference between the 300 mb VSTATs (m) at days 0 of breakdown and onset of Atlantic positive PA events.

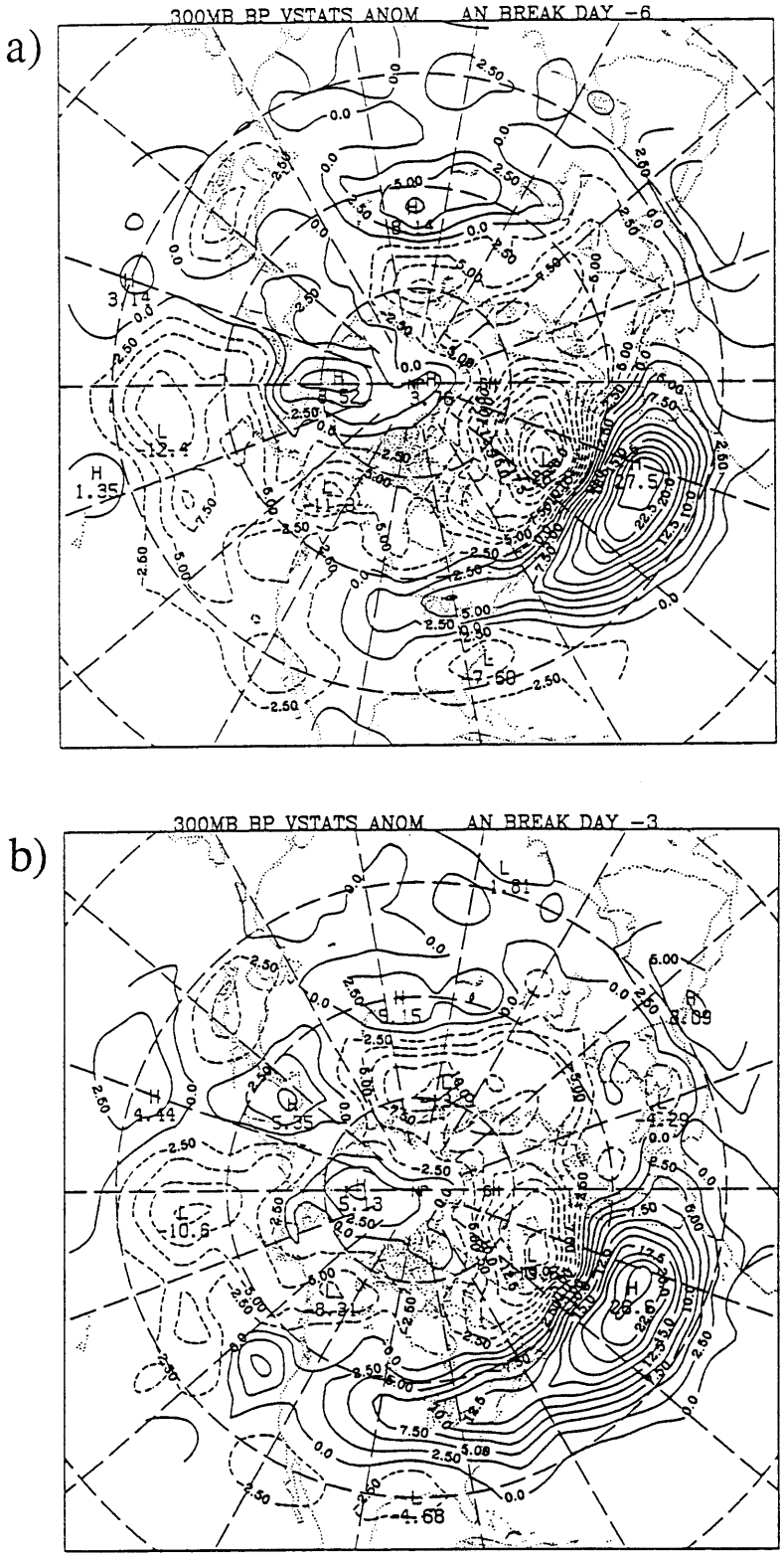

Fig. 4.15. Composite anomalies of the 300 mb VSTATs (m) for days a) -6 and b) -3 during the breakdown of Atlantic negative persistent anomaly cases.

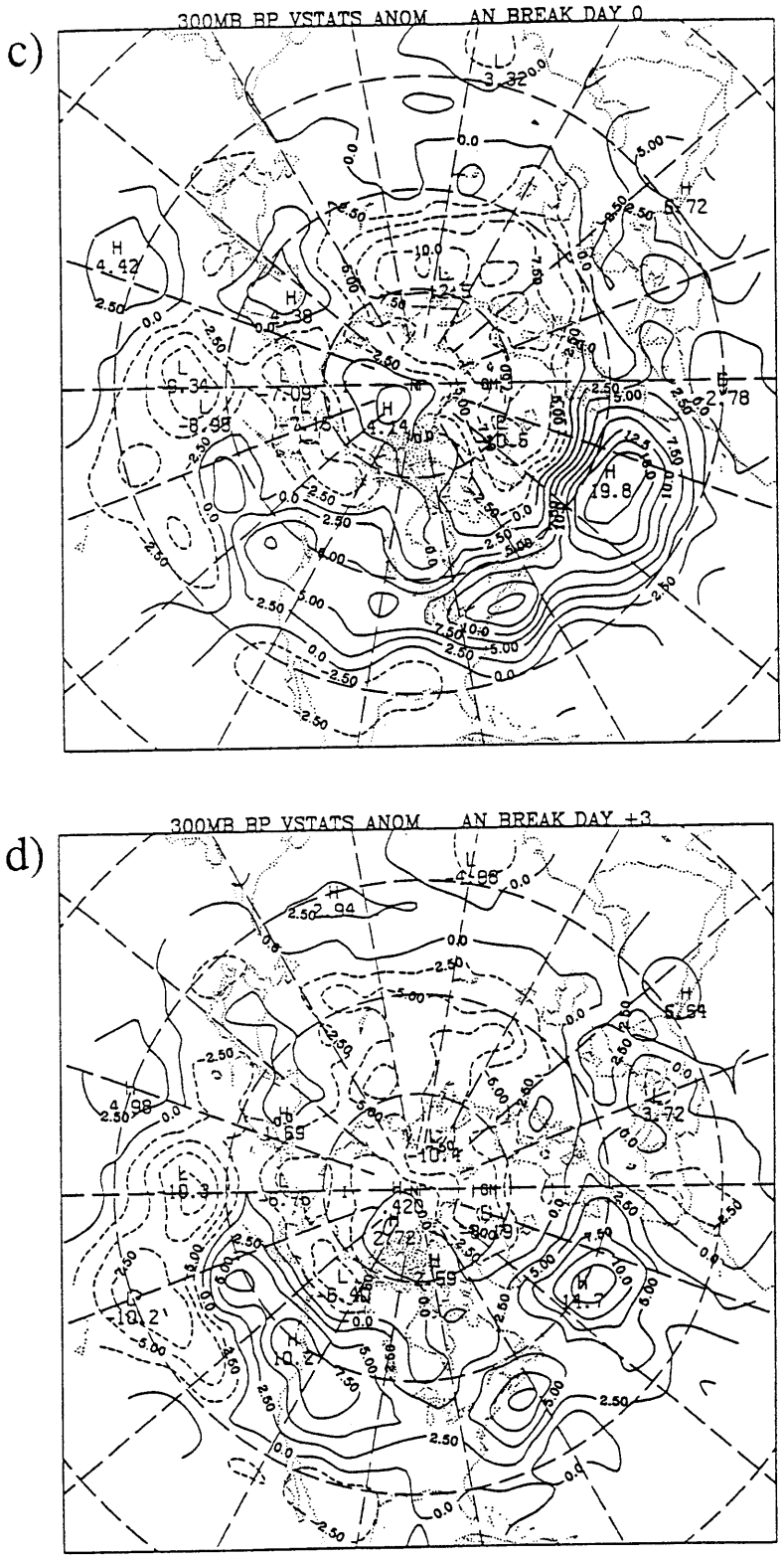

Fig. 4.15 (cont). Composite anomalies of the 300 mb VSTATs (m) for days c) 0 and d) +3 during the breakdown of Atlantic negative persistent anomaly cases.

slowly weakens and reverses during the breakdown phase in association with a westward extension of the primary region of enhanced eddy activity over the Atlantic. Whereas the onset period of the negative PA cases is characterized by a weaker than normal eddy activity over the Atlantic storm track, the breakdown phase is characterized by an anomalously strong storm track. Fig 4.16 shows the differences in eddy activity between the breakdown and onset periods. Relative to onset, the breakdown phase is characterized by an increased level of eddy activity over most of the region near and upstream of the PA. However, unlike the positive PA cases, the upstream VSTAT changes associated with the negative cases appear mainly confined to the North American sector, as suppressed eddy activity over the Pacific remains throughout the breakdown of the negative cases. Although there is a clear westward and northward expansion of the primary region of enhanced eddy activity during breakdown, there is little evidence of any propagation of the primary eddy activity dipole during the breakdown of the large-scale flow anomalies (Fig. 3.12).

The anomalous VSTATs that accompany the breakdown of the Pacific PA cases are shown in Figs. 4.17 and 4.18. Most of the anomalous VSTAT features associated with the Atlantic breakdowns can be identified in the Pacific cases as well. Prior to the breakdown of the Pacific positive (negative) cases, the enhanced (suppressed) eddy activity over eastern Asia characteristic of the onset and mature phase weakens considerably and even reverses sign. However, there is not a clear association of this upstream anomaly weakening with an expansion of the southern half of the principle VSTAT anomaly as in the Atlantic cases. Instead the changes appear to be mostly related to a general weakening of the the eddy activity along the principal storm track. In general, the VSTAT anomaly breakdown sequence for the Pacific cases does not follow as clear a pattern as the Atlantic cases.

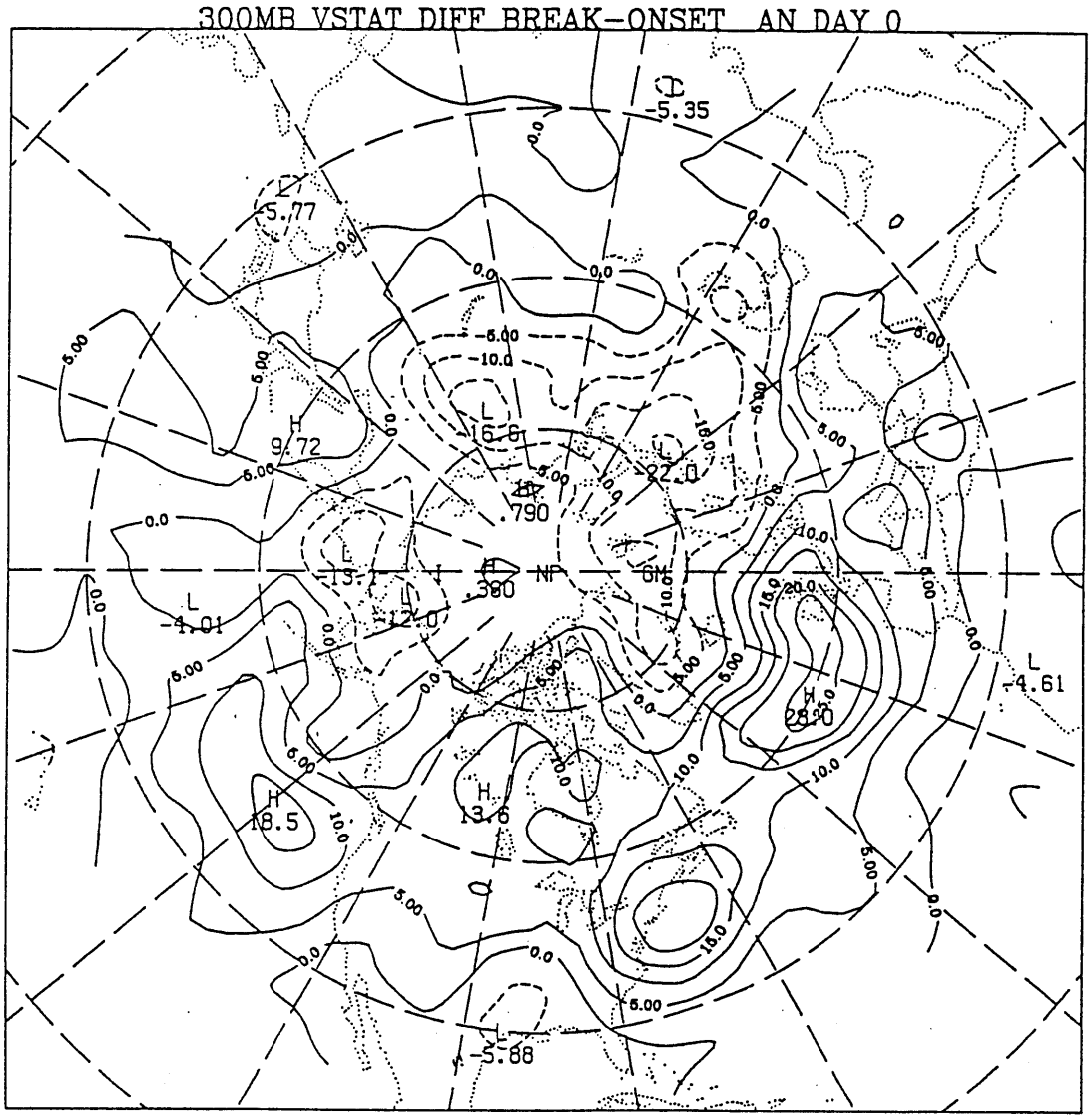

Fig. 4.16. Difference between the 300 mb VSTATs (m) at days 0 of breakdown and onset of Atlantic negative PA events.

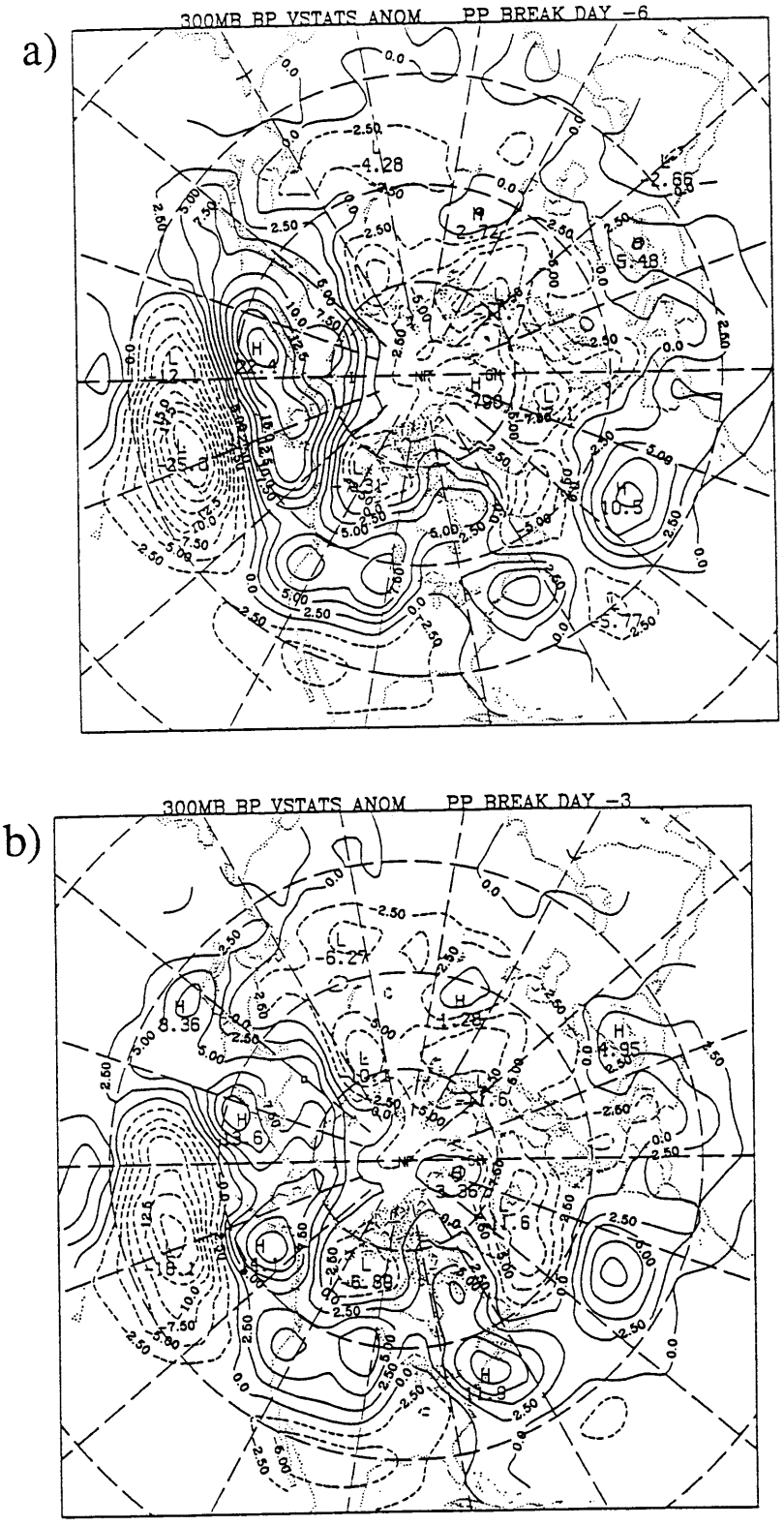

Fig. 4.17. Composite anomalies of the 300 mb VSTATs (m) for days a) -6 and b) -3 during the breakdown of Pacific positive persistent anomaly cases.

c)

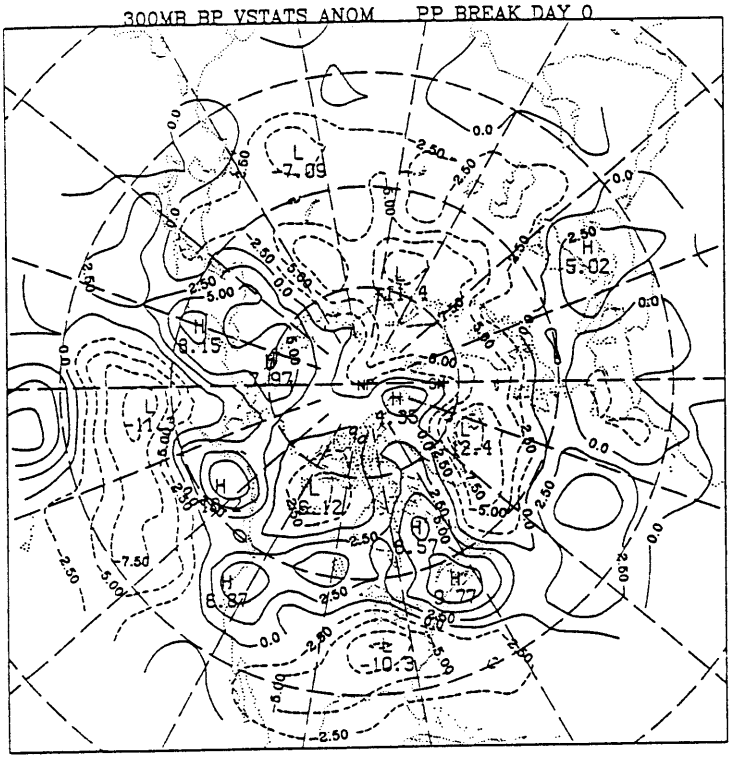

d)

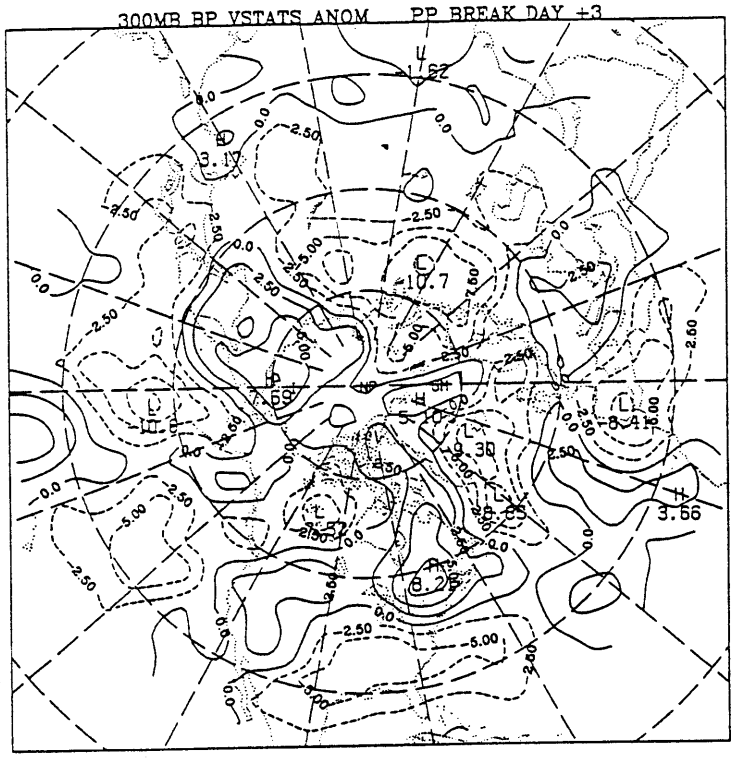

Fig. 4.17 (cont). Composite anomalies of the 300 mb VSTATs (m) for days c) 0 and d) +3 during the breakdown of Pacific positive persistent anomaly cases.

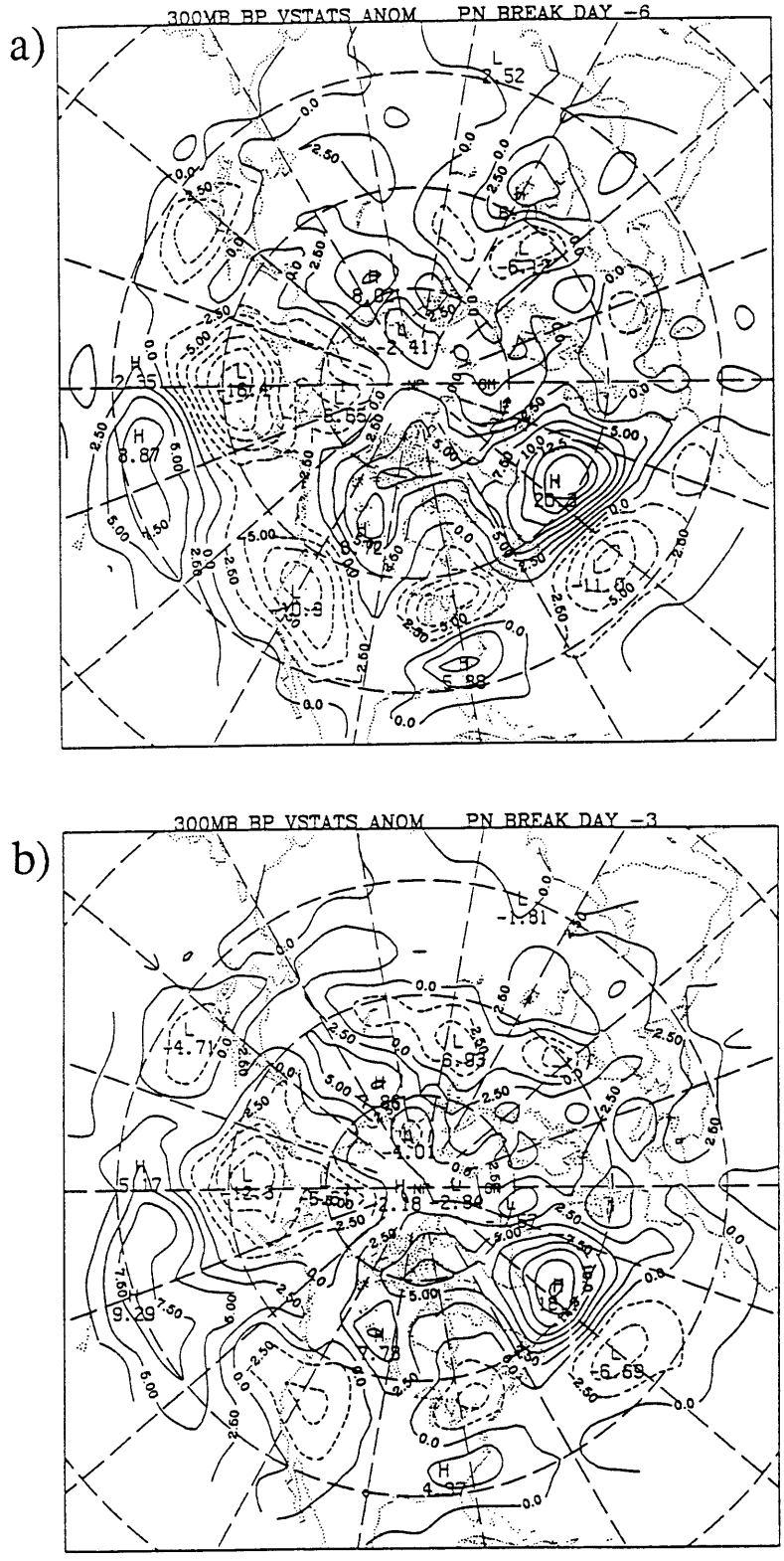

Fig. 4.18. Composite anomalies of the 300 mb VSTATs (m) for days a) -6 and b) -3 during the breakdown of Pacific negative persistent anomaly cases.

c)

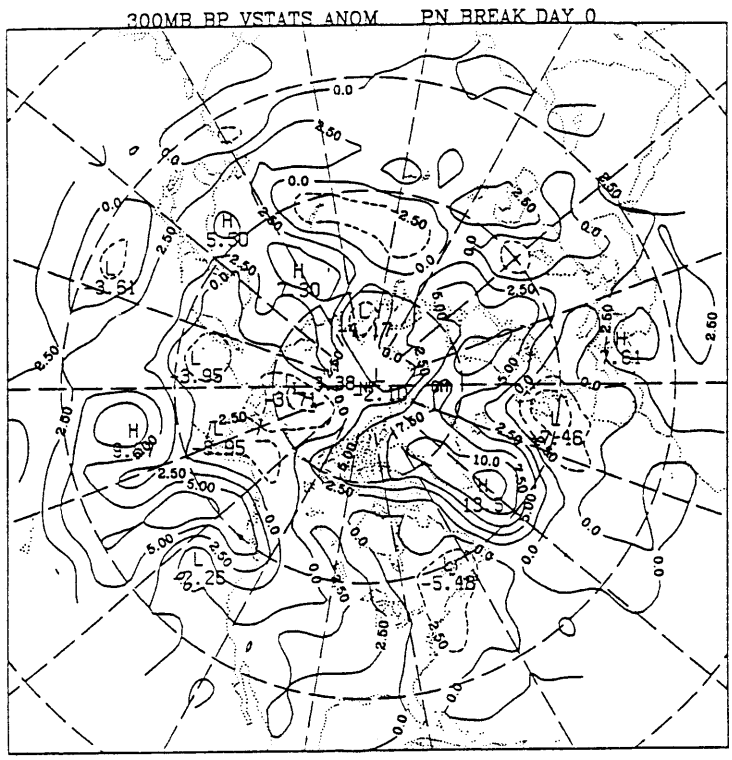

d)

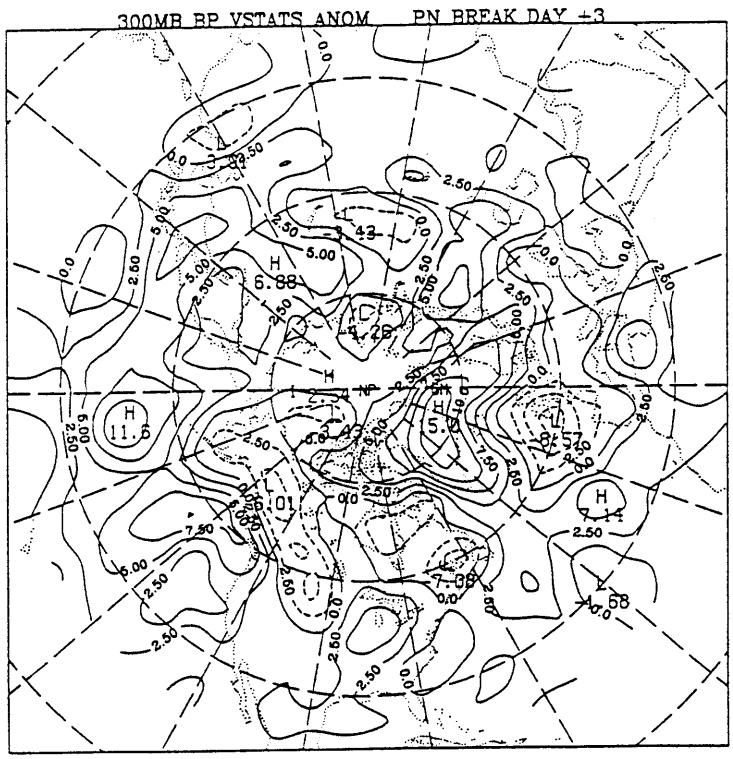

Fig. 4.18 (cont). Composite anomalies of the 300 mb VSTATs (m) for days c) 0 and d) +3 during the breakdown of Pacific negative persistent anomaly cases.

4.5 Eddy Potential Enstrophy and Eddy Heat Fluxes.

In order to provide alternate measures of the changes in eddy activity during the life cycles of persistent anomalies, we present analyses based on two alternative eddy parameters: anomalous quasi-geostrophic eddy potential enstrophy ($q'^2/2$) and anomalous eddy heat fluxes ($V'T'$). Our motivation here is to provide a more complete description of the eddy variations, as well as to verify the basic VSTAT results using different eddy parameters and techniques. These results also provide further confirmation that regions of eddy growth and decay have changed considerably during these times, and therefore that the effects of anomalous eddy forcing terms should be considered in the evolution of the large-scale flow anomalies as addressed in the next chapter.

The quasi-geostrophic eddy potential enstrophy is defined as

$$QGPE = \frac{1}{2} q'^2$$

where q' is the quasi-geostrophic pseudo-potential vorticity

$$q' = \frac{1}{f_o}\nabla^2\Phi' + f_o \frac{\partial}{\partial p}\frac{1}{\sigma}\frac{\partial \Phi'}{\partial p}$$

and Φ' is the eddy geopotential and $\sigma(p)$ is the static stability parameter $\frac{1}{\rho\theta}\frac{\partial\theta}{\partial p}$. The QGPE is evaluated on isobaric surfaces using a hemispheric-mean static stability, geostrophic winds and bandpass filtered quantities for the primed variables. It is an instantaneous measure of the local magnitude of the the synoptic-scale eddies. Thus, during the relatively rapid onset and decay phases of the PA's, QGPE anomalies may present a sharper temporal picture of the eddy activity changes than do the 10-day mean VSTATs.

Fig 4.19 presents the composite anomalies of the 300mb QGPE evaluated at day 0 during the onset of each of the PA types considered here. Comparison with the previous results indicates that the QGPE and VSTAT results are qualitatively similar. The principle QGPE anomaly features include a north-south (Atlantic cases) or northwest-southeast (Pacific cases) aligned anomaly dipole with the northern half of the dipole having the same sign as the developing large-scale geopotential height anomaly. There is also a broad region of anomalous QGPE activity upstream of the key point that has the same sign as the developing PA. As anticipated, QGPE composites are somewhat noisier than the corresponding VSTAT composites since the QGPE analysis technique does not have the same 10-day averaging. The results, however, demonstrate that the eddy activity changes diagnosed during the rapidly changing onset phase of the PAs using the VSTAT technique are not just reflections of the anomalies during the mature phase, but rather are representative of the eddy activity near the center of the 10-day period. QGPE composites at other times in the life cycles (not shown) maintain the same qualitative similarity to the corresponding VSTAT composites. This is consistent with the compositing capturing only the low-frequency variations of eddy activity, as was also shown for the geopotential height analyses (Sec 3.5).

The anomalous horizontal eddy heat fluxes ($\mathbf{V}'T'$) provide another description of the changes in eddy activity that occur during persistent anomalies. The eddy heat fluxes have been computed at 12h intervals throughout the PA life cycles. The heat fluxes were then averaged over various stages of the PA life cycle to provide a compact description of the principle changes occurring during the life cycles. Averages were computed in four stages: *prior* (days -10 to 0 of onset), *onset* (days -5 to +5 of onset), *case* (from day 0 of onset to day 0 of breakdown) and *break* (days -5 to +5 of breakdown). This temporal averaging,

a)

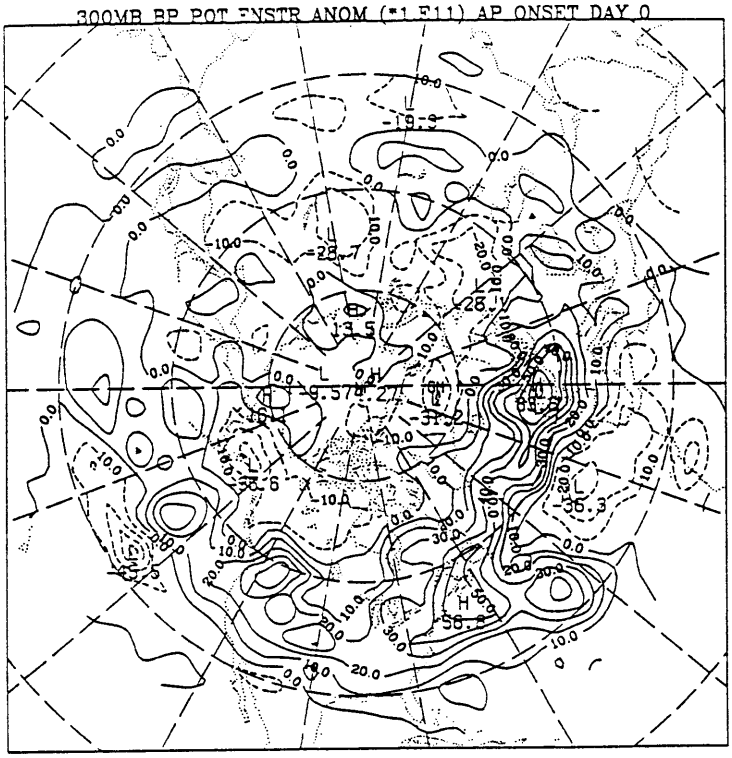

b)

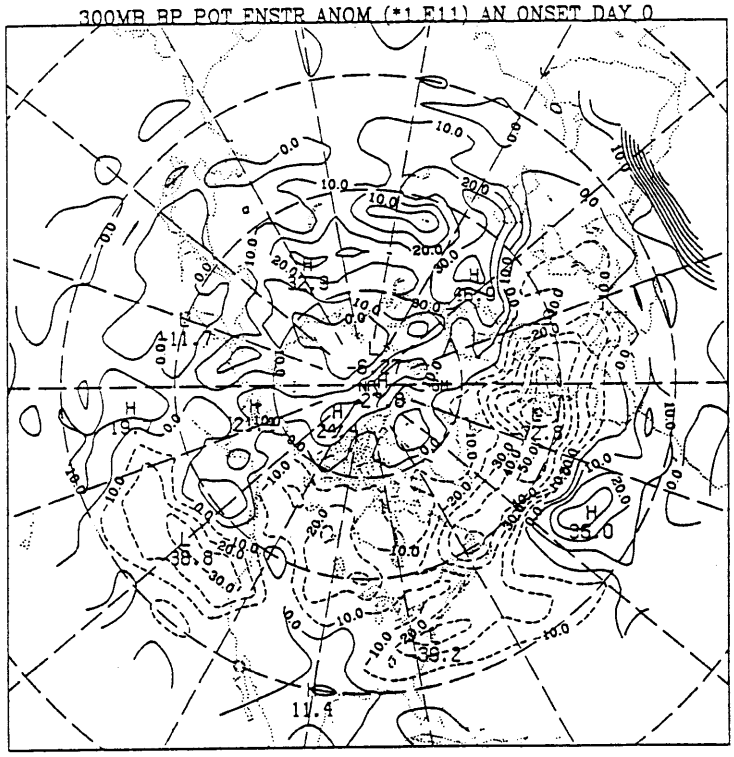

Fig. 4.19. Composite-mean anomalies of the 300mb quasi-geostrophic pseudo-potential enstrophy (s^{-2}) evaluated at day 0 during the onset of a) Atlantic positive and b) Atlantic negative persistent anomaly events. Contour interval 10 x 10^{-11} s^{-2}.

c)

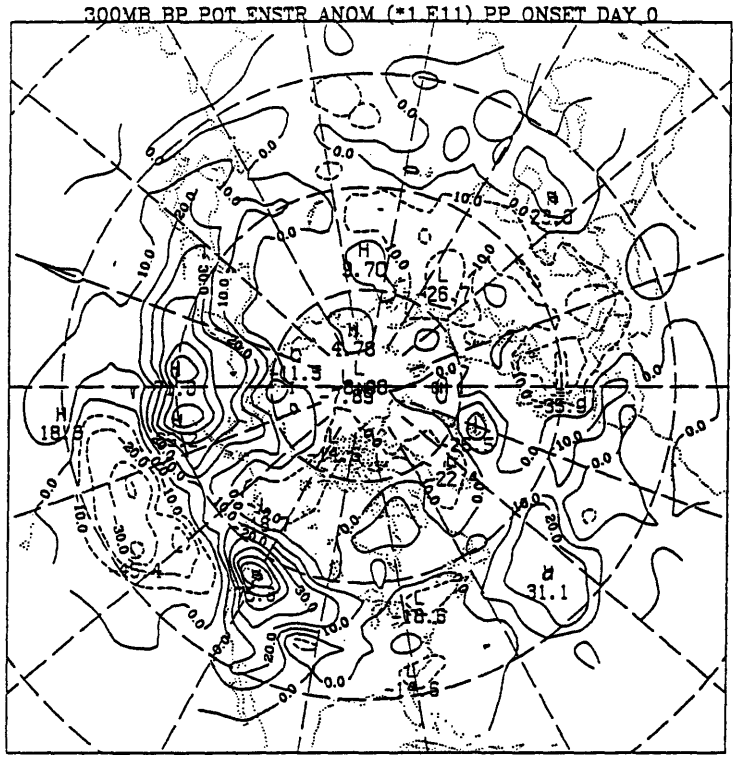

d)

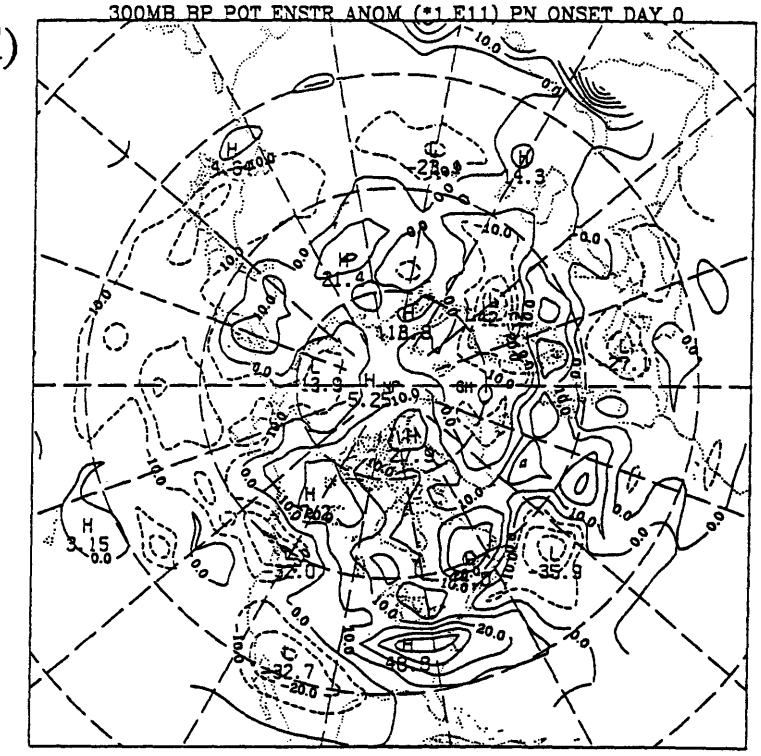

Fig. 4.19 (cont). Composite-mean anomalies of the 300mb quasi-geostrophic pseudo-potential enstrophy (s^{-2}) evaluated at day 0 during the onset of c) Pacific positive and d) Pacific negative persistent anomaly events. Contour interval 10 x 10^{-11} s^{-2}.

followed by the composite averaging[1], ensures that the heat fluxes represent a phase-averaged flux, and not instantaneous pointwise eddy values.

Fig. 4.20 presents the anomalous 700 mb eddy heat flux vectors during the life cycle of the Atlantic positive cases superimposed on the composite-mean 700 mb temperatures. This particular level is chosen as it is typically near the level of maximum synoptic-scale eddy heat fluxes. We see that prior to onset, the anomalous eddy heat fluxes are down the large-scale thermal gradient over a very broad region upstream of the developing PA pattern. These anomalous heat fluxes are well correlated with the anomalous VSTATs observed prior to onset (see Fig. 4.6, day -6) except for an upstream phase shift (approximately 15 degrees) of the heat fluxes. During the onset phase, the broad region of upstream anomalous eddy heat flux shifts eastward and increases in intensity so that very strong anomalous down gradient eddy heat fluxes are found all along and upstream of the main Atlantic storm track. This eddy heat flux pattern is strongly suggestive of anomalously strong baroclinic eddy growth occurring in the region. Rapid synoptic-scale baroclinic growth or "bombs" (Sanders and Gyakum, 1980) during the onset of some blocking cases has also been observed in some case studies (e.g. Colucci, 1985; Tsou and Smith, 1990). Although strong upstream cyclogenesis events appear to proceed the onset of blocking (Nakamura and Wallace, 1990), the occurrence of a bomb is neither a sufficient nor necessary condition for the development of blocking or positive persistent anomalies. The previous VSTAT results suggest that these upstream developments may reflect Petterssen and Smebye (1971) "type-B" or initial-value (Farrell, 1984) development as an abundance of primarily upper-level disturbances propagate into the region and subsequently grow.

---

[1] Recall that the bandpass eddies are generally incoherent with respect to the specific phase in the life cycle of the large-scale life cycle. Thus composite averaging with respect to the large-scale flow essentially averages over many different random phases of the synoptic-scale eddies.

During the mature phase of the PA, the anomalous eddy heat fluxes appear to be primarily dissipative of the large-scale thermal anomaly associated with the PA pattern. Similar relationships were also noted by Dole (1982) and Mullen (1987). Although the immediate upstream region is still characterized by anomalous downgradient heat fluxes, they are considerably weaker than observed during onset. Over the Pacific at this time, most of the anomalous eddy heat fluxes have reversed sign. During the breakdown phase, the anomalous eddy heat fluxes are almost exclusively upgradient over the entire domain (which primarily reflects weaker than normal downgradient fluxes).

During the Atlantic negative life cycle, the anomalous eddy heat fluxes (Fig 4.21) follow a similar cycle but with opposite sign. Although well prior to onset the anomalous heat fluxes are weak and erratic, much of the principle Atlantic storm track region from the Great Lakes eastward through 40W is characterized by weak upgradient anomalous eddy heat fluxes. During the onset period, the anomalous eddy heat fluxes are strong and uniformly upgradient in and upstream of the developing PA, suggesting that weaker than normal baroclinic growth is occurring. During the mature phase, the anomalous eddy heat fluxes again appear generally dissipative of the large-scale thermal anomaly. Immediately upstream of the PA center, the eddy heat fluxes remain anomalously upgradient. However, during the decay phase, these upstream fluxes reverse and have now become downgradient suggesting a return to a more normal or even enhanced baroclinic activity. During the Atlantic negative cases, the anomalous heat fluxes over the Pacific do not seem to follow a consistent pattern as observed during the positive cases.

The composite anomalous eddy heat flux patterns during the Pacific PAs are shown in Figs. 4.22 and 4.23 for the positive and negative cases respectively. The general features of the anomalous heat fluxes that were evident in the Atlantic cases can be seen in these cases as well. The 700 mb anomalous heat fluxes and 300 mb VSTAT anomalies are well correlated. Prior to onset of the positive (negative) cases, anomalous downgradient

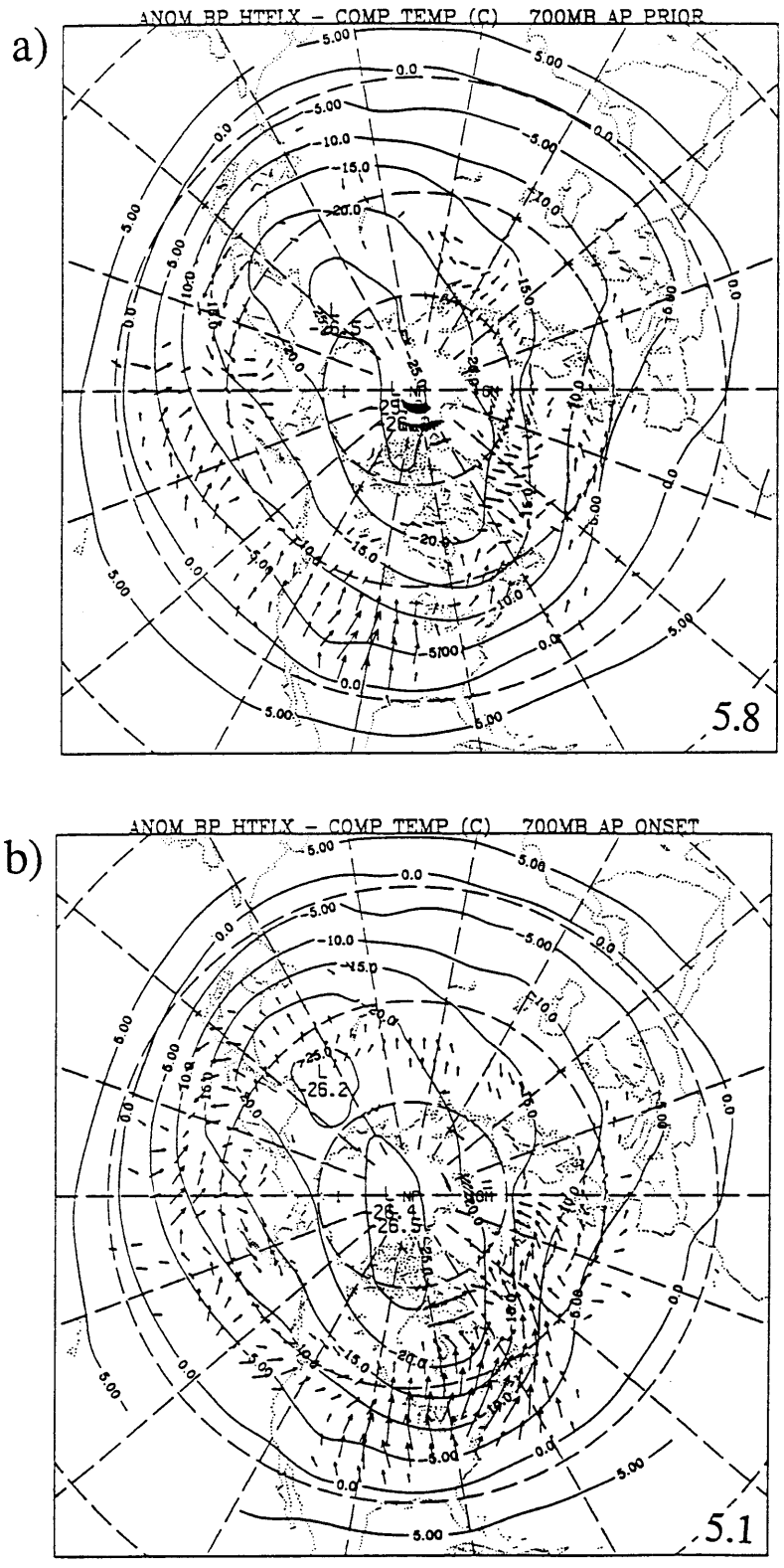

Fig. 4.20. Composite-mean 700mb bandpass heatflux anomaly vectors (C m s^{-1}) and the composite-mean 700 mb temperatures (C) during the a) prior and b) onset phases during the Atlantic positive PA cases. The magnitude of the maximum vector plotted in indicated in the lower-right corner of each panel. The winter mean bandpass heat flux at 700 mb is 15.1 C m s^{-1}.

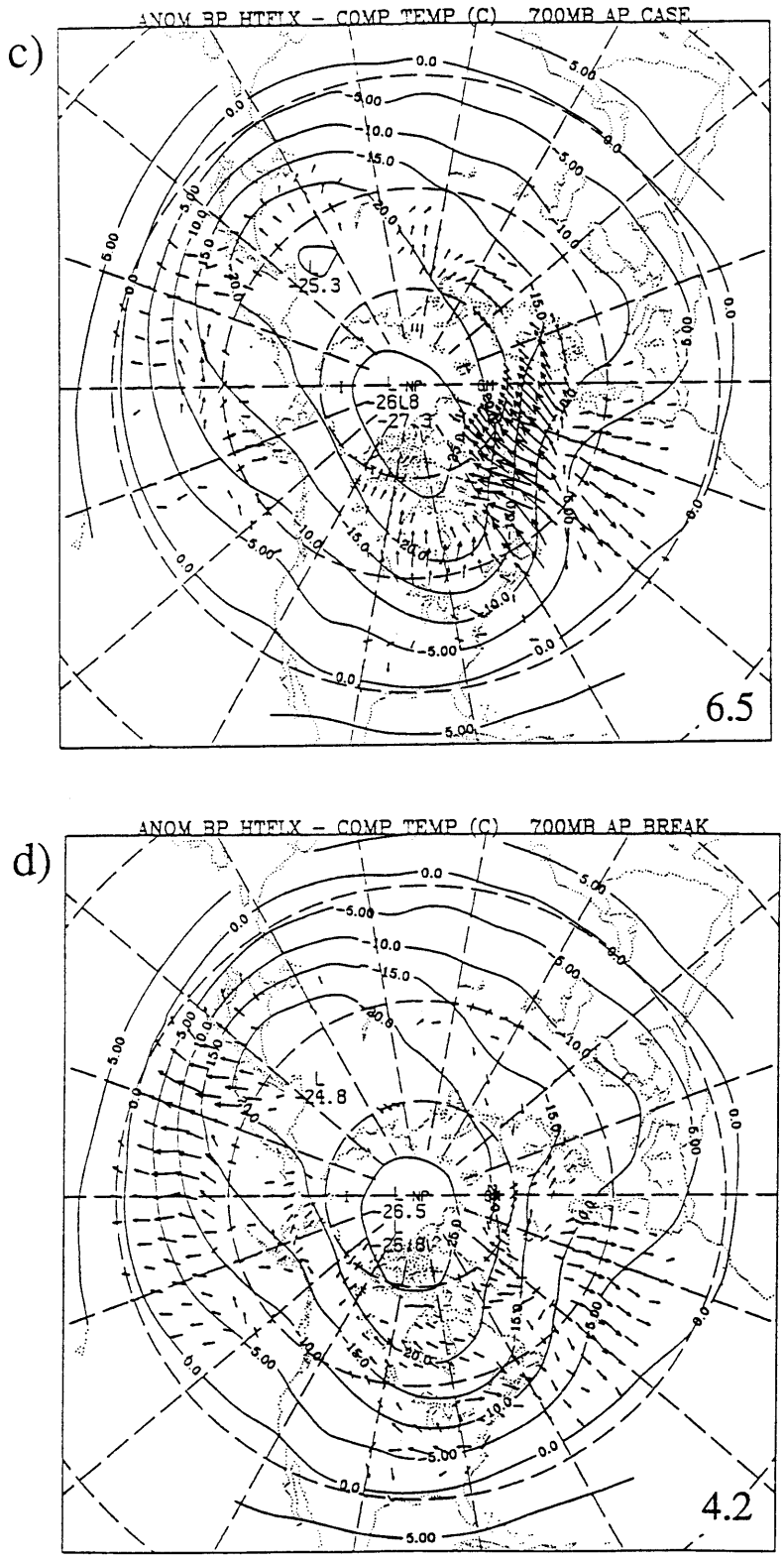

Fig. 4.20 (cont). Composite-mean 700mb bandpass heatflux anomaly vectors (C m s^{-1}) and the composite-mean 700 mb temperatures (C) during the c) case and d) breakdown phases during the Atlantic positive PA cases. The magnitude of the maximum vector plotted in indicated in the lower-right corner of each panel. The winter mean bandpass heat flux at 700 mb is 15.1 C m s^{-1}.

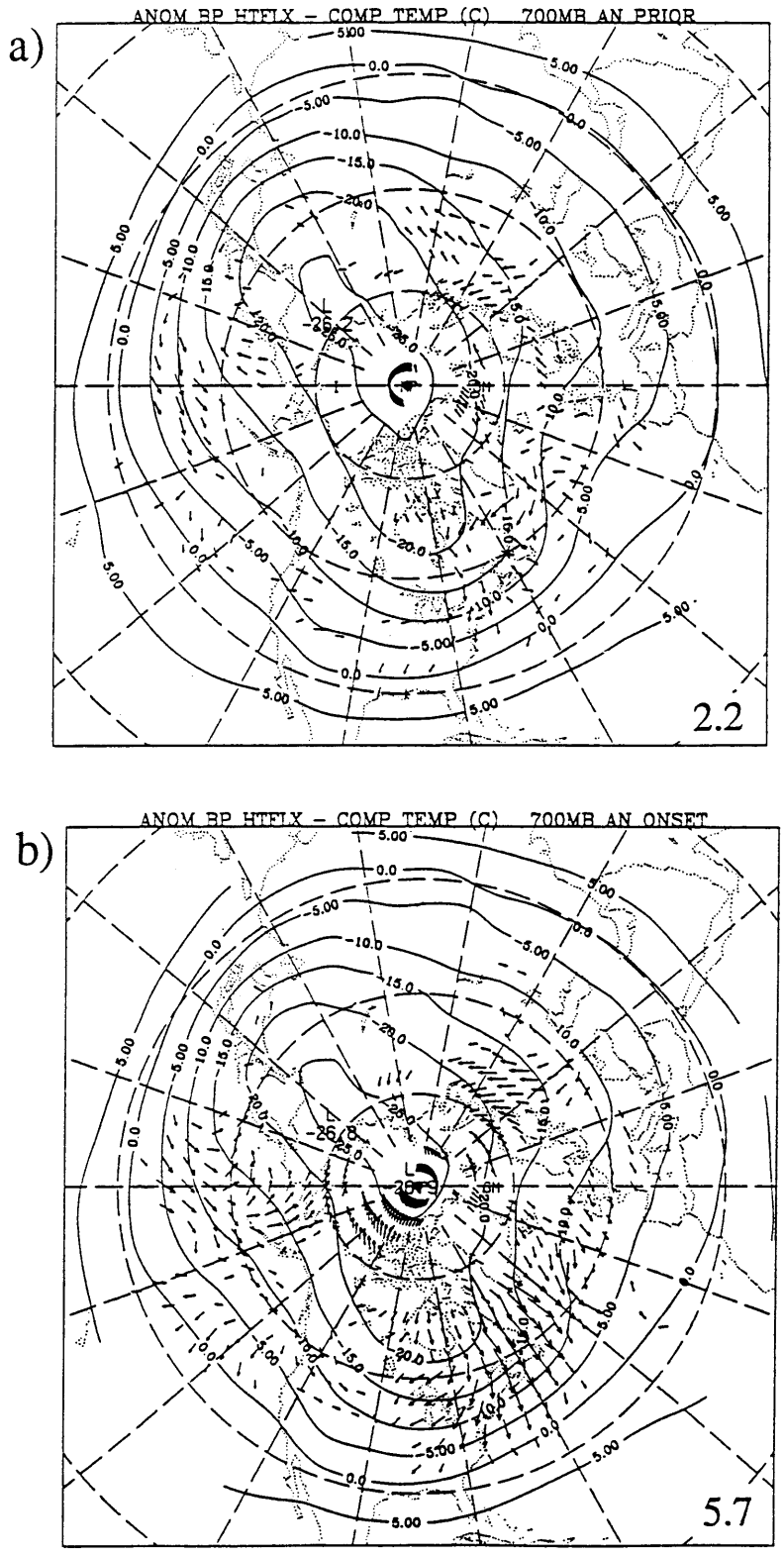

Fig. 4.21. Composite-mean 700mb bandpass heatflux anomaly vectors (C m s^{-1}) and the composite-mean 700 mb temperatures (C) during the a) prior and b) onset phases during the Atlantic negative PA cases. The magnitude of the maximum vector plotted in indicated in the lower-right corner of each panel. The winter mean bandpass heat flux at 700 mb is 15.1 C m s^{-1}.

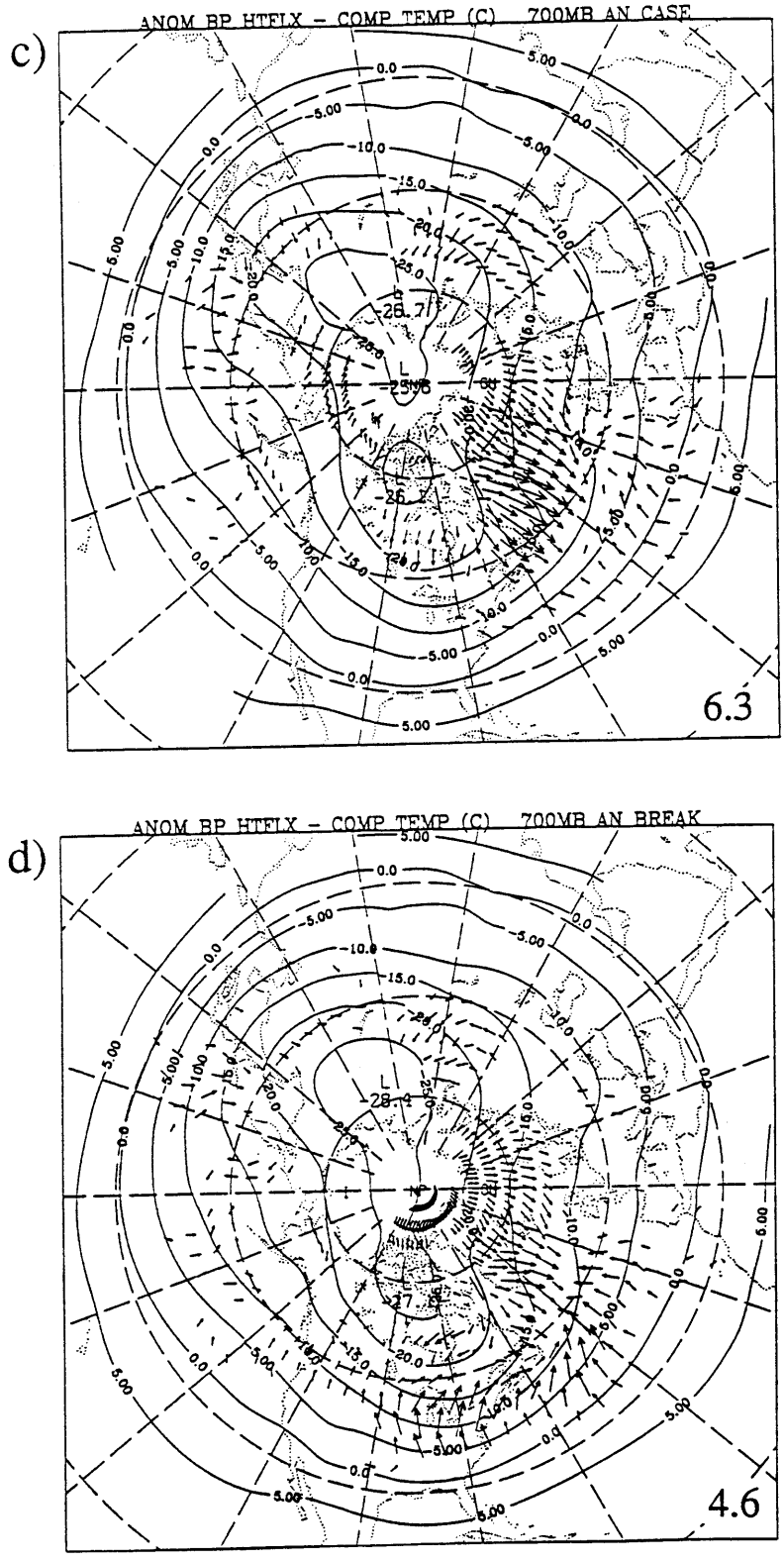

Fig. 4.21 (cont). Composite-mean 700mb bandpass heatflux anomaly vectors (C m s^{-1}) and the composite-mean 700 mb temperatures (C) during the c) case and d) breakdown phases during the Atlantic negative PA cases. The magnitude of the maximum vector plotted in indicated in the lower-right corner of each panel. The winter mean bandpass heat flux at 700 mb is 15.1 C m s^{-1}.

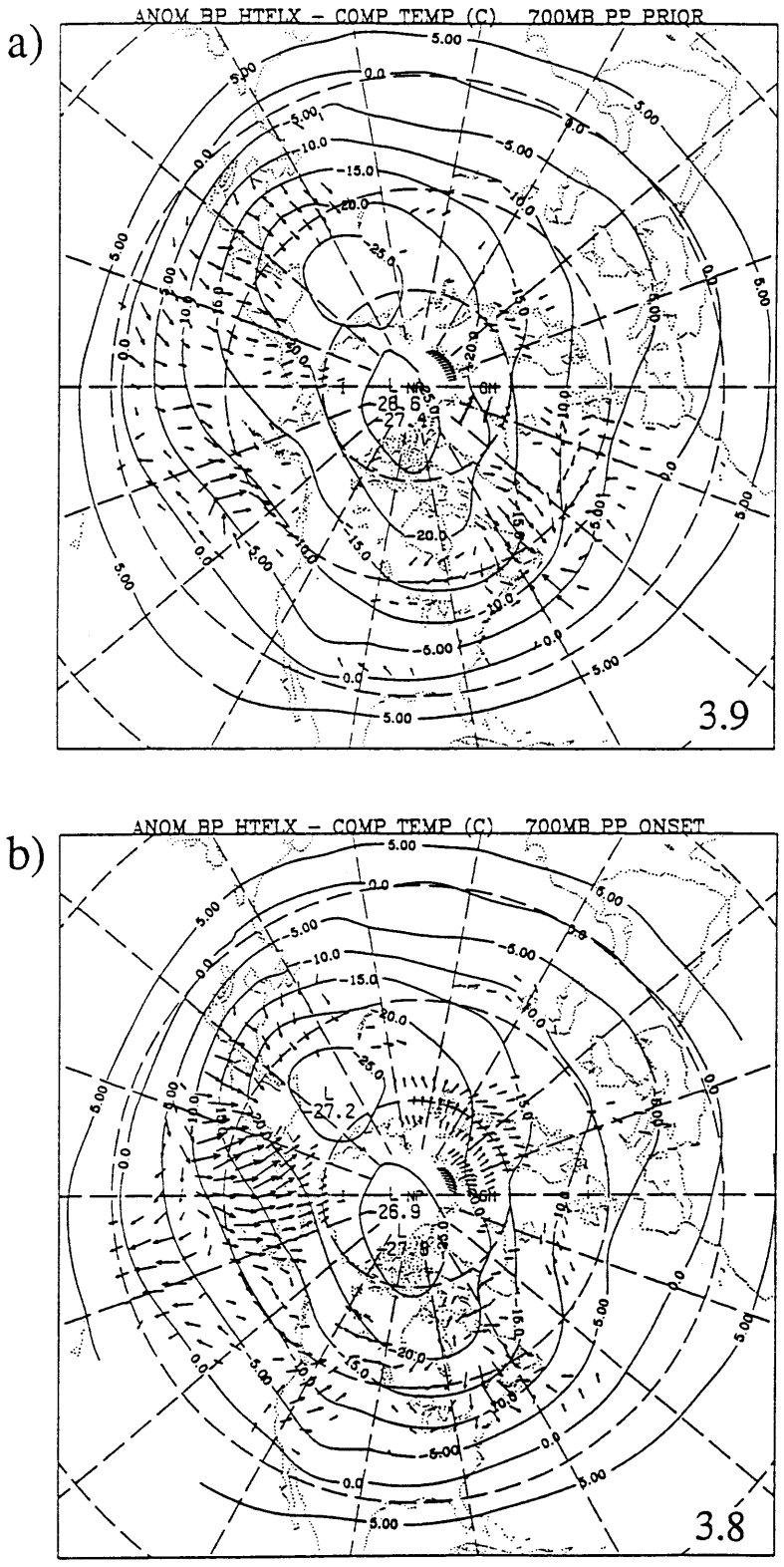

Fig. 4.22. Composite-mean 700mb bandpass heatflux anomaly vectors (C m s^{-1}) and the composite-mean 700 mb temperatures (C) during the a) prior and b) onset phases during the Pacific positive PA cases. The magnitude of the maximum vector plotted in indicated in the lower-right corner of each panel. The winter mean bandpass heat flux at 700 mb is 15.1 C m s^{-1}.

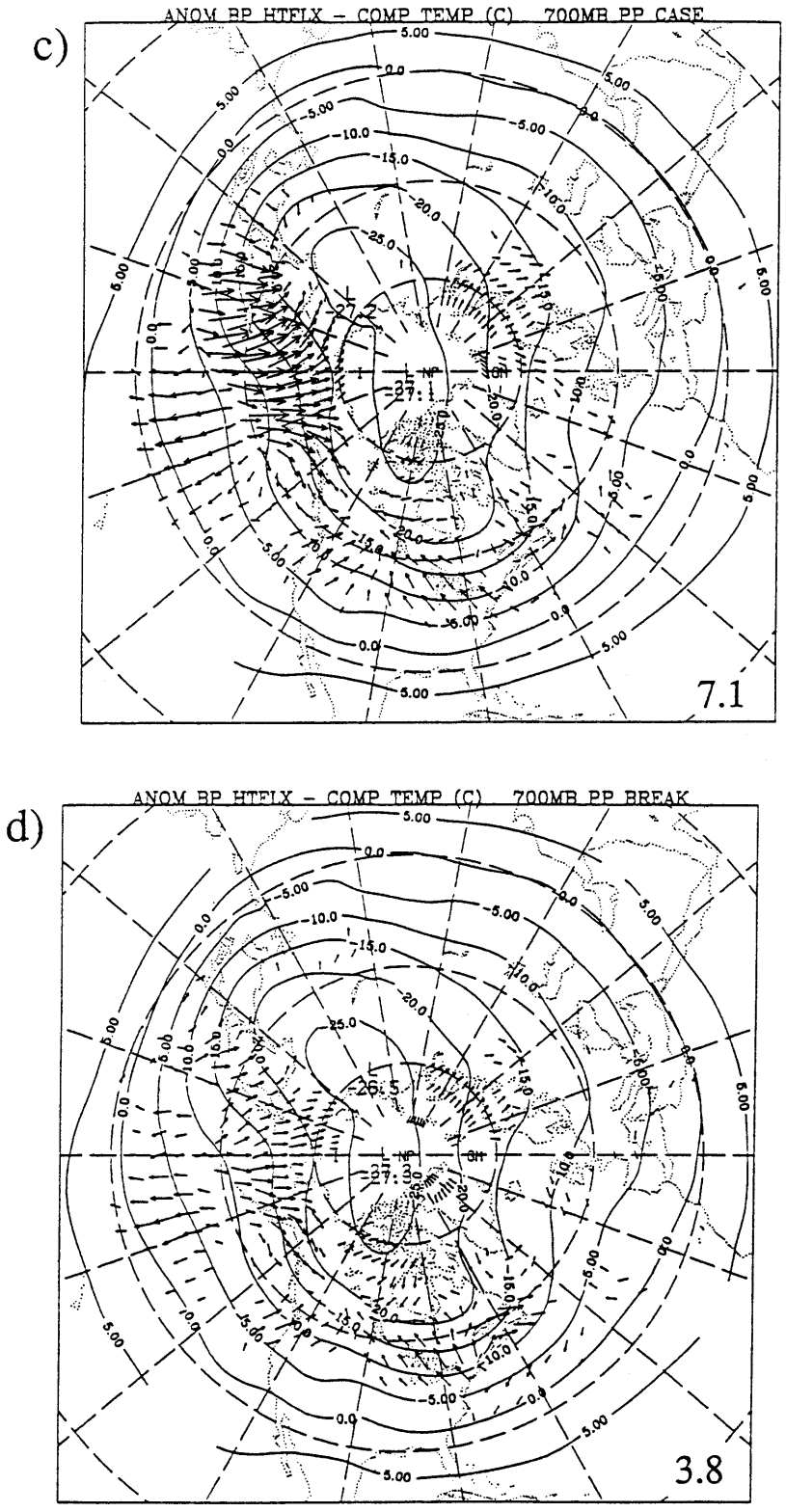

Fig. 4.22 (cont). Composite-mean 700mb bandpass heatflux anomaly vectors (C m s^{-1}) and the composite-mean 700 mb temperatures (C) during the c) case and d) breakdown phases during the Pacific positive PA cases. The magnitude of the maximum vector plotted in indicated in the lower-right corner of each panel. The winter mean bandpass heat flux at 700 mb is 15.1 C m s^{-1}.

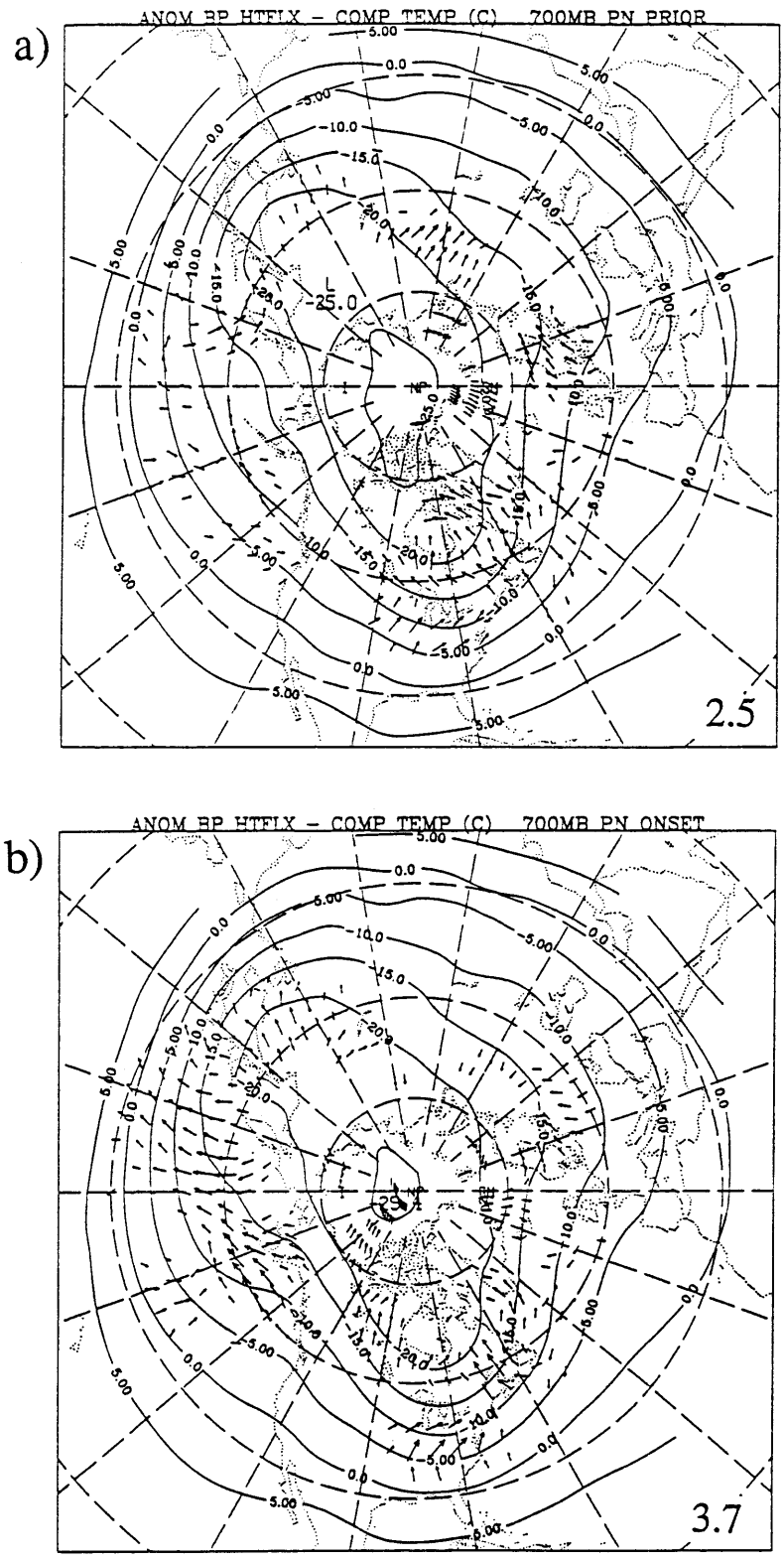

Fig. 4.23. Composite-mean 700mb bandpass heatflux anomaly vectors (C m s^{-1}) and the composite-mean 700 mb temperatures (C) during the a) prior and b) onset phases during the Pacific negative PA cases. The magnitude of the maximum vector plotted in indicated in the lower-right corner of each panel. The winter mean bandpass heat flux at 700 mb is 15.1 C m s^{-1}.

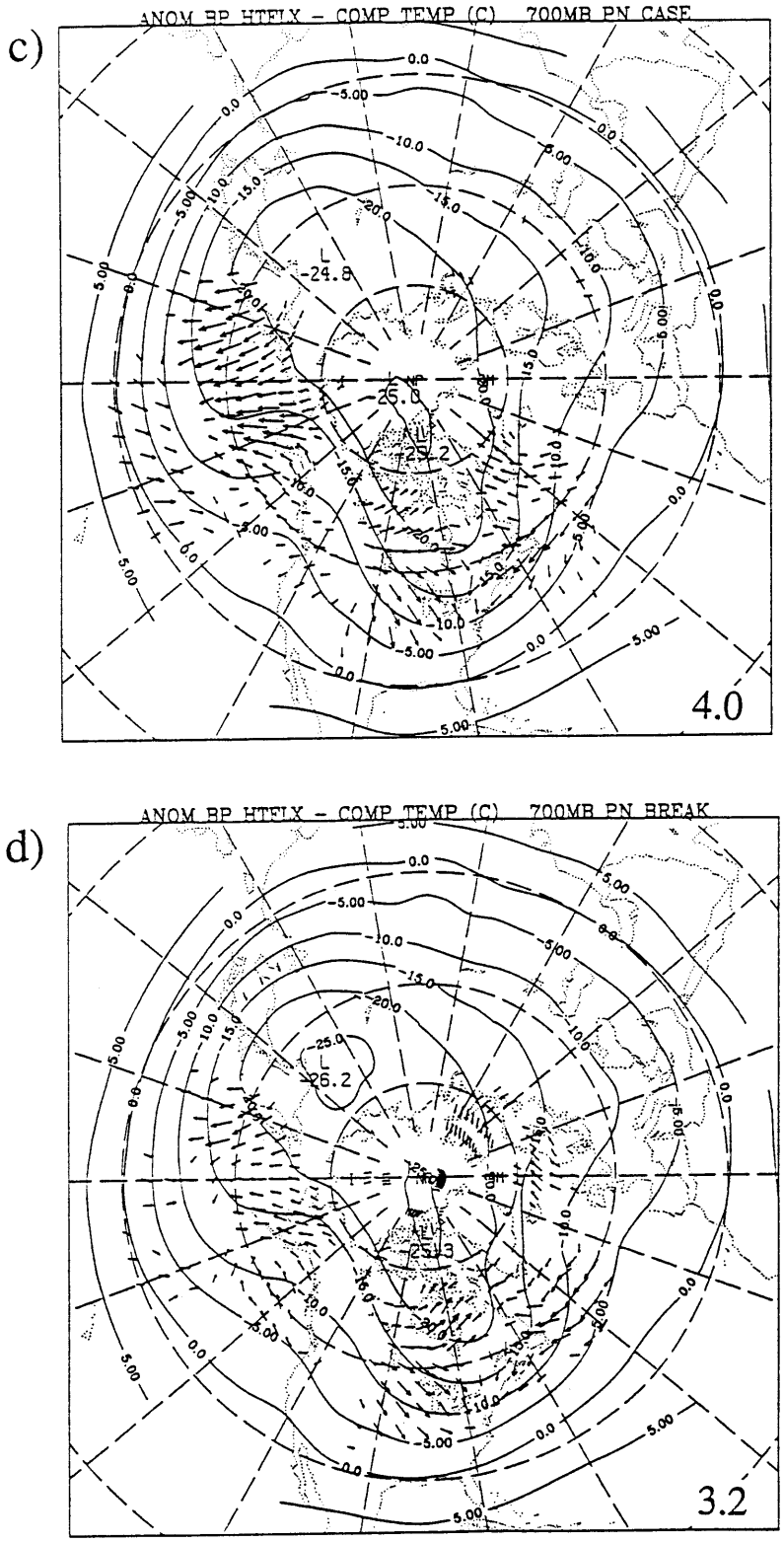

Fig. 4.23 (cont). Composite-mean 700mb bandpass heatflux anomaly vectors (C m s^{-1}) and the composite-mean 700 mb temperatures (C) during the c) case and d) breakdown phases during the Pacific negative PA cases. The magnitude of the maximum vector plotted in indicated in the lower-right corner of each panel. The winter mean bandpass heat flux at 700 mb is 15.1 C m s^{-1}.

(upgradient) eddy heat fluxes are found upstream of the developing PA. These upstream heat flux anomalies intensify during the onset period. During the mature phases, the principal eddy heat fluxes appear dissipative of the large-scale thermal anomaly around the key region, although upstream downgradient (upgradient) eddy heat fluxes persist through the mature phase. During the breakdown phase, the upstream eddy heat fluxes weaken considerably and even reverse sign in some regions. There are considerably more downstream anomalous eddy heat fluxes during the Pacific cases than in the Atlantic composites consistent with the earlier VSTAT analyses. For example, late in the onset phase of the Pacific negative PA pattern, strong baroclinic growth along the eastern U.S. seaboard occurs, as discussed in Sec. 4.3. This cyclogenesis usually occurs as an "Alberta Clipper"-type low drops down along the developing large-scale trough, redevelops off the southeast U.S. coast and then propagates north-eastward along the coast. This is well known to synopticians as a recurrent scenario for major winter storms that effect the eastern U.S. (Sanders, 1986).

4.6 Discussion.

Before proceeding, we will present a summary of the major results of these analyses. The primary systematic aspects of the anomalous synoptic-scale eddy activity during the life cycles of large-scale persistent anomalies are:

- For both the Atlantic and Pacific cases, the principal eddy activity changes can be described by opposite phases of one basic anomaly pattern.

- Central to the basic anomaly pattern is a highly significant eddy activity anomaly dipole that is aligned N-S (or NW-SE) about the key region during the mature phase of the PA. Enhanced eddy activity is found to the north (south) and suppressed eddy activity is found in and to the south (north) of the key region during positive (negative) PA events. The temporal variations

in the magnitude of this dipole appear to be in phase with those of the large-scale flow anomalies.

- Prior to and during positive (negative) PA events, stronger (weaker) than normal eddy activity is found upstream of the key region. These anomalies often appear initially well upstream of the key region, and subsequently propagate eastward to just west of the PA coincident with the time of rapid growth of the large-scale flow anomalies. The upstream region is also characterized by anomalously enhanced (or diminished) baroclinic activity (as depicted by the anomalous eddy heat fluxes) which has the same sign as the PA that subsequently develops.

- The upstream eddy activity anomalies weaken and often reverse sign during the breakdown phase of the persistent anomalies.

The qualitative picture of the changes in eddy activity that occur during the life cycles of Atlantic positive persistent anomalies is as follows: A packet of relatively strong upper-level synoptic-scale eddies propagates eastward from the Pacific and across North America prior to the rapid growth phase of the PA pattern. The eddies within this wave packet undergo further baroclinic growth in and along the western end of the Atlantic storm track, leading to a strongly enhanced western Atlantic storm track. At the same time, the rapidly developing ridge over the eastern Atlantic deflects the eastern end of this storm track northward, resulting in a dipole in eddy activity anomalies near the large-scale ridge. The dipole initially has a positive bias, reflecting overall enhanced eddy activity. During the mature phase, the enhanced baroclinic activity upstream of the key region weakens and the downstream eddy anomaly dipole becomes more symmetric. Eventually the upstream cyclogenesis and eddy activity becomes weaker than normal. This may be partially due to a reduction in the number or intensity of upper-level disturbances propagating eastward from the Pacific. At the same time, the large-scale flow anomaly begins to weaken and the eddy activity near the key region relaxes back towards normal. A very similar scenario exists for

the Pacific positive cases, except that the source for the upstream anomalies appears first over central and eastern Asia.

During the negative PA events, the scenario is also very similar but with opposite sign. We also see that during the negative cases, the large-scale flow has a blocking-like effect but with the principal storm tracks weakened and shifted considerably southward. However, the overall weather conditions in the eddy suppressed regions of positive and negative PAs are likely to still be considerably different. The large-scale subsidence associated with the positive PA events tends to produce dry and warm conditions (Green, 1977) while the weak large-scale ascent during negative PAs is associated with cool and damp weather (Dole, 1982).

The eddy activity anomalies observed upstream well prior to the developments of the large-scale flow are relatively weak compared to the changes directly associated with the mature PA pattern itself. Correspondingly, the statistical significance of these anomalies is relatively low. Fig. 4.24 shows the statistical significance of the 300 mb VSTAT anomalies at day -6 during the onset of each of the PA types. The significance patterns at this time are generally scattered, and the areas covered by significance greater than 90% do not appear to be much greater than 10% of the domain. Thus, based on point-by-point significance tests, one might conclude that much of the eddy activity changes remote to the primary PA pattern discussed earlier in this chapter cannot be distinguished from zero and therefore may represent only sampling variability. However, these remote eddy activity anomalies have good temporal continuity, are nearly equal and opposite in the two phases of PAs, are symmetric about the life cycle of PAs, and can be identified in many of the individual Atlantic and Pacific PA cases. This suggests that the anomaly *patterns* may be more significant than can be ascertained by *pointwise* significance tests.

To illustrate this, consider Fig. 4.25, where the hemispheric-mean (north of 20N) 300 mb VSTAT anomalies during the onset and decay periods of each PA type are plotted. Prior to the positive (negative) developments, the hemisphere is characterized by greater (weaker) than normal eddy activity. During the breakdown phase, a similar but opposite VSTAT anomaly trend is evident, although not as clearly as during onset. These hemispheric-mean VSTAT anomalies tend to lead the large-scale anomalies, particularly prior to onset. The statistical significance, based on the null hypothesis that the positive and negative hemispheric-mean VSTAT anomalies are identical at day -5 of onset, exceed the 97.5% and 99.5% for the Atlantic and Pacific respectively[1]. Therefore, it appears likely that the hemispheric-mean amplitude of the bandpass eddies prior to the onset of positive PAs is typically greater than the corresponding values prior to the onset of negative PAs. Similarly, by comparing the hemispheric-mean VSTAT anomalies between day 0 of onset and day 0 of breakdown, we can conclude that at confidence levels of 99.5% (Atl. pos.), 95% (Atl neg.), 97.5% (Pac. pos.) and 99.5% (Pac. neg.) that the hemispheric mean VSTAT anomalies are weaker (stronger) during breakdown of positive (negative) PAs than during onset.

Although these results suggest that there is a hemispheric-wide signal in the strength of the eddy activity anomalies during the developments, most of the signal is, in fact, contained in smaller regions upstream of the developing PA. Table 4.1 summarizes VSTAT anomalies in regions upstream of each of the developing PAs, 6 days prior to the onset and breakdown. The bounds of the regions chosen were selected to approximately correspond with the largest composite VSTAT anomalies observed at day -6 of onset. The table lists the bounds of the regions, the mean VSTAT anomaly within those bounds, the statistical likelihood that this anomaly is *different from zero*, and the number of individual

[1] These significance values are computing using the technique outlined in Chapter 3 with the sample variances (weighted by the number of cases in each PA type) used as an estimator for the variance. The number of degrees of freedom is thus given by the total number of cases - 2.

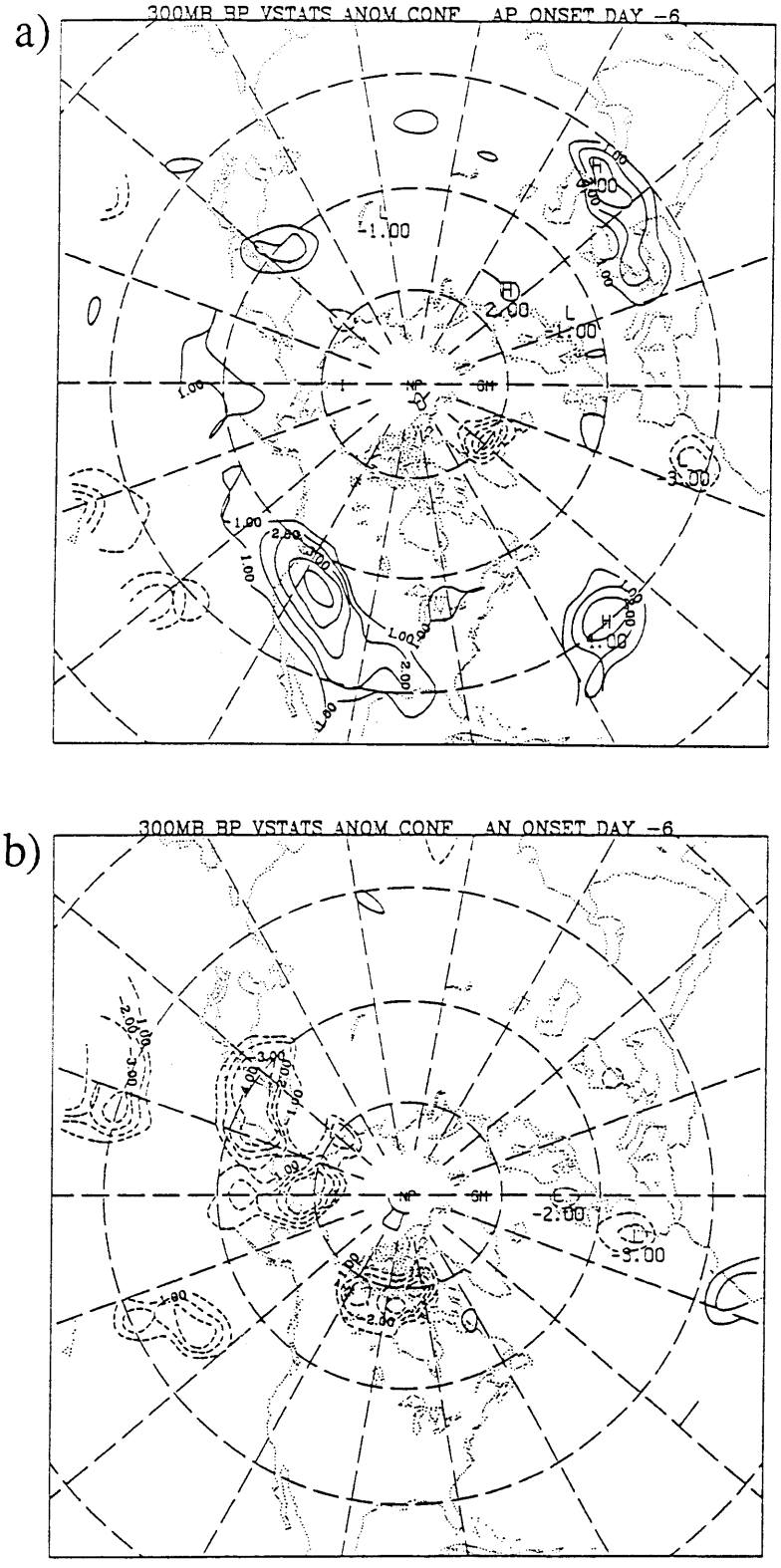

Fig. 4.24. Statistical significance of the 300 mb VSTAT anomalies for day -6 during the onset of a) Atlantic positive and b) Atlantic negative persistent anomaly events. The contours indicate the 90, 95, 97.5, 99 and 99.5 significance levels. Dashed contours imply negative anomalies.

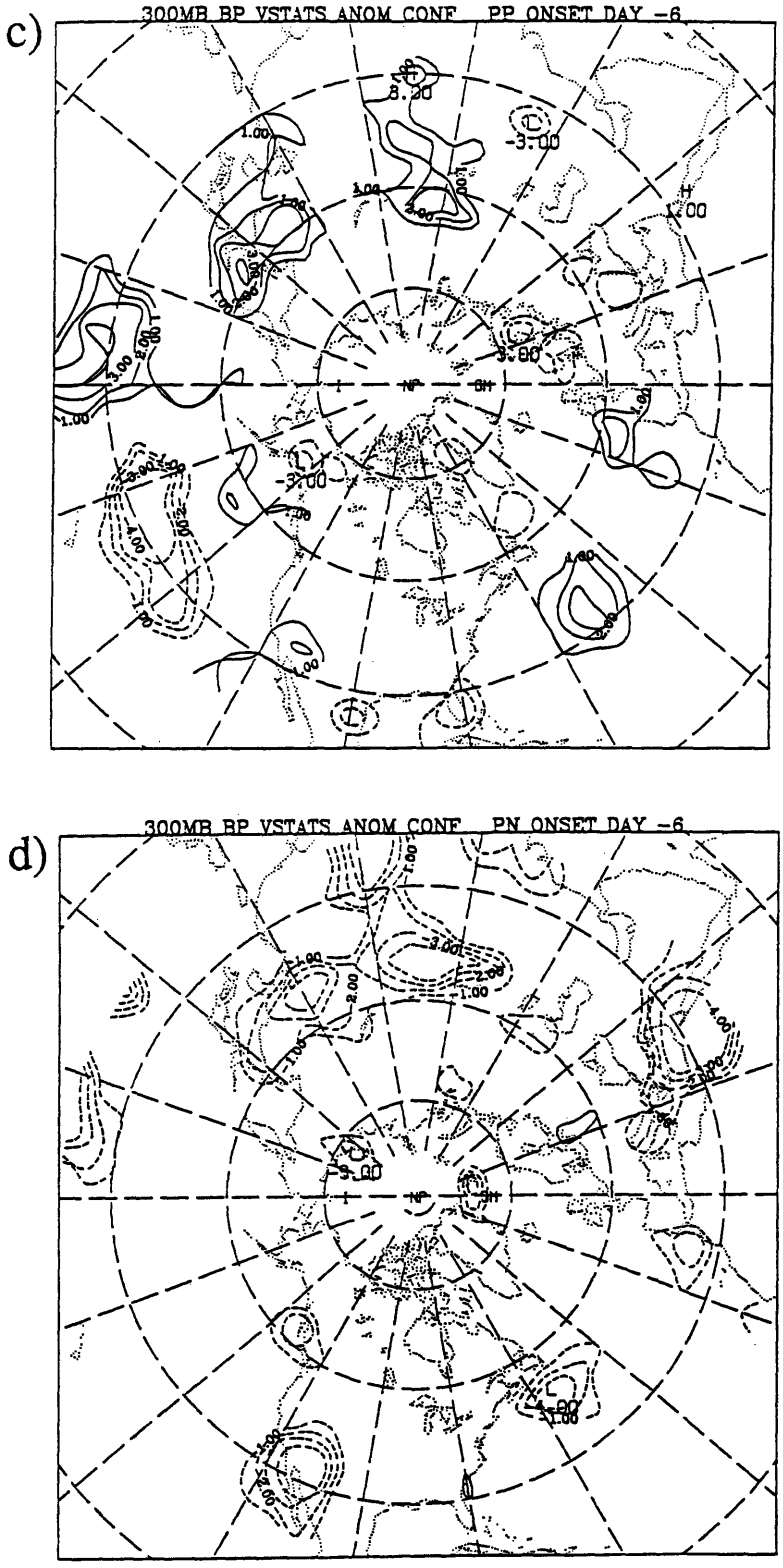

Fig. 4.24 (cont.). Statistical significance of the 300 mb VSTAT anomalies for day -6 during the onset of c) Pacific positive and d) Pacific negative persistent anomaly events. The contours indicate the 90, 95, 97.5, 99 and 99.5 significance levels. Dashed contours imply negative anomalies.

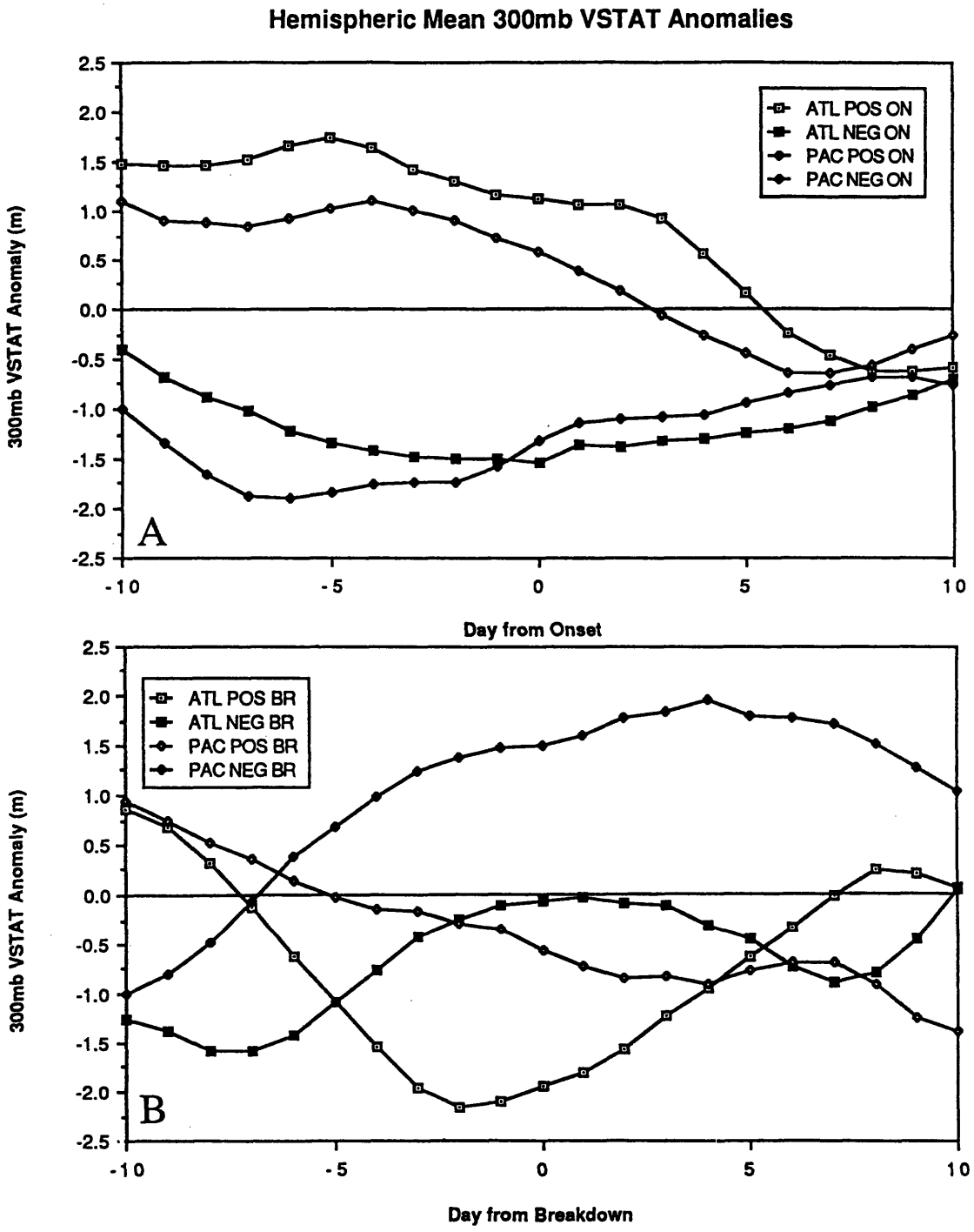

Fig. 4.25. Time series of the hemispheric-mean (north of 20N) 300 mb VSTAT composite anomalies relative to a) the onset and b) the breakdown phase for each of the PA events .

Eddy Activity Changes in Individual Cases

Case Type		ONSET					BREAK				
	Day	Anom	sigf	pos %	neg %	neu %	Anom	sigf	pos %	neg %	neu %
ATL POS 30N - 60N 120E-70W	-6	+8.6	95	12 (67)	5 (28)	1 (5)	-5.1	<90	7 (39)	11 (61)	0 (0)
ATL NEG 30N - 60N 120E - 70W	-6	-6.4	95	4 (20)	14 (70)	2 (10)	-2.5	<90	9 (45)	10 (50)	1 (5)
PAC POS 35N - 60N 60E - 140E	-4	+3.3	98	12 (60)	7 (35)	2 (10)	-2.5	<90	6 (29)	14 (67)	1 (4)
PAC NEG 35N - 60N 60E - 140E	-4	-6.9	99	6 (27)	16 (73)	0 (0)	+1.4	<90	10 (45)	8 (36)	4 (19)

Table 4.1. Composite-mean 300 mb VSTAT anomalies in the indicated regions, the significance level that the anomalies are different from zero and the number of cases that had positive, negative and neutral ($< 0.1\sigma$) anomalies in that region. The table lists values for day -6 during the onset and breakdown of each type of persistent anomaly.

cases that have positive, negative and neutral (<10% of a standard deviation) anomalies in the region. For example, 6 days prior to the onset of the Atlantic positive PAs, the upstream region (30N-60N, 140E-70W) exhibits a mean 300 mb VSTAT anomaly of +8.6 m. There is at least 95% confidence that this composite anomaly is different from zero. Of the 18 Atlantic positive PA cases, 12 were characterized by enhanced eddy activity, 4 by suppressed eddy activity and 2 were considered neutral. At day -6 of breakdown, these trends reverse with a mean anomaly now of -5.6 m and 6, 11 and 2 cases were characterized by positive, negative and neutral anomalies respectively.

Although an exhaustive search for regions or times in which the VSTAT anomalies optimally predicted the onset or breakdown of PAs was not made, a check of several regions other than those used in Table 4.1 indicated that the predictive power of the VSTAT anomalies could not be significantly improved upon over that already presented. Further, no single data point was found for any PA type at which the VSTAT anomalies correctly predicted the onset or breakdown of all cases. Therefore it seems likely that broad upstream enhanced (suppressed) synoptic-scale eddy activity, although favorable, is not a necessary condition for the formation of positive (negative) persistent anomalies. Further, these upstream VSTAT anomalies are not a sufficient condition for PA onset or decay. This was determined by searching for all cases in which the regional VSTAT anomalies exceeded the mean anomalies presented in Table 4.1 for at least 10 days. In general, only about 1/3 of these "VSTAT persistent anomaly" cases actually lead to the development of a downstream PA at the key regions within 10 days. Therefore, synoptic-scale eddy activity by itself can only be used to predict the likelihood that a specific PA event will occur. However, by combining the VSTAT anomalies with other predictive parameters (e.g. a enhanced subtropical ridge in the eastern Atlantic prior to positive Atlantic PA cases) some useful skill in empirical long-range forecasting may be possible.

The generality of the VSTAT results to flows that do not meet the PA identification criteria is demonstrated in Fig 4.26. Here the correlation coefficient between the lowpass 300 mb heights at the Atlantic key point and the 300 mb VSTATs observed 6 days earlier is computed. The correlations are dominated by a dipole structure about the key point with an extrema magnitude of about 0.4. (The correlation coefficients for a 0 day lag are about 0.7). Most of the upstream region identified by the VSTAT analyses as having enhanced eddy activity during PA events is characterized by a weak but positive correlation coefficient with peak correlations of about 0.2. Therefore anomalous geopotential heights over the North Atlantic are more likely to be preceded by eddy activity anomalies of the same sign far upstream. Correlation coefficients for the Pacific key point (not shown) shows a similar structure although the positive correlations do not extend far into Asia.

We now wish to briefly discuss why the synoptic-scale eddy activity changes during persistent anomalies, focusing particularly on eddy activity changes observed during the mature phase of the persistent anomalies. Three hypothesis are suggested to explain the observed differences. They are:

1) The observed anomalies are doppler-shifted artifacts of bandpass temporal filtering a red mean wave power spectra in a varying mean-flow.

2) The paths of the synoptic-scale eddies are altered by a differing large-scale steering flow.

3) The principal regions of synoptic-scale eddy growth and decay have been altered.

The first hypothesis is suggested by the close correlation between the eddy activity anomalies and the anomalous large-scale zonal flow. However this explanation is at best incomplete, since results of anomalous eddy activity calculations using a spatial filter to

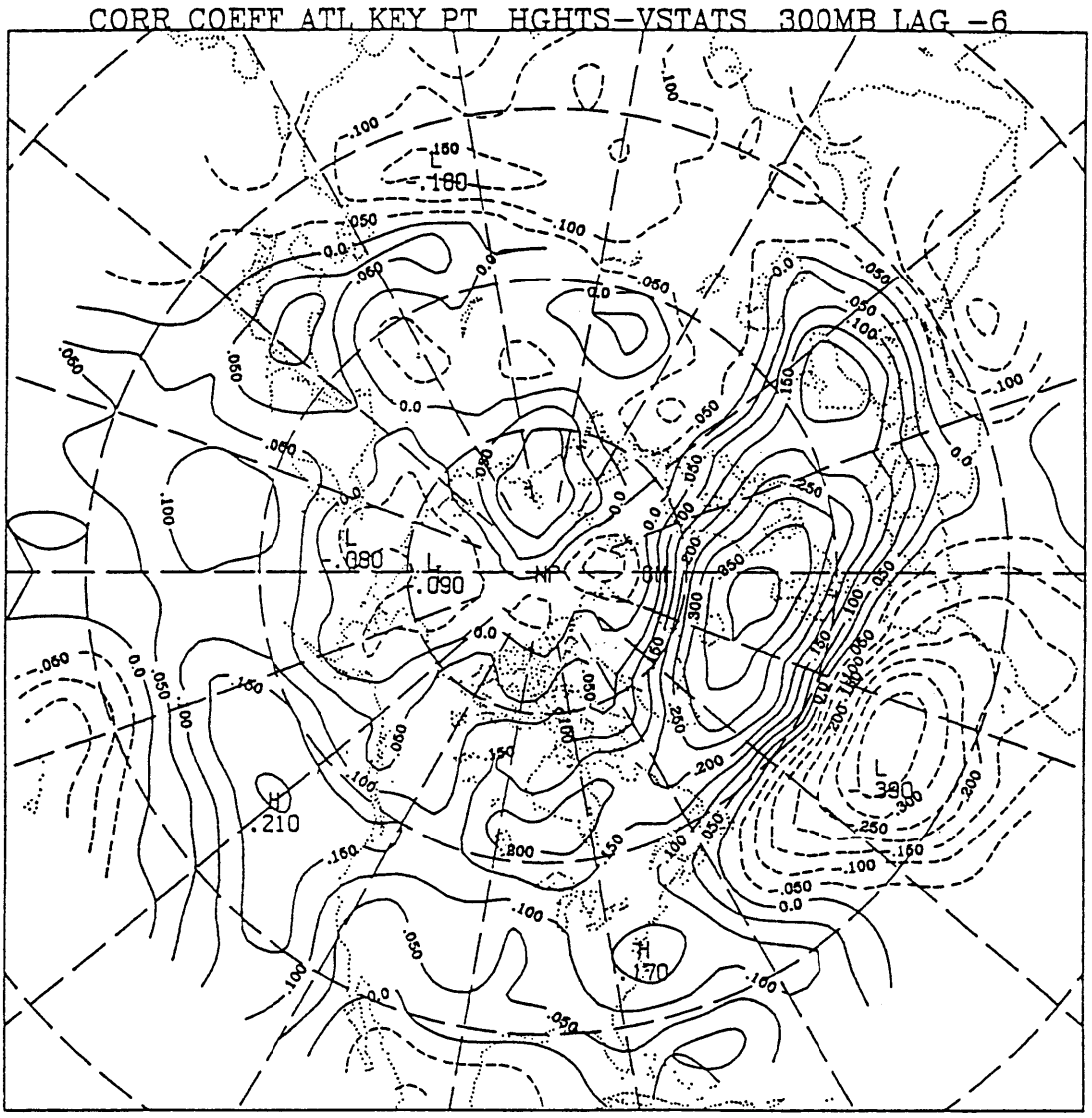

Fig. 4.26. Correlation coefficient between the lowpass 300 mb heights at the Atlantic key point (50N 25W) and the 300 mb VSTATs observed 6 days earlier.

sample the synoptic-scale eddies (Appendix B) as well as observations of the storm track changes (Figs. 4.6 and 4.7), which are not based on any filtering, convincingly demonstrate that the bandpass VSTAT results are not mere artifacts. Further, by computing the maximum changes in eddy frequencies that may occur from the doppler shifting effect, and then comparing the changes to mean wave power spectra (not shown), it can be demonstrated that the mean power spectra is not red enough to account for the observed eddy activity anomalies.

The second hypothesis relies on the observation that synoptic-scale eddies primarily follow the large-scale anomalous flow as was demonstrated earlier using the tracks of surface cyclones. The steering of eddies by an anomalous large-scale diffluent flow has generally been considered the primary "blocking" mechanism, as the eddies are essentially advected to the north or to the south of the block. The percentage of the eddies passing to the north or to the south of the block then depends largely upon the amount of the large-scale flow passing on either side of the blocking anticyclone.

A similar effect can also occur during negative PAs. Here the eddies are funneled by the large-scale confluent flow on the upstream side of the PA into a narrow channel south of the climatological-mean storm track. Regions along this channel will likely exhibit enhanced synoptic-scale eddy activity, while regions on either side of the channel will observe a weaker than normal eddy activity. Thus, in this sense, negative persistent anomalies can also essentially have a "blocking" effect by limiting the eddy activity in certain regions.

Many factors other than advection by the large-scale flow may influence the particular track that a cyclone follows. These include the β effect, orography, diabatic heating, friction, non-linear interactions with the mean flow and interactions with other disturbances. However, the high correlation between the anomalous large-scale flow and

the observed cyclone tracks shown earlier suggests that anomalous advection plays a first-order role in changing the cyclone paths, and thus in determining the local changes in eddy activity observed during mature persistent anomalies.

The third hypothesis proposed to explain the eddy activity anomalies during PAs focuses on changes in the growth characteristics of the eddies. The anomalous heat fluxes shown in Figs. 4.18-4.21 suggest that there are indeed changes in the geographical distribution of cyclogenesis. This is further supported by contrasting the first analyzed positions of all cyclones occurring during each of the PA events. Such an analysis (not shown) indicates that there are considerable differences in the general regions where cyclones first occur between opposite phases of the PAs. Most notable are the regions just east of Greenland and just south of Alaska, which become relatively strong cyclogenetic regions during mature positive Atlantic and Pacific cases respectively. Further south, in and near the key regions, there is considerable cyclogenesis during the negative events that is virtually absent in the positive cases. Other subtle differences are apparent as well. For example, along the Gulf Coast of the U.S. there is considerably more cyclogenetic activity during both Atlantic and Pacific negative cases.

To further assess the role that baroclinic variations play in the observed cyclogenesis changes, anomalies in the baroclinic growth parameter

$$\sigma = \frac{f}{N}\frac{\partial U}{\partial Z}$$

were computed throughout the life cycles of PA events. The growth rates of both infinitesimal disturbances in an unstable mean flow (Charney, 1947; Eady, 1949) as well as a finite amplitude baroclinic growth (Farrell, 1985) depend on the magnitude of σ. (In the latter theory, the growth rates also depend upon the magnitudes and configurations of the initial perturbations). This baroclinic growth parameter was computed using lowpass-

filtered data and then averaged over all cases. Fig. 4.27 shows the composite anomalies in the 700 mb baroclinicity at day +6 during the onset of each of the PA types. In general, the baroclinicity anomalies are closely correlated with the eddy activity anomalies, except for an approximate 15 degree upstream shift in the baroclinicity. This same spatial relationship also exists between the climatological mean distribution of baroclinicity (not shown) and the mean VSTATs. Further, the ratio of the magnitudes of the baroclinicity and VSTAT anomalies is approximately equal to those obtained from climatological-mean values. Therefore, it appears that changes in the large-scale baroclinicity associated with PAs likely play a significant role in organizing the growth regions of the synoptic-scale eddies as in climatological mean conditions. However, there are no apparent systematic large-scale changes in baroclinicity well before the onset and breakdown of PAs that would readily explain the upstream eddy anomalies observed during those times.

Another reason for the observed changes in regional cyclogenesis may be related to changes in lee cyclogenesis activity. This would most likely play a role in the regions near Iceland, in the northeast part of the Gulf of Alaska and in eastern Alberta. These regions are just downstream of where the large-scale flow during positive PA events have a considerable component over the high terrain of Greenland, the Aleutian and Alaskan Ranges and the Canadian Rockies respectively. By inspection of the individual case surface maps, these regions have frequent events of rapid cyclogenesis during the positive PA cases. However, since these regions are also generally characterized by enhanced baroclinicity, it is unclear what the relative importance of baroclinic and orographic effects may be.

4.7 Summary

This chapter documented the changes in synoptic-scale eddy activity that accompany the large-scale flow changes associated with the life cycles of persistent anomalies. In

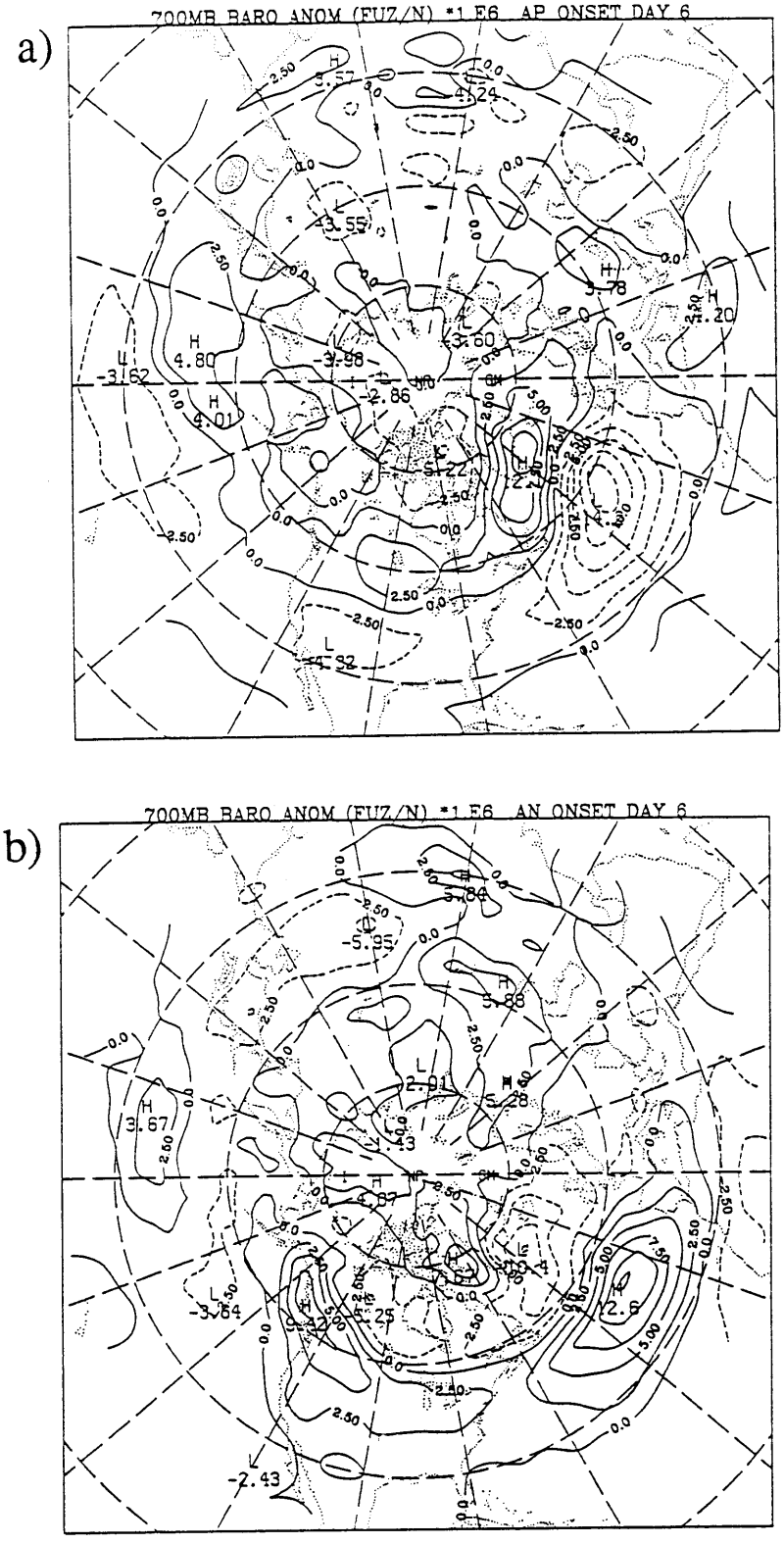

Fig. 4.27. Composite-mean anomalies of the baroclinic growth parameter (fU_Z/N) for day +6 during the onset of a) Atlantic positive and b) Atlantic negative cases (units s^{-1}).

c)

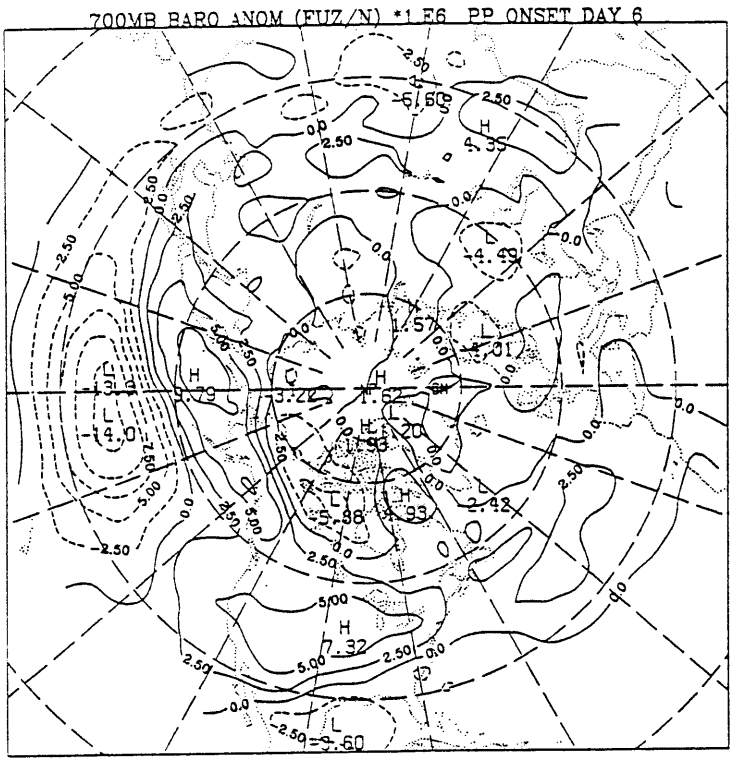

d)

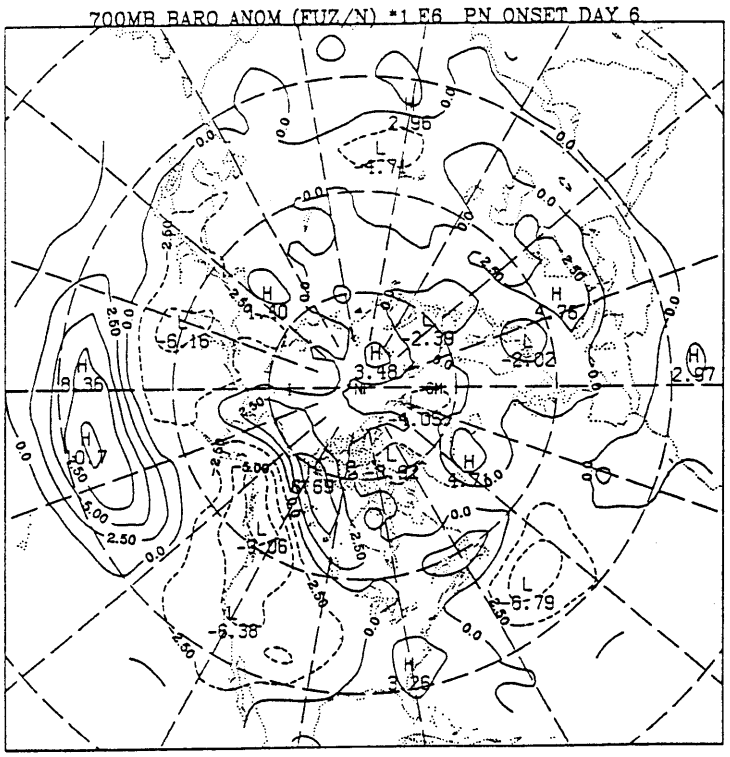

Fig. 4.27 (cont). Composite-mean anomalies of the baroclinic growth parameter (fU_Z/N) for day +6 during the onset of c) Pacific positive and d) Pacific negative cases (units s^{-1}).

general, the eddy activity tends to follow the strongest large-scale flow throughout the PA life cycles. The largest and most significant of the eddy activity changes are directly associated with the primary PA flow pattern itself. However, weaker eddy activity changes are also found remote to the PA patterns. Upstream eddy activity anomalies with the same sign as the tendency of the large-scale flow anomalies were also found. This association, combined with the observations of anomalous eddy heat and vorticity fluxes (not shown) during the life cycles of the PAs, suggests that the eddies may also be playing a significant role in determining the evolution of the large scale flow. A more quantitative assessment of the role of the eddies in forcing the large-scale flow is the subject of the next chapter.

Chapter 5
Eddy Forcing of Persistent Anomalies

5.1 Introduction

In this chapter we investigate the potential role of synoptic-scale eddies in forcing the large-scale flow during the life cycles of persistent anomalies. Synoptic-scale eddy forcing is an important (although generally not the largest) term in the forcing of zonal (Pfeffer, 1981) and time mean flows (Lau and Holopainian, 1987). From the analyses of the preceding chapter, we anticipate that there will be significant changes in the distribution and magnitude of synoptic-scale eddy forcing throughout the life cycles of PAs associated with the changes in eddy activity. Here we are will attempt to determine how that anomalous forcing varies in relationship to the life cycles of PAs.

Dole (1982) computed time-mean budget analyses of the heat, vorticity and potential vorticity equations during mature Atlantic PAs. He broke his budgets into contributions from time-mean quantities and time-deviation (eddy) quantities. He found that the phase of upper-level transient eddy vorticity flux divergence patterns are generally situated just upstream of the large-scale vorticity center, acting to maintain the large-scale flow against time-mean advection and divergence. The transient eddy heat fluxes were found to be generally dissipative of the large-scale thermal anomalies. The eddy potential vorticity fluxes had qualitatively similar structure to the upper-level eddy vorticity flux patterns.

Mullen (1987) examined the composite structure of synoptic-scale eddy fluxes of pseudopotential vorticity during mature blocking events, and concluded that the eddy

induced circulation pattern was in an approximate quadrature relationship with the large-scale anomaly pattern. This suggested that the eddy forcing was approximately balancing time-mean advection (as suggested by Austin, 1980) rather than maintaining the block against dissipation (as suggested by Green, 1977). Further, the magnitude of the eddy forcing was large in the sense that the spinup time scale for the development of the blocking patterns implied by the eddy forcing is comparable to the observed development time scale.

There have been several other observational studies stressing the importance of eddy fluxes in the budgets of mature blocking flows (e.g. Hoskins *et al.*,1983; Illari and Marshall, 1983; Illari, 1984; Trenberth, 1986; Hoskins and Sardeshmukh, 1987; Holopainen and Fortelius, 1987). In this chapter we wish to extend these studies in several important aspects. First we wish to more clearly isolate the anomalous part of the eddy forcing from the climatological mean part and then determine the relationships with the anomalous aspects of the large-scale flow. We also wish to extend these studies by examining the role of anomalous eddy forcing throughout the entire life cycles of both positive and negative persistent anomaly events. In doing so, we hope that a more complete picture of the systematic interactions between the large-scale flow the synoptic-scale eddies will begin to emerge.

5.2 Basic Diagnostic Framework

One of the more common frameworks in which eddy-mean flow interactions are studied is by decomposing the variables of the governing equations into terms involving time-mean quantities and departures from the time-mean values. For example, consider the quasi-geostrophic, pseudo-potential vorticity equation

$$\frac{dq}{dt} = F_{NC}$$

in which the change of pseudo-potential vorticity (PV) is conserved following the (horizontal) geostrophic flow in the absence of diabatic heating and frictional processes. If the derivative is expanded and the variables are broken into time mean ($\overline{x}$) terms and eddy terms defined as deviations from the time-mean (x'), then the PV conservation equation becomes

$$\frac{\partial q'}{\partial t} + \overline{\mathbf{V}}\cdot\nabla\overline{q} + \overline{\mathbf{V}}\cdot\nabla q' + \mathbf{V}'\cdot\nabla\overline{q} + \mathbf{V}'\cdot\nabla q' = \overline{F_{NC}} + F'_{NC} \qquad (1)$$

where the time derivative of the time-mean PV is set to zero. Taking the time-mean of the equation, uncorrelated eddy terms drop out leaving

$$\overline{\partial q'/\partial t} + \overline{\mathbf{V}}\cdot\nabla\overline{q} + \overline{\mathbf{V}'\cdot\nabla q'} = \overline{F_{NC}}.$$

Usually the time-mean eddy PV storage term is assumed small. Since the geostrophic advecting flow is nondivergent, the advection terms are usually written in flux form

$$\nabla\cdot(\overline{\mathbf{V}}\overline{q}) + \overline{\nabla\cdot\mathbf{V}'q'} = \overline{F_{NC}} \qquad (2)$$

In the absence of sources and sinks, the time-mean and the eddy PV flux divergences must be in balance. Illari (1984) used this framework to study the monthly-mean PV budget during a strong European blocking episode. She found a qualitative balance between the time-mean flux divergence and the eddy-flux divergence, a result which basically implies the relative smallness of the non-conservative terms (although nonconservative processes may have had an important indirect role by influencing the eddy parts of the flow).

In order to readily interpret results obtained in such a time-mean / eddy framework, it is usually assumed that the time-mean and eddy parts of the flow can be associated with different physical phenomena. Often, there is at least an implicit assumption that the eddy terms are associated with travelling synoptic-scale disturbances, while the time-mean terms represent the sole effects of the large-scale phenomena. However, a simple example by

which such an interpretation would break down is if the large-scale phenomena were a slowly propagating Rossby wave. As the ridge or trough of the wave passes, one may have a nearly stationary, long-lived PA event. By applying (1) to the observations near the time of passage of the ridge or trough, a balance between the time-mean and transient terms would emerge. However, association of the transient eddy terms with synoptic-scale eddies would be erroneous in this case, as the only dynamical process occurring is large-scale Rossby wave propagation.

Dole (1989) shows that the composite evolutions of persistent anomalies do not appear to have a prolonged steady state phase. Therefore instead of adopting the conventional time-mean / eddy decomposition, we modify (1) by breaking the flow into slowly evolving terms ($\tilde{x}$) and faster eddy terms (x'). The conservation equation for the evolution of the slow part of the flow then becomes

$$\frac{\partial \tilde{q}}{\partial t} + \tilde{\mathbf{V}} \cdot \nabla \tilde{q} + \mathbf{V}' \cdot \nabla q' + CT = \tilde{F}_{NC} .$$

Correlations between the slow and fast parts of the flow may also excite low-frequency fluctuations which are represented by the term CT. Holopainen and Fortelius (1987) used this framework to study a single blocking event, employing a 6-day filter to separate the low and high frequency components of the flow[1]. However they note that in individual cases application to the relatively rapid evolving onset and breakdown stages may not be warranted as there may not be a clear separation of time-scales between the synoptic-scale eddies and the developing blocking flow as they defined it.

In this study we have been focusing on the composite-mean relationships between the synoptic-scale eddies with the evolving large-scale flow associated with the PAs. The analyses of Chapter 3 showed that, for all cases, to a very good approximation, the

[1]Actually, they break their quantities into slow and fast parts but still solve the conservation equation in a 10-day time mean framework.

composite-mean evolution of PAs can be represented by the lowpass-filtered fields, with higher-frequency fluctuations generally incoherent to the large-scale evolution. Therefore, if we write our conservation equation in terms of lowpass-filtered (x_{LP}) and bandpass-filtered (x_{BP}) quantities, the equation for the evolution of the lowpass part of the flow becomes

$$\frac{\partial q_{LP}}{\partial t} + \mathbf{V}_{LP} \cdot \nabla q_{LP} + (\mathbf{V}_{BP} \cdot \nabla q_{BP})_{LP} + CT_{LP} = (F_{NC})_{LP}.$$

If the LP and BP filters do not cover the full spectrum of motions, then an additional spectral gap term (SG) is required for balance. Forming the composite mean (<x>) of this conservation equation we obtain

$$\frac{\partial \langle q_{LP} \rangle}{\partial t} + \langle \mathbf{V}_{LP} \cdot \nabla q_{LP} \rangle + \langle \mathbf{V}_{BP} \cdot \nabla q_{BP} \rangle_{LP} + \langle CT_{LP} \rangle = \langle F_{NC} \rangle_{LP}. \qquad (3)$$

The composite cross term in this equation will tend to vanish since the phase (with respect to the lowpass evolution) of the cross term is determined by the phase of the bandpass features. Since the bandpass fields tend to be incoherent to the lowpass development, so too are the cross terms. Therefore, aside from a possible remaining <SG> term, the composite-lowpass evolution is determined to a good approximation by the self-advection of the lowpass flow, the divergent part of the bandpass PV fluxes and the nonconservative effects. Although this equation is not as simple as (2), there is a clearer association of physical phenomena with the terms in (3). In particular, the bandpass terms are clearly associated with the synoptic-scale eddies. This approach, therefore, allows us to more directly examine the effects of the synoptic-scale eddies on the evolution of the low-frequency flow.

Since we are interested in low-frequency circulation anomalies and the anomalous aspects of the eddy forcing associated with these anomalies, for many of the diagnostics, the climatological-mean part of the eddy forcing has been removed. This enables us to

more readily ascertain whether the anomalous eddy forcing may be playing a significant role in the evolution of the low-frequency anomalies. Of course a complete analysis of the evolution requires that contributions from all budget terms be determined. That is not our intent here. Rather, we focus on the more specific question of whether the anomalous aspects of the bandpass eddy forcings are likely to significantly influence the evolutions of the low-frequency anomalies. As discussed in Chapter 1, the answer to this has significant practical implications for long-range weather prediction.

5.3 E-vector analyses.

In recent years, several new methods have been proposed for diagnosing the transient eddy effects on mean flows. Holopainen (1984) and Holopainen and Fortelius (1987) discuss the usefulness and limitations of many of these methodologies. In this section, we present the results of application of the extended Eliassen-Palm vector (E-vector) technique to PAs. E-vectors are essentially three-dimensional generalizations to time-mean flows of the Eliassen-Palm (Andrews and McIntyre, 1976; Edmon *et al.*, 1980) flux vectors for zonal-mean flows. They were first derived by Hoskins *et al.* (1983) with alternative forms introduced by Plumb (1985, 1986) and Trenberth (1986). Summaries of the important properties of E-vectors can be found in Plumb (1986) and Lau (1988). These include:

- The zonal and meridional quasi-geostrophic momentum equations may be transformed in such a manner that the net accelerations of the zonal and meridional components of the time-mean flow are given respectively by divergences of the set of vectors $\mathbf{E}_u$ and $\mathbf{E}_v$.

- The E-vector divergences are proportional to the meridional and zonal eddy pseudopotential vorticity fluxes.

- For plane waves, the $\mathbf{E_u}$-vector subtends an angle with the local east equal to half of the same angle of the minor axis of the wave[1]. The vertical component of $\mathbf{E_u}$ indicates the vertical tilt of the wave. The E-vectors can therefore be used to deduce the characteristic shapes and orientations of the eddies.

- For slowly varying mean flows, $\mathbf{E_u}$-vectors point in the direction of the mean eddy group velocity relative to the mean flow.

In this study we will use of Trenberth's (1986) quasi-geostrophic E-vector formulation in spherical coordinates. He shows that the time-mean horizontal momentum equations may be written in the form (using a log pressure vertical coordinate $z=\ln(p_o/p)$)

$$D\bar{u} - \frac{\overline{uv}\tan\phi}{a} - fv^* = \frac{1}{\cos\phi}\nabla\cdot\mathbf{E_u} + F_x$$

$$D\bar{v} + \frac{\bar{u}^2\tan\phi}{a} + fu^* = \frac{1}{\cos\phi}\nabla\cdot\mathbf{E_v} + F_y$$

where "a" is the earths radius, ϕ is latitude, f is the Coriolis parameter, u* and v* are the time-mean residual circulations, D represents the substantial time derivative, and the overbar is a time-mean operator. The two E-vectors are given by

$$\mathbf{E_u} = \left[\tfrac{1}{2}(\overline{v'^2} - \overline{u'^2})\mathbf{i},\ -\overline{u'v'}\mathbf{j},\ fR\frac{\overline{v'T'}}{S}\mathbf{k}\right]\cos\phi$$

$$\mathbf{E_v} = \left[-\overline{u'v'}\mathbf{i},\ -\tfrac{1}{2}(\overline{v'^2} - \overline{u'^2})\mathbf{j},\ -fR\frac{\overline{u'T'}}{S}\mathbf{k}\right]\cos\phi$$

[1] This, and the next point, are only true for the Plumb and Trenberth formulations. In the Hoskins et. al. version, the vector is parallel to the minor axis, but the group velocity subtends half of the angle with east.

where u', v' and T' are the eddy momentum and temperature components, S is the static stability that is assumed to vary in the vertical alone, and R is the gas constant. The divergence operator in this coordinate system takes the form

$$\nabla = \left[\frac{\partial}{\partial x}, \frac{1}{\cos\phi}\frac{\partial}{\partial y}, \frac{1}{\rho_0}\frac{\partial}{\partial z}\right]$$

and density is given by $\rho_0 (z) = \rho_{00} e^{-z}$. The horizontal and vertical components of the **E**-vectors are related to the horizontal momentum and heat fluxes, respectively, and are therefore sometimes referred to as the barotropic and baroclinic parts. The divergence of the horizontal term alone is equal to the eddy relative vorticity flux.

Hoskins *et al.* (1983) formulate their **E**-vector representation in terms of the zonal momentum alone. They argue that the zonal derivatives of the eddy statistics are usually much smaller than the meridional derivatives and therefore to a good approximation they may be neglected. They also consider the zonal eddy heat fluxes small. The eddy forced meridional flow in their formulation is just that necessary to maintain the total flow nondivergent. Accordingly, they derive only a single zonal $\mathbf{E_u}$-vector that does not have a factor of $\frac{1}{2}$ in the ith component. Plumb's (1986) form is rather similar to Trenberth's but includes additional terms related the eddy available potential energy. The extra terms make Plumb's formulation provide a more exact relationship between the direction of **E** and the eddy group velocity, but do not force the rotational part of the the large-scale flow.

The zonal barotropic forcing of the mean flow by the eddies is given by the horizontal divergence of $\mathbf{E_u}$ and the meridional acceleration by the curl of $\mathbf{E_u}$. Thus, with the exception of the effect of the relatively small zonal eddy heat fluxes, much of the relevant information on eddy structure, group velocity and mean flow forcing can be qualitatively obtained by examining vector plots of the horizontal components of $\mathbf{E_u}$

overlayed on contours of the northward eddy heat flux for the level of maximum heat fluxes, as suggested by Hoskins *et al.* (1983).

Fig. 5.1 shows the midwinter-mean 300 mb $\mathbf{E}_u$ vectors and the corresponding 700 mb northward eddy heat fluxes computed using bandpass filtered eddy statistics. These two levels were chosen as being near the maximum amplitudes of their represented quantities. Several general characteristics of the bandpass eddies can be ascertained from this plot. First the magnitude of the barotropic $\mathbf{E}_u$ vectors tends to be well correlated with maps of geopotential height RMS variability such as the winter-mean VSTATs shown in Fig. 4.2. The maximum vector magnitudes lie near the two zonally elongated axes that have previously been identified as the principal storm tracks. The storm tracks achieve their maximum intensity downstream of the regions of large eddy heat fluxes consistent with the eddies growing primarily through baroclinic growth processes as they propagate eastward. The $\mathbf{E}_u$ vectors are generally directed eastward implying that $v'^2 > u'^2$ and thus that the bandpass eddies are predominantly meridionally elongated. There is an overall divergence of **E** out of the storm tracks, implying that the eddies are barotropically forcing an eastward acceleration of the time-mean zonal jets. This eastward acceleration appears to reach maximum values just east of the maximum growth regions with a relative minimum located over the western oceans. The fanning out of the E-vectors from the storm tracks implies that the eddies are bow-shaped with maximum eastward extension near the latitude of the jet, an observation supported by Blackmon *et al.* (1984a,b). This characteristic shape of the eddies is often referred to as trough and ridge tilting, and implies a westerly momentum flux into the jets. To the north and south of storm tracks, the **i**-components of the $\mathbf{E}_u$ vectors tend to weaken. This structure yields a positive curl of $\mathbf{E}_u$ to the north and a negative curl to the south and thus a tendency for the eddies to also attempt to induce a diffluent mean flow. The **E** vectors also show some tendency to be directed southward

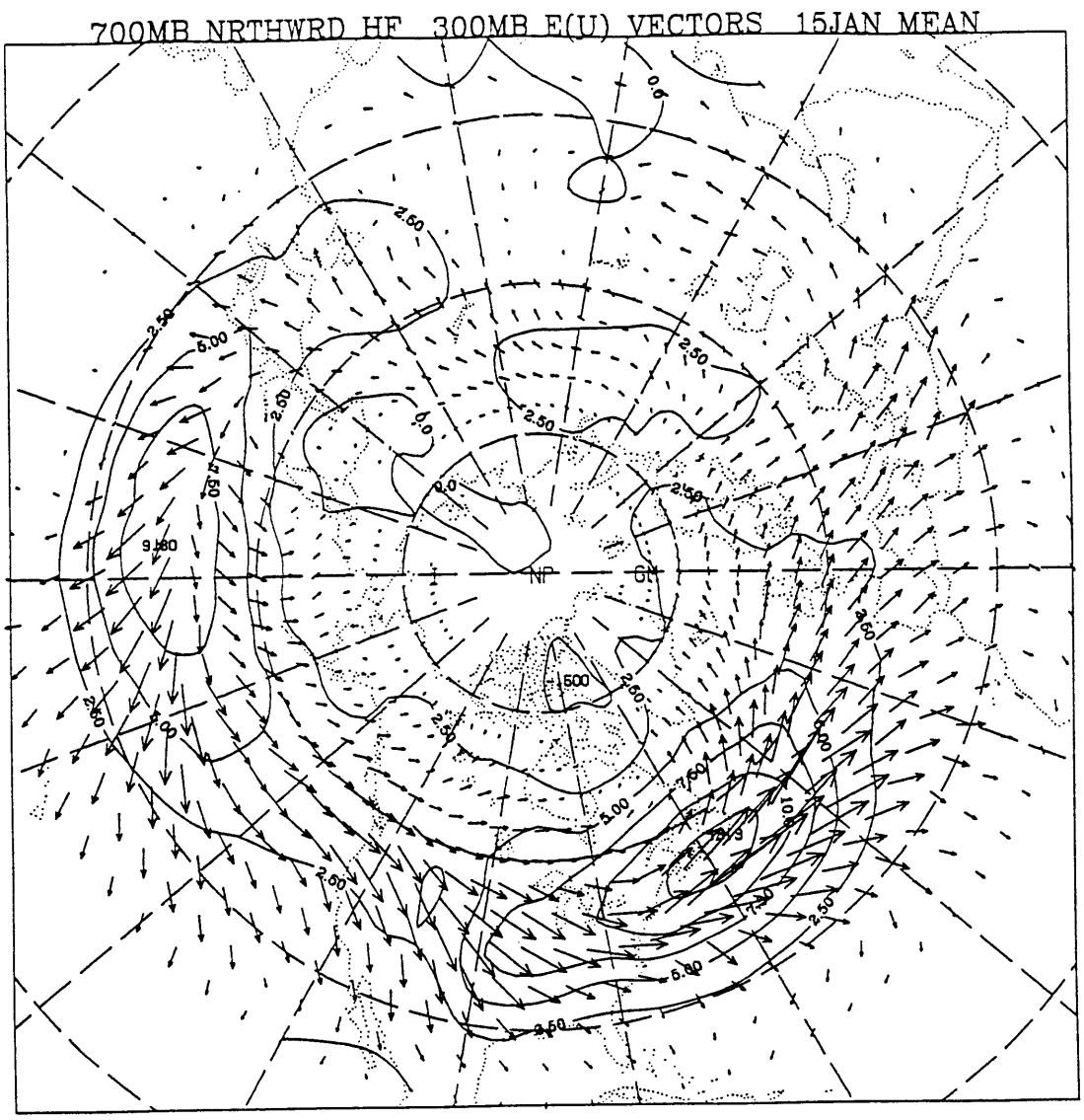

Fig. 5.1 Wintermean 700 mb northward bandpass heat flux (contours, contour interval 2.5 C m s^{-1}) and 300 mb bandpass E_u vectors. The means are computed by evaluating the first four Fourier harmonics of the seasonal cycles on 15 January.

into the tropics, particularly over the central Pacific, implying a tendency toward equatorward propagation of eddy activity.

The northward eddy heat fluxes imply that the eddies tilt predominantly westward (i.e. upshear) with height. The tendency for the northward heat fluxes to be a maximum near 700 mb implies that they tend to force a eastward mean-flow acceleration at low levels and a westward acceleration at upper levels. Thus the baroclinic eddy processes are acting to decrease the shear of the time mean flow and therefore to provide a net downward flux of westerly momentum. Of course, the net effect of the eddies on the mean circulation tendencies, particularly near the surface, must take into account the δ-function potential vorticity tendency implied by the eddy heat fluxes along the lower boundary (Bretherton, 1966).

The Atlantic and Pacific storm tracks as depicted by this plot display several noticeable differences. The Atlantic track appears more intense and more zonally confined than its Pacific counterpart. This suggests that the eddy activity along Atlantic track is characterized by somewhat faster growing but somewhat shorter-lived disturbances. The maximum intensity along the Atlantic track is also near the eastern North American coast, whereas along the Pacific track the maximum intensity appears over the central North Pacific. The overall pattern is consistent with the notion that disturbances from the Pacific frequently propagate into the Atlantic track, but that Atlantic disturbances seldom propagate to the Pacific.

In order to apply the **E**-vector technique to PA flows, we use the general approach outlined in the previous section. That is, we employ composite-mean bandpass **E**-vectors (whose divergence is equal to the composite-mean divergence of the eddy PV flux in Eq. 2) to diagnose the eddy feedbacks on the slowly evolving composite-mean flow. The **E**-vectors are also time-averaged over several phases of the life cycles of the large-scale flow

anomalies, as discussed in Chapter 3. This averaging technique approximates the lowpass filter applied to (3). We then compute a geopotential tendency that would be needed to maintain the forced large-scale flow in geostrophic balance. This geopotential tendency is computed by first forming a relative vorticity tendency associated with the divergences of both the zonal and meridional E-vectors, i.e.

$$\frac{\partial \zeta}{\partial t} = \frac{\partial}{\partial x} \nabla \cdot \mathbf{E}_v - \frac{1}{\cos\phi} \frac{\partial}{\partial y} (\cos\phi \, \nabla \cdot \mathbf{E}_u)$$

A geopotential height tendency ($\partial\Phi/\partial t$) is then computed from this vorticity tendency using

$$\frac{\partial \Phi}{\partial t} = \frac{f}{g} \nabla^{-2} \frac{\partial \zeta}{\partial t} \, . \qquad (4)$$

The Laplacian is inverted using a standard relaxation technique subject to the boundary conditions that there is no height tendency at 20N. Lau (1988) used a similar methodology to display the patterns of eddy forcings and found that the solutions were generally insensitive to the exact location of the southern boundary. Patterns of eddy forcings displayed using this technique are smoother and easier to interpret than plots of the vorticity flux divergences from which they are derived. Shutts (1986) shows that plots of eddy vorticity flux divergences can often be overwhelmed by small scale variations that make it difficult to deduce the important and systematic aspects of the eddy feedbacks.

Lau and Holopainen (1984) show that the effects of 300 mb eddy relative vorticity fluxes tend to dominate the effects due to the heat fluxes. They also found that the vorticity fluxes tend to have an overall equivalent barotropic structure and that the effect of their induced secondary circulations is small. Therefore we anticipate that the barotropic E-vector calculations well approximate the upper tropospheric response to the eddy forcings and thus we will initially limit the discussion to those tendencies. Later in this section we will include the baroclinic tendencies in the calculation, and in the next section we will report on the results of a full three dimensional calculation. It is also important to point out

that these calculations diagnose only the initial linear large-scale response to the eddy forcings, and are not necessarily representative of the ultimate effects of the synoptic-scale eddies on the large-scale flow.

Fig. 5.2 shows the anomalous part of the composite 300 mb horizontal $\mathbf{E}_u$ vectors and the 700 mb heat fluxes associated with the bandpass eddies during four stages of the life-cycles of the Atlantic positive patterns. Fig. 5.3 shows the corresponding barotropic geopotential height tendencies for the same periods. The spatial distributions of the magnitude of the anomalous E-vectors are closely correlated with the anomalous VSTATs discussed in the previous chapter. The anomalous northward heat fluxes correspond closely with the anomalous heat flux vectors described in the previous chapter and attest to the overall dominance of the meridional component of the heat flux. When inspecting the anomalous E-vectors, note that one can not directly distinguish between changes in the mean shapes and orientations of the eddies and changes in eddy amplitude as the sources of the anomalous vectors. However, patterns of the magnitude of the anomalous E-vectors broadly coincide with patterns of the anomalous VSTATs from the previous chapters, suggesting that amplitude variations are playing an important role in the E-vector variations.

Prior to the onset of the Atlantic positive cases, a packet of stronger than normal eddy activity is found upstream over the eastern Pacific and North American regions. Maximum magnitudes of the anomalous E-vectors are found at the eastern edge of an elongated region of anomalous northward heat fluxes. The magnitude of this anomalous eddy activity falls off sharply near the east coast of the North America. Over the central Atlantic, a strongly convergent pattern of anomalous E-vectors is found southwest of the key point (50N 25W), indicating anomalous easterly forcing (i.e. westerly directed) of the mean flow by the eddies. The corresponding height tendencies have a maximum located about 15 degrees upstream of the key point. Height rises are also found along the east

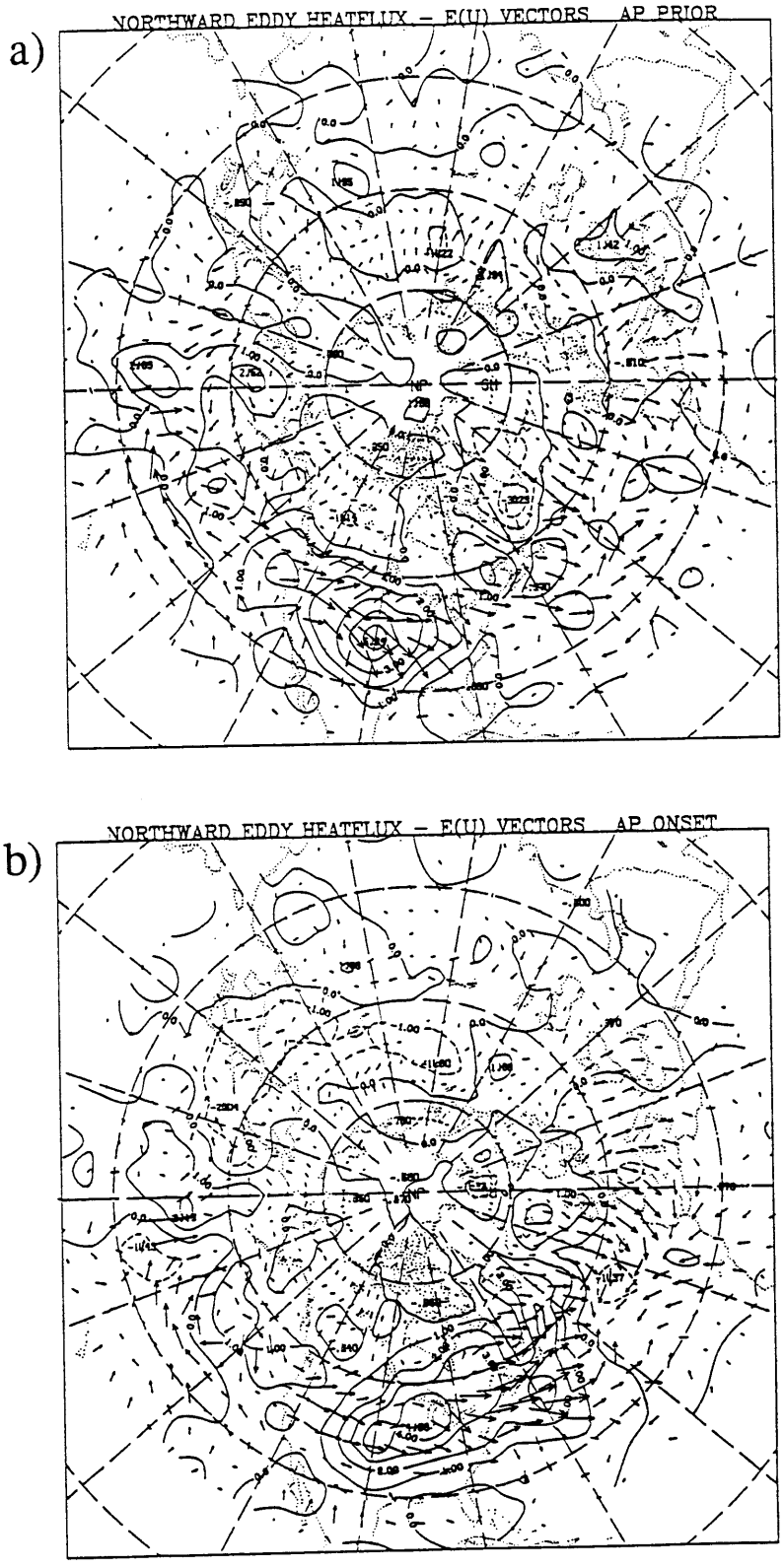

Fig. 5.2 Composite anomalous northward 700 mb bandpass heatflux (contour interval 1C m s^{-1}, negative contours dashed) and composite anomalous 300 mb bandpass $\mathbf{E}_u$ vectors during Atlantic positive PA events. Composites are time averaged over a) the 10 days prior to day 0 of onset and b) the 10 days centered on day 0 of onset.

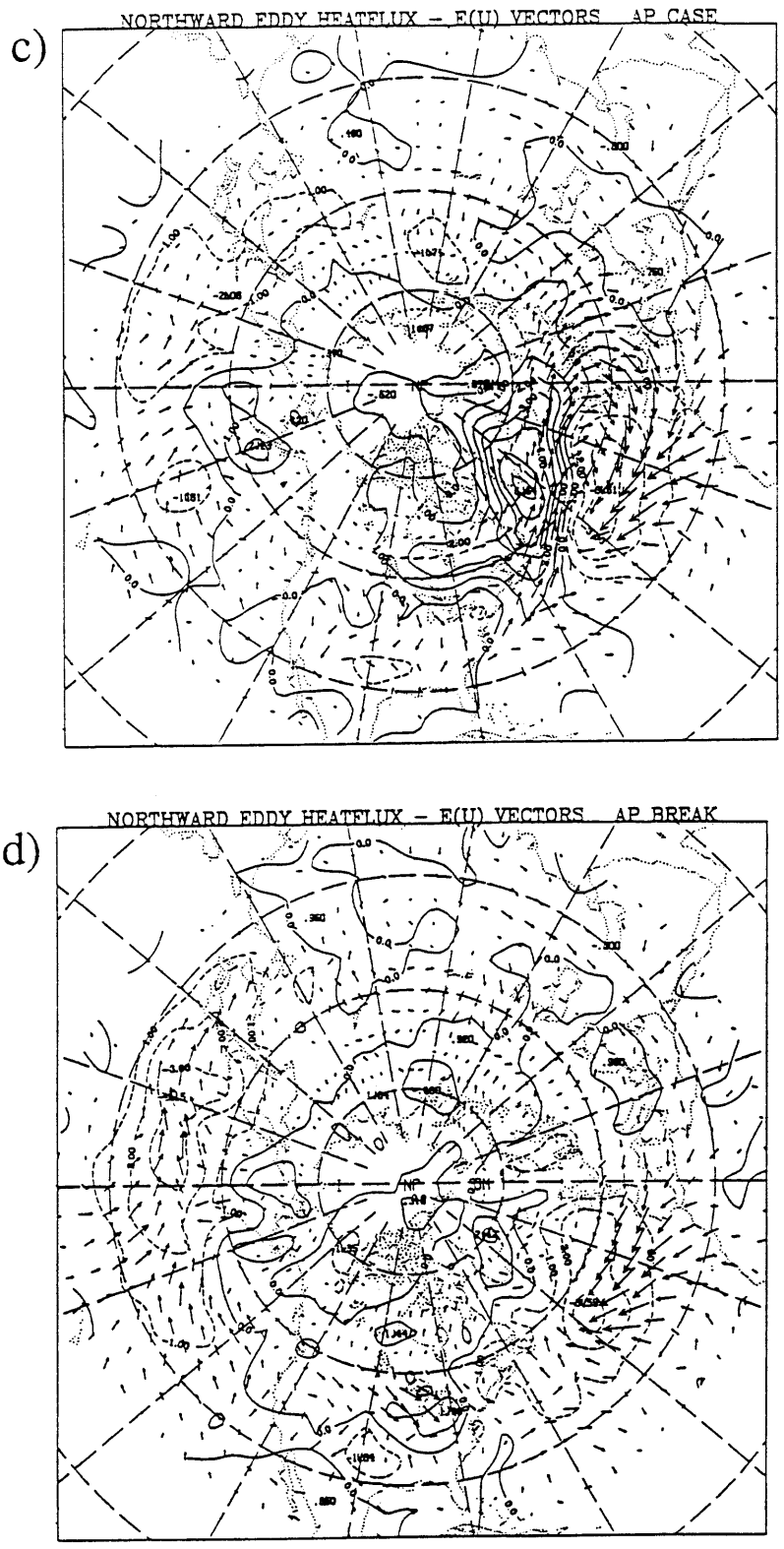

Fig. 5.2 (cont.) Composite anomalous northward 700 mb bandpass heatflux (contour interval 1C m s^{-1}, negative contours dashed) and composite anomalous 300 mb bandpass E_u vectors during Atlantic positive PA events. Composites are time averaged over c) the case duration and d) the 10 days centered on day 0 of breakdown.

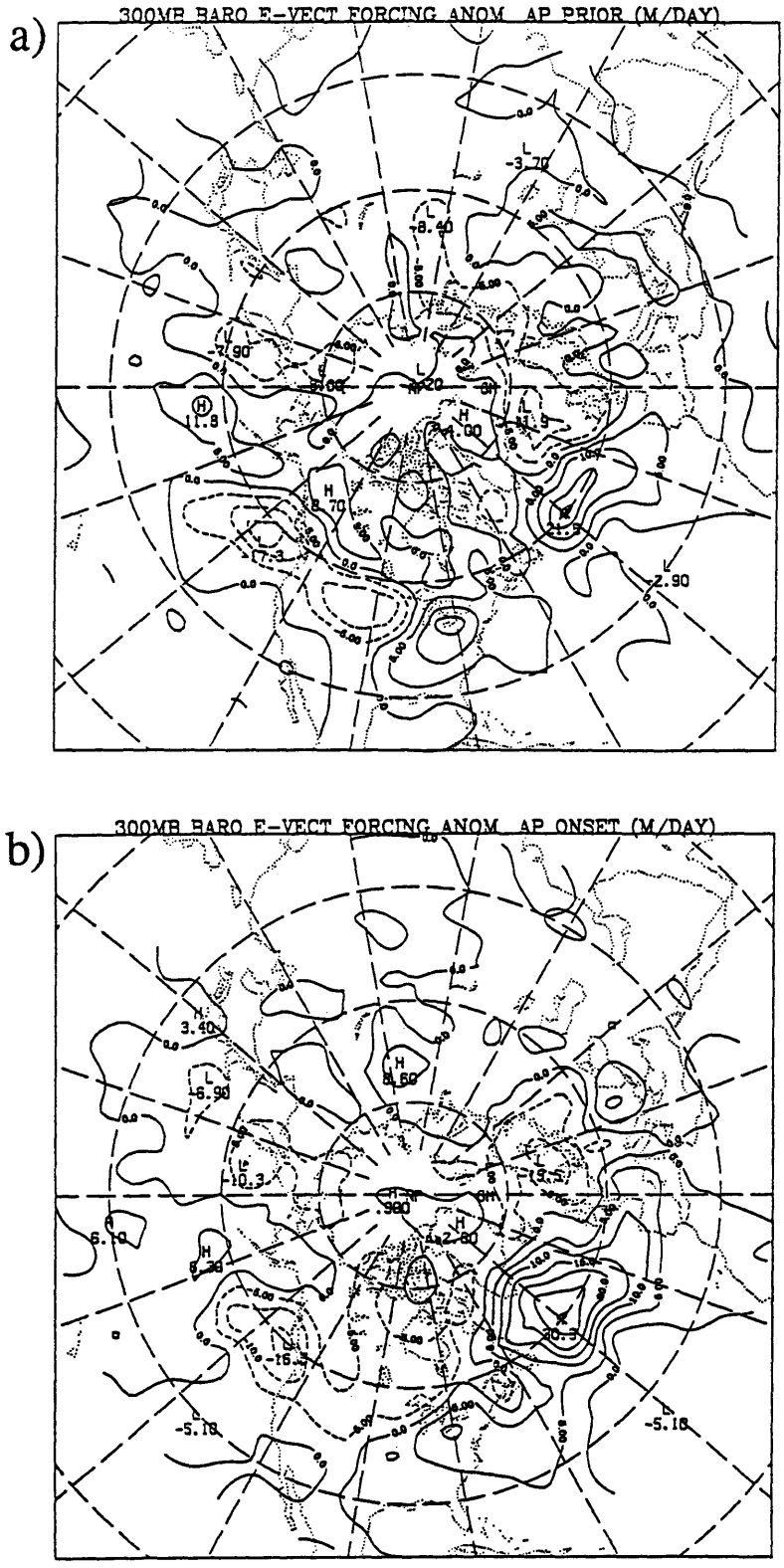

Fig. 5.3. Composite 300 mb geopotential height tendencies due to the time-averaged anomalous barotropic components of the E-vectors during Atlantic positive PAs. Shown are a) the 10 days prior to day 0 of onset and b) the 10 days centered on day 0 of onset. Contour interval is 6 m day^{-1} and negative contours are dashed.

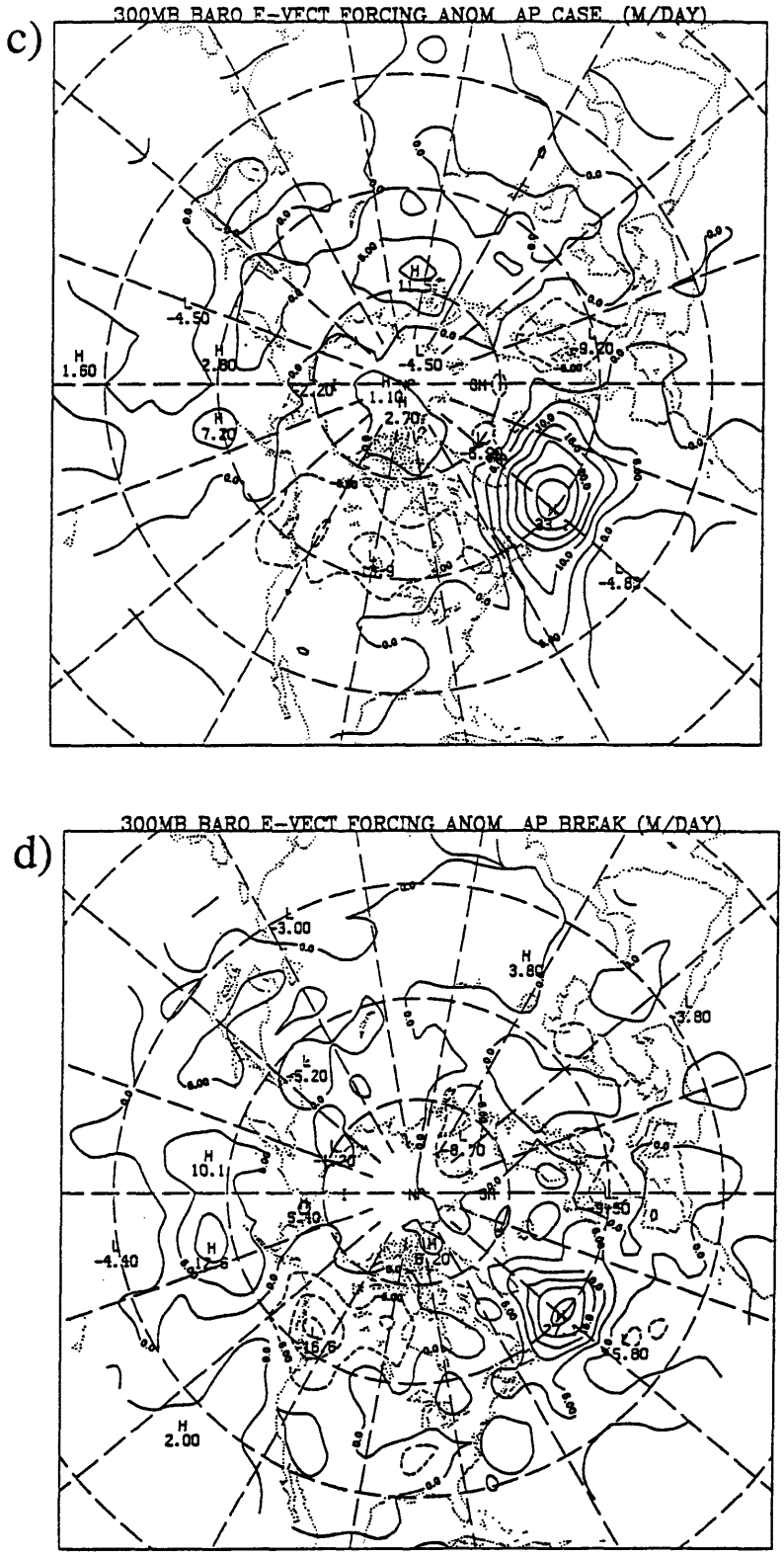

Fig. 5.3 (cont.). Composite 300 mb geopotential height tendencies due to the time-averaged anomalous barotropic components of the E-vectors during Atlantic positive PAs. Shown are c) the case duration average and d) the average over the 10 days centered on day 0 of breakdown. Contour interval is 6 m day^{-1} and negative contours are dashed.

coast, and are associated with the leading edge of the the anomalous eddy packet. During the onset period, the upstream anomalous eddy activity has propagated further east and amplified. The leading edge of the associated packet of anomalous eddy activity now reaches into the central Atlantic. At the same time, most of the E-vectors over the eastern North Atlantic have an anomalous westward component, reflecting weaker than normal eddy activity in that region. The anomalous eddy heat fluxes at this time are strong and downgradient over the eastern half of North America. Just off the coast there is a meridionally extended region of anomalous northward heat fluxes extending from the tropics all the way to the pole. Examination of individual cases suggests that this anomalous northward heat flux is most often associated with strong warm advection ahead of a slowly propagating cold frontal troughs. Fig 5.4 shows the mean sea-level pressure and 1000 to 500 mb thickness pattern during a particularly striking example of this. The height tendencies for this time, show height rises over most of the North Atlantic, with a maximum value of approximately 30 m/day[1]. This implies a spin-up time scale for the large-scale flow anomaly due to the eddy forcings alone of about 10 days, quite close to the observed growth time scale of the composite PA pattern.

During the mature phase of the PAs, the anomalous E-vector activity continues to shift eastward, although anomalously strong eastward directed E-vectors are still found upstream of the key region. The primary storm track is shifted considerably north over the central Atlantic at this time, reflected by the eastward pointing anomalous E-vectors north of the large-scale flow anomaly and westward pointing vectors to the south. There is strong tendency for the E-vectors to rotate about the key point, thus locally forcing the meridional flow southward. The corresponding height tendencies indicate a large anticyclonic circulation tendency centered about 15 degrees upstream of the key point. The

---

[1] An estimate of the magnitude of the large-scale vorticity tendencies can be estimated by dividing the height tendencies by 5×10^6 m sec assuming a plane wave 3 horizontal structure. Thus a 30 m day $^{-1}$ height tendency approximately corresponds to a 6×10^{-6} s^{-1} day $^{-1}$ vorticity tendency.

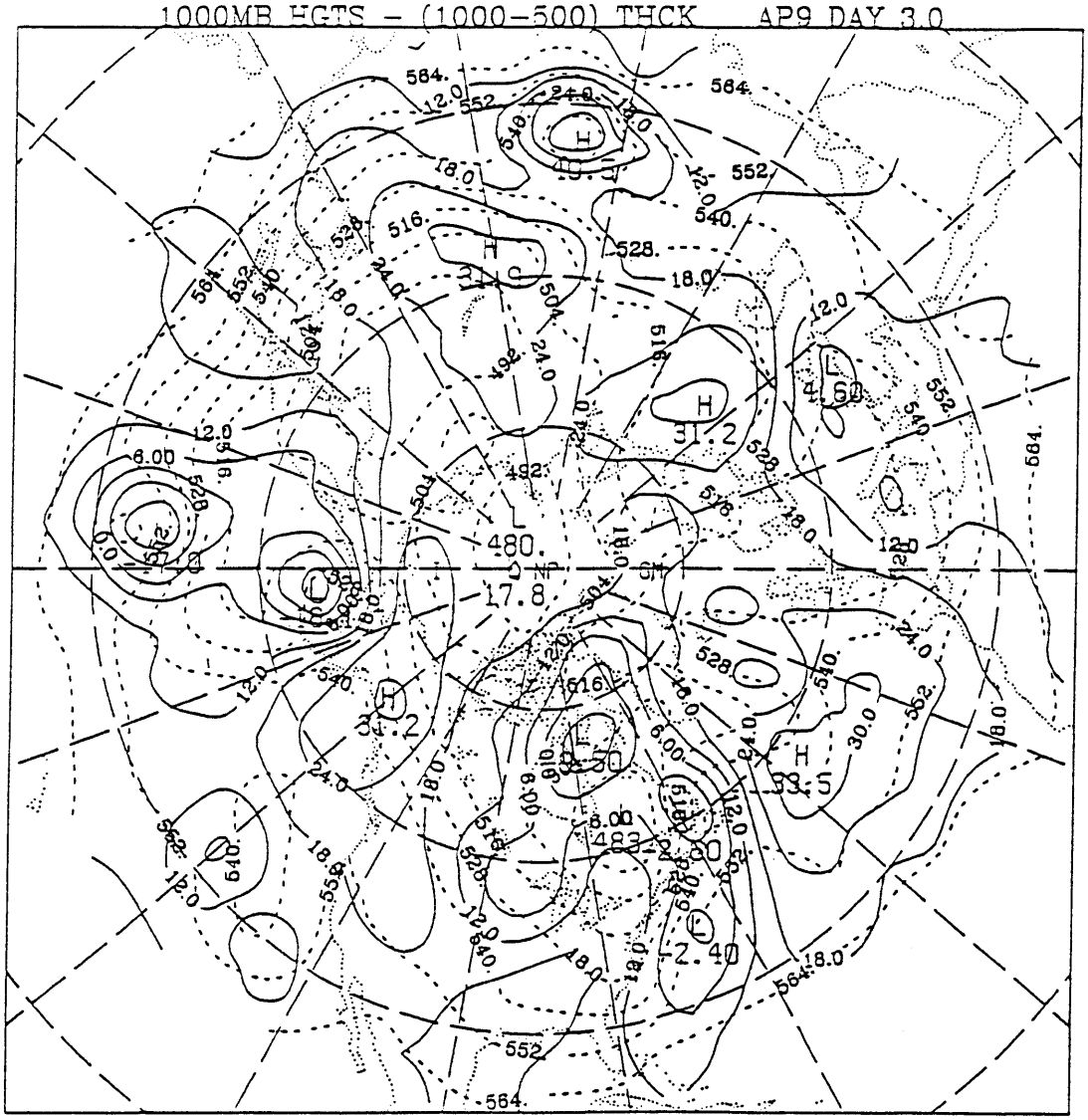

Fig. 5.4 1000 mb heights (solid, contour interval 6 dam) and 1000 mb to 500 mb thickness (dashed, contour inteval 12 dam) during the onset of AP9.

phase shift between the large-scale flow anomaly and the eddy forcing represents approximately 1/6th to1/8th of the wavelength of the large-scale anomaly. Thus our results appear intermediate between Green's (1977) in-phase and Austin's (1980) quadrature phase relationships and in qualitative agreement with results described earlier by Dole (1982), suggesting that the eddies play a significant role in balancing both large-scale advection and dissipation.

During the breakdown phase, the anomalous E-vector pattern weakens considerably, with a small area of convergence upstream of the key region and a corresponding small region of positive height tendencies. There is little evidence that the eddies have any enhanced tendency to force the PA anomaly westward during breakdown, as is often observed for the large-scale flow (e.g. Dole, 1989).

Although the geopotential height tendency patterns during the onset and mature phases of the Atlantic positive PAs are very similar, they are associated with quite different patterns in the E-vectors. During the onset phase, the principal height rises appear largely associated with the leading edge of the anomalous wave packet propagating into the Atlantic. This wave packet was evident in the VSTAT calculations in the previous chapter, and apparently has its origins over the Pacific Ocean. The wave packet undergoes considerable amplification as it crosses North America. As it propagates into the central Atlantic its leading edge is characterized by a strong zonal gradient in the E-vectors, which induces a anomalous westward acceleration of the large-scale flow. The onset pattern appears largely independent of the developing large-scale flow, although the structure of leading edge of the packet may be somewhat modified by the weakly developed large-scale flow at this time. Therefore, it appears that anomalously strong upstream synoptic-scale eddy activity is playing an important role in the development of the Atlantic positive PA pattern. This development scenario is reminiscent of the development stage of sudden stratospheric warming events (Holton, 1981) where a vertically propagating planetary wave

packet propagates upward into the stratosphere. The leading edge of this planetary-wave packet is associated with a vertical convergence of **E**, and thus a easterly acceleration of the time-mean flow. In the Atlantic positive PA cases however, it is the horizontal propagation of a synoptic-scale wave packet that appears to be inducing the anomalous westward acceleration leading to development of the split flow over the central Atlantic.

During the mature phase of the Atlantic positive PA pattern, the eddy forced height tendencies appear to be primarily related to the effects of a northward shifted storm track. The westward pointing E-vectors in and south of the key region (associated with the weaker than normal eddy activity in that region) lead to strong convergence of the E-vectors on the upstream side of the key region. At the same time, the strong rotational part of vectors is forcing a southward acceleration near the key point. Since the large-scale flow anomaly tends to dictate the spatial patterns of anomalous eddy activity near the key region, through the effects of both steering and modified eddy growth and decay regions, the anomalous forcing during the mature phase is apparently a self-maintaining interaction with the synoptic-scale eddies.

Similar anomalous E-vectors and height tendency analyses during the life cycles of the composite Atlantic negative PA cases are shown in Figs. 5.5 and 5.6 respectively. Well prior to onset, the anomalous eddy activity is generally weak, as indicated by the magnitude of the anomalous E-vectors and the northward heat fluxes. Over much of the Pacific and North America, the westward pointing anomalous E-vectors are related to weaker than normal eddy activity, as discussed in the VSTAT results from the previous chapter. The corresponding height tendencies for this period are also weak and erratic. During the onset phase, however, the eddy activity continues to decreases, particularly along the Atlantic storm track west of the key point where strong westward pointing anomalous E-vectors are found. The corresponding barotropic height tendencies are negative over much of the North Atlantic at this time, with a minimum height tendency of

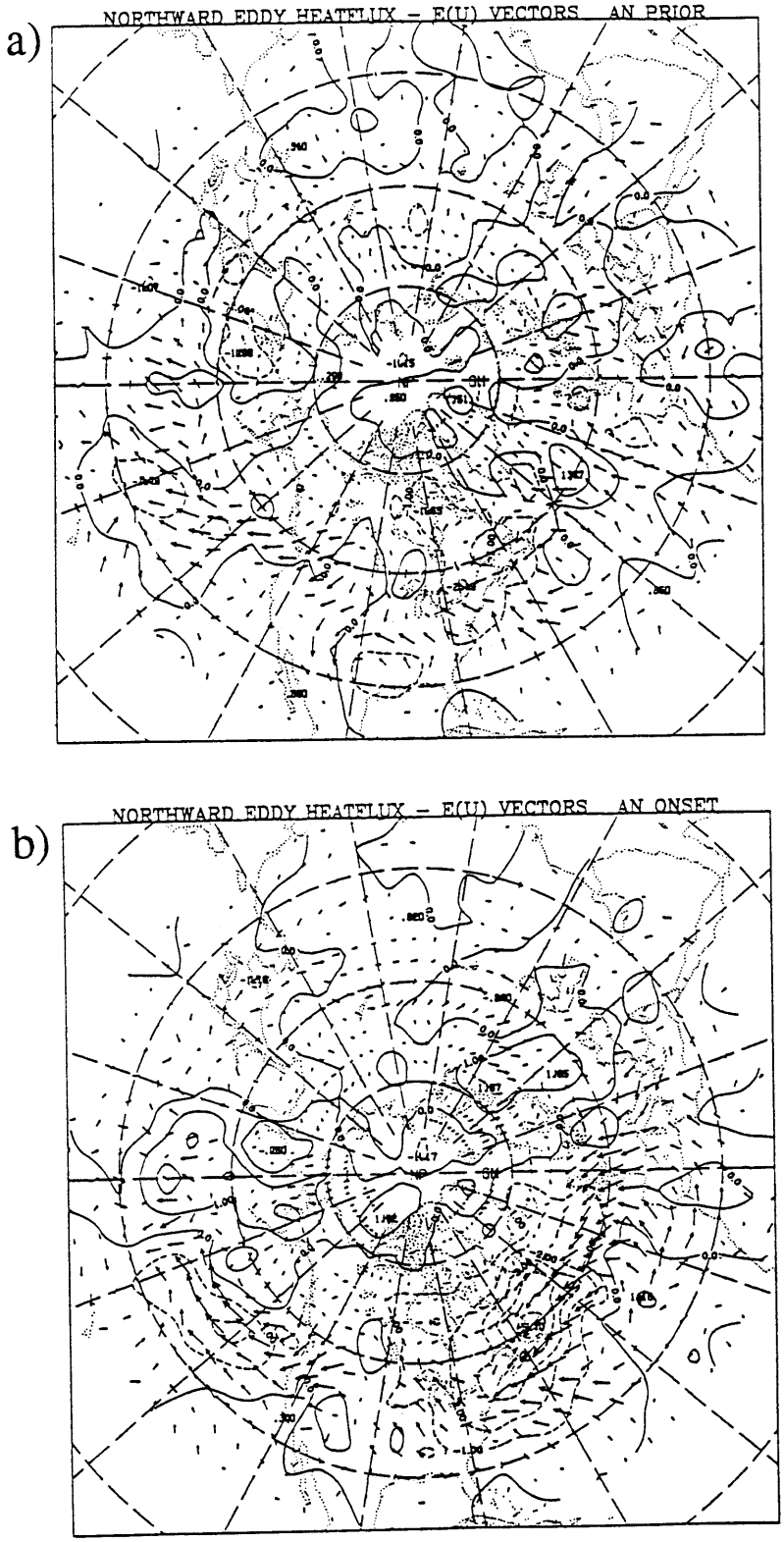

Fig. 5.5 Composite anomalous northward 700 mb bandpass heat flux (contour interval 1C m s^{-1}, negative contours dashed) and composite anomalous 300 mb bandpass E_u vectors during Atlantic negative PA events. Composites are time averaged over a) the 10 days prior to day 0 of onset and b) the 10 days centered on day 0 of onset.

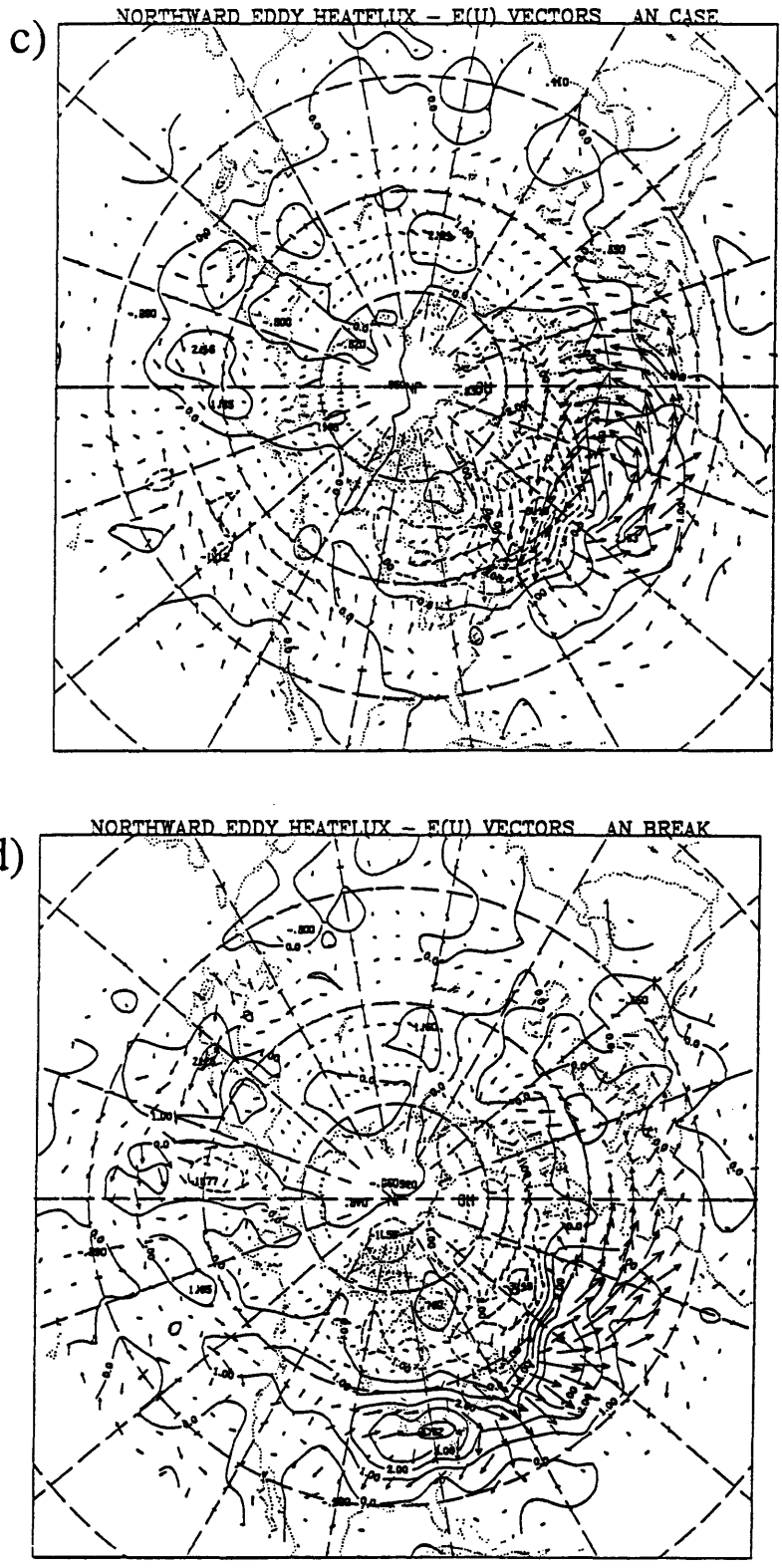

Fig. 5.5 (cont.) Composite anomalous northward 700 mb bandpass heat flux (contour interval 1C m s^{-1}, negative contours dashed) and composite anomalous 300 mb bandpass E_u vectors during Atlantic negative PA events. Composites are time averaged over c) the case duration and d) the 10 days centered on day 0 of breakdown.

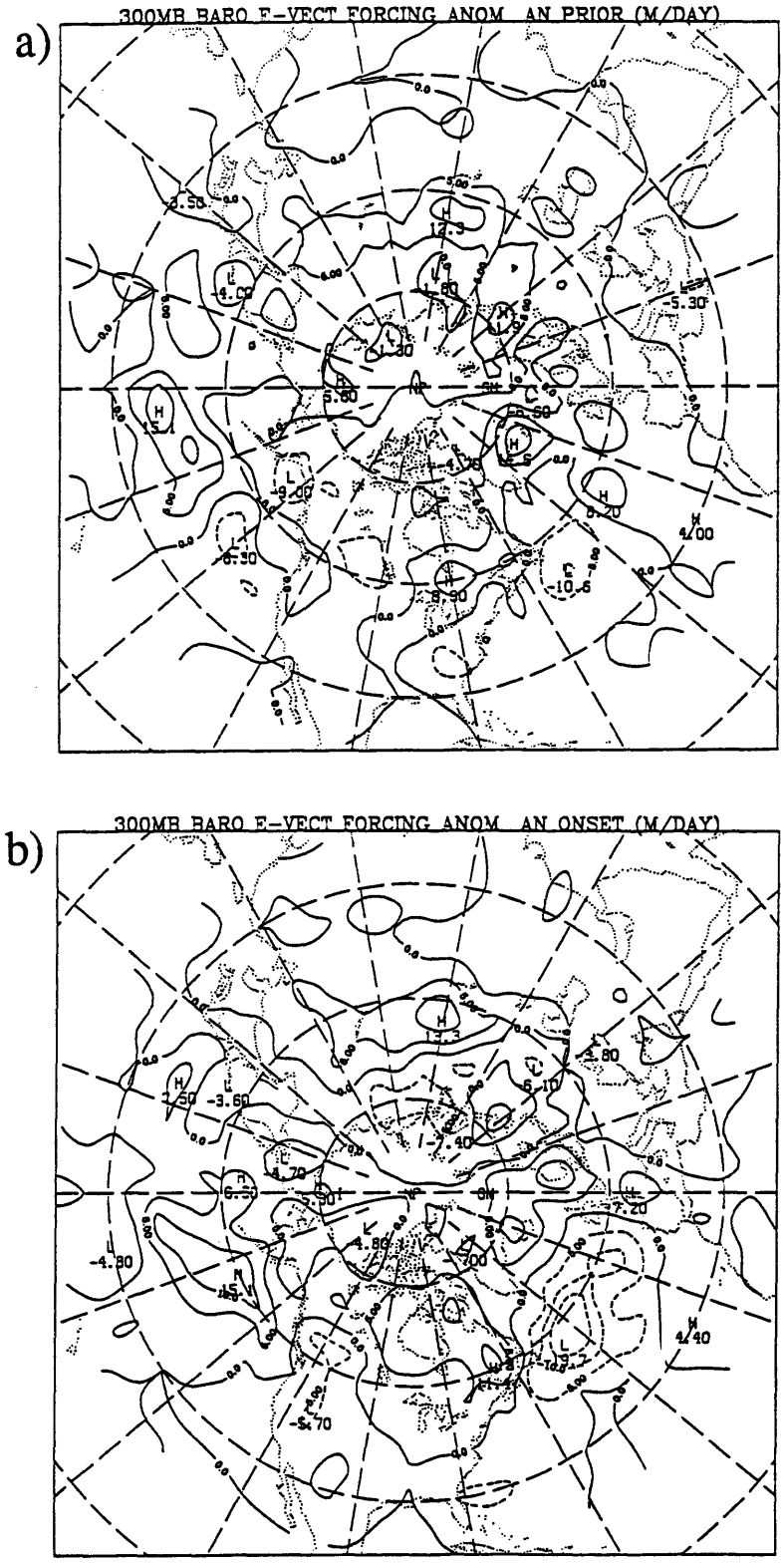

Fig. 5.6. Composite 300 mb geopotential height tendencies due to the time-averaged anomalous barotropic components of the E-vectors during Atlantic negative PAs. Shown are a) the 10 days prior to day 0 of onset and b) the 10 days centered on day 0 of onset. Contour interval is 6 m day^{-1} and negative contours are dashed.

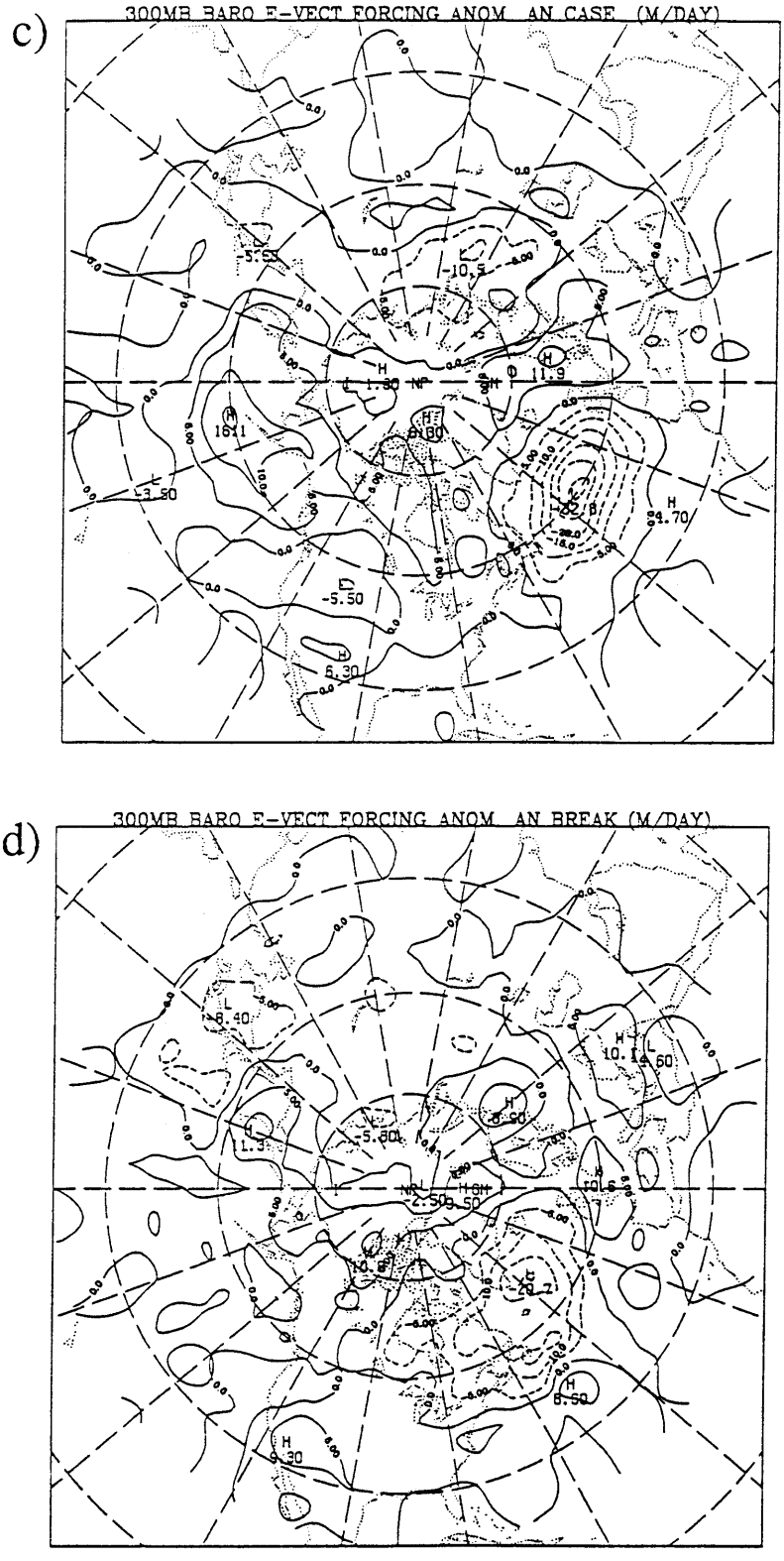

Fig. 5.6 (cont.). Composite 300 mb geopotential height tendencies due to the time-averaged anomalous barotropic components of the E-vectors during Atlantic negative PAs. Shown are c) the case duration average and d) the average over the 10 days centered on day 0 of breakdown. Contour interval is 6 m day^{-1} and negative contours are dashed.

about -20 m/day located about 20 degrees upstream of the developing large-scale anomaly center.

During the mature Atlantic negative PA phase, the patterns of anomalous E-vectors are characterized by a strong gyre centered just upstream of the key point, indicating northward acceleration of the large-scale flow by the eddies is occurring near the center of the large-scale anomaly. To the south of the key point, strongly divergent vectors associated with the anomalous eddy growth imply an anomalous eastward acceleration of the mean flow. To the north of the key region, an inverse pattern is found with anomalous convergence associated with weaker than normal eddy activity. The corresponding height tendencies strongly resemble the large-scale anomaly (Fig. 3.7), but are shifted about 10 degrees upstream. The magnitude of the anomalous forcing indicates that the time scale to spin up the flow to the observed large-scale anomaly is again, about 10 days.

During the breakdown phase of the Atlantic negative pattern, enhanced eddy activity expands westward from south of the key point into North America, as indicated by both the heat fluxes and the E-vectors. Over North America, the anomalous patterns are somewhat similar those found during the onset phase of the Atlantic positive cases. However, closer to the key region the patterns still resemble the mature negative anomaly cases. The westward-directed anomalous E-vectors that characterized the region just north of the key point during the mature phase have weakened considerably. The corresponding height tendency pattern has also weakened and is shifted somewhat northwestward.

Overall, the barotropic eddy forcing pattern during Atlantic negative PAs strongly resembles that of the Atlantic positive PAs, but with opposite sign. The pattern of geopotential height tendencies throughout the life cycles of the negative PA cases can broadly be described by a stationary pattern that resembles the large-scale flow anomaly shifted by about 15 degrees upstream. However, the corresponding anomalous E-vector

patterns from which the stationary height tendency pattern is deduced undergo considerable variation through the life cycles. The E-vector patterns during the negative cases resemble the patterns during the positive cases but with opposite sign. However, the packet of anomalous eddy activity that propagates into the key region prior to and during the onset of the positive cases is not as well defined in the negative cases. Rather, most of the upstream region during the onset of the negative cases is characterized by westward pointing anomalous E-vectors and by reduced eddy heat fluxes that do not seem to have temporarily consistent boundaries which would clearly define an anomalous wave packet.

The anomalous E-vectors and associated barotropic height tendencies for the Pacific positive PA cases are shown in Fig. 5.7 and 5.8 respectively. In many respects, the anomalous E-vector and heat flux patterns for the Pacific cases resemble those found for the Atlantic cases. Prior to and during onset of these cases, enhanced eddy activity upstream of the key region is indicated by the anomalous eastward pointing E-vectors and enhanced eddy heat fluxes. During the mature phase of these cases, the storm track is shifted well north of its climatological-mean position, and accordingly, the anomalous E-vectors tend to have large rotational component around the key point. South of the key point there is a strong zonal convergence in the vectors, indicating a tendency for anomalous eddy activity to accelerate the large-scale flow westward. The corresponding barotropic geopotential height tendency pattern has height rises centered near the key point. As in the Atlantic cases, the time scale associated with this forcing to spin up the observed large-scale anomaly pattern is about 10 days. However, unlike the Atlantic cases, throughout the PA life cycle the barotropic forcing during the Pacific cases is geographically in-phase with the large-scale flow anomaly. The forcing tends to drift northward during the life cycle, a tendency also apparent in the large-scale flow anomaly (Figs. 3.11 and 3.16). Over eastern Asia there are relatively strong negative barotropic height tendencies (~15 m day^{-1}) during both the onset and mature phases of the PA,

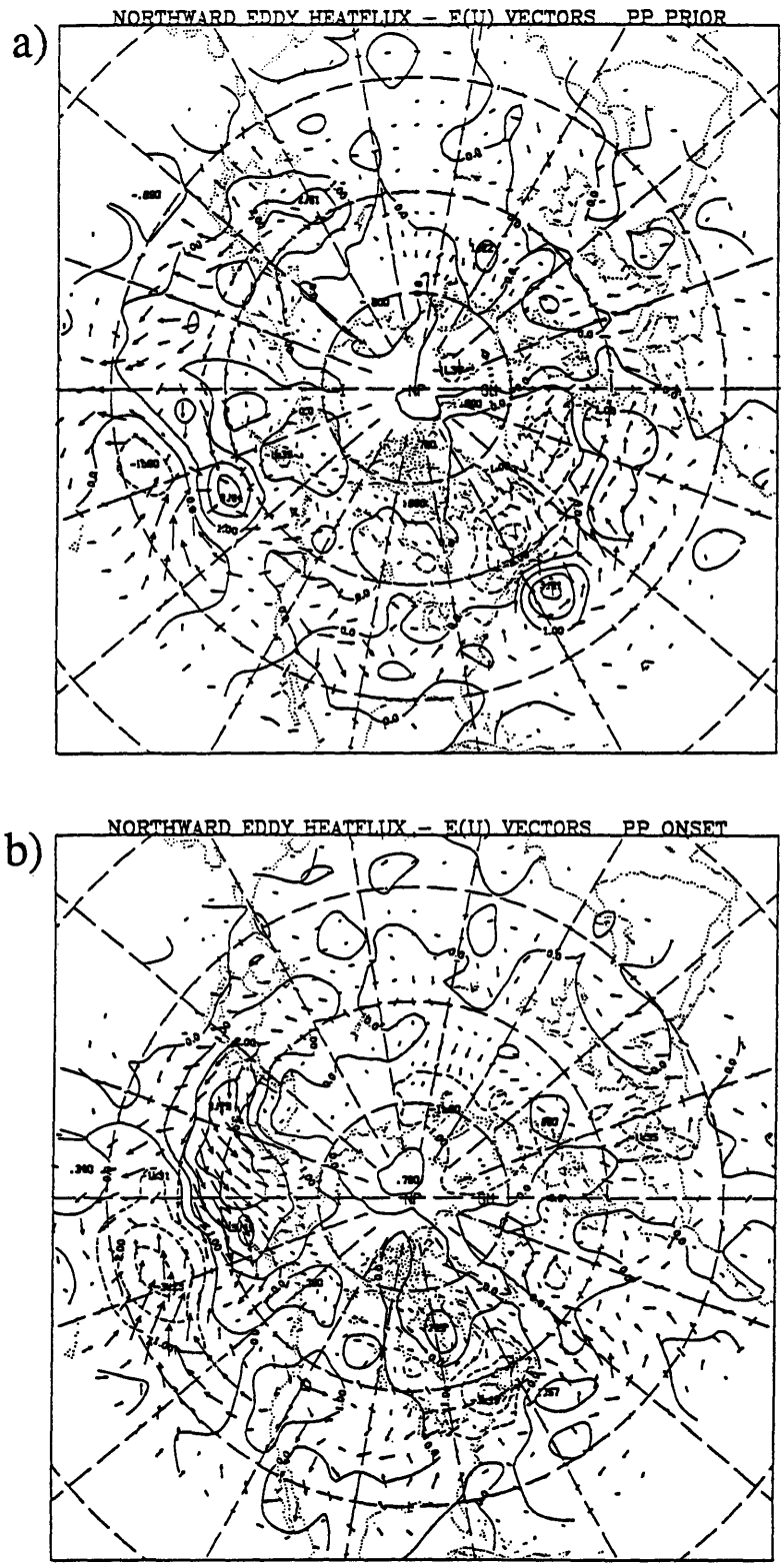

Fig. 5.7 Composite anomalous northward 700 mb bandpass heat flux (contour interval 1C m s^{-1}, negative contours dashed) and composite anomalous 300 mb bandpass E_u vectors during Pacific positive PA events. Composites are time averaged over a) the 10 days prior to day 0 of onset and b) the 10 days centered on day 0 of onset.

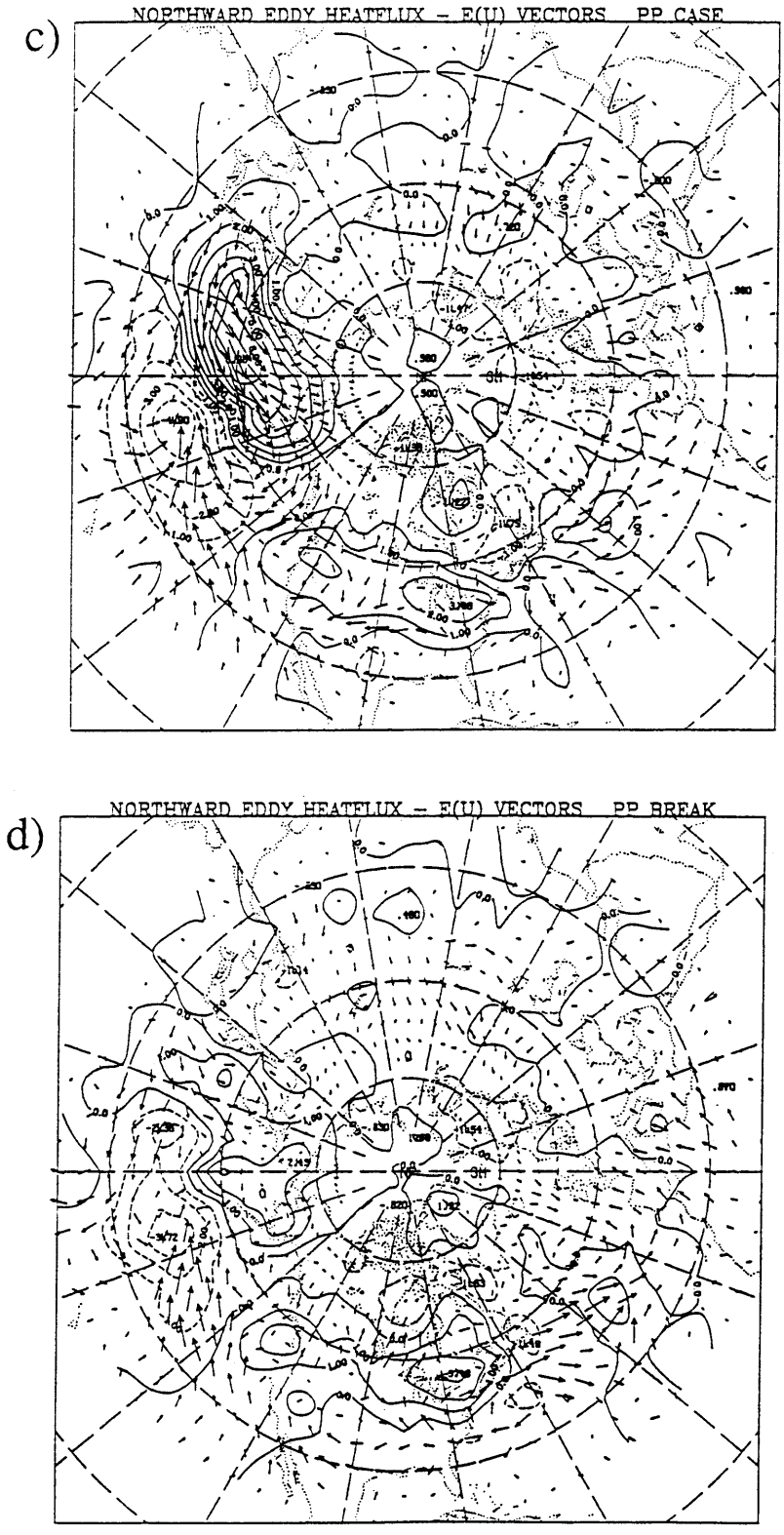

Fig. 5.7 (cont.) Composite anomalous northward 700 mb bandpass heat flux (contour interval 1C m s^{-1}, negative contours dashed) and composite anomalous 300 mb bandpass $\mathbf{E}_u$ vectors during Pacific positive PA events. Composites are time averaged over c) the case duration and d) the 10 days centered on day 0 of breakdown.

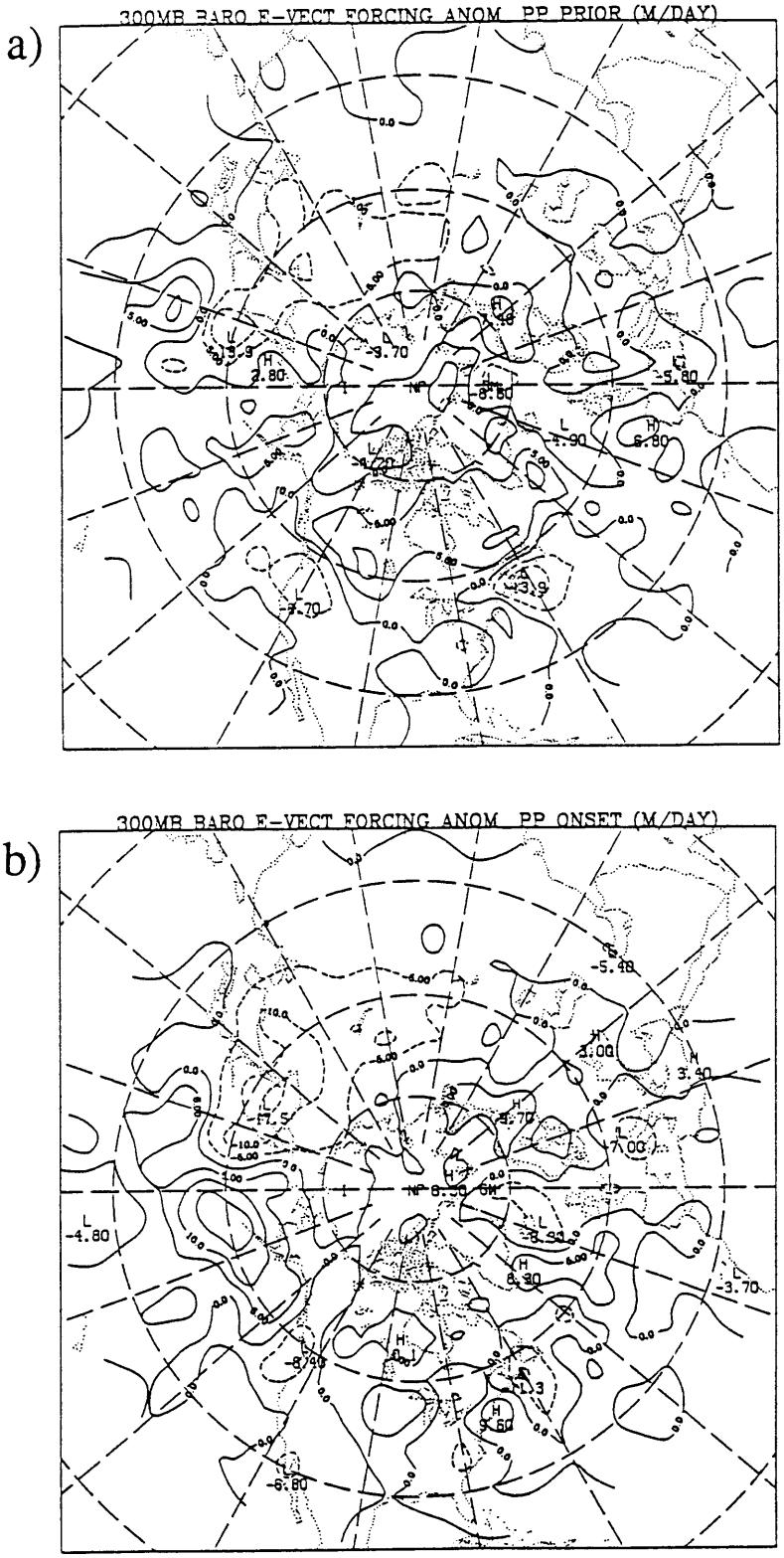

Fig. 5.8. Composite 300 mb geopotential height tendencies due to the time-averaged anomalous barotropic components of the E-vectors during Pacific positive PAs. Shown are a) the 10 days prior to day 0 of onset and b) the 10 days centered on day 0 of onset. Contour interval is 6 m day^{-1} and negative contours are dashed.

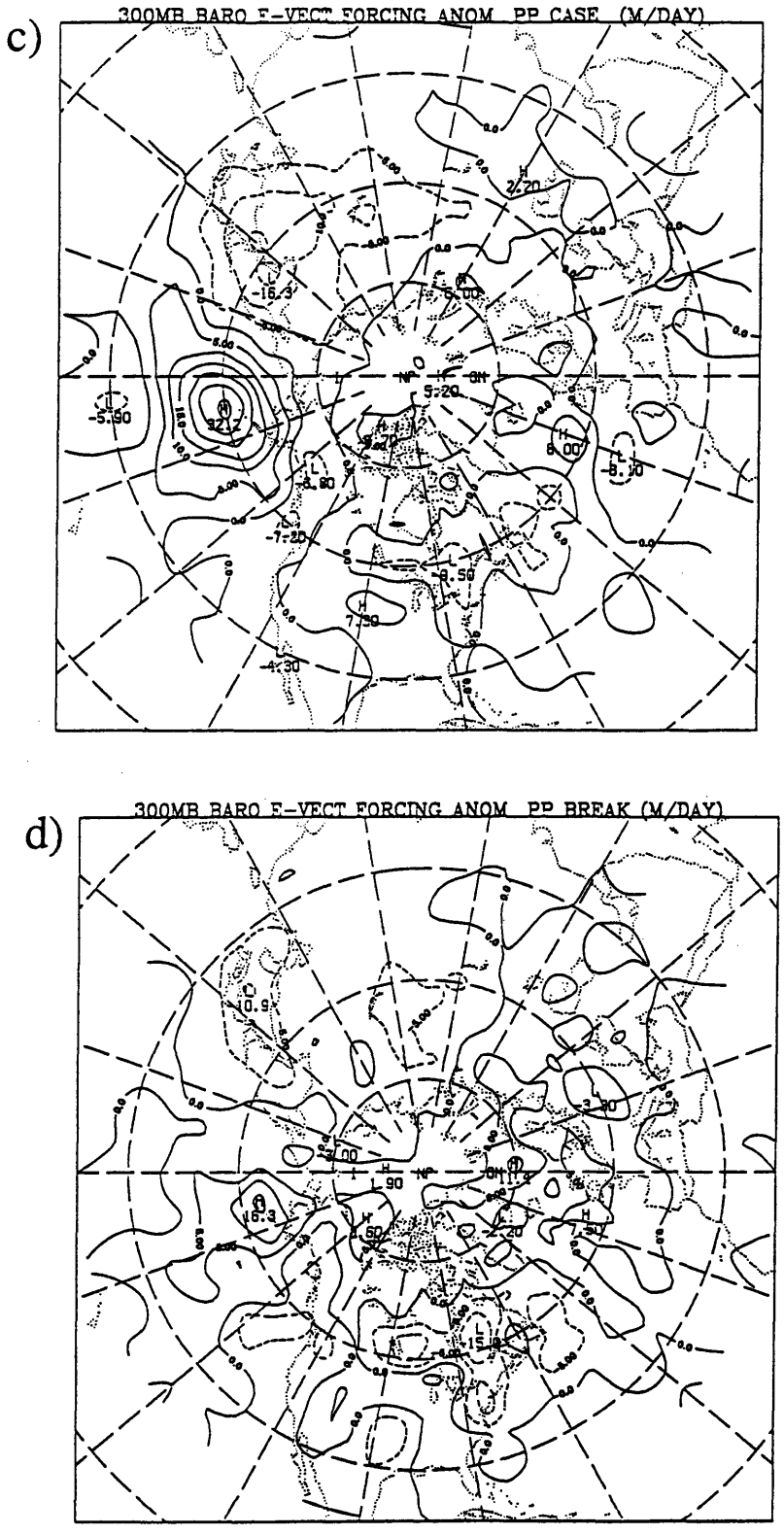

Fig. 5.8 (cont.). Composite 300 mb geopotential height tendencies due to the time-averaged anomalous barotropic components of the E-vectors during Pacific positive PAs. Shown are c) the case duration average and d) the average over the 10 days centered on day 0 of breakdown. Contour interval is 6 m day^{-1} and negative contours are dashed.

although large-scale negative height anomalies are not observed there. Further downstream of the key region, there are negative height tendencies over much of eastern Canada during the mature and breakdown phases. These height tendencies seem to be associated with an enhanced storm track across the Great Lakes and into the central Atlantic. However again, the observed geopotential height composite anomalies do not show any clear local response to this eddy forcing.

One possible explanation why the Pacific barotropic forcing tends to occur over the large-scale flow anomaly while the Atlantic forcing tends to occur upstream of the large-scale flow anomaly may have to do with the position of each of the PA patterns with respect to the stationary waves. The Atlantic key point lies near a ridge in the stationary wave pattern, with the PA induced diffluence on the upstream side tending to enhance that climatological-mean diffluence. One the other hand, there is a relatively large separation between the Pacific PA key point and the nearest stationary wave ridge, so that a positive mutual enhancement of the diffluence pattern tends not to occur. If eddy straining and dissipation in diffluent flow regions is the primary cause for the zonal gradient in $\mathbf{E}_u$ (and thus the westward acceleration) that occurs near the PA centers, then we may expect that this process would be more efficient further upstream of the Atlantic key point than of the Pacific key point. That is to say, if the eddies must experience a critical amount of deformation in diffluent flow regions before significant enhancement of eddy dissipation occurs, than that critical point will more likely lie further upstream in the Atlantic cases than in the Pacific cases. The fact that the magnitudes of the barotropic forcings for the Atlantic and Pacific cases are so similar despite different large-scale diffluent patterns, suggests that the operating mechanism is nonlinear and perhaps is easily saturated. A somewhat different dynamical balance for the Pacific cases than the Atlantic cases is suggested by these analyses, as the barotropic eddy forcing apparently does not balance the advection of the PA downstream by the climatological-mean flow.

The anomalous E-vectors and associated height tendencies during the life cycles of the Pacific negative PA cases are shown in Figs. 5.9 and 5.10, respectively. As anticipated from the VSTAT calculations in the previous chapters, the patterns of anomalous eddy activity as indicated by the anomalous E-vectors have the smallest magnitudes of the four PA types considered. Nonetheless the patterns do resemble the corresponding patterns from the Atlantic negative cases, and also tend to be directed opposite to the patterns observed in the Pacific positive cases. Prior to and during onset, weaker than normal eddy activity and associated westward pointing anomalous E-vectors induce a negative height tendency over the key point. During the mature phase, the southward and eastward shifted storm track is evident in the E-vector patterns, with westward pointing vectors north of the key point and eastward directed vectors to the south. As in the previous cases examined, the varying E-vector patterns throughout the life cycle yield approximately the same height tendency pattern with maximum height falls noted over or even just east of the key point. During the breakdown phase, the height tendencies remains basically intact. Outside of the key region, weak height rises are found over Siberia and the Pacific Northwest region of the U.S. throughout most of the life cycle. The latter region is indeed a region of substantial positive height anomalies during these cases, and there appears to be some positive eddy forcing of this anomaly. However, the magnitudes of the eddy forcing for this downstream anomaly as well as for the principal anomaly itself are weak, and by themselves are not sufficient to account for the observed developments.

Fig 5.11 shows the total geopotential height tendencies (including the baroclinic components) during the onset phase of each of the the PA cases. For the Atlantic cases, the results are qualitatively unchanged when the baroclinic terms are included. The extreme height tendencies still imply a 10 day time scale for the eddy forcing to spin up the observed large-scale flow anomaly. The point of maximum height tendencies during the Atlantic positive cases is now more nearly over the key point (rather than upstream) in this

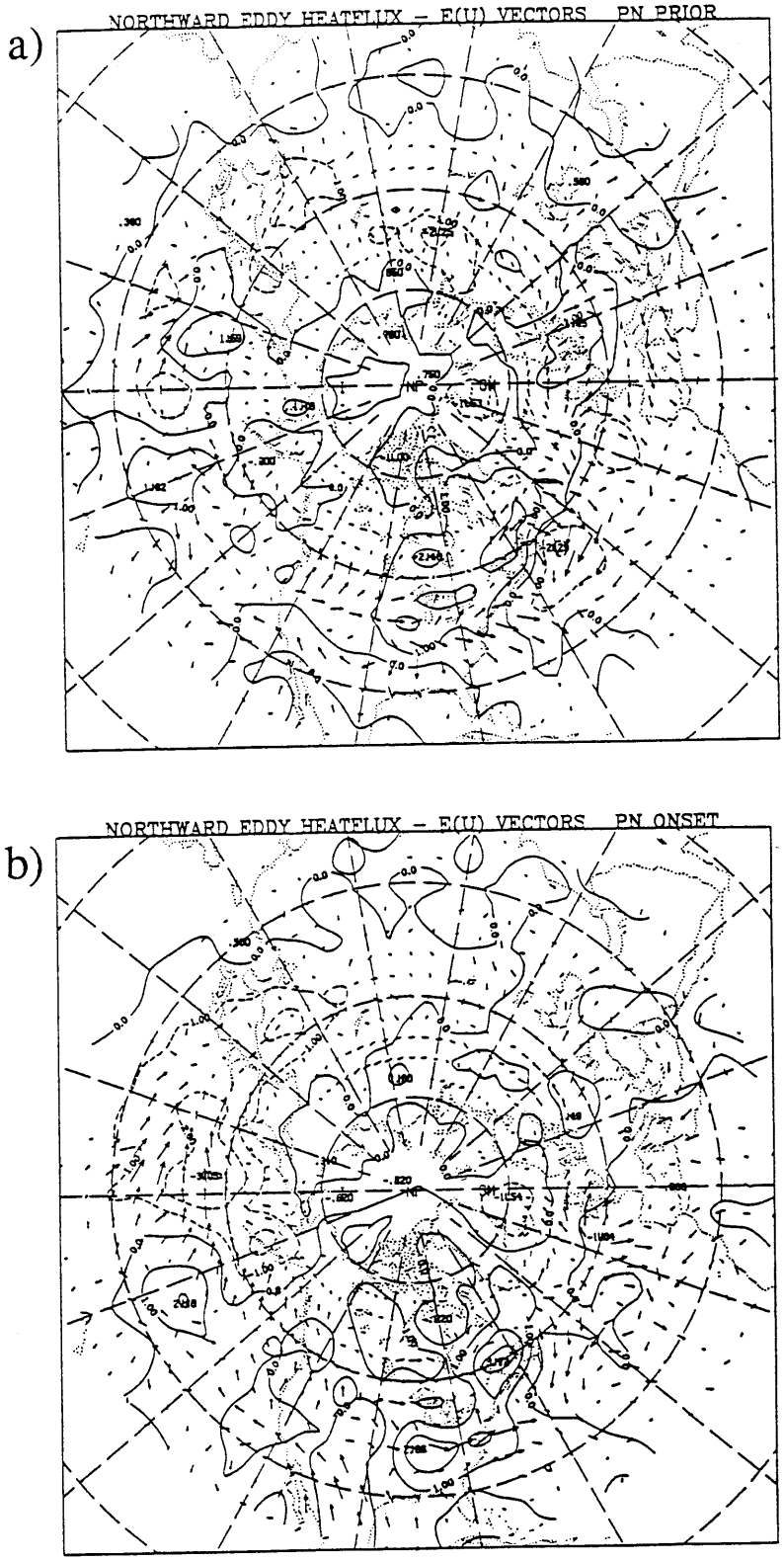

Fig. 5.9 Composite anomalous northward 700 mb bandpass heat flux (contour interval 1C m s^{-1}, negative contours dashed) and composite anomalous 300 mb bandpass $\mathbf{E_u}$ vectors during Pacific negative PA events. Composites are time averaged over a) the 10 days prior to day 0 of onset and b) the 10 days centered on day 0 of onset.

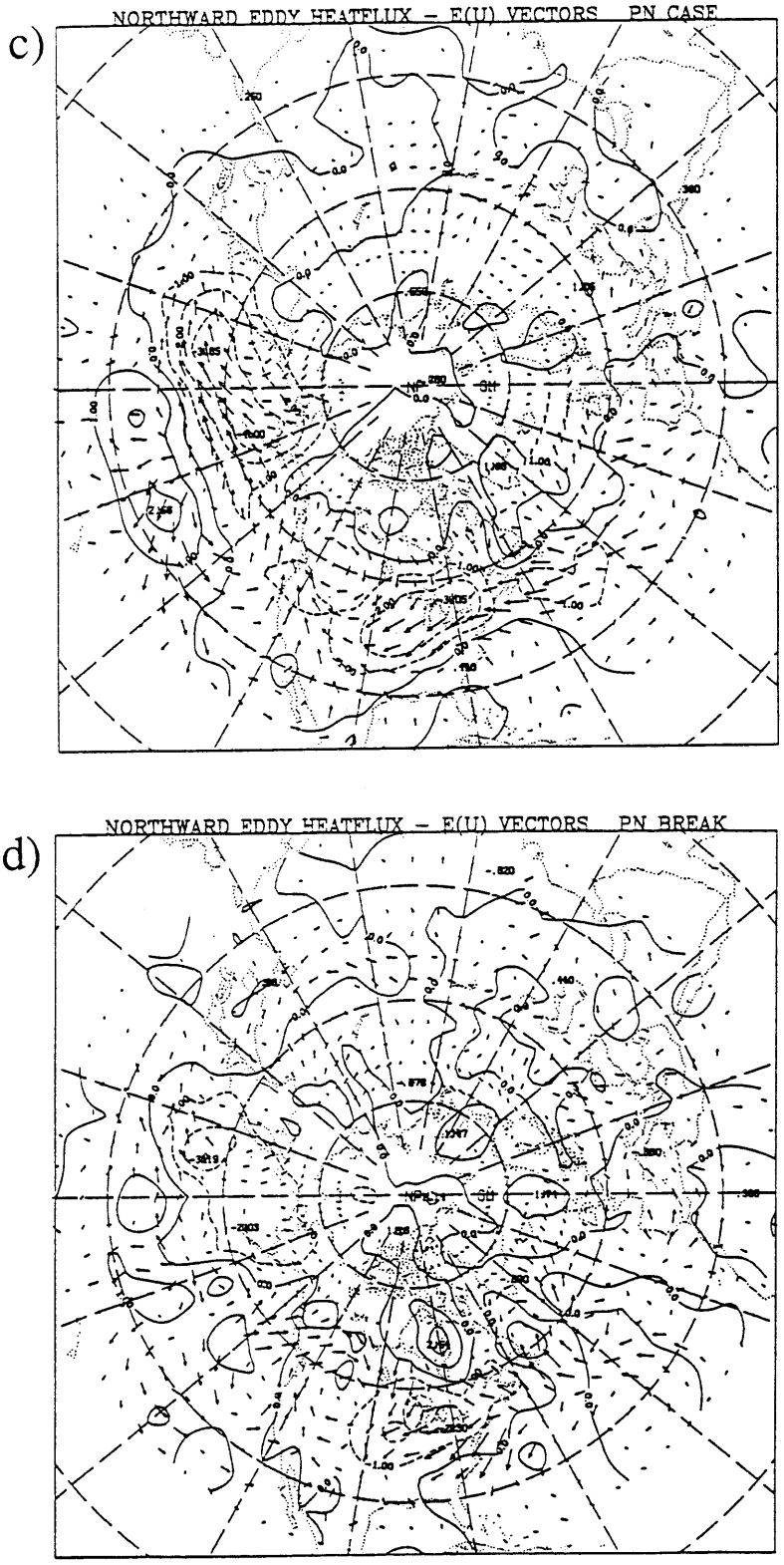

Fig. 5.9 (cont.) Composite anomalous northward 700 mb bandpass heat flux (contour interval 1C m s^{-1}, negative contours dashed) and composite anomalous 300 mb bandpass E_u vectors during Pacific negative PA events. Composites are time averaged over c) the case duration and d) the 10 days centered on day 0 of breakdown.

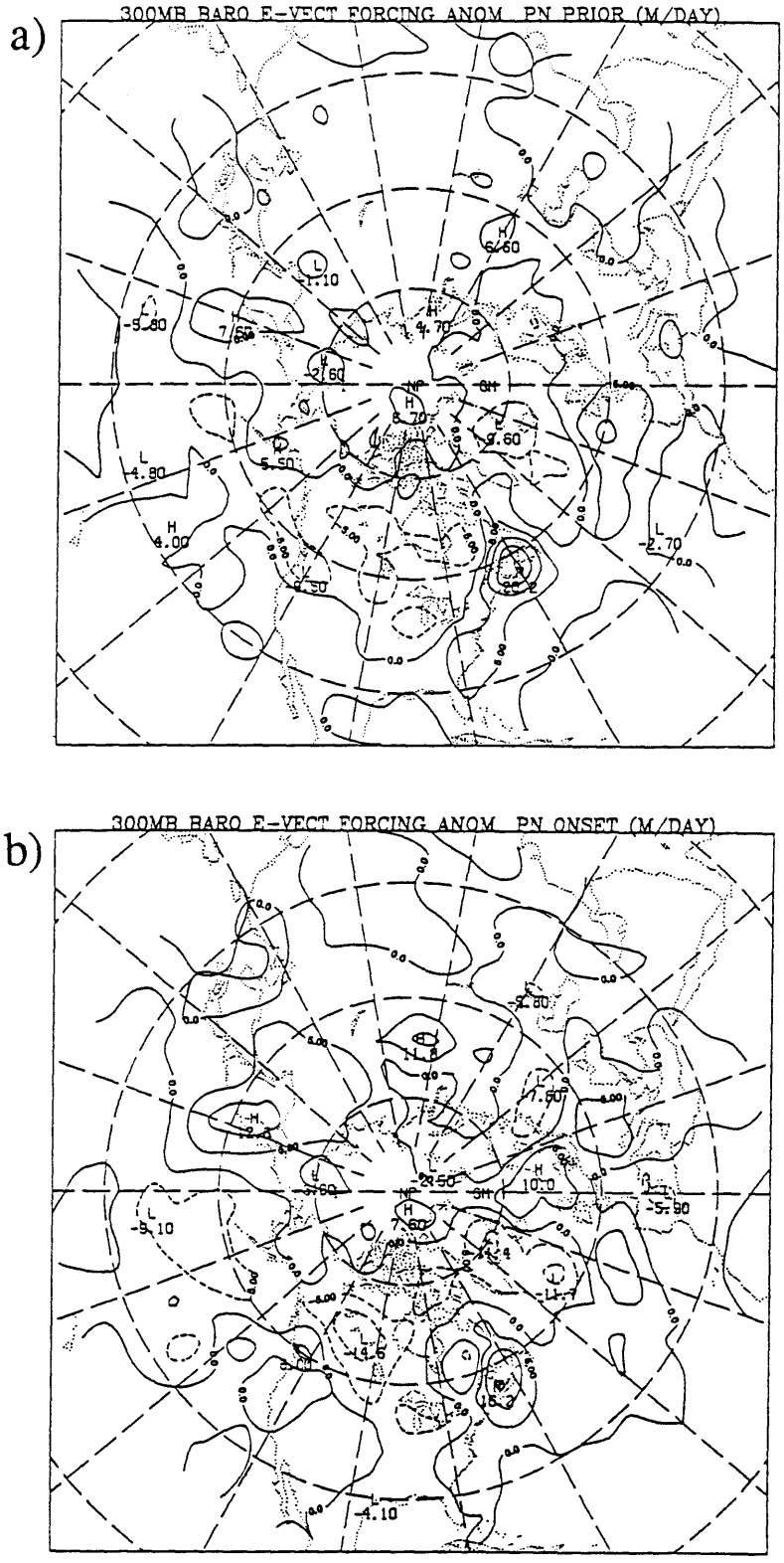

Fig. 5.10. Composite 300 mb geopotential height tendencies due to the time-averaged anomalous barotropic components of the **E**-vectors during Pacific negative PAs. Shown are a) the 10 days prior to day 0 of onset and b) the 10 days centered on day 0 of onset. Contour interval is 6 m day^{-1} and negative contours are dashed.

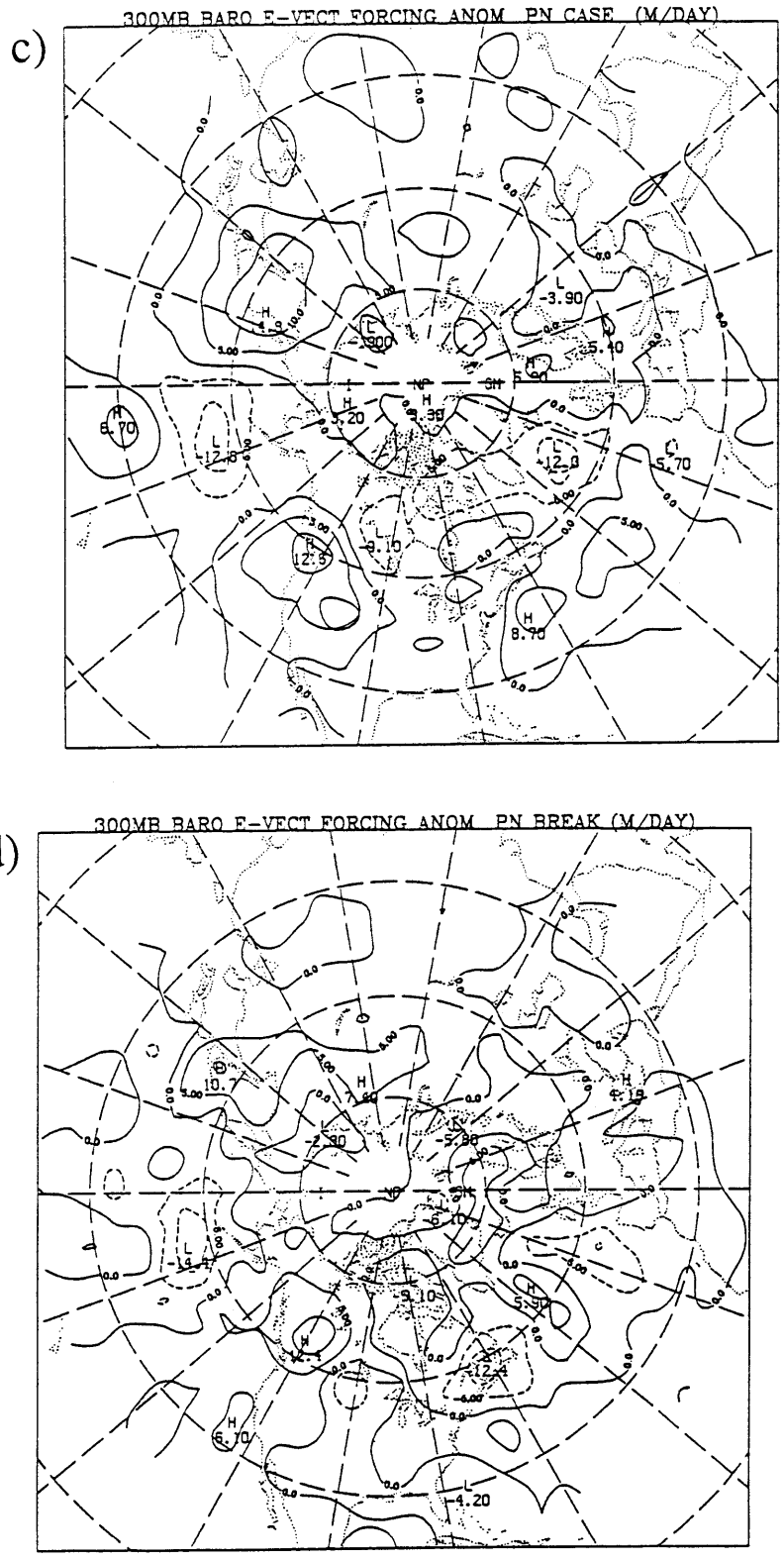

Fig. 5.10 (cont.). Composite 300 mb geopotential height tendencies due to the time-averaged anomalous barotropic components of the **E**-vectors during Pacific negative PAs. Shown are c) the case duration average and d) the average over the 10 days centered on day 0 of breakdown. Contour interval is 6 m day^{-1} and negative contours are dashed.

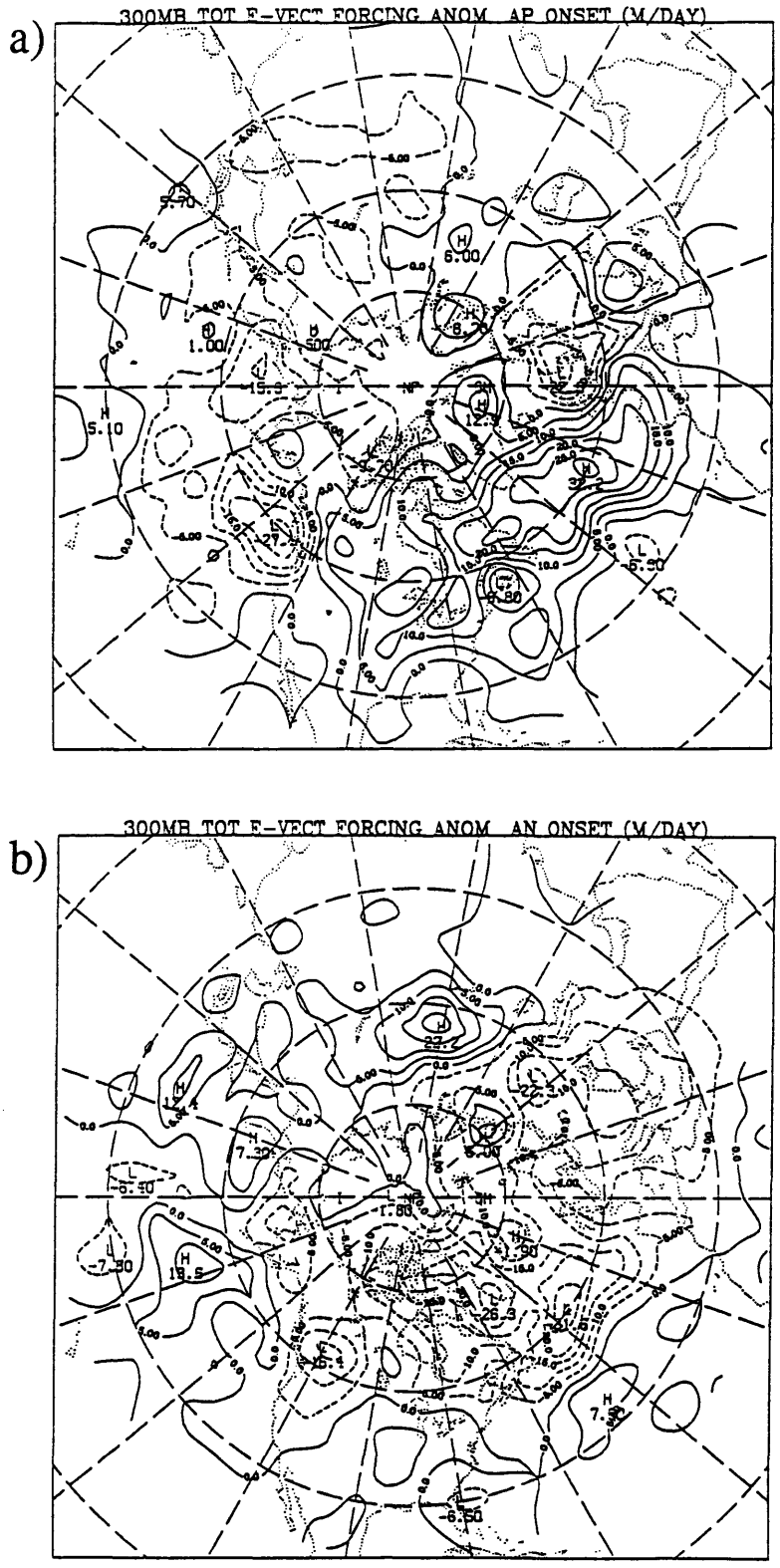

Fig. 5.11. Composite 300 mb anomalous geopotential height tendencies due to both the barotropic and baroclinic components of the bandpass E-vectors averaged over the 10 days centered on day 0 of onset for a) Atlantic positive and b) Atlantic negative PA events. Contour interval is 6 m day^{-1} and negative contours are dashed.

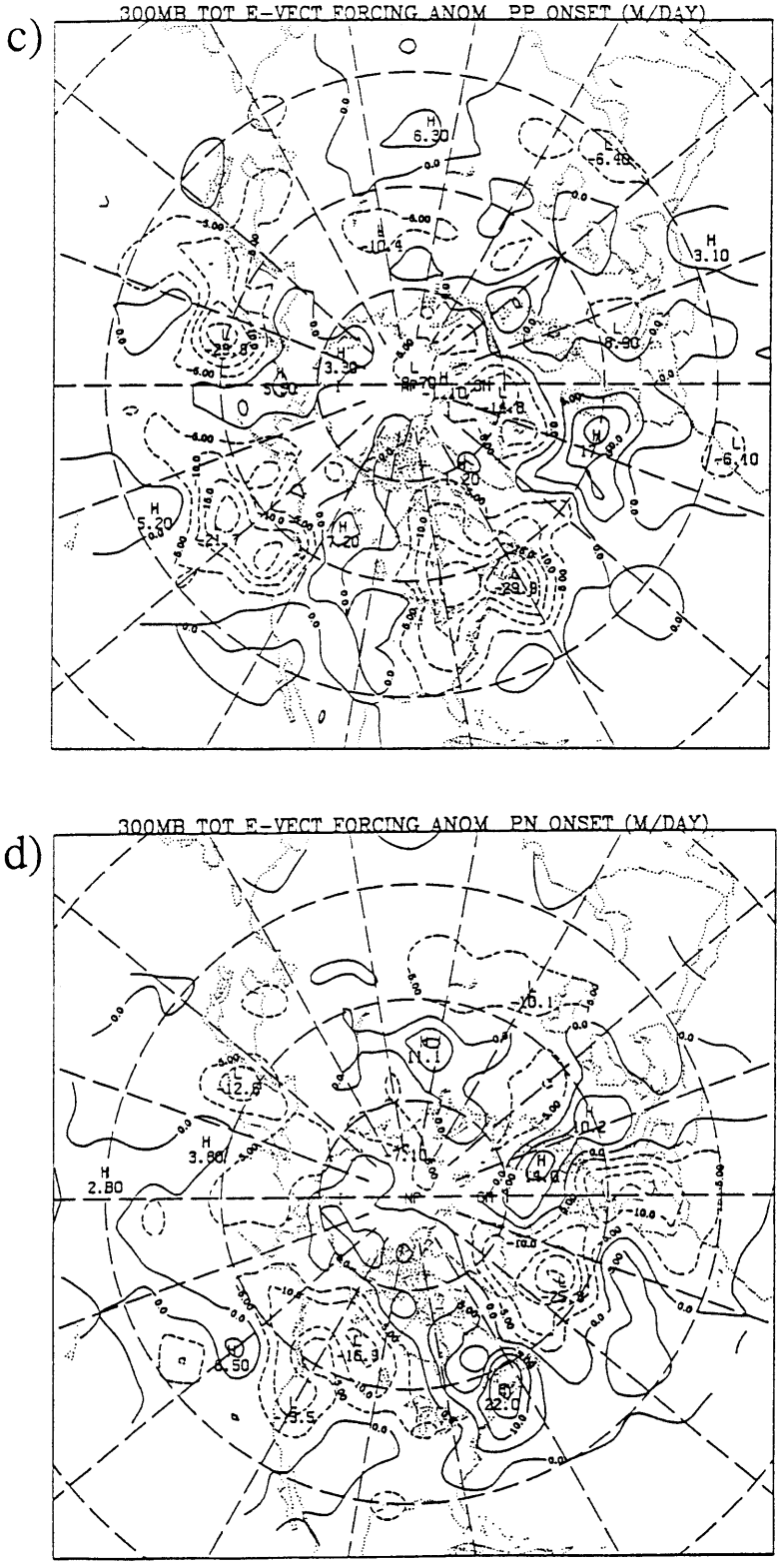

Fig. 5.11 (cont.). Composite 300 mb anomalous geopotential height tendencies due to both the barotropic and baroclinic components of the bandpass **E**-vectors averaged over the 10 days centered on day 0 of onset for a) Pacific positive and b) Pacific negative PA events. Contour interval is 6 m day^{-1} and negative contours are dashed.

calculation, although the overall height tendency pattern is still upstream biased. The total Atlantic negative results primarily differ from the barotropic results by having a broadened region of height falls to the north of the key point, and an enhanced height tendency just upstream of the key region.

The Pacific cases show quite different geopotential height tendency patterns when the baroclinic terms are included. The anomalous baroclinic eddy forcing during the onset of Pacific positive PAs tends to be negative over most of the Pacific basin. Consequently, the total height rises over the Pacific have a very strong negative bias, with only very small height rises remaining over the key point, although the eddy induced relative vorticity tendencies are still strongly anticyclonic. During the Pacific negative case onset, the total height tendencies over the Pacific are weak, although the tendency is still to accelerate the climatological-mean jet eastward.

The geopotential height tendencies associated with the baroclinic parts of the anomalous E-vectors prior to and during the onset of the Atlantic PA cases are generally centered just upstream from the barotropic forcings. Thus, during onset, the heat and vorticity forcings appear to cooperate to excite the large-scale flow anomaly. However, during the mature phase of Atlantic cases and generally throughout the life cycles of the Pacific cases, the baroclinic forcing tends to be out of phase with the barotropic forcing and to be dissipative of the large-scale flow anomaly. The change in phase of the anomalous baroclinic forcing during the Atlantic cases is due in part to both a eastward shift in the anomalous eddy growth regions and significant changes in the patterns of zonal eddy heat fluxes.

Significance patterns corresponding to the composite anomaly E-vector components have also been computed. The patterns for the individual components barotropic part of the E-vectors (not shown) are similar but weaker the VSTAT significance patterns shown in

Chapter 4. The weaker significance is expected since the E-vectors are second moment eddy statistics, and are thus more subject to pointwise variability. However, the integrated height tendency results are not as susceptible to small scale noise and tend to have higher levels of significance. For example, Fig. 5.12 shows the statistical significance based on the null hypothesis that the total (barotropic plus baroclinic) anomalous height tendencies during the mature phase of each of the PAs is zero. These significance patterns largely reflect the magnitude of the composite height tendency anomalies. Near the Atlantic key points, broad regions of greater than 90% confidence are found near the key points. For the Pacific cases, the significance patterns near the key points are weaker, although considerable significance is found for the upstream (Pacific positive) and downstream (Pacific negative) tendencies. In general, the significance associated with the anomalous barotropic and baroclinic height tendencies individually tends to be greater than the total significance, as the baroclinic and barotropic processes tend to oppose one another during the mature phase of the PAs.

We have also examined the anomalous E-vectors and the implied geopotential height tendencies at 700 mb. The results (not shown) are similar to those displayed for the 300 mb analyses. The anomalous barotropic forcing is slightly more than half of the 300 mb forcing and tends to have an overall equivalent barotropic structure similar to the climatological-mean results of Lau and Holopainen (1984). The anomalous heat fluxes also tend to have to similar patterns to the 300 mb patterns. Examination of the vertical structure of the anomalous heat fluxes (not shown) indicates that they tend to be largest just below 700 mb. Thus, the vertical derivative of the anomalous eddy heat fluxes (which forces the mean flow) tends to have the same sign at both 300 and 700 mb.

We now wish to examine in greater detail the temporal relationships between the eddy forcing patterns and the large-scale flow anomalies. If the eddy forcing is responsible for the large-scale anomaly evolution, then there should be a positive correlation between

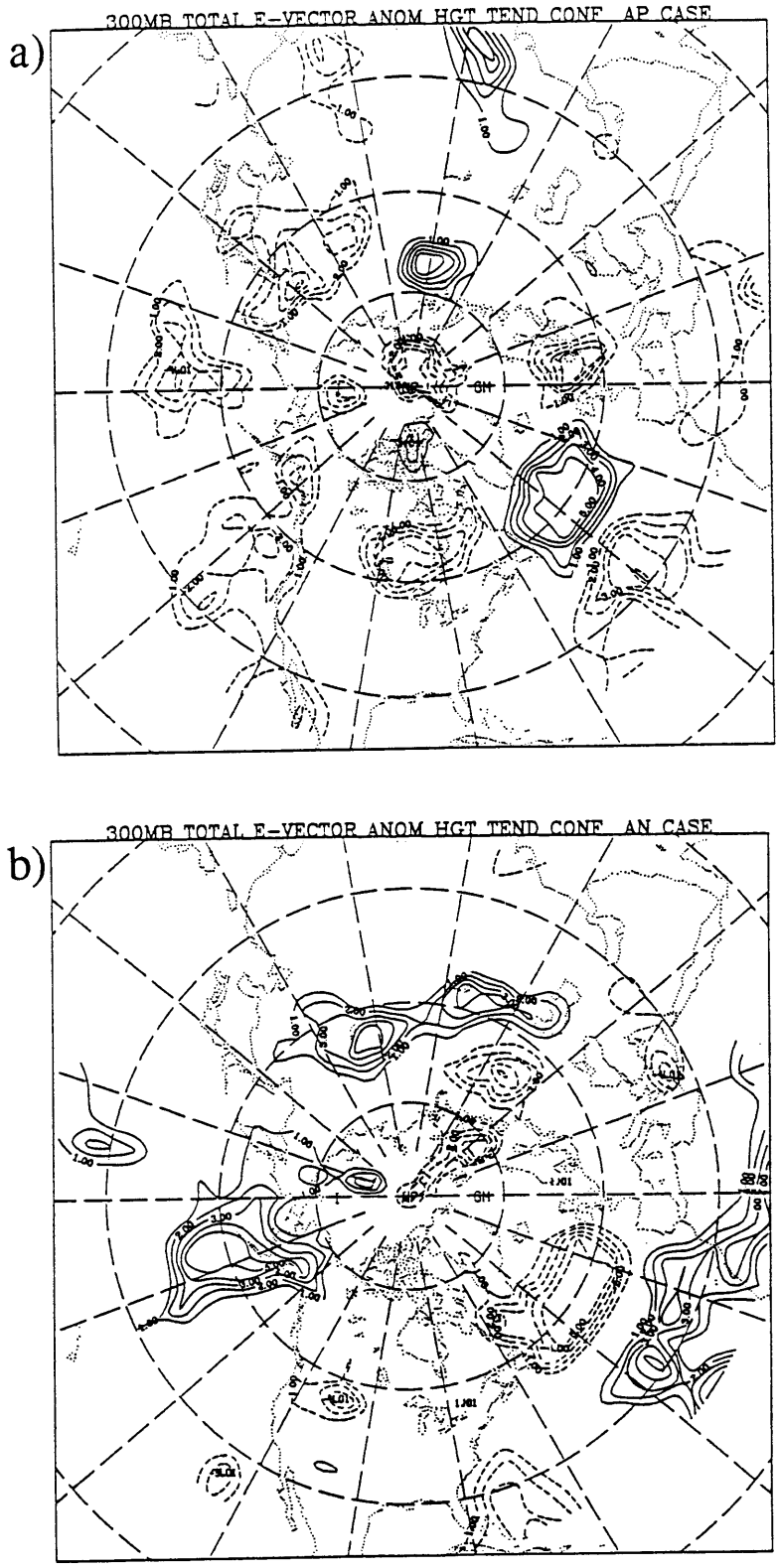

Fig. 5.12. Statistical significance of the total (barotropic plus baroclinic) anomalous 300 mb geopotential height tendencies during the mature phase of a) Atlantic positive and b) Atlantic negative PA events. Contours levels indicate the 90, 95, 97.5, 99 and 99.5 significance levels. Dashed contours imply negative anomalies.

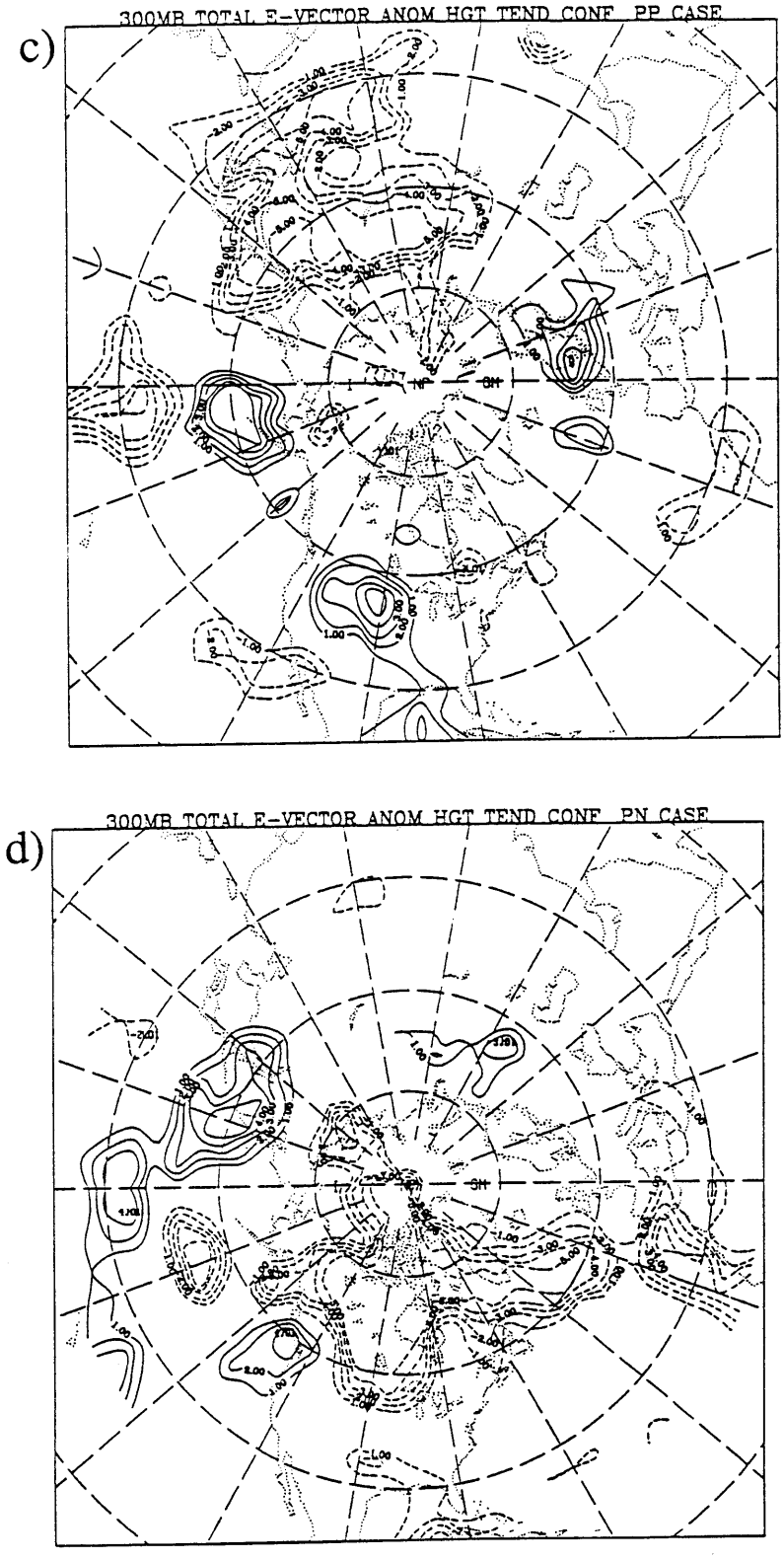

Fig. 5.12 (cont.). Statistical significance of the total (barotropic plus baroclinic) anomalous 300 mb geopotential height tendencies during the mature phase of c) Pacific positive and d) Pacific negative PA events. Contours levels indicate the 90, 95, 97.5, 99 and 99.5 significance levels. Dashed contours imply negative anomalies.

the forcing and the tendency of the large-scale flow. In order to examine this possibility, we have computed two-day mean eddy forced anomalous 300 mb height tendencies at two day intervals during the onset and breakdown of the PAs. The tendencies were averaged over a 30 degree grid square centered on the grid point 15 degrees upstream of the Atlantic key point (Atlantic PA cases) and on the Pacific key point (Pacific PA cases). The observed 300 mb anomalous geopotential heights for the same periods were also noted at each of the key points. The eddy tendencies have been normalized by the magnitude of the maximum observed value during the time series for each PA type. The observed heights have also been normalized in a similar fashion.

The results for the onset period are shown in Fig. 5.13. For the Atlantic positive cases, the barotropic forcing pattern leads the large-scale flow evolution by about 5 days, whereas the baroclinic forcing leads by about 8 days. During the onset of the Atlantic negative cases, both the baroclinic and barotropic forcings lead by about 2 and 4 days, respectively. For the Pacific positive cases, the barotropic forcing in nearly in-phase with the large-scale flow, while the baroclinic forcing patterns are nearly out of phase. A similar pattern is evident for the Pacific negative cases. Therefore, these temporal relationships suggest that the anomalous eddy activity during the Atlantic cases can play a positive role in both the development and maintenance of the large-scale flow anomalies. However, the anomalous eddy forcing during the Pacific cases may only be able to maintain the large-scale flow anomalies.

The time series of eddy forcing during the breakdown of the PAs is shown in Fig. 5.14. In general, the barotropic forcings for all the types remains in phase with the large-scale flow during breakdown. The baroclinic forcings generally appear to play a dissipative role throughout the breakdowns although there is no evidence in these results of a sudden increase in the magnitude of the baroclinic eddy forcing that might trigger the

breakdowns. There is also little clear evidence that the eddies are trying to resist the breakdowns of the large-scale patterns except perhaps in the Pacific negative cases.

To summarize the E-vector results, the anomalous height tendencies in the upper troposphere induced by the eddy barotropic (vorticity fluxes) lie somewhat upstream of the key regions for the Atlantic cases (approximately 1/8th of a wavelength) and over the key region for the Pacific cases. The patterns of the anomalous barotropic forcing tend to be geographically stationary throughout the life cycles of PAs. The barotropic forcing term tends to lead the large-scale evolution in the Atlantic, particularly during the Atlantic positive cases. Except for the Pacific negative cases, the magnitude of the anomalous eddy forcing implies spinup time scales comparable to those observed. Inclusion of the baroclinic terms does not qualitatively change the results for the Atlantic development cases but does appear to significantly influence the total eddy induced geopotential tendencies associated with the Pacific cases. The temporal relationships between the eddies and the large-scale flow suggest that the eddies are also likely to be playing a significant role in the developments of the Atlantic PA cases.

5.4 Three-dimensional geopotential tendencies.

One of the shortcomings of the E-vector technique for diagnosing the eddy feedbacks on the mean flow is that they are evaluated at only a single level and, therefore, that the effects of PV tendencies at other levels and temperature tendencies at the boundaries are not explicitly considered. Lau and Holopainen (1984) have developed an alternative diagnostic approach which relates the instantaneous height tendencies to the divergence of the eddy potential vorticity fluxes in the interior together with the eddy heat fluxes at the boundaries. Specifically, they write the quasi-geostrophic pseueo-potential vorticity equation as

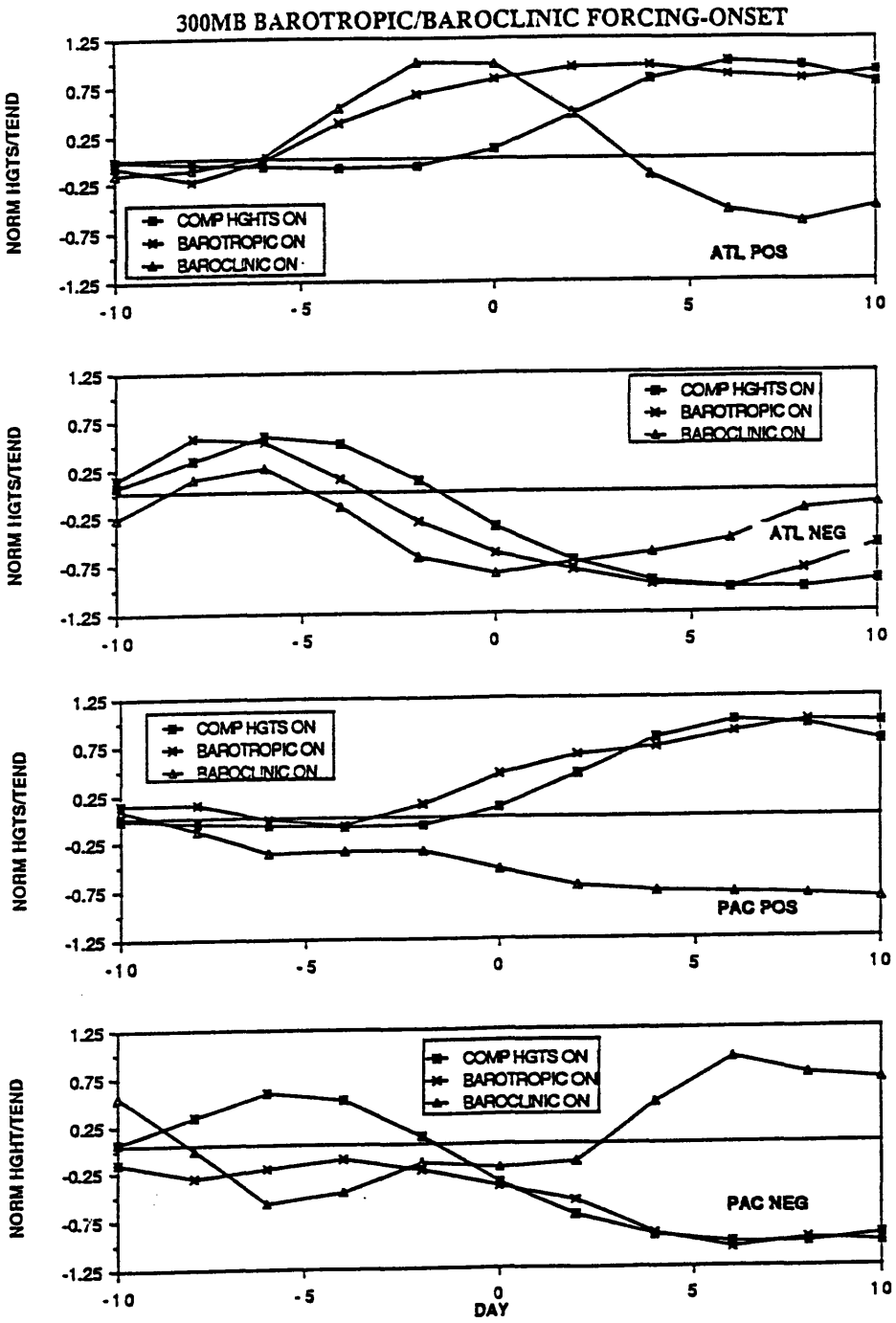

Fig. 5.13. Time series of the composite anomalous 300 mb eddy forced barotropic and baroclinic geopotential height tendencies averaged over a 30 degree wide grid square located 15 degrees west of the key points and the observed 300 mb height anomalies at the key point during the onset of each of the PA patterns. The tendency curves have been normalized by the magnitude of the maximum observed (either barotropic or baroclinic) forcing for each PA while the observed height anomaly curve is normalized by the maximum observed heights.

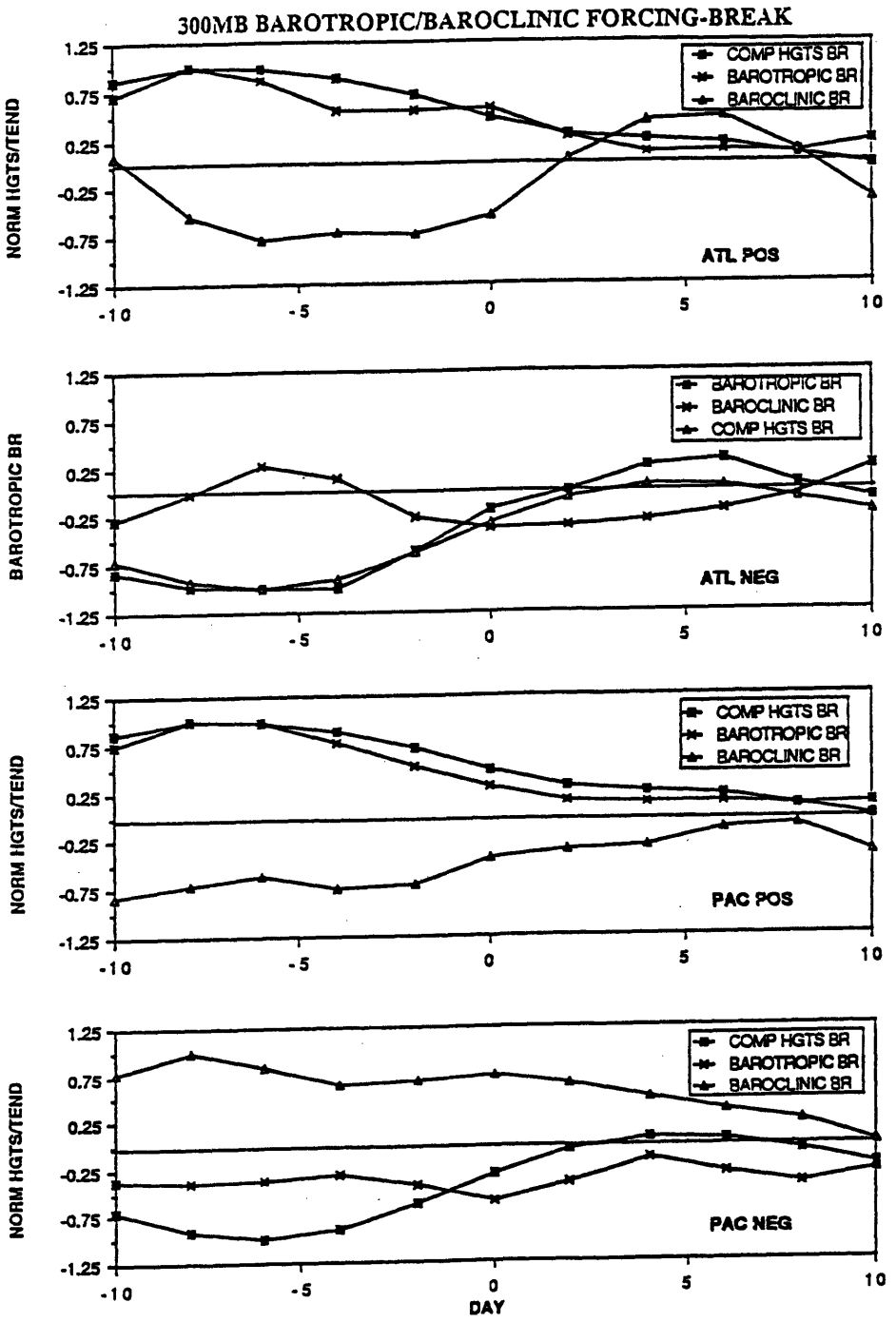

Fig. 5.14. Time series of the composite anomalous 300 mb eddy forced barotropic and baroclinic geopotential height tendencies averaged over a 30 degree wide grid square located 15 degrees west of the key points and the observed 300 mb height anomalies at the key point during the breakdown of each of the PA patterns. The tendency curves have been normalized by the magnitude of the maximum observed (either barotropic or baroclinic) forcing for each PA while the observed height anomaly curve is normalized by the maximum observed heights.

$$\left\{ \frac{1}{f}\nabla^2 + f\frac{\partial}{\partial p}\left(\frac{1}{\sigma}\frac{\partial}{\partial p}\right)\right\} \frac{\partial \Phi}{\partial t} = D + R \qquad (4)$$

where Φ is the geopotential. The static stability ($\sigma = -(\alpha/\theta)(\partial\theta/\partial p)$) is assumed to be a function of pressure alone so that (4) is a separable elliptic equation for the height tendencies. The D term represents the contributions by eddy forcing, and may be written as

$$D = f\frac{\partial}{\partial p}\left(\frac{\nabla\cdot\overline{\mathbf{V}'\theta'}}{S}\right) - \nabla\cdot\overline{\mathbf{V}'\zeta'} \qquad (5)$$

Note that this term is equal to the divergence of the eddy potential vorticity flux. The R term contains all other contributions to the PV budget, including mean advection and non-conservative terms. Evaluation of (4) with R set to zero gives the geopotential tendencies that result from the eddy forcing term D. The boundary conditions used in solving (4) are

$$\frac{\partial}{\partial p}\left(\frac{\partial \Phi}{\partial t}\right) = \frac{R}{p}\nabla\cdot\overline{\mathbf{V}'T'} \qquad (6)$$

applied at 1000 and 100 mb.

This technique has been used previously by Lau and Holopainen (1984) to assess the effects of forcing by the bandpass eddies on the climatological-mean Northern Hemisphere wintertime flow, by Holopainen and Fortelius (1987) to study the maintenance of European blocking event and by Mullen (1987) to examine the maintenance of composite blocking events over the Pacific and the Atlantic by synoptic-scale eddies in both the NMC dataset and in a GCM. In the latter studies, the tendencies appeared to be structured so as to maintain the block if large-scale advection is important (i.e. positive height tendencies located approximately one-quarter wavelength upstream of the blocking ridges). However there are considerable similarities between the tendency patterns obtained in the blocking cases and the climatological-mean flows as reported by Lau and Holopainen (1984). Thus,

it is difficult to determine the degree to which the eddy forcing during the blocking events was, in fact, anomalous.

Therefore, we have applied this technique to the PA cases including only the anomalous part of eddy forcing. The motivation is to verify the single level E-vector tendency results from the previous section. Mullen (1989, personal communication) indicated that his upper-tropospheric results could be well approximated those obtained using by the E-vector tendency method. We have obtained the code used by Mullen (and previously by Lau) and have applied it as provided, except that our solution is obtained on a grid with a horizontal resolution that matches our dataset, rather than the gaussian grid used by Mullen. We have also corrected an error in the coefficent applied to the upper boundary heat fluxes. Because the eddy heat fluxes are so small at 100 mb this correction is generally trivial. The solution to the set (4-6) is then obtained by expanding the appropriate fields into a set of zonal Fourier harmonics and then solving for each component in the y-p plane. In the following, results have been obtained for zonal wavenumbers less than 11. The final solution is then obtained by summing over all components. The eddy forcings were first determined from mandatory level data, and were then interpolated to a 50 mb vertical resolution using cubic-splines. Because of the cost involved in determining the 26-year climatological-mean eddy statistics at all levels, we have approximated these statistics by averaging 840 samples of bandpass eddy statistics that occurred at least 10 days before or 10 days after each PA case. The patterns of climatological-mean height tendencies due to these approximate mean eddy fluxes are very similar to those reported by Lau and Holpainein (1984).

The 300 mb anomalous geopotential height tendencies during the mature phase of each of the PA cases are shown in Fig. 5.15. These results agree with the mature E-vector tendencies in all respects except:

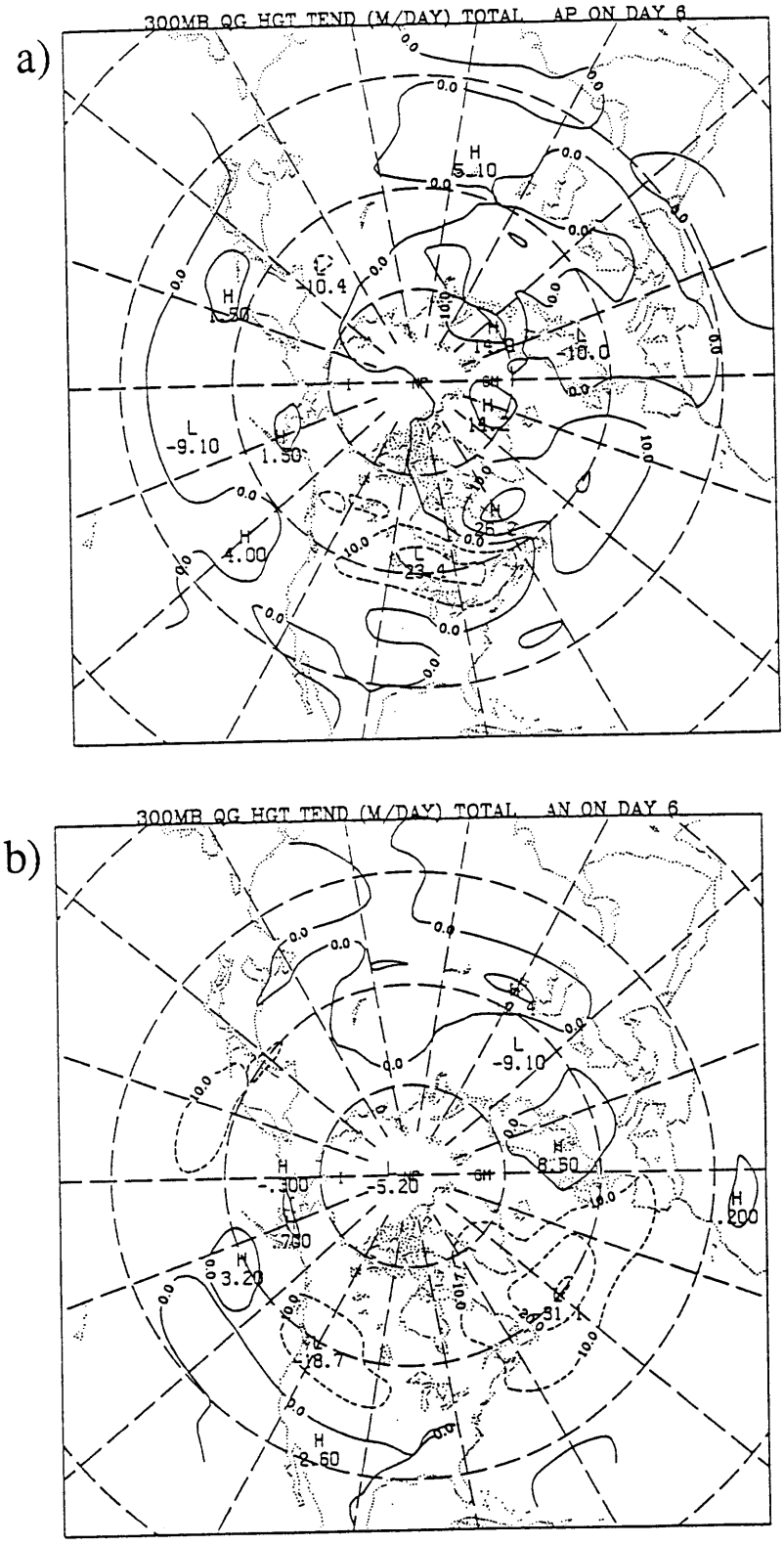

Fig. 5.15. Composite anomalous 300 mb geopotential height tendencies computed using the Holopainen and Lau three dimensional QGPV flux technique. Results are shown for day +6 during the onset of a) Atlantic positive and b) Atlantic negative PA events. Contour interval is 10 m day^{-1} and negative tendencies are dashed.

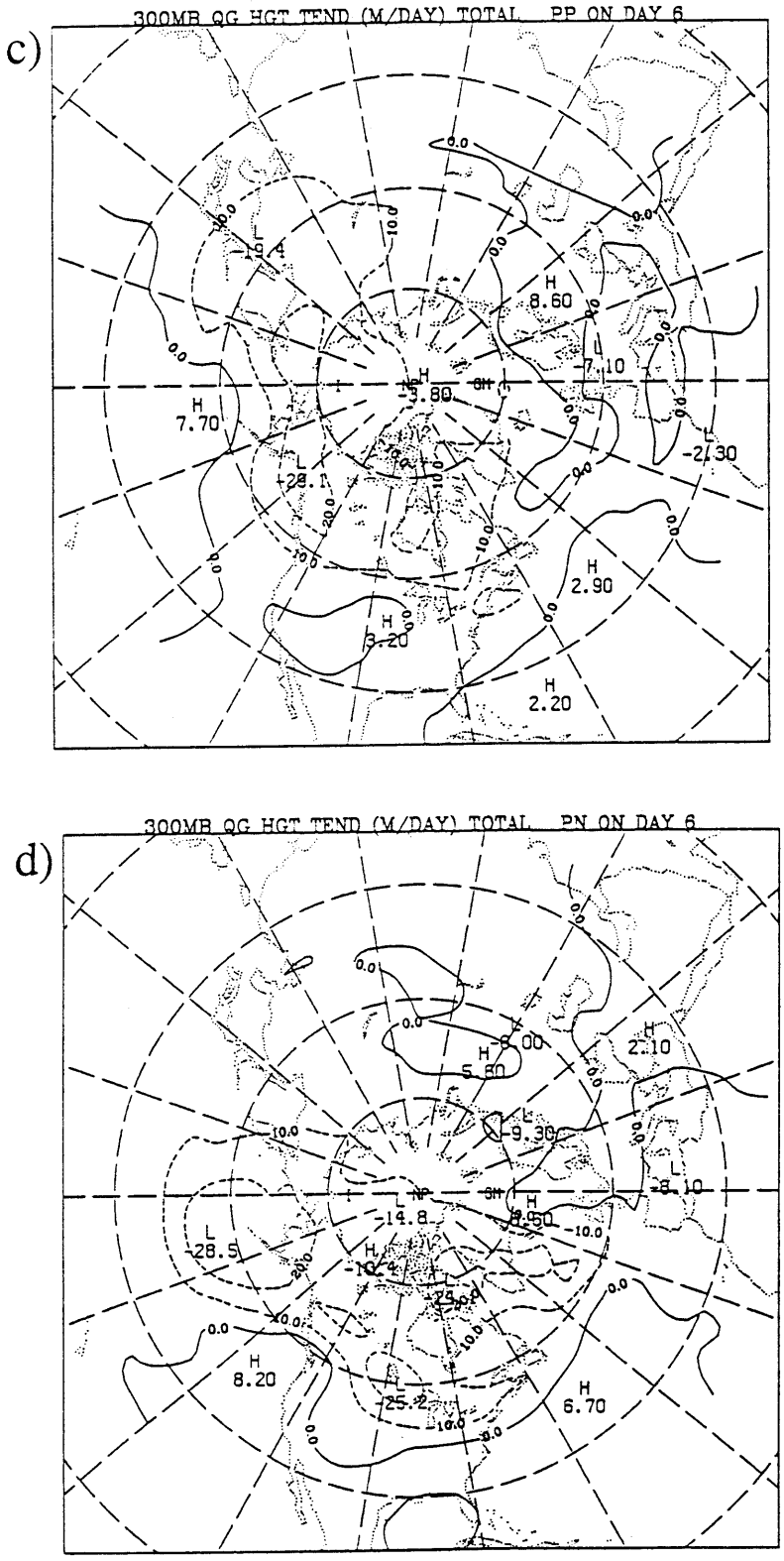

Fig. 5.15 (cont.). Composite anomalous 300 mb geopotential height tendencies computed using the Holopainen and Lau three dimensional QGPV flux technique. Results are shown for day +6 during the onset of c) Pacific positive and d) Pacific negative PA events. Contour interval is 10 m day^{-1} and negative tendencies are dashed.

- The magnitude of the height tendencies associated with Pacific negative cases are considerably greater, and are now very similar to their counterparts over the Atlantic. However, unlike the Atlantic negative cases, the Pacific negative height tendencies do not have a phase shift upstream from the key point.

- The Pacific positive cases show only modest height rises over the key region. However, the eddies are still tending to induce anticyclonic vorticity at or just upstream of the key point, with large negative height tendencies located to the west, north and east of the key point.

- The three-dimensional tendencies have less small-scale structure than the corresponding **E**-vector tendencies. This is likely due to spectral truncation and to the additional smoothing implicit in the fully three-dimensional inversion of the Laplacian operator.

The corresponding 1000 mb anomalous height tendencies are shown in Fig. 5.16. The results show that, in general, the eddies are forcing approximately equivalent barotropic structures. Large anomalous positive 1000 mb height tendencies (and therefore positive surface pressure tendencies) are found at or just upstream of the key regions during the positive PA cases. Large 1000 mb height falls are found 15 degrees west and 4 degrees north of the Atlantic and Pacific negative PA centers respectively. There is also some indication that the eddies are forcing the downstream wave train observed during the Pacific negative cases, especially at the surface. The implied surface pressure tendencies associated with the 1000 mb height tendencies can be estimated (using the hydrostatic equation) by multiplying the height tendencies by .12 mb m^{-1}. Thus during the Pacific negative cases, the anomalous eddy heat fluxes are inducing pressure falls of about 7 mb day^{-1}. Holopainen and Fortelius (1987) discuss the nature of these large surface pressure tendencies and indicate that they are primarily a result of the Ferrel cell circulations induced by the eddy heat fluxes. Through the Coriolis torque the heat flux induced secondary circulation accelerates the mean flow along the storm tracks. They suggest that the

accelerations implied by these tendencies will generally not be realized, as they will be largely balanced by surface stress. However, significant overestimation of the surface potential temperature fluxes by the geostropic winds probably also contributes to these anomalously large surface tendencies.

The mean 300 mb to 1000 mb temperature tendencies can be qualitatively estimated by examining the difference between the height tendencies, i.e. the thickness tendencies. The thickness anomalies are negative for the two positive cases and positive for the negative cases. Since the large-scale temperature anomalies have the same sign as the PA itself (Dole 1986), the eddies are acting to reduce the mature large-scale temperature anomalies, as was also apparent in the earlier analyes.

Results for other times during the life cycles of PAs (not shown) have similar relationships with the **E**-vector tendency results from the previous section. In general, the **E**-vectors are found to well represent the upper-level geopotential height tendencies for the Atlantic cases as computed by the Lau and Holopainen tendency method. For the Pacific negative cases, the latter method indicates more of a role for the eddies in the negative cases than indicated by the **E**-vectors. The disparity in the relative roles of the eddies between the Atlantic and Pacific positive cases that our results indicate was also apparent (but was not noted) in the results obtained by Mullen (1987). His results indicate only about half the tendencies in his Pacific cases as in the Atlantic cases. He also found less of a tendency for the eddy forcing to lie upstream of the key region, in the Pacific cases (but again not noted), as we have also observed here.

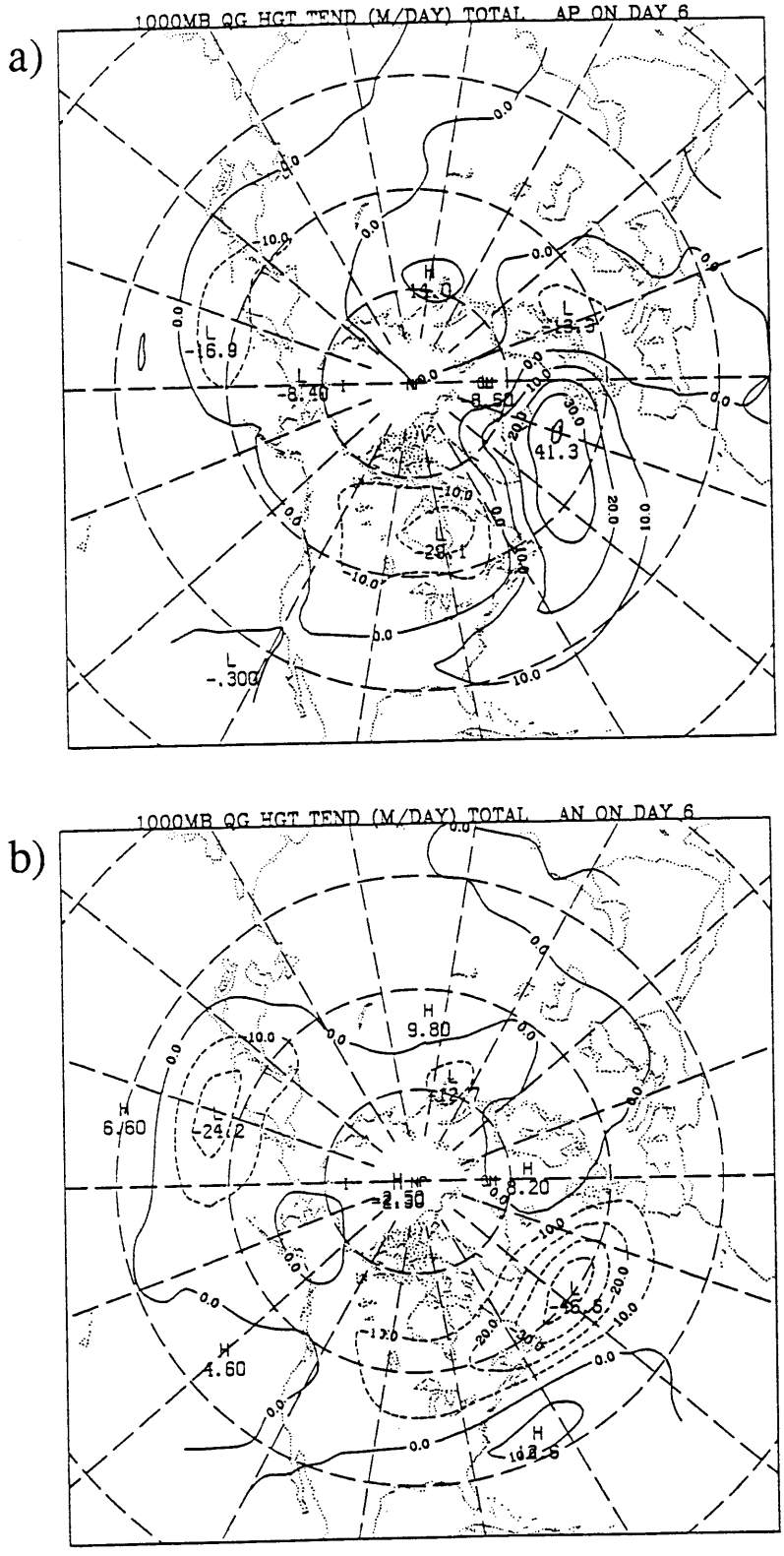

Fig. 5.16. Composite anomalous 1000 mb geopotential height tendencies computed using the Holopainen and Lau three dimensional QGPV flux technique. Results are shown for day +6 during the onset of a) Atlantic positive and b) Atlantic negative PA events. Contour interval is 10 m day^{-1} and negative tendencies are dashed.

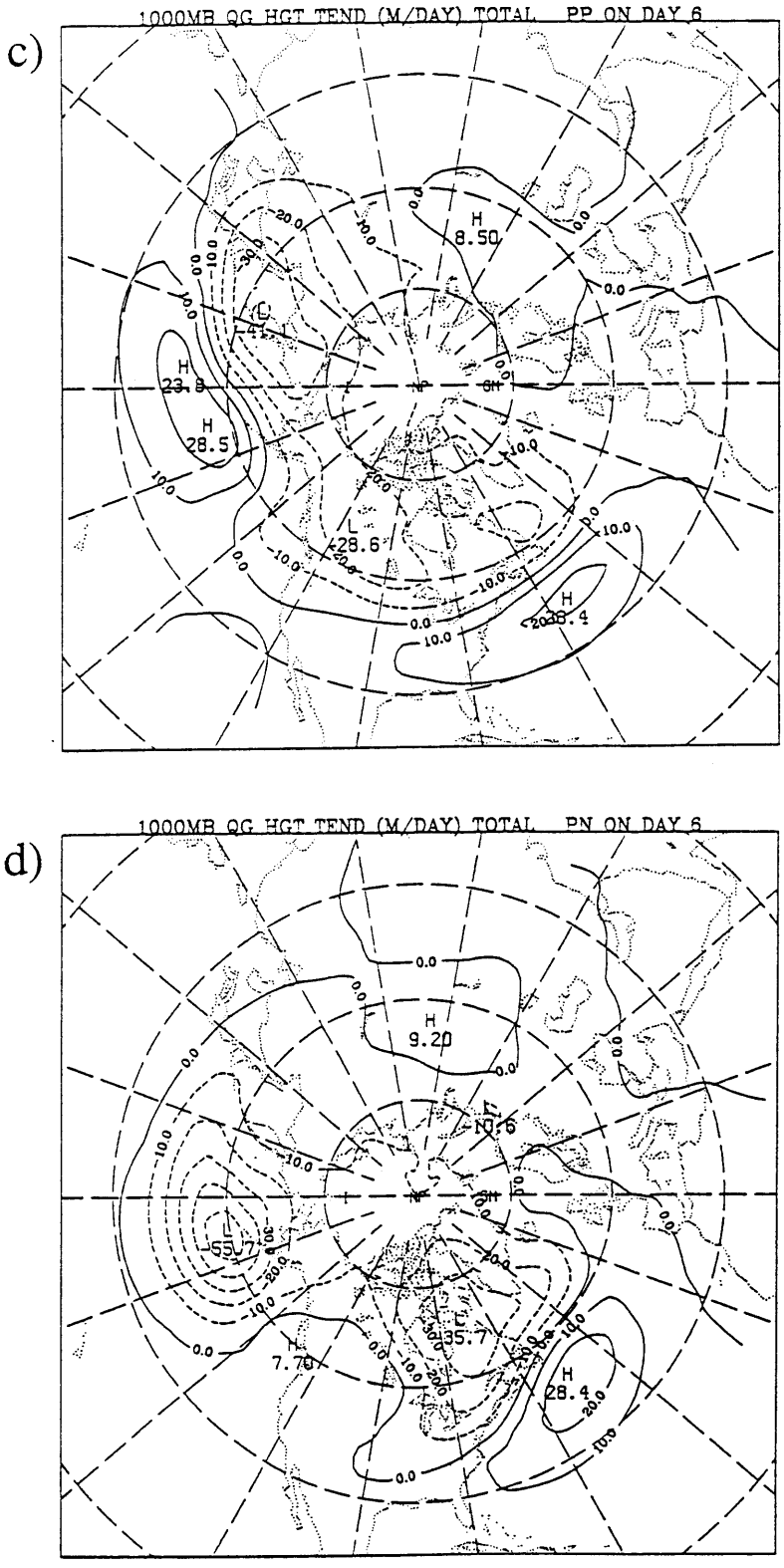

Fig. 5.16 (cont.). Composite anomalous 1000 mb geopotential height tendencies computed using the Holopainen and Lau three dimensional QGPV flux technique. Results are shown for day +6 during the onset of c) Pacific positive and d) Pacific negative PA events. Contour interval is 10 m day^{-1} and negative tendencies are dashed.

5.5 Barotropic response to the eddy forcings.

Our results so far indicate that the eddies appear to play a significant role in the initiation and maintenance of the Atlantic events. The role of the eddies during the Pacific cases is not as clear, although they also appear to have a positive role. However, so far we have only considered the forcing of the mean flow by the eddies, and not the net response to that eddy forcing. Pierrehumburt (1986) considers the responses of several simple flows to idealized eddy forcings. He notes that the barotropic response will be in quadrature with the forcing, if the dominate balance is between forcing and advection by the large-scale flow. However, if the forcing is balanced by dissipation, then the response tends to be more in phase with the forcing. The actual response in particular cases will obviously depend upon the exact structure of the forcing, mean flow and dissipation.

In this section we will estimate the large-scale response to anomalous eddy forcing using a hemispheric barotropic forecast model governed by the equation

$$\frac{\partial \zeta}{\partial t} + \mathbf{V}\cdot\nabla(\zeta+f) = E + F_C + \varepsilon\nabla^2\zeta \qquad (7)$$

where ζ ($=\nabla^2\Phi/f$) is the relative vorticity , Φ is the geopotential, E is the anomalous eddy forcing and F_C is the climatological-mean forcing. The latter is computed as that forcing which is necessary to maintain the climatological-mean flow stationary and contains an implicit effect of the climatological-mean eddies. We have solved (7) in spherical coordinates using a damping parameter $\varepsilon = 1.8 \times 10^5$ $m^2\ s^{-1}$. This choice provides e-folding damping time scale of about 5 hours for the smallest resolvable waves, about 20 days at the PA scales and at least 50 days for the stationary waves.

The model is run on a 2x5 degree latitude-longitude grid that generally matches our dataset. The zonal resolution is halved at 76N and again at 84N to avoid extremely short grid spacings near the pole. The model is initialized with observed height data from our

NMC dataset between 20N and the pole. Between 20N and the equator the initial vorticity field is assumed to linearly decay to zero. The model is run with a 15 minute centered time step (which ensures CFL stability) and the horizontal derivatives are computed using centered differences.

Our approach is as follows: We initialize the model with the observed composite-mean lowpass 300 mb heights observed at day -5 of onset. We then run the model for 10 days using the stationary anomalous eddy forcing computed using the barotropic part of (3) averaged over the 10 day onset period. We then compare the results to a control run in which the anomalous eddy forcing is set to zero. Here we will consider only the Atlantic cases, as these cases have the most prominent eddy forcings. Consistent with the model, we only consider the barotropic part of the anomalous eddy forcing. Since the anomalous eddy heat fluxes appear to play a positive role in the initiation of Atlantic PAs, the use of only the barotropic part of the eddy forcing may result in a conservative estimate to the upper-level atmospheric response.

Fig 5.17 shows the geopotential height differences between the forced and unforced 10-day runs of the model for both the Atlantic positive and negative PA cases. For the positive PA cases, the maximum geopotential height response is at 50N 20W, just east of the key point. The structure and magnitude of the Atlantic positive response is very similar to the geopotential anomalies observed at day 0 of onset (i.e. approximately halfway through the observed development). For the negative Atlantic PA case, the response is similar but with opposite sign and about 25 degrees further downstream. Therefore the bandpass barotropic forcings during the onset of Atlantic PAs roughly account for half of the observed developments, although the responses are located somewhat too far downstream. The downstream tendency for the modeled developments may be partially due to the use of 300 mb data for our model. The relatively stronger flow at 300 mb compared to the equivalent barotropic level may tend to overemphasize the role of advection

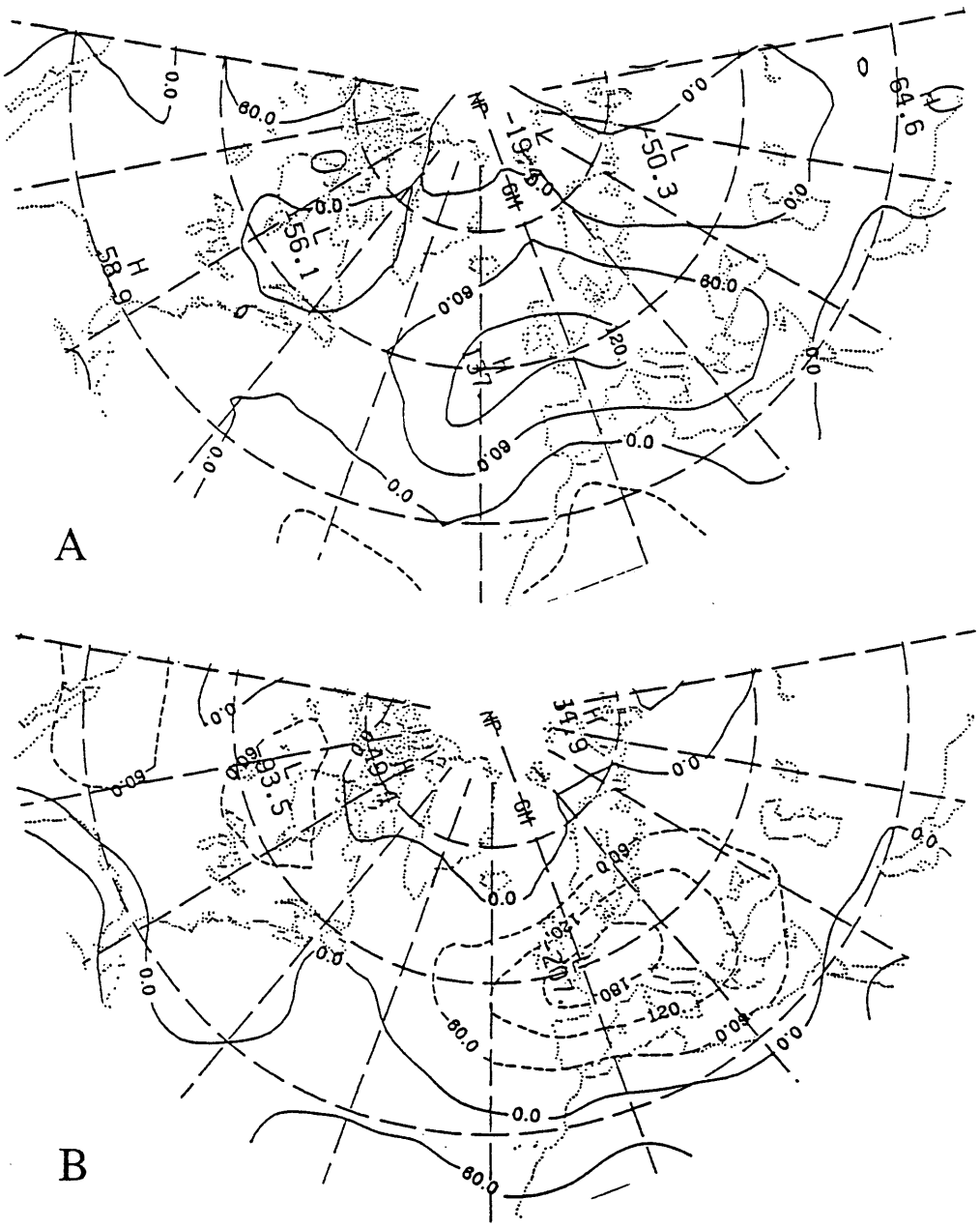

Fig. 5.17. Differences between the 300 mb geopotential heights between 10 day runs of a barotropic model forced with the anomalous barotropic eddy forcing and an unforced control run for the a) Atlantic positive and b) Atlantic negative cases. Contour interval is 60 m and negative contours are dashed.

compared to dissipation of the forced waves, and thus lead to a response to far downstream. When the anomalous vorticity tendencies induced by the upper-level eddy heat fluxes are included (not shown) the response shifts about 10 degrees westward for the positive PA cases but remains approximately stationary for the Atlantic negative cases.

5.6 Discussion

In this chapter we have examined the potential role of anomalous forcing by the synoptic-scale eddies during the life cycles of persistent anomalies. We have found that the eddies force anomalous geopotential height tendencies (and therefore vorticity tendencies) having similar structures to the large-scale flow anomalies, with magnitudes comparable to those required to spinup the observed anomalies in the time scales of the developments. For the Atlantic cases, the upper-level anomalous tendencies induced by the eddies are centered upstream of the large-scale flow anomaly by about 1/8 wavelength. For these cases, the barotropic part of the forcing appears to lead the large-scale flow anomalies, particularly for the positive cases. When the baroclinic forcing is included, the forcing just upstream of the key region clearly leads the large-scale developments. For the Pacific cases, the results are less clear. Although the barotropic forcing of the Pacific positive cases is similar to that found the Atlantic, inclusion of the baroclinic forcing significantly reduces the net eddy feedbacks. The Pacific negative cases appear to have the weakest eddy forcings. The results from three-dimensional QG tendency calculations generally confirm those obtained from the E-vector forcings evaluated at 300 mb, but do suggest a somewhat greater significance for the eddies in the Pacific negative cases, particularly near the surface. Integrations of the barotropic vorticity equation forced with the observationally diagnosed anomalous eddy forcing patterns during onset of the Atlantic cases are able to

produce structures that resemble the large-scale flow anomalies, although the model simulated anomalies have magnitudes only approximately half as large as observed.

The anomalous barotropic and baroclinic eddy forcings are generally out of phase throughout the Pacific cases and during the latter stages of the Atlantic cases, with the baroclinic forcing having a tendency to dissipate the thermal anomalies associated with the PA. This is most apparent in the Atlantic positive cases where the strong baroclinic wave activity to the north of the key region produces significantly enhanced heat flux divergence over the PA. Since there are both significant anomalous zonal eddy heat fluxes and significant zonal gradients in the eddy magnitudes in this region, it is possible that the E-vector formulation of Hoskins *et al.* (1983) may not fully capture all of the eddy feedbacks.

It is important to note that the results presented in this section are based solely on bandpass filtered eddy statistics. Results of several parallel calculations using different temporal and spacial filters are presented in Appendix B. These results (as well as those of Blackmon, 1976 and Wallace *et al.*, 1988) suggest that the highpass eddies (with 0-2.5 day periods) ignored by the bandpass filter have similar characteristics as the bandpass eddies. The mean magnitudes of flucuations with frequencies in the highpass range are typically about 20% of the bandpass magnitudes. Therefore we may expect the the eddy feedbacks of all modes between 0 and 6 days will be somewhat larger (about 1.4 times) than the bandpass results alone[1]. If this simple argument can be carried through to the anomalous response of the barotropic model, then we would expect to account for up to 75% of the observed Atlantic PA developments. This could occur if the eddies account for about 3/4th of the developments in all cases or, alternatively, if 3/4 of the cases studied were primarily forced by the eddies. Examination of individual cases suggests that the latter is more likely, as several Atlantic positive cases had eddy feedback patterns that did not completely

[1] The eddy feedbacks on the large-scale flow depend on quadratic eddy terms. Thus a 20% increase in eddy magnitude may lead to a 44% increase in eddy forcing.

fit the composite picture. Nonetheless, the bandpass results presented in this chapter are, if anything, likely to be a conservative estimate of the total synoptic-scale eddy forcing.

In part, our results appear consistent with the eddy straining hypothesis proposed by Shutts (1983, 1986) as a mechanism for blocking maintenance and by Haines and Marshall (1987) for blocking initiation. As discussed in Chapter 2, the slowing and kinematic elongation of eddies in the diffluent regions upstream of blocks is a central concept in this hypothesis. The straining or deformation of eddies in these regions enhances the destruction of eddy enstrophy and thus enhances the irreversible downgradient PV fluxes. The mechanism would manifest itself as a zonal gradient in the magnitude of the E-vectors as the eddy magnitude decreases through the diffluent region, a finding indeed supported by our analyses. As this effect occurs in the climatological-mean, a reduction and/or shift in it appears to have a role in the development of Atlantic negative PAs as well. We have also computed anomalous values of the eddy enstrophy normalized by the local magnitude of the large-scale PV gradient ($q'^2 / 2|\nabla\bar{q}|$). The results (not shown) indicate anomalously high (low) values upstream of developing positive (negative) PAs and thus a potential for the eddies to anomalously destroy (enhance) the mean PV gradients.

We note that changes in the eddy activity other than those that can be attributed to eddy straining and enstrophy destruction appear to have substantial influences on the anomalous eddy forcing patterns. For instance, there is apparently a packet of stronger than normal eddy activity that propagates into the Atlantic during onset of Atlantic positive cases. The passage of the leading edge of this wave packet decelerates the mean flow, a mechanism that is reminiscent of some some sudden stratospheric warming theories. We also note that stronger than normal cyclongenesis north of positive PAs and south of negative PAs leads to barotropic accelerations consistent with eddy maintenance of the PA patterns, although the associated eddy heat fluxes appear to primarily dissipate the

anomalies. Our calculations show that the barotropic effects generally dominate, as the total effects of the eddies act in a sense to maintain the fully developed anomalous flow patterns.

Finally we note that our results may not be inconsistent with the suggestions of Farrell (1989). He describes a blocking mechanism in which large excursions of low potential vorticity air are advected northward by properly configured eddies developing in a diffluent large-scale flow. The troughs are squeezed to frontal scales between the low PV pools generated by northward advection by these eddies. Since we can not necessarily distinguish between true diffusion or an observational "diffusion" (i.e. contraction of eddy scale to below the observational resolution), we can not necessarily rule out Farrell's hypothesis.

Chapter 6

A Case Study

6.1 Introduction

In this chapter we present the results of a case study of the life cycle of a major positive persistent anomaly event over the North Atlantic. Our motivation here is to present and describe synoptic analyses for a case which illustrates the composite analyses presented the preceding chapters. Our discussion will be mainly qualitative, with particular emphasis on the interactions of synoptic-scale systems with the evolving large-scale flow anomalies. In doing so, we hope to gain a clearer insight into the synoptic manifestations of the eddy processes identified in the analyses of the previous chapters.

6.2 Case Selection and General Features.

We have chosen to investigate an Atlantic positive PA event as the composite results for those cases appeared to be most clear. Although the Atlantic negative composite results are equally interesting, those cases are often associated with suppressed eddy activity, so that for a descriptive case study, the number of tangible synoptic-scale features to describe are often limited. On the other hand, the Atlantic positive PA events are generally associated with enhanced eddy activity, so that the cyclone-scale features on the synoptic charts can generally be readily identified.

The particular case that we investigate (AP16 in Appendix A) was subjectively chosen as the one case whose evolution was best characterized by the previous composite analyses. Interesting features of the evolution of this case include an overlap between our PA case and the blocking event studied by Shutts (1986). Our PA case starts on 02

February 1983, 0000 UTC and lasts for 13 days (4 days less than the average) until 15 February 1983 1200 UTC. Although Shutts (1986) notes that the blocking was initiated much earlier, he focuses on the period between 12 February and 16 February. However this period is actually during the breakdown phase of the PA event as defined by the selection criteria at the key point. Therefore, we will focus on the evolution of the flow leading up to Shutts' case. Other noteworthy aspects of this particular case are that it occurred during the strong El Niño winter of 1982-83 (Kok and Opsteegh, 1985), that a very long-lived Pacific negative PA case was in progress (both of these features are likely coincidental and not general to Atlantic positive PAs) and that the Megalopolitan snow storm (Sanders and Bosart, 1985), which produced over a foot of snow over much of the Northeast U.S., occurred during the mature phase of the event.

6.3 Case Generality.

To illustrate the resemblance of this case to the composite results, we first present the VSTAT and E-vector analyses that were used in the analyses of the previous chapters. Fig. 6.1 shows the anomalous 300 mb bandpass VSTATs on day 0 and day +6 during the onset of this case. The patterns of anomalous eddy activity are very similar to the composite patterns shown in Figs. 4.4b and 4.6 for the Atlantic positive PA case. Throughout the development of this case, stronger than normal eddy activity is found upstream of the key point over most of the Pacific and eastern U.S. The Pacific and Atlantic storm tracks during this time are weakly connected through a track over southern California and Northern Mexico. The highpass VSTATs (Appendix B) show better continuity between the anomalous Pacific and Atlantic storm tracks. As synoptic-scale systems propagate eastward from the Pacific, they cross the Rocky Mountains and then redevelop along the Gulf of Mexico and southeastern U.S. coasts. On day 0, the eastern

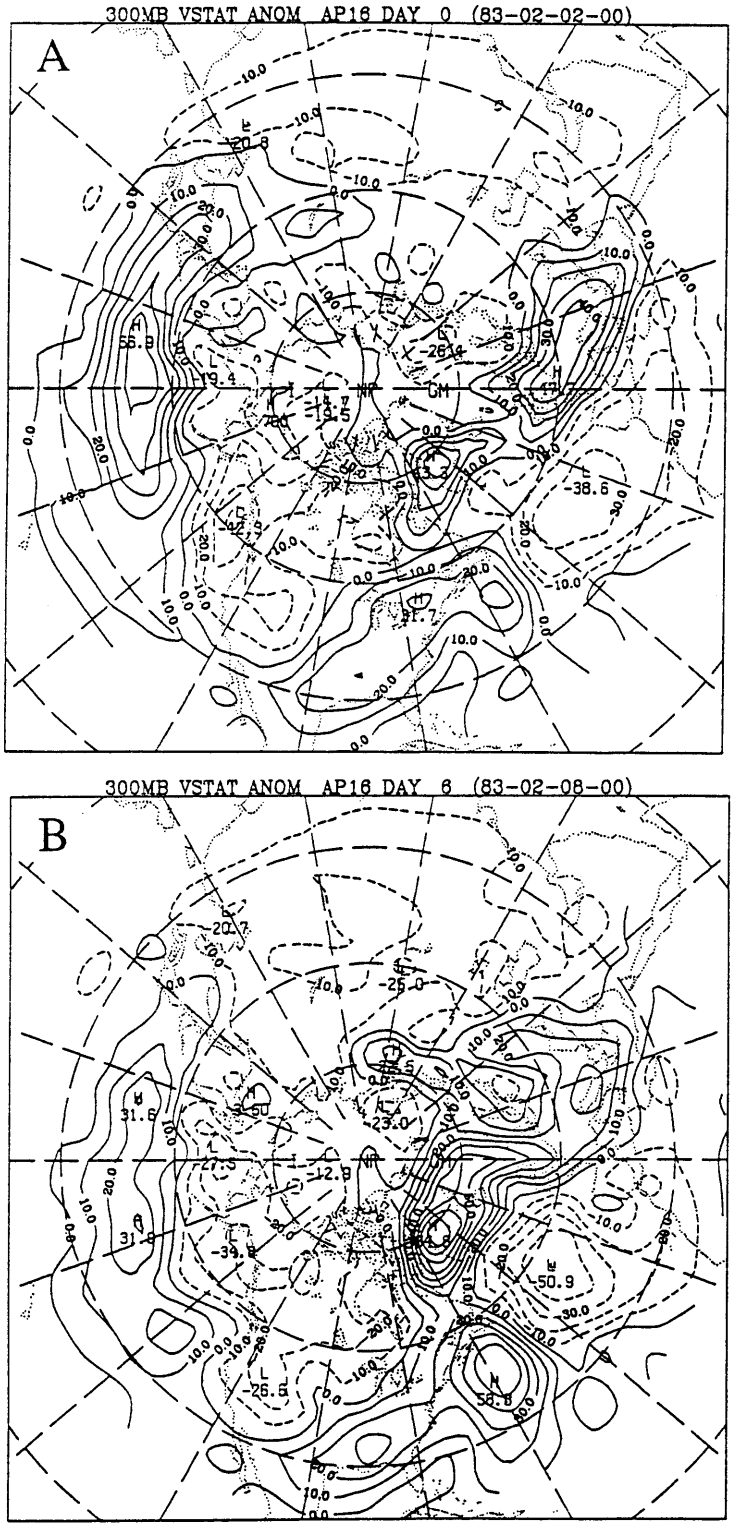

Fig. 6.1 Anomalous 300 mb bandpass VSTATs for a) day 0 during the onset of AP16 (02-Feb-83 00 UTC) and b) day +6 during onset (08-Feb-83 00 UTC). Contour interval 10 m; negative contours dashed.

end of the Atlantic storm track already shows indications of a northward deflection as the characteristic VSTAT dipole has begun to develop over the central Atlantic. By day +6, the anomalous eddy activity over the Pacific has weakened, a tendency also evident in the composite analyses. The anomalous eddy activity over the western Atlantic at this time has increased and the dipole structure over the central Atlantic has become more prominent. The magnitude of these changes over the central North Atlantic are quite large, comparable to the climatological-mean bandpass variability. Although the case VSTAT anomalies are somewhat larger than the composite anomalies, the overall patterns are very similar.

The anomalous 300 mb $\mathbf{E}_u$-vectors and associated barotropic geopotential height tendencies averaged over the onset and mature (case duration) periods for this case are shown in Figs. 6.2 and 6.3 respectively. During the onset period, the enhanced eddy activity over the Pacific is associated with an anomalous tendency to barotropically accelerate the mean Pacific jet. This is actually one of the few Pacific negative PA cases that have significant eddy forcing of the large-scale flow anomaly. The **E**-vector pattern over northern Mexico and the southern U.S. is particularly interesting. Although the anomalous **E**-vectors are directed poleward, the orientation of the total **E**-vectors (not shown) at this time are generally eastward, as the climatological-mean vectors (Fig. 5.1) have a strong southward component in this region. This suggests that the synoptic-scale eddy activity that normally propagates southward into the tropics in this region is instead being channeled on a more zonal course. At this time, substantial anomalous anticyclonic eddy forcing is occurring about 20 degrees upstream of the key point with the maximum diagnosed height tendencies due to the eddies near 35 m day^{-1}.

During the mature phase of the event, the anomalous **E**-vector activity shifts considerably eastward. The corresponding anomalous height tendencies have remained nearly stationary but have increased in magnitude up to about 60 m day^{-1}. The anomalous **E**-vectors suggest that considerable eddy growth is occurring during this period between

Greenland and Iceland which is associated with a barotropic eastward acceleration of the anomalous jet. However the heat transports associated with this baroclinic eddy growth are simultaneously acting to weaken the anomalous upper-level flow.

Overall, the general patterns of anomalous eddy activity obtained for this case are very similar to the composite patterns, although the magnitudes of the anomalies are somewhat greater. The primary differences are associated with the track of the upstream anomalous eddy activity. Although there is indeed enhanced synoptic-scale activity over the Pacific prior to this case, the connection with the Atlantic storm track is through the southern U.S., rather than through a more northern route apparent in the composite analyses. In particular, the anomalous **E**-vectors have substantial northward components which correspond to a reduced southward component of the propagation of the synoptic-scale eddies.

6.4 Synoptic evolution.

In this section we present a qualitative description of the synoptic events associated with this case. We concentrate mainly on the the mean sea level (MSL) pressure and 1000 to 500 mb thickness analyses, and the tropopause potential temperature and wind analyses. Here, the tropopause is defined as the 1.5 PVU[1] surface. Danielsen and Hipskind (1980) indicate that this surface essentially separates stratospheric from tropospheric air. Similar to the effect of thermal perturbations on the lower boundary (but with opposite sign), relatively warm air (in the potential temperature sense) at the tropopause is associated with anticyclonic circulations and cold anomalies with cyclonic circulations. As most of the upper-level PV gradient is concentrated along the tropopause (Davis, 1990), maps of the

[1] We adopt the approximate form of Ertel's PV ($Q = -g (f+\zeta) (\partial\theta/\partial p)$) where one PVU unit is equal to 1 x 10^{-6} K m^2 s^{-1} kg^{-1}.

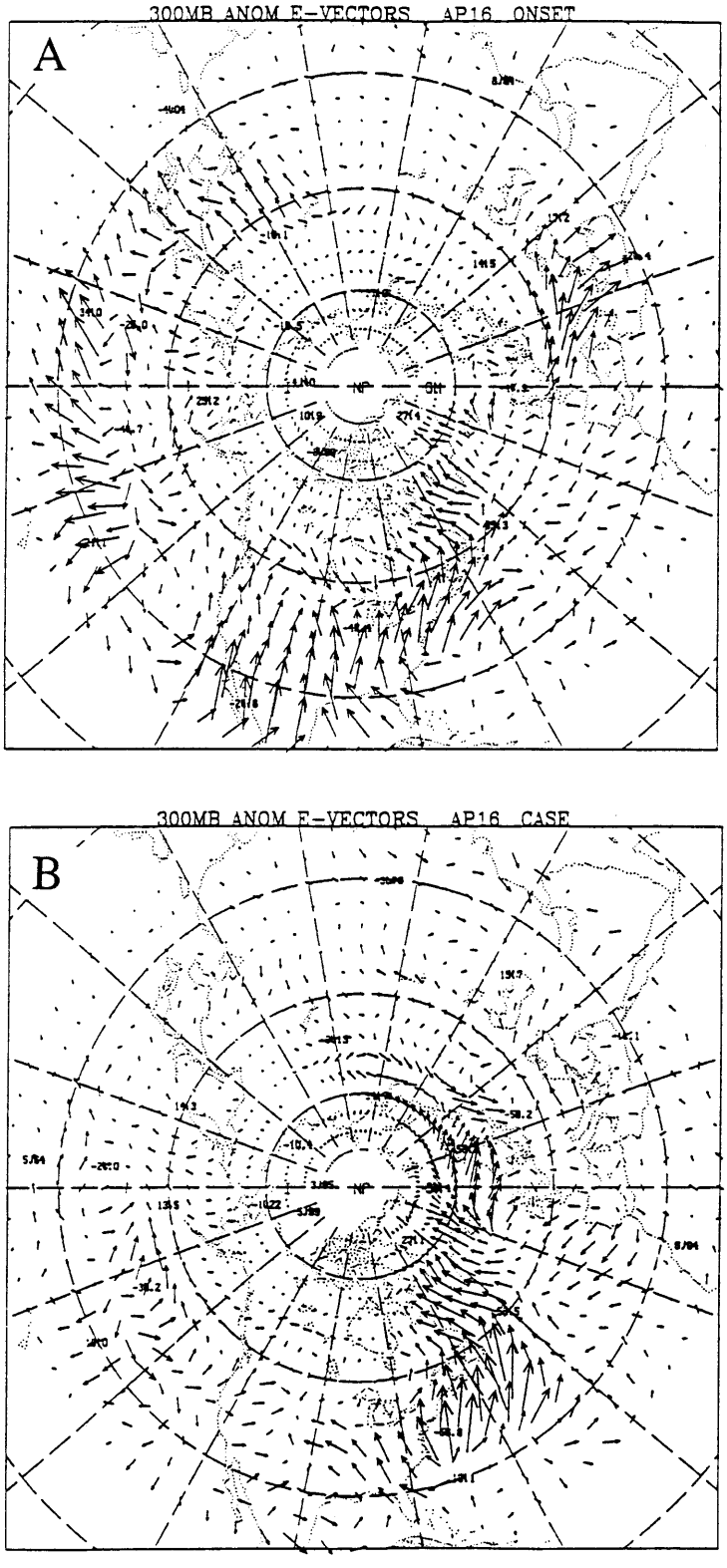

Fig 6.2 Anomalous 300 mb bandpass **E**-vectors averaged over a) the 10 days centered on day 0 of onset of AP16 and b) the case duration of AP16.

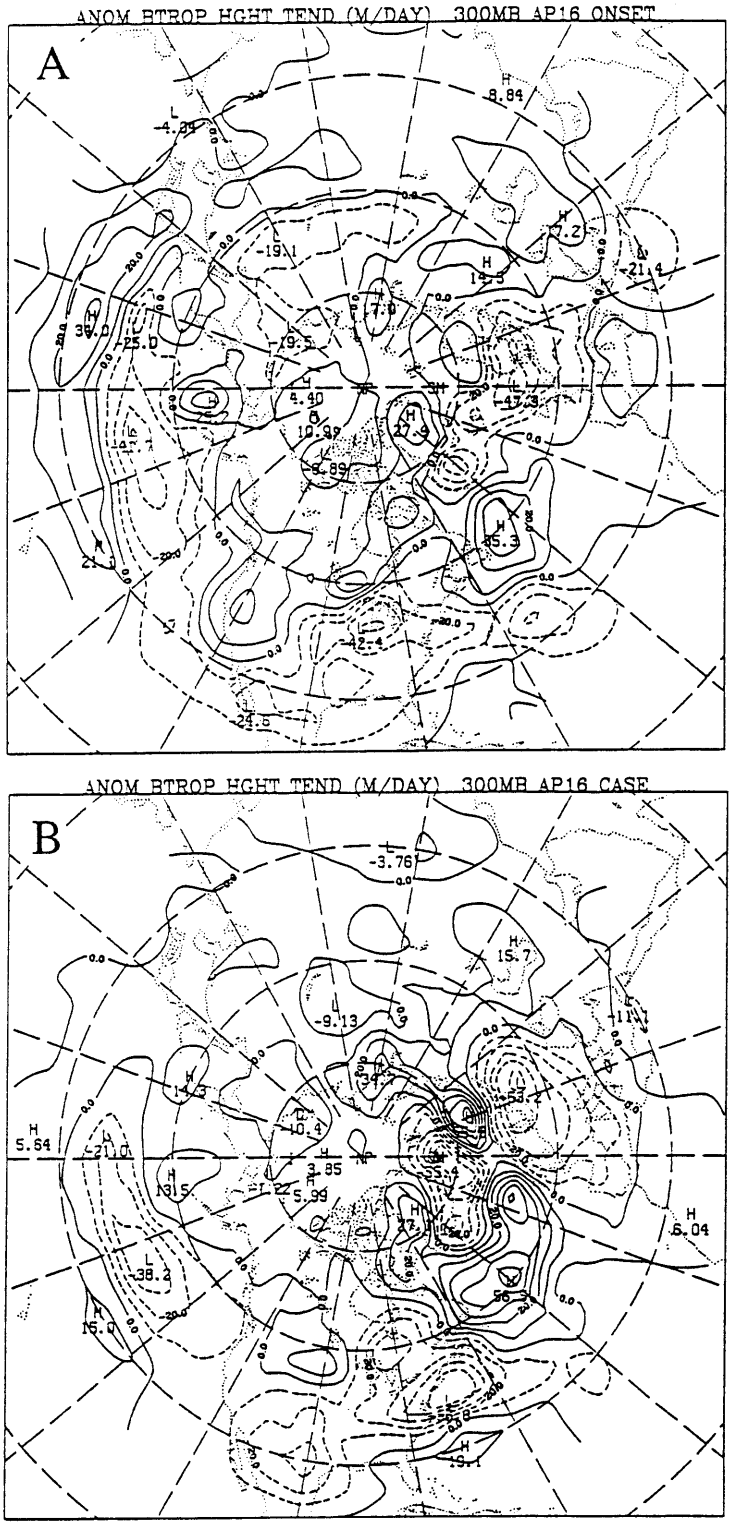

Fig. 6.3 Anomalous 300 mb height tendencies computed from the barotropic component of the **E**-vectors that have been averaged over a) the 10 days centered on day 0 of onset of AP16 and b) the case duration of AP16. Contour interval 10 m day^{-1}; negative contours dashed.

location of the tropopause in isentropic coordinates contain a significant amount of information on the general characteristics of the upper-level flow field. Also, since both potential temperature and PV are conserved following adiabatic and inviscid flow, potential temperature on a constant PV surface is a useful tracer of air parcel motions. For a more thorough discussion on the use and significance of isentropic PV analyses, see the recent review by Hoskins *et al.* (1985).

Tropopause maps were constructed by first computing the PV on isentropic surfaces at 5K intervals in a manner described by Crum and Stevens (1988). The transformation from the isentropic maps to the 1.5 PVU surface was then made using linear interpolation between isentropic levels. The MSL pressure and thickness analyses computed from the NMC gridded data and have been compared to the available DIFAX charts in the MIT archives. The loss of some of the small-scale details of the gridded analyses compared to the archived maps is generally inconsequential to the following discussion.

Figs. 6.4 through 6.11 show the sequence of tropopause potential temperature and wind analyses and the MSL pressure and thickness analyses at 2 day intervals for the times from day -5 to day +15 of onset. (Note that day +15 following onset corresponds to day +2 of breakdown.) The day 0 charts are also included in this sequence to highlight a synoptic-scale development that occurs on that day.

On day -5 , the principal features of the MSL analyses (Fig 6.4a) are the large Aleutian and Icelandic lows and an anomalously strong subtropical high located just east of Portugal. The Icelandic low is shifted about 40 degrees east of its climatological-mean position at this time. South of the Aleutian low and extending into North America a series of 5 mid-latitude synoptic-scale eddies are located near longitudes 160E (off the chart), 175W, 140W, 105W and 80W. The northward eddy heat flux over the western Pacific (not shown) is anomalously strong at this time, suggesting that enhanced baroclinic growth

is leading to this strong set of synoptic-scale eddies. The tropopause analysis for this time (Fig. 6.5a) shows these same synoptic-scale disturbances as a prominent set of warm ridges and cold troughs.

By day -3 (Figs. 6.4b and 6.5b), the family of synoptic-scale disturbances has propagated eastward about 20 to 25 degrees but the large-scale pattern has changed little. The surface cyclone east of Florida on day -5 has deepened about 10 mb and moved into the western Atlantic where it is approaching a region of strong baroclinicity to the north of the subtropical high. By day -1 (Figs. 6.4b and 6.5b) the surface cyclone has deepened to 962 mb while an anticyclone originally over Canada has propagated into the North Atlantic and has begun to merge with subtropical ridge east of Iberia. Between days -1 and +1 (Figs. 6.6 and 6.7), the surface cyclone that was over the western U.S. on day -5, has propagated into the central Atlantic and appears as a deep meridionally elongated trough ahead of the subtropical high. At the tropopause, the associated cold trough obtains a similar shape. Ahead of this trough, a closed-pool of anomalously warm (>350K) air has developed near 30N 35W perhaps aided by diabatic processes. Surface pressures at the key point have risen by 18 mb between days -5 and day 0, as the subtropical high builds toward the northwest.

Centered on day 0 (Figs. 6.6b and 6.7b), a major cyclogenesis event occurs over the eastern U.S. Concurrent with this development, a dramatic 15K warming occurs at the tropopause on the east side of the system. This warming is likely diabatically induced, as the development is accompanied by over 1 inch precipitation over much of the eastern half of the U.S., with many stations reporting in excess of 3 inches.

By day +3 (Figs. 6.6c and 6.7c), a cold trough on the tropopause that had earlier separated the two apparent diabatically generated warm pools had become quite meridionally elongated and essentially disappears in the analysis. This meridional

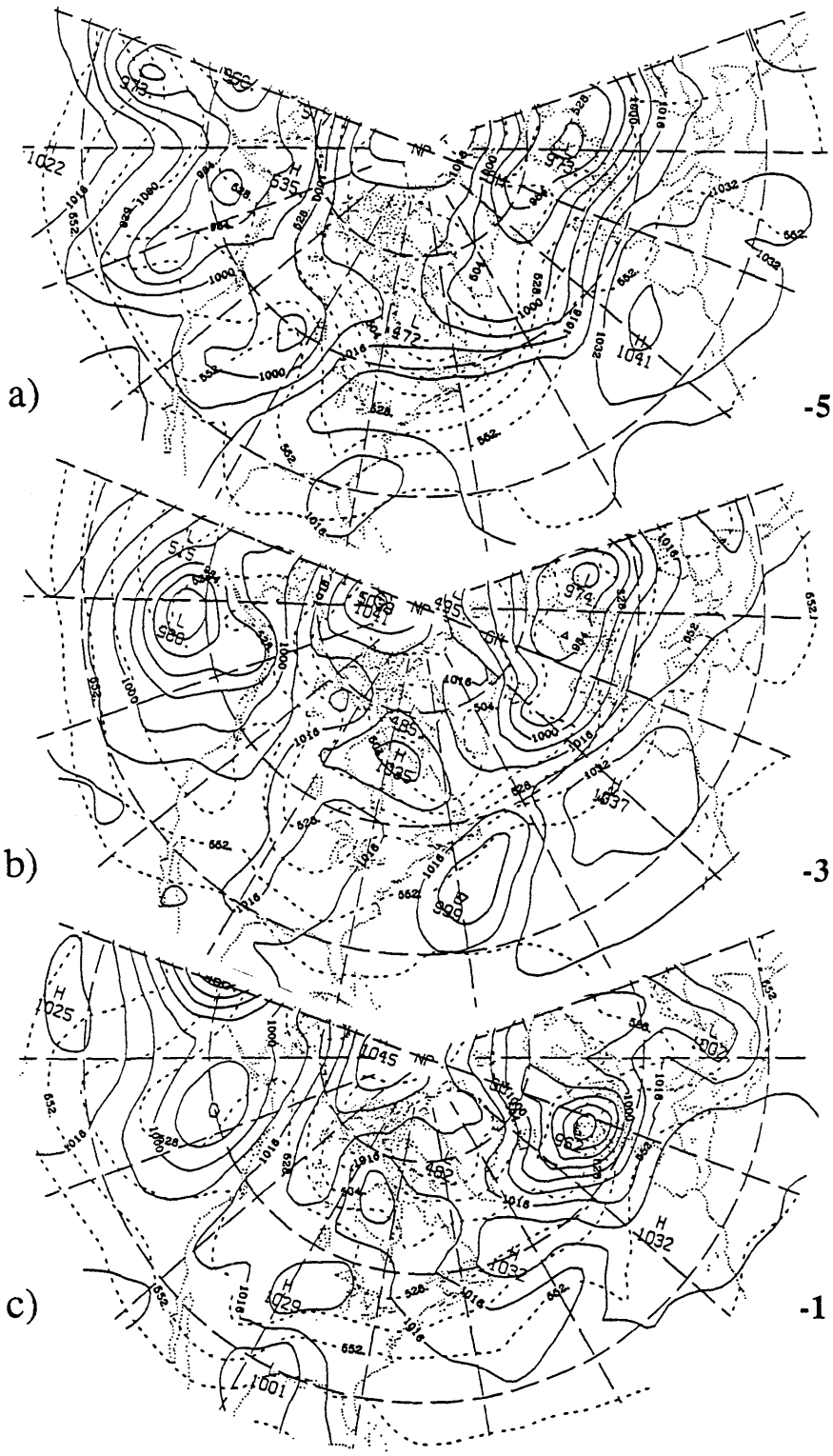

Fig. 6.4. Sequence of a) MSL pressure (solid, contour interval 8 mb) and 1000 mb to 500 mb thickness (dashed, contour interval 12 dam) for days a) -5, b) -3 and c) -1 relative to onset of AP16.

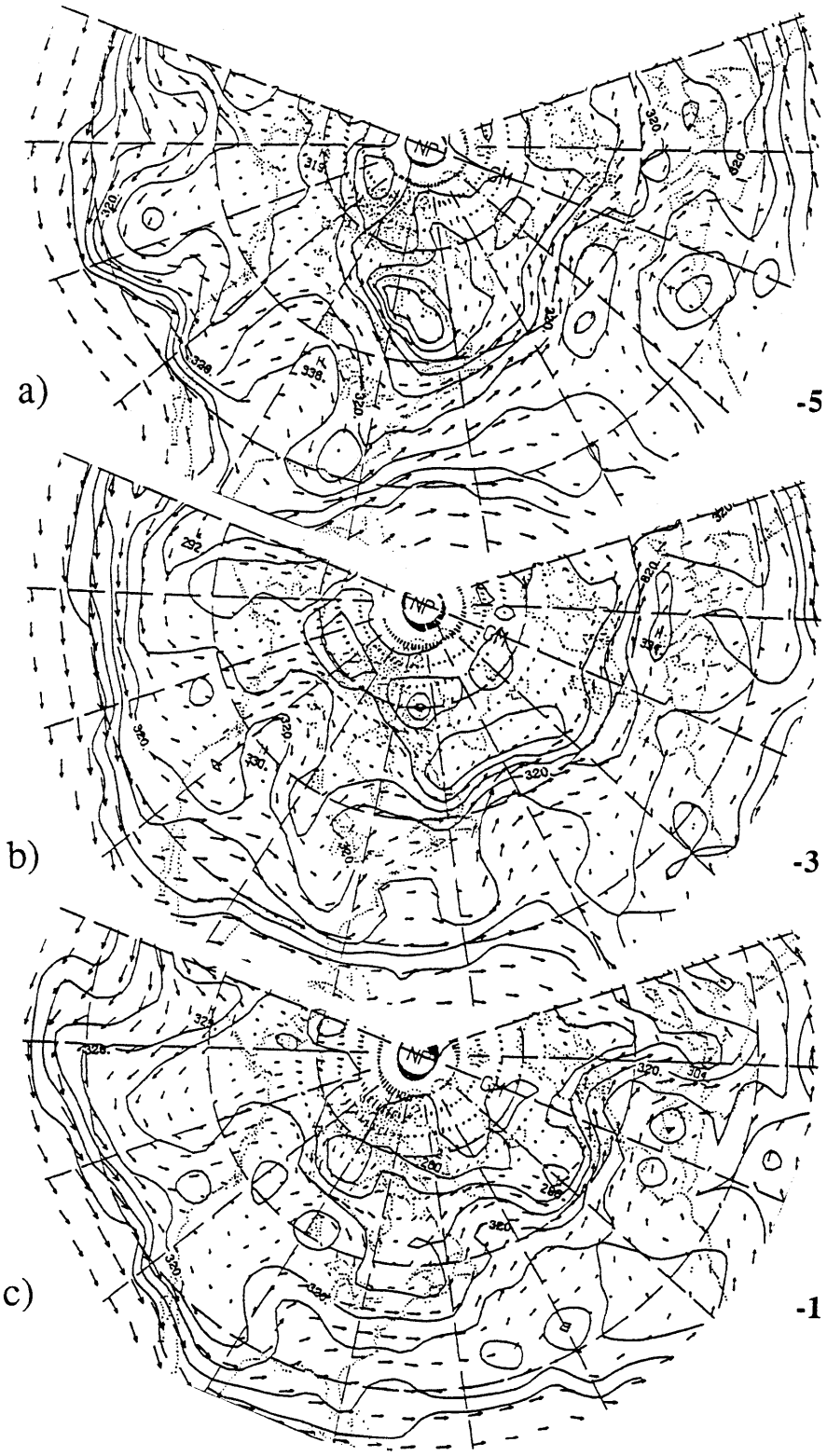

Fig 6.5 As in Fig 6.4 except for potential temperature (contour interval 10K) and the observed wind vectors on the 1.5 PVU surface.

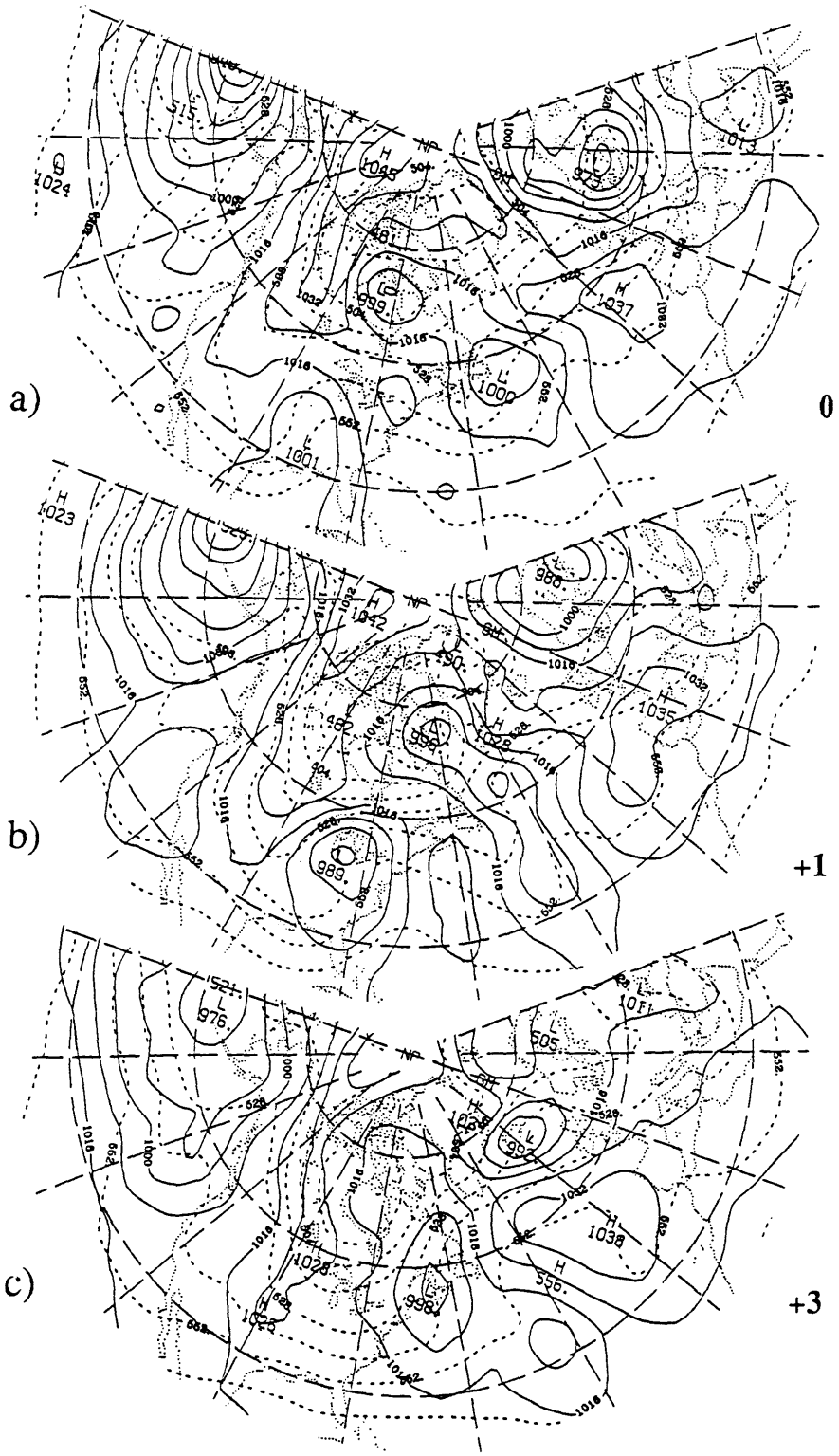

Fig. 6.6. Sequence of a) MSL pressure (solid, contour interval 8 mb) and 1000 mb to 500 mb thickness (dashed, contour interval 12 dam) for days a) 0, b) +1 and c) +3 relative to onset of AP16.

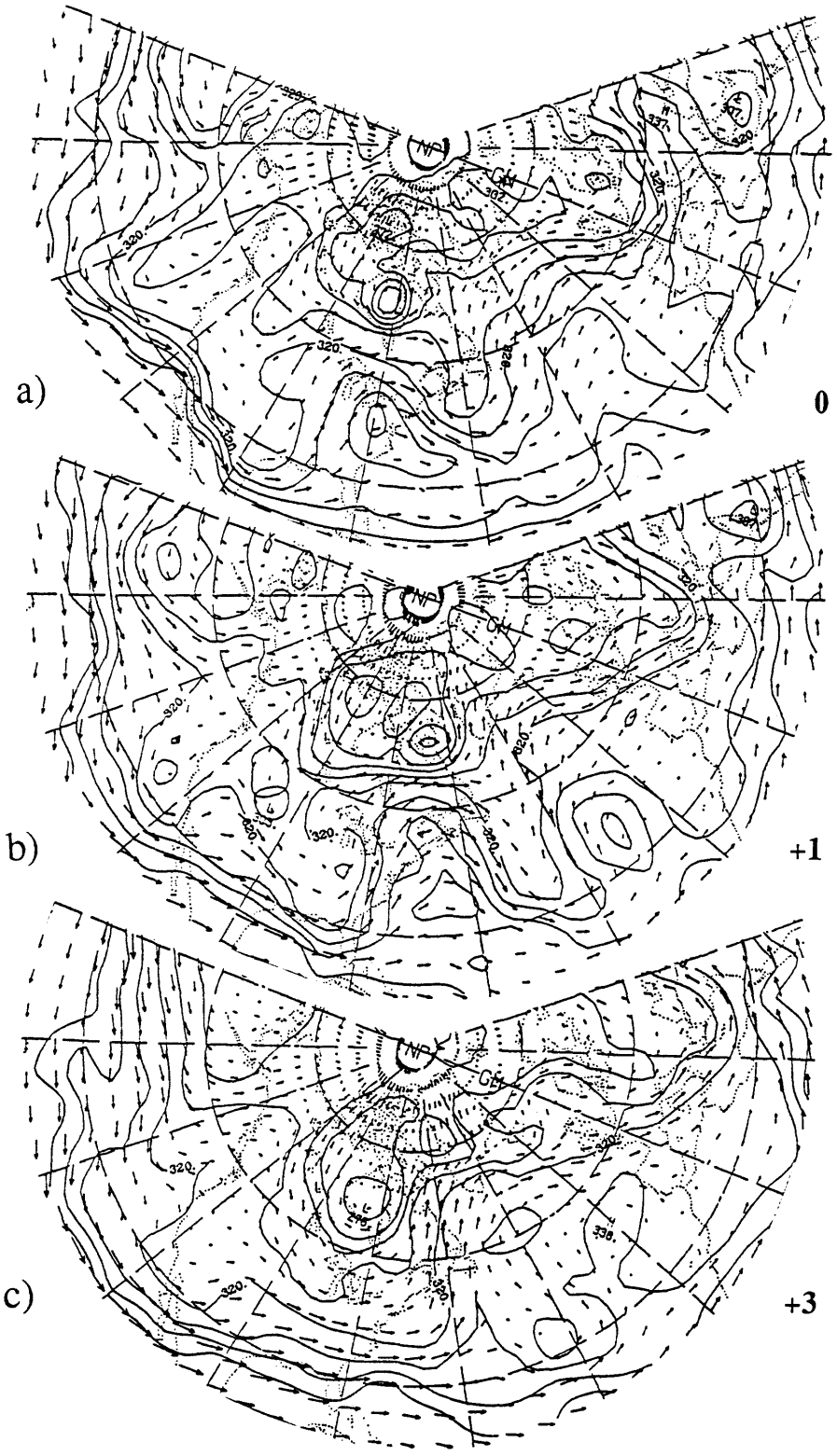

Fig 6.7. As in Fig 6.6 except for potential temperature (contour interval 10K) and the observed wind vectors on the 1.5 PVU surface.

elongation and eventual dissipation of synoptic-scale enstrophy strongly resembles the eddy straining mechanism proposed by Shutts (1983), and is associated with an irreversible downgradient transport of eddy potential vorticity. A second cyclone that was located over Michigan cyclone on day +1, has propagated towards the Canadian Maritimes by day +3, and also acquires a meridionally-elongated shape. On its northeast flank, strong warm advection is evident at both the surface and on the tropopause. The tropospheric warm pool associated with the development of this system has merged with the other warm pool to produce a large region of warm air and anticyclonic flow over the central Atlantic, coinciding with the onset of the PA. Also at this time, a rapidly deepening surface cyclone appears near Iceland along the strong baroclinic zone to the north of the developing PA.

By day +5 (Figs. 6.8a and 6.9a), the PA pattern has reached a well developed phase, although continued intensification of the pattern appears to still be occurring. This development is associated with a very long north-south aligned cold trough that is advecting a large tropopause warm air pool (originally created during the major cyclogenesis event over the eastern U.S.) northward. Tropopause temperatures have risen by about 30K over the 10 day period in the region near Iceland with surface pressures rising to 1042 mb. The rapidly deepening cyclone near Iceland on day +3 has propagated southeastward into Europe and has advected a large pool of cold air southward east of the PA.

On day +6 (not shown), the trough that was originally the strong day 0 cyclone development continues to meridionally elongate and collapse, although its southern end remains as a weak cool pool on the tropopause near 35N 40W. Its northern end has moved across Greenland and has led to another rapidly deepening cyclone just north of Iceland. The circulation associated with this cyclone advects part of the anomalously warm PA air eastward. At the same time, cold advection around the central European low has pushed

cold air westward. By day +7 (Figs. 6.8b and 6.9b), the combination of these processes has lead to a reversal of the temperature gradient throughout the troposphere over Europe and the initiation of a classic high-over-low blocking pattern over Europe. The process of this block formation is at the expense of the PA and shows how synoptic-scale disturbances on the north side of the PA play an important role in dissipating the local thermal anomaly that characterizes the PA.

Also on day +7, a new cyclone develops along the U.S. southeast coast in response to another upper-level trough that propagated across North America. The circulation associated with this trough renews the warm advection into the polar regions just west of Greenland helping to replenish the warm air lost to the European block formation. Note that at this time, the number and intensity of synoptic-scale disturbances over the Pacific and Western North America has diminished relative to earlier times during the evolution.

By day +9 (Figs. 6.8c and 6.9c), the cyclone on the upstream side of the PA has weakened considerably (its central pressure on day +8 was 988 mb) and has become meridionally elongated. The circulation on the south and west side of the trough is advecting cold air into the western Atlantic, which begins to reestablish zonal flow at mid-latitudes. The warm pool that had advected eastward over Europe has completely detached from the PA and is drifting further eastward over the Northern Soviet Union. At this time, the beginning of the Megalopolitan snow storm (Sanders and Bosart, 1985) is evident as a small low over northern Florida. By day +11 (Figs. 6.10a and 6.11a), which is near the time of the start of Shutts' analyses, the Megalopolatian storm has deepened considerably but retains a relatively small scale. Near Greenland, yet another surface cyclone development is occurring. Its associated circulation begins to advect another pocket of warm air into Northern Europe. By day +13 (Figs. 6.10b and 6.11b), the Megalopolitan storm has become north-south meridionally elongated and continues to advect warm air northward along a narrow stream into the polar regions. By this time,

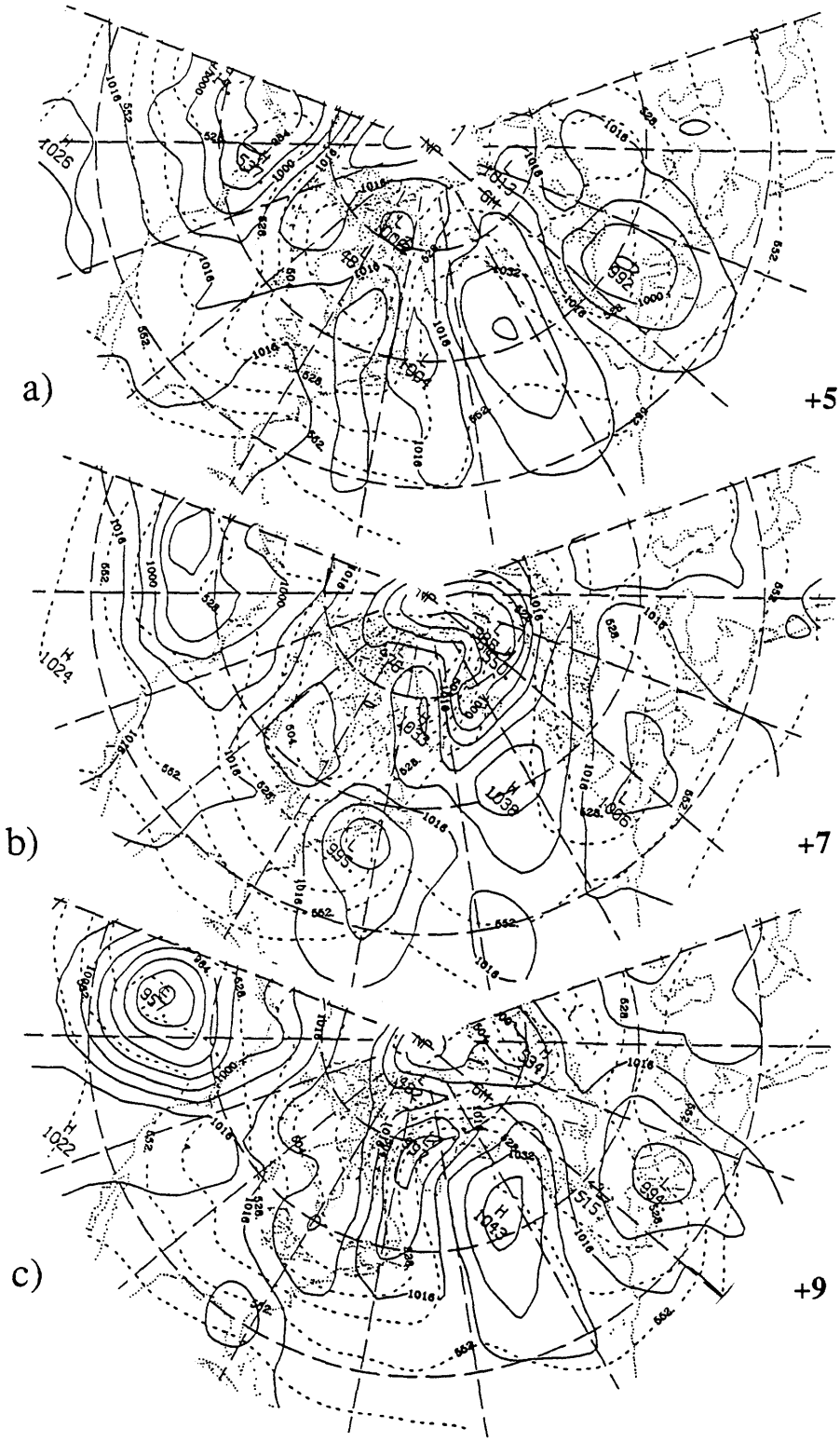

Fig. 6.8. Sequence of a) MSL pressure (solid, contour interval 8 mb) and 1000 mb to 500 mb thickness (dashed, contour interval 12 dam) for days a) +5, b) +7 and c) +9 relative to onset of AP16.

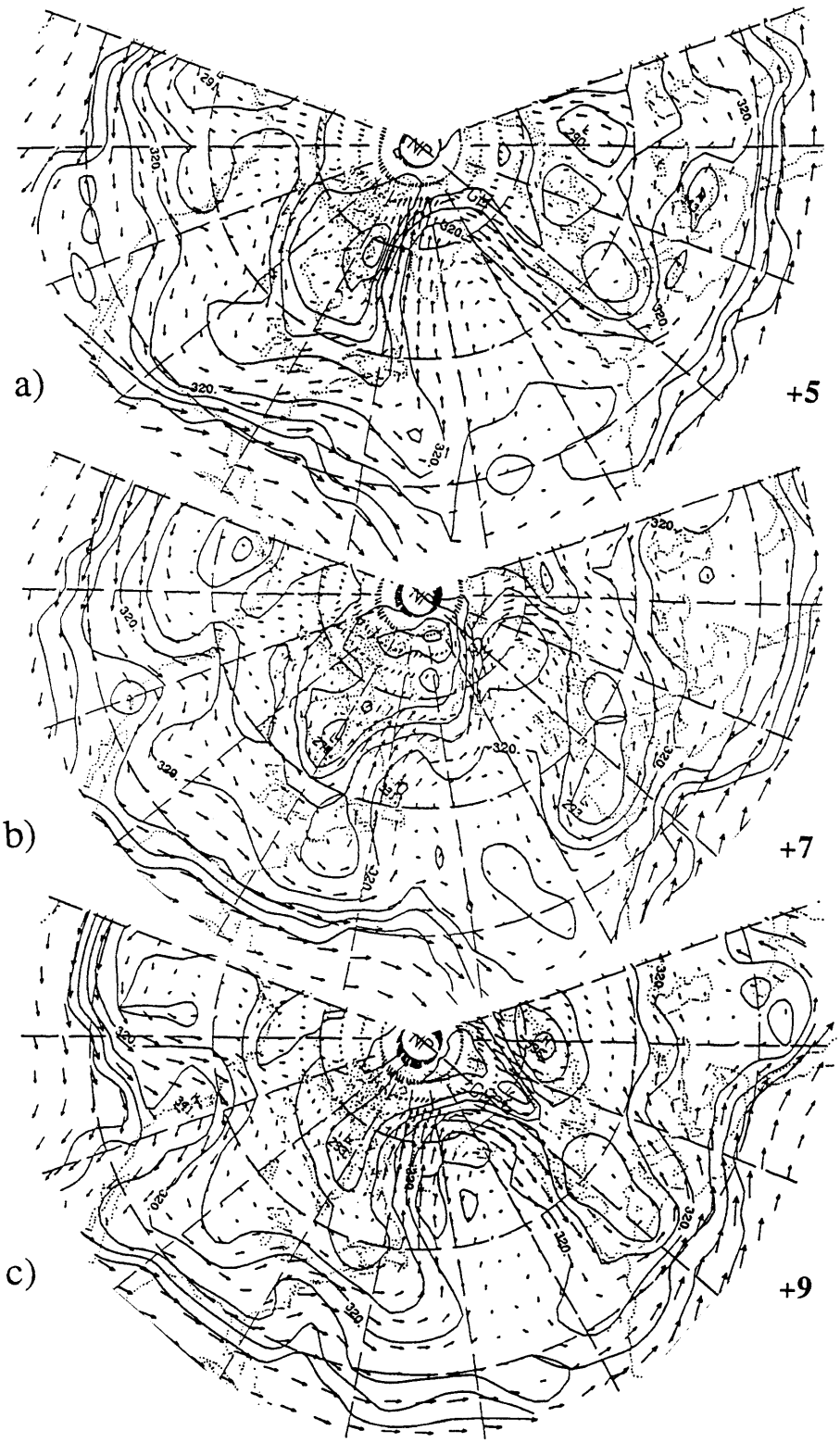

Fig 6.9. As in Fig 6.8 except for potential temperature (contour interval 10K) and the observed wind vectors on the 1.5 PVU surface.

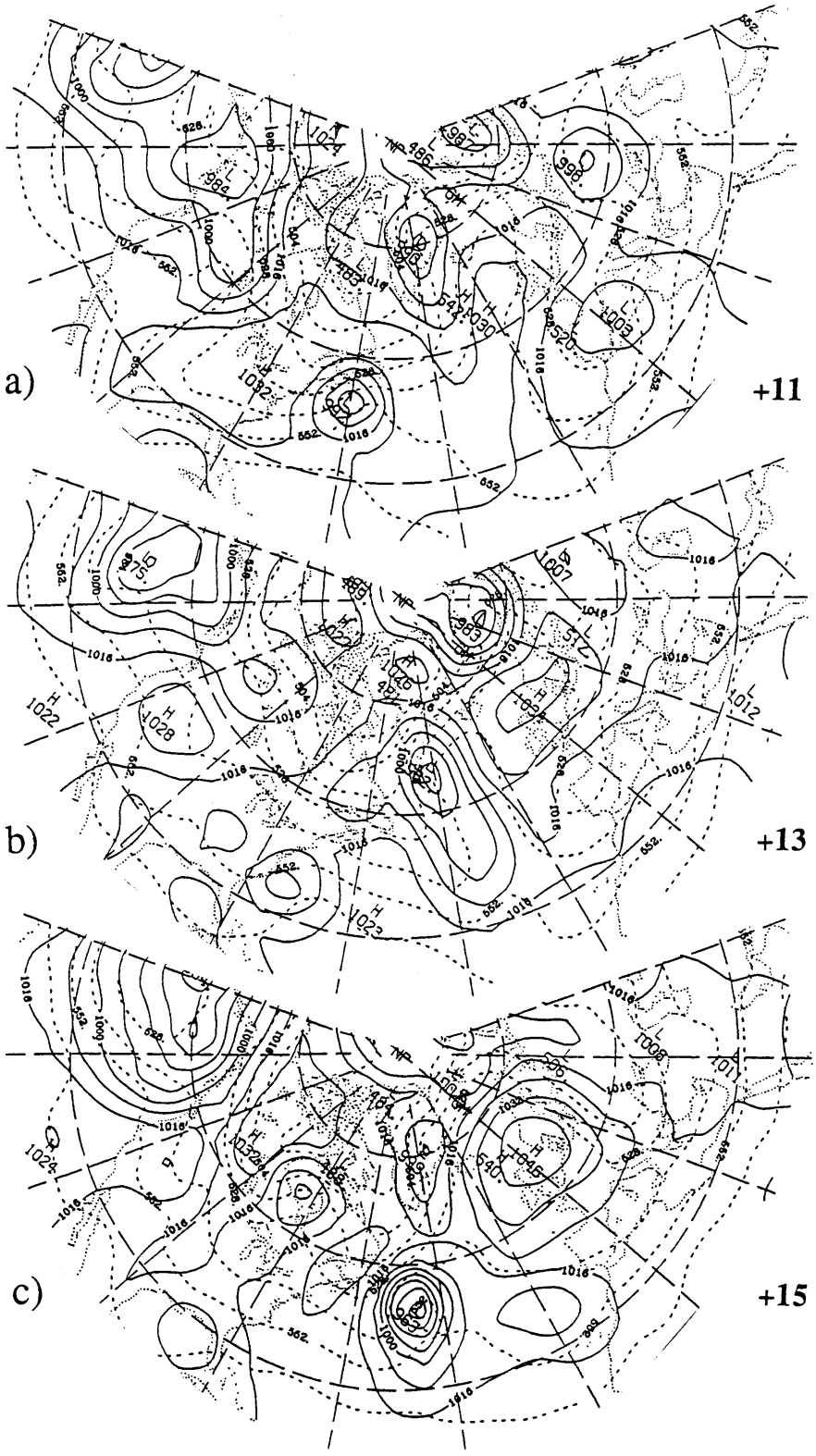

Fig. 6.10. Sequence of a) MSL pressure (solid, contour interval 8 mb) and 1000 mb to 500 mb thickness (dashed, contour interval 12 dam) for days a) +11, b) +13 and c) +15 relative to onset of AP16. Day +13 of onset is equivalent to day 0 of breakdown.

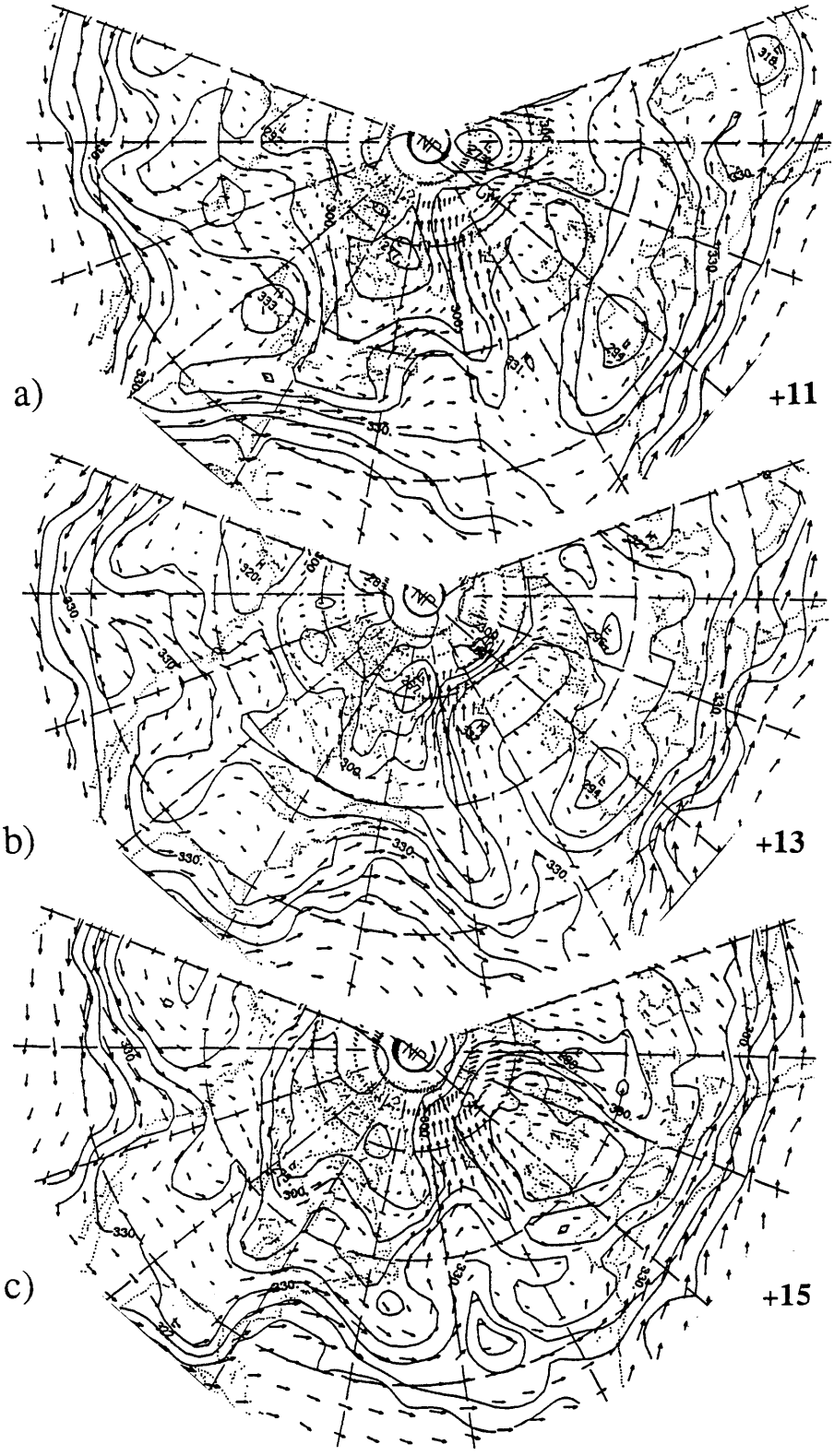

Fig 6.11. As in Fig 6.10 except for potential temperature (contour interval 10K) and the observed wind vectors on the 1.5 PVU surface.

however, the latest Greenland low has advected another large pool of the warm air associated with the PA into Northern Europe. Associated with this advection is an eastward shift of the major surface anticyclone and the reestablishment of a high-over-low block over Europe. At the same time, to the south of the Megalopolitan, cold air advection into the central Atlantic further reestablishes the midlatitude zonal flow. The combination of the loss of considerable warm air into northern Europe and the cold advection into the central Atlantic is essentially the demise of the PA event. By day +15 (day +2 of breakdown), a new rapidly deepening cyclone off the U.S. develops and propagates eastward. However, as it takes a much more southerly route than its predecessors, it does not appear to significantly reestablish the anomalous pattern over the key region. Subsequent analyses (not shown) show that the reestablished European block was short lived, as the warm pool of air at the tropopause that characterized it, continued to drift eastward over the Soviet Union.

6.6 Discussion

During the three week period (day -5 to +15) of discussion for this case, at least 6 major surface cyclones crossed the 60W meridian between 30N and 70N. In addition, at least 5 cyclones developed after day +2 east of Greenland and subsequently propagated eastward or southeastward into Europe. There were six cyclogenesis events with origins over the southeast U.S., all of which were associated with cold troughs along the tropopause that had propagated into the region from over the Pacific. As these systems developed and propagated eastward, they became strongly meridionally elongated. This elongation was usually most evident in the structure of the surface cyclones and in the cold troughs on the tropopause. Ahead of these elongated disturbances, strong warm advection brought (and later replenished) anomalously warm air far over the North Atlantic. The

narrow cold troughs usually eventually dissolved between the warm air pockets ahead of them and the warm pocket developing behind them. The cyclogenesis events in the far northern Atlantic apparently had a dissipative effect of the thermal structure of the PA, as they were directly associated with advection of warm air associated with the PA eastward into Northern Europe. This was most evident on days +9 and +13, when pockets of warm air were cutoff from the top of the warm PA by eastward advection associated with a synoptic-scale disturbance. The second event was most dramatic and played a substantial role in the breakdown of the PA.

Although we have often focused on the baroclinic processes occurring during this PA event, the barotropic processes also played a substantial role in the evolution, as demonstrated by the barotropic height tendencies (Figs. 6.3 and 6.4). These barotropic processes were related to the collapse and subsequent decay of the cold troughs on the east side of the PA, the northward shift in storm track and the rapid cyclogenesis events east of Greenland.

Diabatic processes also apparently played a significant role in several of the eddy developments, particularly during the cyclogenesis event that occurred over the eastern U.S. near day 0. The warming associated with the large-scale latent heat release appeared to produce significant warming of the tropopause over the North Atlantic, which subsequently helped in the development of the PA. Although a complete thermodynamic analysis was not attempted, it would likely indicate that diabatic processes had an important role in the overall warming of the PA region. However, it would be erroneous to attribute the increase of the enstrophy of the large-scale directly to the diabatic processes. Rather, these processes appeared to play a significant role in increasing the enstrophy of the synoptic-scale eddies. These eddies subsequently stretched meridionally and compressed zonally in the strong diffluent region upstream of the PA. The narrowing of the eddies continued until, in most cases, individual synoptic features could no longer be tracked.

Thus this downscale eddy enstrophy cascade eventually led to dissipation of the eddies, and an irreversible downgradient transport of PV. Diabatic processes may have also played a role in the destruction of upper-level eddy enstrophy late in the eddy life cycles, when the troughs became meridionally elongated and nearly equivalent barotropic.

Chapter 7

Summary and Conclusions

We have performed an observational study to identify the systematic interactions between synoptic-scale eddies and the large-scale flow during the life cycles of wintertime persistent flow anomalies. We have been motivated by a lack of a general and concise picture of how synoptic-scale eddies interact with the larger-scale modes of low frequency variability. We have also been motivated by the practical issue of relatively poor dynamical weather predication into the time ranges normally associated with LFV. Although the behavior of synoptic-scale eddies has been extensively studied for the mature phase of blocking, there have been few observational studies during the other phases of the life cycles of blocking. Further, there have been almost no studies of the synoptic-scale eddy interactions associated with the negative (zonal) phases of LFV.

In this thesis, we have focused on composite studies of the wintertime persistent anomalies as defined by Dole and Gordon (1983). We concentrated on identifying the anomalous aspects of the eddy interactions with the life cycles of PAs. We approached the problem by attempting to answer two basic questions: First, how do the synoptic-scale eddies behave throughout the life cycles of persistent anomalies? Second, how do the eddies feedback and influence the evolution of the large-scale flow? These questions were the focus of the results described in Chapters 4 and 5, respectively. In Chapter 6, we provided additional diagnostic and synoptic analyses of an Atlantic positive PA case to further illustrate many of the composite results.

We found that there are large and systematic changes in the patterns of anomalous eddy activity throughout the life cycles of PAs. The patterns displayed a remarkable degree

of symmetry between positive and negative phases of PAs, with corresponding Atlantic and Pacific cases also showing many similarities. Prior to the development of the large-scale flow patterns, we found significant changes in the degree of the hemispheric-mean synoptic-scale eddy activity, with increased (suppressed) mean eddy activity preceding the development of positive (negative) persistent anomalies. During the developments, anomalous eddy activity having the same sign as the tendency of the large-scale flow anomalies were found immediately upstream of the key region. During the mature phase, the anomalous eddy activity pattern was generally characterized by a N-S aligned dipole pattern, with enhanced eddy activity found to the north (south) and suppressed activity to the south (north) of the key point during positive (negative) PA events. Upstream of the mature PAs, the sign of the anomalous eddy activity remained the same as that of the large-scale flow anomaly until just prior to breakdown, when the anomalous eddy activity weakened and in many cases changed sign.

During the Atlantic positive PA cases, a relatively well defined packet of anomalous eddy activity was evident in the composite analyses over the Pacific at least 6 days prior to onset. This activity subsequently propagated eastward to just upstream of the key region as the large-scale flow anomalies were developing most rapidly. For the other cases, it was not possible to identify a temporally consistent anomalous propagating wave packet, although trends similar to the Atlantic positive cases were still evident. The magnitudes of the composite eddy activity anomalies during mature PA events were approximately 50% of the local climatological-mean values, although the mature Pacific negative cases had anomalies only about half as large as the other cases. The mature Pacific cases also had significant changes in eddy activity far downstream that were apparently associated with the large-scale wavetrain patterns that are characteristic of these cases. Particular striking was an anomalous Atlantic storm track during the Pacific negative cases that was aligned northeastward along the eastern U.S. seaboard.

The changes in eddy activity associated with the mature PAs appeared related to changes in both the advection (steering) by the large-scale flow and to changes in the large-scale baroclinicity and associated favored regions of cyclogenesis as well as changes in the patterns of eddy dissipation. Some of the more significant of the cyclogenesis changes were found in the regions to the north of the mature positive PAs, where rapid cyclogenesis events were found to be unusually common. In general, the maxima in anomalous eddy activity were found to be located about 15 degrees downstream from the maxima of 700 mb anomalous baroclinicity (fUz/N) and downstream of 700 mb anomalous eddy heat fluxes, a relationship similar to that found in the climatological-mean fields. This suggests that the same mechanisms controlling mean synoptic-scale eddy activity are also evident on the time-scales of the persistent anomalies, as was suggested by Dole (1982). However, the far upstream eddy activity anomalies well prior to the onset of the PAs do not bear a clear relation to any baroclinicity anomalies, although they are associated with anomalous eddy heat fluxes. Understanding their origin remains an important unresolved question. We also found that upstream eddy activity anomalies alone are neither a necessary nor sufficient condition for the occurrence of a PA, although lag correlation analyses indicate that eddy activity changes upstream have some weak predictive power as to the sign of the subsequent downstream large-scale geopotential height anomalies.

To diagnose the eddy feedbacks on the large-scale flow, we have made use of a variety of diagnostic techniques. The **E**-vector method proved to be a particularly useful and compact description of many important eddy characteristics, including forcing by the eddies of the large-scale flow. For the Atlantic cases, we found large upper-level anomalous eddy forcings due to the divergence of the barotropic (eddy vorticity flux) part of anomalous **E**-vectors throughout the life cycles of the PAs. The magnitude of the geopotential height tendencies induced by the anomalous eddy forcings is about 30 m/day, which implies a spinup time scale similar to that observed for the large-scale flow.

Temporally, the barotropic forcing tends to lead the development of the Atlantic cases by 2 to 4 days, but during breakdown appears to be mainly in-phase with the large-scale changes. Geographically, the forcing is centered about 1/8 wavelength upstream of the large-scale circulation center. The barotropic forcing pattern tends to be stationary throughout the life cycle of the Atlantic cases, although the associated patterns of anomalous E-vectors vary considerably. Including the somewhat weaker baroclinic (eddy heat flux) effects, the patterns of anomalous eddy forcings for the Atlantic cases do not change appreciably. However the baroclinic terms temporally lead the large-scale Atlantic developments by about 6 to 8 days, so that during the mature and decay phases, the baroclinic terms are generally dissipative of the large-scale flow anomaly. For the Atlantic cases, a significant portion of this dissipative effect appears to be directly associated with a hyperactive storm track between Greenland and Scandinavia.

During the Pacific PA cases, the results are somewhat less clear. The upper-level barotropic forcing patterns associated with the Pacific positive cases are large and of the correct sign, but do not show any significant phase shift between the large-scale flow either temporally or geographically. Throughout the life cycles of the positive PA cases, the upper-level baroclinic forcing patterns are nearly out of phase with the large-scale flow. For the Pacific negative cases, the magnitudes of the eddy feedbacks are about half that found during the other three PA cases, as anticipated from the relatively small associated changes in eddy activity.

Our interpretations based on the upper-level E-vector analyses were generally confirmed using Lau and Holopainen's (1984) complete three-dimensional height tendency technique, although the results suggested a somewhat stronger role for the anomalous eddies in the maintenance of the Pacific negative PAs. The anomalous surface pressure tendencies forced by the eddies were large (~5 mb day^{-1}) and had the same sign and similar structures to the observed large-scale flow anomalies. Considering the simplicity of the E-

vector technique, as well as the additional information on eddy structure and propagation implicit in the vectors, we found the E-vector method conceptionally superior to the tendency technique for studying eddy changes in association with the large-scale flow anomalies. The Hoskins *et al.* (1983) formulation of the E-vectors, however, which ignores zonal variations in the eddy statistics as well as zonal eddy heat fluxes, may not be as quantitatively suitable as the other formulations for examining the anomalous aspects of eddy interactions during PAs, as it ignores terms that are not necessarily small in some of the circumstances encountered.

A hemispheric barotropic model was also used to estimate the response of the atmosphere to the anomalous eddy forcing. By comparing runs during the onset of the Atlantic PA cases which were forced with anomalous eddy vorticity forcings to corresponding unforced control runs, we concluded that the anomalous eddy forcing could produce about half of the observed large-scale developments. It was suggested that the net response may be increased substantially if the highest frequency components (0-2.5 day) of the eddy activity were included.

A case study of one of the Atlantic positive PA events provided a clearer synoptic interpretation of the composite results. Most of the features of the composite analyses could be identified in this case, including a set of eastward propagating anomalous synoptic-scale waves that existed well prior to development, large changes in the storm tracks during the mature phase, including enhanced cyclogenesis north of the PA and to the east of Greenland, straining and dissipation of the eddies as they entered the diffluent flow region upstream of the PA, and strong eddy interactions with the large-scale flow anomaly. The study also suggested that diabatic heating may play an indirect role in the large-scale development by directly increasing the enstrophy of the eddies which in turn, weakens the large-scale PV gradient as the eddies dissipate.

In a very recent study, Nakamura and Wallace (1990) have also studied the composite anomalous eddy activity changes associated with relatively strong occurrences and the major teleconnection patterns. Their results are generally consistent with our results, although they found a somewhat more enhanced (suppressed) storm track to the south of positive (negative) mature height anomalies. This is likely due to the fact that their key points were generally located further north than ours, so that a larger percentage of the mean flow (and synoptic-scale eddies) passed to the south of the key regions. Our results are also considerably more extensive than the 500 mb height analyses provided by Nakamura and Wallace. In another recent study, Lau (1988) identified the leading EOF patterns of the large-scale flow associated with changes in the monthly-mean synoptic-scale eddy activity, as well as the barotropic eddy feedbacks on the EOF patterns. Although our approach was quite different than Lau's, our general results also appear to be qualitatively consistent with his.

The results of the eddy forcing calculations for the Atlantic cases also appear consistent with other observational studies that have identified synoptic-scale eddy forcing as having a significant role in maintaining blocking flow patterns. Here we have extended the calculations by considering only the anomalous part of the eddy forcings, by computing the eddy feedbacks during negative (zonal) persistent flow anomalies, and by computing the eddy forcing during the entire life cycles of composite PAs. We have found that the synoptic-scale eddy feedbacks during the Atlantic cases present a picture consistent with the eddies playing a first-order role in determining the evolution of the large-scale flow anomalies. The results for the Pacific cases are less clear, and cast doubt on whether the eddies are playing a primary role in determining those evolutions. This difference is consistent with the calculations of Hansen and Chen (1982) and Mullen (1987), who have found a larger role for the synoptic-scale feedbacks during Atlantic blocking cases than during Pacific blocking cases. Hansen and Chen (1982) suggested that their Pacific

blocking case grew primarily through energy extraction by a planetary-scale wave directly from the basic state flow. Dole and Black (1990) found similar results for composite negative PAs over the Pacific. Further, Black (1990) finds that such large-scale energy extraction is not as clear during the Atlantic PA cases. Understanding why there are apparently such differences between the Atlantic and Pacific cases remains an important unresolved question.

When evaluating the eddy feedback results it is important to note the quasi-geostropic approximations on which the diagnostics are based. We found that the most restictive assumption to be a horizontally invariant static stability. Tests using a slowly varying basic state static stability to modulate the heat fluxes in the three dimensional height tendency calculations (not shown) indicated up to 50% changes in the effect of the heat fluxes[1]. Similar variations in results for the 300 mb E-vector calculations were also found when a local rather than a hemispheric-mean value for static stability was used. These results should be expected, since PAs are accompanied by large thermal anomalies and significant changes in the height of the tropopause. Results from tests using both geostrophic and observed horizontal winds in the E-vector calculations, however, were basically indistinguishable. It was also suggested that a significant overestimation of the surface potential temperature fluxes by the 1000 mb geostrophic flow may be partially responsible for the large surface pressure tendencies that have been calculated. Recent formulations of the height tendency equation in a non-QG framework by Smith and Tsou (1988) may provide a useful tool to test the effects of a variable static stability and other non-QG effects on the roles of the eddies in forcing the large-scale flow patterns.

Our results provide an observational benchmark upon which interactions between synoptic-scale eddies and the large-scale flow in GCMs can be compared. Low resolution

---

[1]This calculation was not entirely consistent, however, as the separable form of height tendency equation was still solved

GCMs typically have relatively poor representations of the observed LFV of the atmosphere. Our results suggest that this may be in part due to a poor representation of the synoptic-scale eddies that would be expected in low resolution models. It will be of interest to compare our results to similar calculations based on more recent long-term, high resolution GCM runs.

Finally, we note that our results may have significant implications for the prospects of dynamical long-range weather prediction. Our findings suggest that, for at least some forms of major LFV, both the details of the initial state and the evolution of the synoptic-scale systems appear to be critical for determining the evolution of the large-scale flow. Our results also suggest an alternative explanation to Palmer's (1988) finding that there is relatively high forecast skill during negative Pacific PA patterns. Since interactions between the synoptic-scale eddies and the large-scale flow are weakest during the Pacific negative cases, the evolution of the large-scale flow in these cases may also display to least sensitivity the the relatively poorly predicted synoptic-scale eddies.

Appendix A

Composite Case Dates

A description of the methodology used to select the persistent anomaly cases used for this study can be found in Chapter 3. In summary, cases were identified at key points whenever the magnitude of the lowpass filtered 500 mb heights exceeded ±100 m for at least 10 consecutive days during the winter season (defined as the 120 days starting 15 November). The key points used were 50N 25W for the Atlantic cases and 46N 170W for the Pacific cases. The dataset covered the winters 1962-63 through 1986-87. The following statistics on the cases were compiled:

Case Type	No. of Cases	Mean Duration	Stand. Dev.
Atl. Pos.	18	17.2 days	9.2 days
Atl. Neg.	20	16.2 days	7.6 days
Pac. Pos.	21	14.2 days	3.9 days
Pac. Neg.	22	20.0 days	12.6 days

The specific starting dates and durations of the cases used are:

Type	Starting Date and Time	Duration (days)
Atlantic Positive	21 Jan 64 12Z	20.0
" "	17 Dec 64 00Z	10.0
" "	01 Feb 65 00Z	21.0
" "	02 Jan 67 12Z	12.5
" "	24 Dec 67 12Z	11.5
" "	20 Jan 68 00Z	15.5

" "	25 Dec 68 00Z	10.5
" "	30 Jan 69 12Z	16.5
" "	24 Feb 70 12Z	10.5
" "	23 Jan 73 12Z	36.0
" "	29 Dec 74 12Z	10.0
" "	03 Dec 75 00Z	26.5
" "	08 Jan 76 00Z	18.5
" "	26 Dec 77 12Z	10.0
" "	26 Dec 80 00Z	42.0
" "	02 Feb 83 00Z	13.0
" "	05 Feb 84 00Z	12.0
" "	23 Jan 86 12Z	13.5
Atlantic Negative	09 Dec 63 12Z	12.0
" "	13 Feb 64 12Z	17.5
" "	31 Dec 65 12Z	11.5
" "	17 Jan 66 00Z	42.5
" "	18 Jan 67 12Z	11.5
" "	12 Feb 67 12Z	13.5
" "	08 Jan 69 00Z	18.5
" "	08 Jan 70 00Z	20.5
" "	04 Jan 71 00Z	23.5
" "	05 Jan 72 12Z	12.0
" "	30 Jan 7212Z	13.0
" "	01 Jan 74 00Z	14.0
" "	24 Jan 74 00Z	10.0
" "	01 Dec 77 00Z	11.0
" "	15 Feb 78 12Z	16.5
" "	01 Dec 78 00Z	14.5
" "	10 Dec 81 12Z	26.0
" "	13 Dec 83 00Z	12.0
" "	05 Feb 85 00Z	10.0
" "	02 Dec 86 12Z	13.5

Pacific Positive	10 Dec 64 00Z	10.0
" "	23 Dec 64 12Z	14.0
" "	21 Dec 65 00Z	13.0
" "	10 Feb 66 00Z	25.0
" "	29 Dec 67 12Z	20.5
" "	09 Dec 68 12Z	11.5
" "	31 Dec 68 00Z	15.0
" "	23 Jan 69 00Z	16.5
" "	16 Dec 70 00Z	13.5
" "	17 Jan 71 12Z	10.0
" "	24 Feb 71 12Z	10.5
" "	08 Dec 71 12Z	17.0
" "	16 Feb 72 12Z	11.5
" "	22 Feb 74 12Z	12.5
" "	01 Jan 75 00Z	20.0
" "	12 Dec 78 12Z	14.0
" "	03 Feb 79 12Z	14.0
" "	01 Dec 79 00Z	11.0
" "	25 Dec 81 00Z	10.0
" "	13 Dec 84 12Z	14.5
" "	02 Feb 85 12Z	14.5
Pacific Negative	16 Dec 63 00Z	17.0
" "	24 Jan 64 00Z	12.5
" "	09 Jan 65 00Z	12.0
" "	30 Jan 67 00Z	12.0
" "	05 Feb 68 00Z	30.0
" "	16 Dec 69 12Z	17.5
" "	28 Jan 70 12Z	25.5
" "	04 Feb 7112Z	15.5
" "	17 Dec 73 00Z	11.0
" "	16 Dec 75 12Z	12.0
" "	24 Jan 76 00Z	10.5
" "	10 Dec 76 00Z	15.0

" "	01 Jan 77 00Z	52.5
" "	10 Feb 78 00Z	28.5
" "	04 Feb 80 00Z	11.0
" "	28 Dec 80 12Z	22.5
" "	11 Dec 81 00Z	12.5
" "	13 Jan 83 12Z	56.0
" "	30 Dec 84 00Z	14.0
" "	17 Dec 85 00Z	11.5
" "	26 Jan 86 00Z	19.5
" "	06 Dec 86 12Z	26.5

Appendix B

Alternate Filtering Results

In this appendix we present the results of diagnostic calculations of eddy interactions with persistent anomalous flows similar to those discussed in Chapters 3 and 4 but based on somewhat different methodologies for identifying the synoptic-scale eddies. The motivation is to test the robustness of our previous to variations in the filtering schemes. Here we present the results obtained using two alternative filtering schemes: 1) a highpass temporal filter that retains modes with periods less than about 6 days and 2) a spatial filter that retains most features with wavelengths less than about 3500 km.

The particular highpass filter is the 31-point filter described by Wallace *et al.* (1988) that has a half-power response at a frequency of 0.18 day^{-1}. It has essentially the same 6-day low-frequency cut-off as the Blackmon bandpass filter, but also includes contributions from the high frequency (0-2.5 day period) eddies. We have highpass filtered both the 300 mb and 1000 mb geopotential heights, and have then performed a highpass VSTAT calculation in the manner described in Chapter 4. Here we will focus on the 300 mb results, as the 1000 mb results are qualitatively similar.

Composite-mean anomalies of the 300 mb highpass VSTATs for day +6 during onset of each of the PA cases are shown in Fig. A2.1. These patterns are nearly identical to the bandpass VSTAT anomaly patterns presented in Chapter 4. There is no indication during negative PAs of an enhanced eddy activity over the southern part of the eddy activity anomaly dipole. It was speculated that a significant fraction of synoptic-scale eddy energy may be shifted into higher frequencies in the regions of anomalously fast zonal flow, such as those present in the negative PA event. Magnitudes of the highpass filtered (0-6 day)

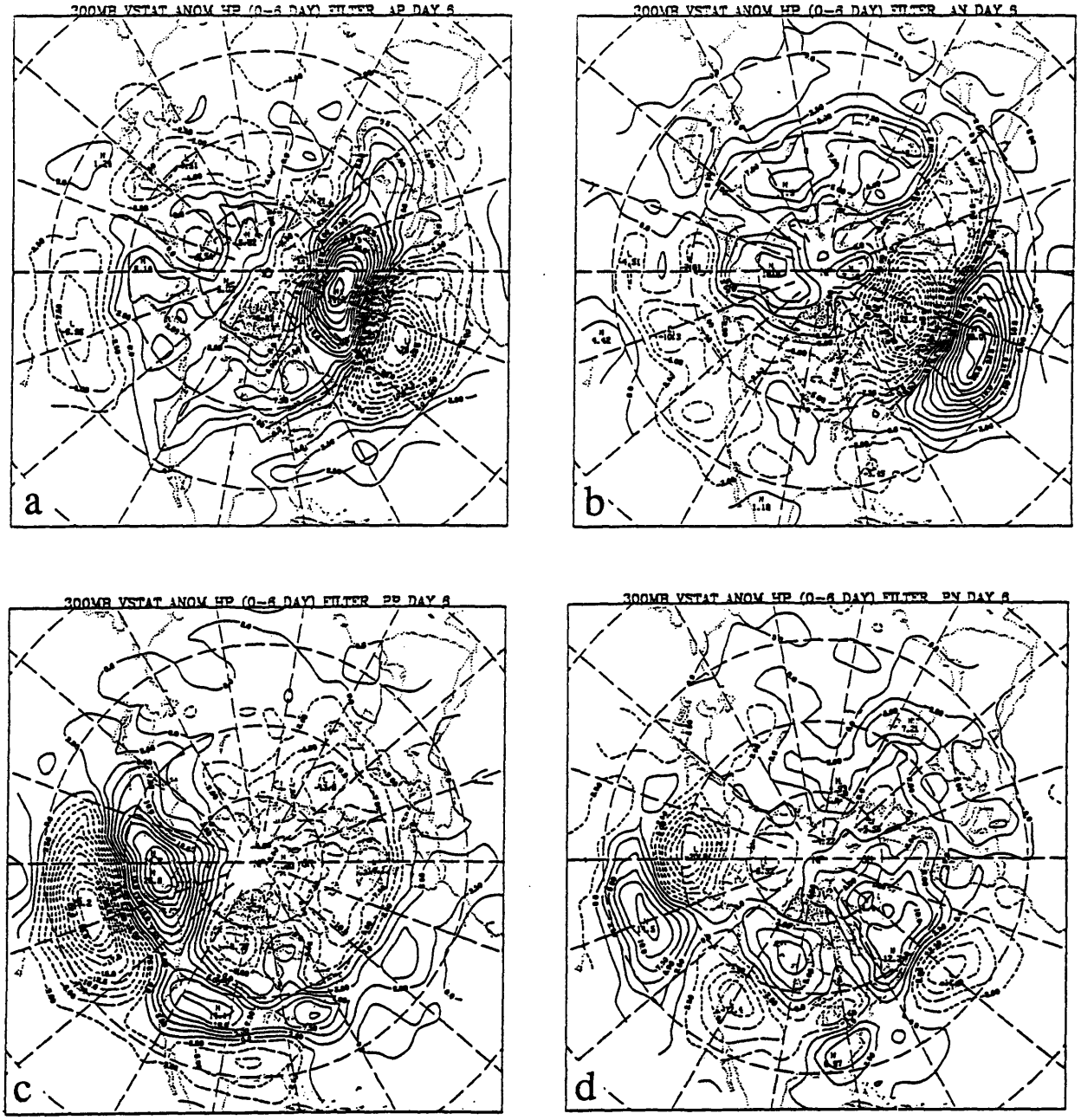

Fig. A2.1 Composite VSTAT anomalies computed using highpass-filtered (0-6 day) 300 mb geopotential heights for day +6 of a) Atlantic positive b) Atlantic negative c) Pacific positive and d) Pacific negative PA events. Contour interval 2.5 m; negative contours are dashed.

anomalies exceed the corresponding bandpass (2.5-6 day) anomaly magnitudes by about 20%. This enhancement is about as expected, based on Blackmon's (1976) results for the differences in RMS variance between his bandpass (2.5-6 day) and highpass (0-2.5 day) filters. Since highpass eddies have characteristics very similar to the bandpass eddies (Blackmon, 1976), we expect that inclusion of the highpass eddies in our diagnostic calculations of eddy forcing in Chapter 5 would yield similar patterns but with increased magnitudes. Since eddy mean-flow interactions depend upon quadratic eddy terms (e.g. u'^2, $v'T'$) we anticipate that a 20% increase in eddy magnitude would roughly yield a 40% increase in the eddy forcing.

The second alternative filtering technique is based upon Barnes (1973) objective analysis (OA) technique. The use of the Barnes OA scheme to spatially filter data is discussed by Maddox (1980). The Barnes OA technique begins by assigning Gaussian weights to the observed data based on their distance from each grid point in the analysis field. A first guess gridded analysis is then created as the weighted sum of all observations whose associated weights exceed an arbitrary threshold. A correction is applied to the first guess based upon the errors between the first-guess grid and the observations. The errors are multiplied by a slightly modified weighting function and the analysis repeated. Parameters of the analysis are the width of the Gaussian weight function, the weight modification parameter for the second pass and the minimum allowed weight threshold. The scheme is essentially a lowpass spatial filter that removes the small-scale variations in the data field. The bounds of the lowpass filter depend upon the (non-unique) choices of the analysis parameters. We make use of the Barnes OA technique to determine the lowpass spatial modes in the NMC dataset using the already gridded data as proxy observations. We then subtract the lowpass OA grids from the original grids to obtain the smaller-scale components of the original grid.

Our particular choice of OA parameters yields a filter response curve as shown in Fig. A2.2. The half power point for this filter is at about 3000 km with wavelengths greater than about 4000km virtually eliminated. Although this filter does not capture all synoptic-scale variability, it ensures that phenomena with the scales normally associated with PAs will not substantially influence the filtered results. Successful application of the Barnes OA scheme requires equally distributed data about the analysis point in order to avoid erroneous extrapolation. This is indeed a problem in our calculations, as the subtropical regions show considerable southward extrapolation of the mean midlatitude jets. Therefore, in the following discussion, the results south of about 30 to 35N need to be treated with caution. Fig A2.3 shows an example of a 300 mb spatially filtered analysis along with the corresponding bandpass temporal filter analysis for one of the days during the case discussed in Chapter 6. The extrapolation effect is particularly evident over the western subtropical Pacific, but otherwise, the spatial and temporal filters reveal broadly similar features. The OA filter retains smaller-scale phenomena and is thus characterized by sharper gradients. It also appears to have an greater integrated response than the bandpass filter.

Fig A2.4 shows the composite-mean anomalies in the VSTAT function computed using spatially-filtered 300mb height data for day +6 during the onset of each of the PA patterns. All aspects of the principal results described in Chapter 4 for the bandpass VSTATs can be identified in these plots. The principal eddy activity changes during mature PAs consist of an dipole in eddy activity characteristic of a meridionally shifted storm track and an upstream enhancement of eddy activity having the same sign as the PA. The magnitude of the spatial VSTAT anomalies is somewhat greater than the bandpass VSTAT anomalies and is very similar to the highpass VSTAT anomalies shown in Fig A2.2. During the positive PA events, the positions of the maximum spatial VSTAT anomalies to the north of the key points are shifted about eastward 5 to 10 degrees. This may be due to

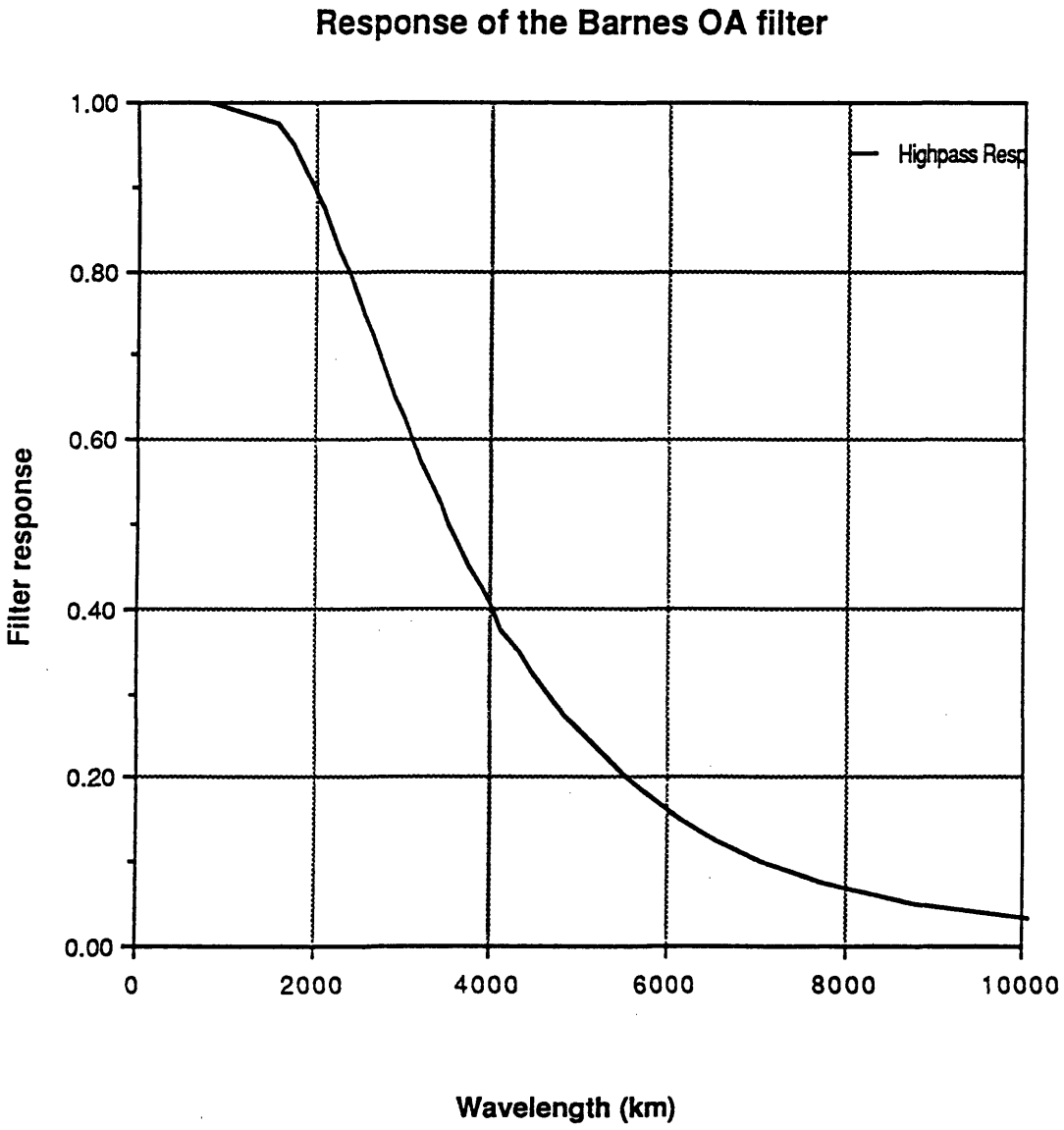

Fig. A2.2 Response curve of the Barnes objective analysis spacial filter used to isolate the smaller-scale fluctuations in the NMC data set.

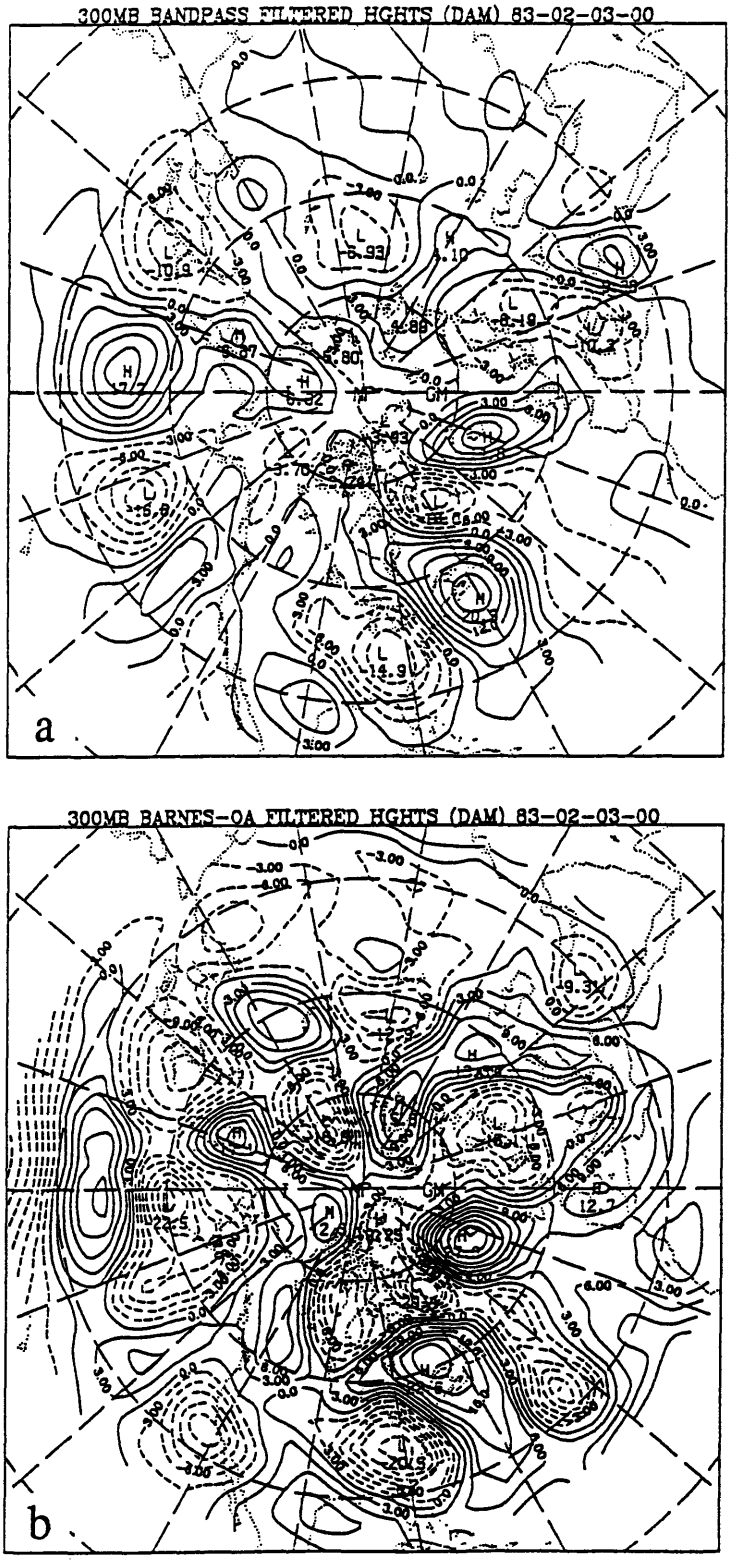

Fig. A2.3 Examples of a) a bandpass-filtered and b) a Barnes objective analysis filtered analyses. Contour interval 3 dam; negative contours dashed.

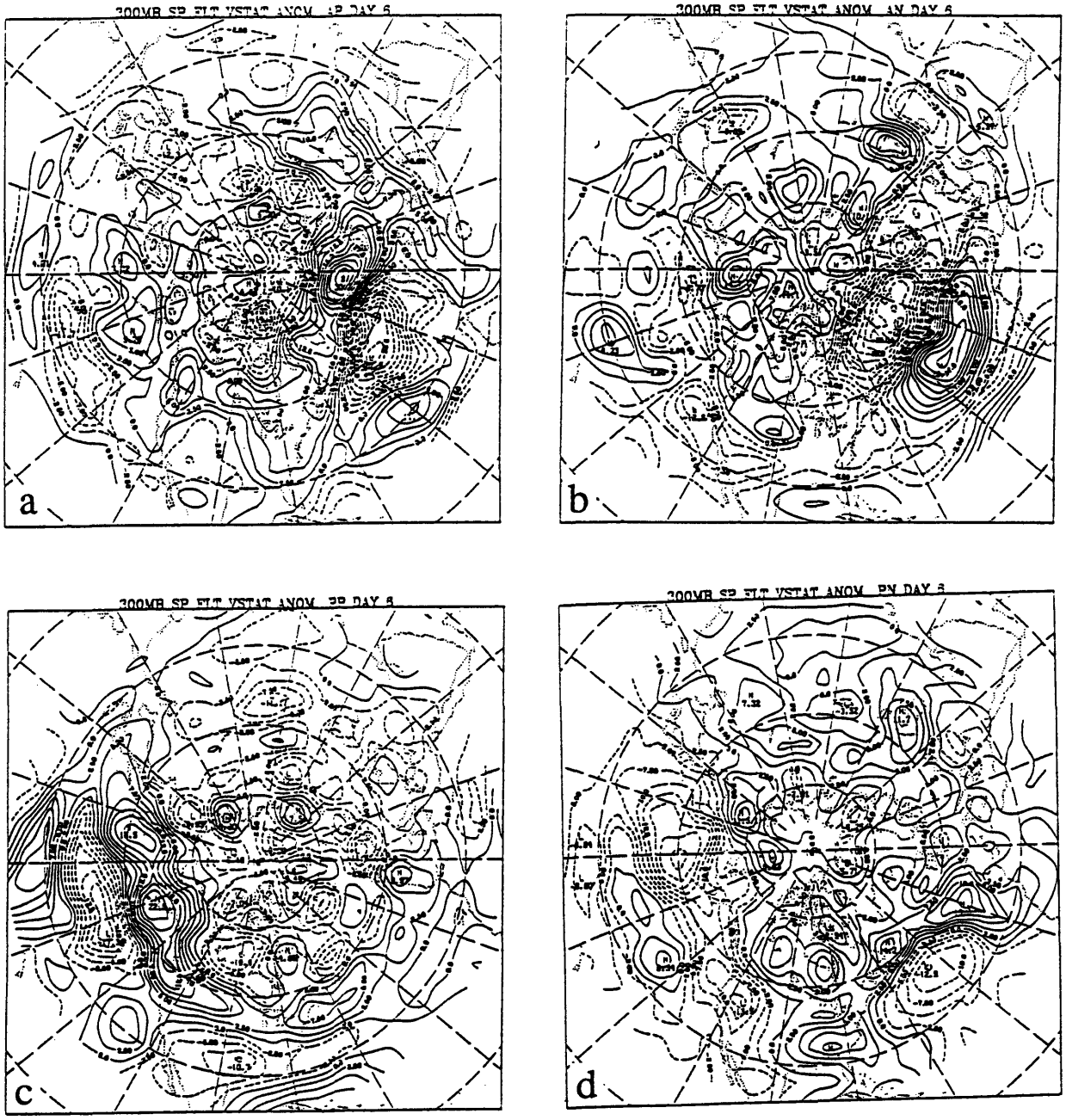

Fig. A2.4 Composite 300 mb VSTAT anomalies computed using the Barnes OA spatially filtered analyses for day +6 of a) Atlantic positive b) Atlantic negative c) Pacific positive and d) Pacific negative PA events. Contour interval 2.5 m; negative contours are dashed.

a greater sensitivity of the spatial filter to the eastward-propagating rapid cyclogenesis events that are common in those areas during positive PA events. The spatial filter VSTAT anomalies also indicate more of a storm track enhancement to the south of the PA events with the overall pattern having more of the "sandwich" structure described by Nakamura and Wallace (1990). However, as mentioned earlier, results from the southern part of our analysis region need to treated with caution.

We have also calculated the barotropic components of Trenberth's (1986) E-vectors at 300 mb using winds computed geostrophically from the spatially-filtered height data. Fig. A2.5 shows the resulting anomalous 300 mb height tendencies during the onset period of each of the PA patterns. These patterns are very similar in structure, position and magnitude to the bandpass barotropic E-vector forcing presented in Chapter 5. There is a much clearer eddy forcing signal for the Atlantic cases than for the Pacific, with the anomalous eddy forcing during the Pacific negative cases relatively very small. The time series of the barotropic eddy forcing computed using the spatially filtered data (not shown) throughout the life cycles of the Atlantic PAs display a tendency for the eddy forcing patterns to be geographically stationary, but to temporally lead the development of the large-scale flow. Whereas the maximum eddy forced height tendency is about 27 m day^{-1} just upstream of the key point during the onset period of the Atlantic positive PAs, its maximum during the case average (not shown) increases to only 30 m day^{-1}.

Computation of the spatially filtered grids requires significantly more computer time than do the temporally filtered grids. In general, the temporal filter requires 16 multiplications and 16 additions per grid point per time whereas the spatial filtering technique typically requires 600 multiplications and additions per grid point per time. Therefore we have limited our application of the OA filtering to the 300 mb heights alone. Given that the spatially filtered results are very similar to the bandpass filtered results, we have no reason to suspect the same for other levels and parameters. Therefore future

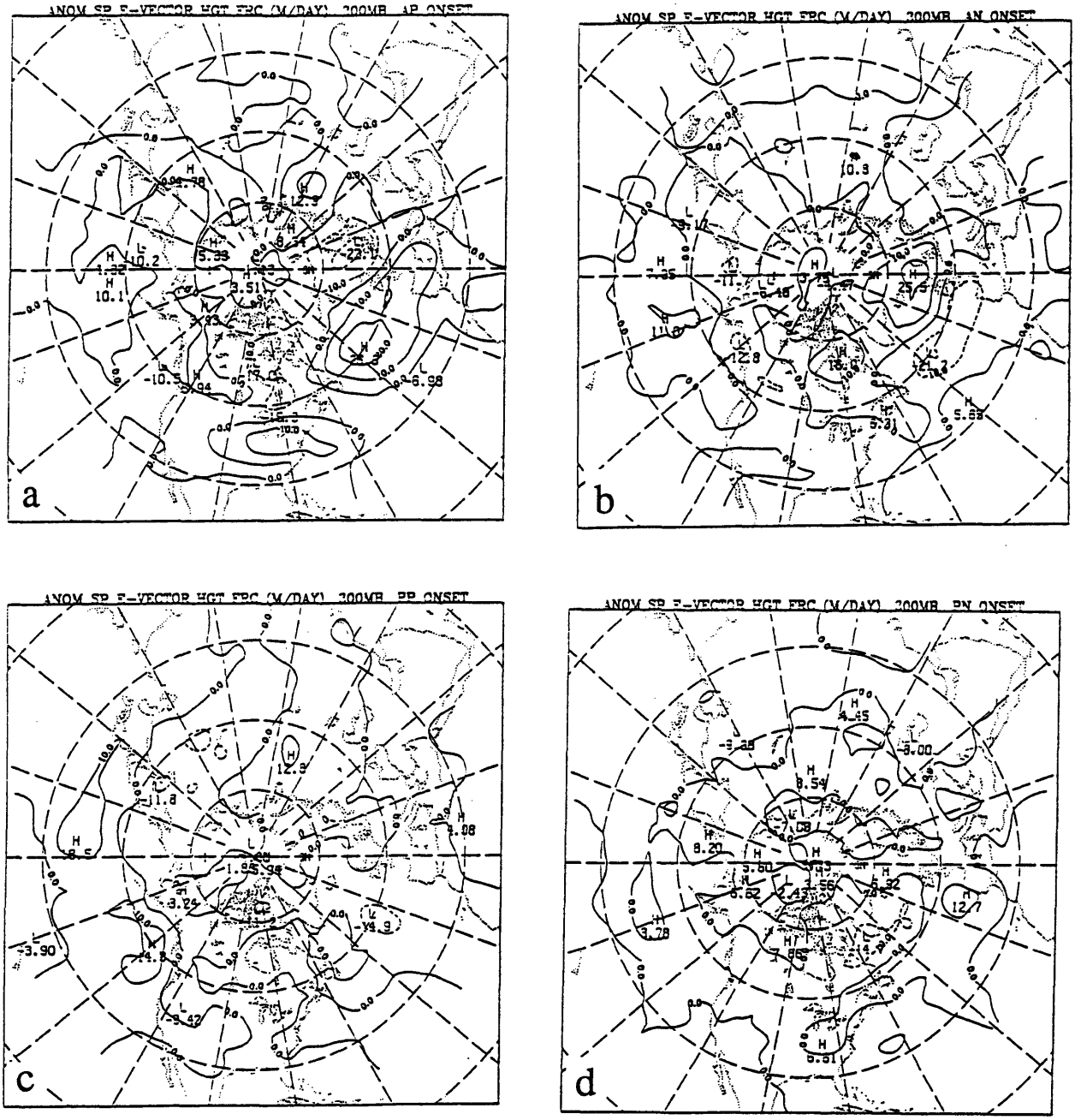

Fig A2.5 Composite 300 mb geopotential height tendencies computed using E-vectors formed using spatially-filtered height data. Plots are averaged over the 10 day period centered on day 0 of onset for a) Atlantic positive b) Atlantic negative c) Pacific positive and d) Pacific negative PA events. Contour interval 10 m day^{-1}; negative contours are dashed.

studies based on synoptic-scale filtered statistics may be most efficiently performed using the temporal filter, without any particular loss of generality.

List of References

Anderson, J.R., and J.R. Gyakum, 1989: A diagnostic study of Pacific basin circulation regimes as determined from extratropical cyclone tracks. *Mon. Wea. Rev.*, **117**, 2672-2686.

Andrews, D.G. and M.E.McIntyre, 1976: Planetary waves in horizontal and vertical shear: The generalized Eliassen-Palm relation and the mean zonal acceleration. *J. Atmos. Sci.*, **33**, 2031-2048.

Austin, J.F., 1980: The blocking of middle latitude westerly winds by planetary waves. *Quart.J. Roy. Meteor. Soc.*, **106**, 327-350.

Barnes, S.L., 1973: Mesoscale objective map analysis using weighted time series observations. NOAA Tech. Memo. ERL, NSSL-62, 60 pp.

Bell, G.D. and L.F. Bosart, 1989: A 15-year climatology of northern hemipshere 500 mb closed cyclone and anticyclone centers. *Mon. Wea. Rev.*, **117**, 2142-2163.

Benzi, R., P. Malguzzi, A. Speranza and A. Sutera, 1986: The statistical properties of general atmospheric circulation: Observational evidence and a minimal theory of bimodality. *Quart. J. Roy. Meteor. Soc.*, **112**, 661-674.

Bengtsson, L., 1985: Medium range forecasting at the ECMWF. *Adv. Geophys.*, **28**, 3-54.

Berggren, R., B. Bolin and C.G. Rossby, 1949: An aerological study of zonal motion, its perturbation and breakdown. *Tellus*, **1**, 14-37.

Black, R.X., 1990: Diagnostic study of the time evolution of persistent anomalies. M.I.T. Dept. of Earth, Atmospheric and Planetary Sciences, Ph.D. thesis.

Blackmon, M.L., 1976: A climatological spectral study of the 500 mb geopotential height of the Northern Hemisphere. *J. Atmos. Sci.*, **33**, 1607-1623.

_____, J.M. Wallace, N.C. Lau and S.L. Mullen, 1977: An observational study of the Northern Hemisphere wintertime circulation. *J. Atmos. Sci.*, **34**, 1040-1053.

_____, Y.-H. Lee and J. M. Wallace, 1984a: Horizontal structure of 500mb height fluctuations wiht long, intermediate and short time scales. *J. Atmos. Sci.*, **41**, 961-979.

_____, Y.-H. Lee, J. M. Wallace and H.-H. Hsu, 1984b: Time variations of 500mb height fluctuations with long, intermediate and short rime scales as decuded from lag-correlation statistics. *J. Atmos. Sci*, **43**, 981-991.

Bretherton, F. P., 1966: Critical layer instability in baroclinic flows. *Quart. J. Roy. Meteor. Soc.*, **92**, 325-334.

Brooks, C.E.P. and N. Carruthers, 1953: *Handbook of Statistical Methods in Meteorology*. Her Majesty's Stationary Office, London.

Charney, J.G., 1947: The dynamics of long waves in a baroclinic westerly current. *J. Meteor.*, **4**, 135-162.

_____, and J. G. DeVore, 1979: Multiple-flow equilibria in the atmosphere and blocking. *J. Atmos. Sci.*, **36**, 1157-1176.

_____, and D.M.Straus, 1980: Form-drag instability, mutiple equilibria and propagating planetary waves in baroclinic, orographically forced planetary wave systems. *J. Atmos. Sci.*, **37**, 1157-1176.

_____, J. Shukla and K.C. Mo, 1981: Comparison of a barotropic blocking theory with observation. *J. Atmos. Sci.*, **30**, 762-779.

Colucci, S.J., 1985: Explosive cyclogenesis and large-scale circulation changes: Implications for the onset of blocking. *J. Atmos. Sci.*, **42**, 2701-2717.

_____, 1987: Comparative diagnosis of blocking versus nonblocking planerary-scale circulation changes during synoptic-scale cyclogenesis. *J. Atmos. Sci.*, **44**, 125-139.

Crum, F.X. and D.E. Stevens, 1988: A case study of atmospheric blocking using isentropic analysis. *Mon. Wea. Rev.*, **116**, 223-241.

Danielsen, E. and R.S. Hipskind, 1980: Stratospheric-troposhperic exchange at polar latitudes in summer. *J. Geophys. Rev.*, **85**, pp.

DaSilva, A.M., 1989: The role of temporal changes of the zonal wind on the excitation of large-scale transients. M.I.T. Dept. of Earth, Atmospheric and Planetary Sciences, Ph.D. thesis.

Davis, C., 1990: Cyclogenesis diagnosed using potential vorticity. M.I.T. Dept. of Earth, Atmospheric and Planetary Sciences, Ph. D. thesis.

Dey, C.H., 1989: The evolution of objective analysis methodology at the National Meteorological Center. *Wea. Forecasting*, **4**, 297-312.

Dole, R. M., 1982: Persistent anomalies of the extratropical northern hemisphere wintertime circulation. M.I.T. Dept. of Meteorology and Physical Oceanography, Ph.D. thesis.

_____, and N.D. Gordon, 1983: Persistent anomalies of the extratropical Northern Hemisphere wintertime circulation: Geographical distribution and regional persistence characteristics. *Mon. Wea. Rev.*, **111**, 1567-1586.

_____, 1986a: Persistent anomalies of the extratropical Northern Hemisphere wintertime circulation: Structure. *Mon. Wea. Rev.*, **114**, 178-207.

_____, 1986b: The life cycles of persistent anomalies and blocking over the North Pacific. *Adv. Geophys.*, **29**, 31-69.

_____, 1989: Life cycles of persistent anomalies. Part I: Evolution of the 500mb height anomalies. *Mon. Wea. Rev.*, **117**, 177-211

_____, and R.X. Black, 1990: Life cycles of persistent anomalies. Part II: The development of persistent negative height anomalies over the North Pacific Ocean. *Mon. Wea. Rev.*, **118**, 824-826.

Eady, E.T., 1949: Long waves and cyclone waves. *Tellus*, **1**, 33-52.

Ebisuzaki, W.N., 1986: Interactions between long and synoptic-scale waves in a simple model. M.I.T. Dept. of Earth, Atmospheric and Planetary Sciences, Ph.D. thesis.

Edmon, H.J., B.J.Hoskins and M.E.McIntyre, 1980: Eliassen-Palm cross sections for the troposphere. *J. Atmos. Sci.*, **37**, 2600-2616.

Egger, J., W., Metz and G. Müller, 1986: Forcing of planetary-scale blocking anticyclones by synoptic-scale eddies. *Adv. Geophys.*, **29**, 183-198.

Farrell, B.J., 1984: Modal and nonmodal baroclinic waves. *J. Atmos. Sci.*, **41**, 668-673.

_____, 1985: Transient growth of damped baroclinic waves. *J. Atmos. Sci.*, **42**, 2718-2727.

_____, 1989: Transient development in confluent and diffluent flow. *J. Atmos. Sci.*, **46**, 3279-3288.

Frankignoul, C., 1985: Sea surface temperature anomalies, planetary waves and air-sea feedback in the middle latitudes. *Rev. Geophys.*, **23**, 357-390.

Frederiksen, J.S., 1979: Baroclinic instability of zonal flows and planetary waves in multilevel models on a sphere. *J. Atmos. Sci.*, **36**, 2320-2335.

_____, 1982: A unified three-dimensional instability theory of the onset of blocking and cyclogenesis. *J. Atmos. Sci.*, **39**, 969-982.

_____, 1983: Disturbances and eddy fluxes in Northern Hemipshere flows: Instability of three-dimensional January and July flows. *J. Atmos. Sci.*, **40**, 836-855.

_____, 1986: Instability theory and nonlinear evolution of blocks and mature anomalies. *Adv. Geophys.*, **29**, 277-303.

Gall, R., R. Blakeslee and R.C.J. Somerville, 1979: Cyclone-scale forcing of ultra-long waves. *J. Atmos. Sci.*, **36**, 1692-1698.

Green, J.S.A., 1977: The weather during July 1976: some dynamical considerations of the drought. *Weather*, **32**, 120-128.

Gyakum, J.R., J.R.Anderson, R.H. Grumm and E.L.Gruner, 1989: North Pacific cold-season cyclone activity: 1975 through 1983. *Mon. Wea. Rev.*,**117**, 1141-1155.

Haines, K. and J. Marshall, 1987: Eddy-forced coherent structures as a prototype of atmospheric blocking. *Quart. J. Roy. Meteor. Soc.*, **113**, 681-704.

_____ and P. Malanotte-Rizzoli, 1990: Isolated anomalies in westerly jetstreams: A unified approach. Submitted to *J. Atmos. Sci.*.

Hansen, A.R., and T.-C. Chen, 1982. A spectral energetics analysis of atmospheric blocking. *Mon. Wea. Rev.*, **110**, 1146-1165.

_____, and A. Sutera, 1984: A comparison of the spectral energy and enstrophy budgets of blocking versus non-blocking periods. *Tellus*, **36**, 52-63.

_____, 1986: Observational characteristics of atmospheric planetary waves with bimodal amplitude distribution. *Adv. Gephys.*, **29**, 101-133.

Held, I.M., S.W. Lyons and S. Nigam, 1989: Transients and the extratropical response to El Niño. *J. Atmos. Sci.*, **46**, 163-174.

Holopainen, E. O., 1984: Statistical local effect of synoptic-scale transient eddies on the time-mean flow in the northern extratropics in winter. *J. Atmos. Sci.*, **41**, 2505-2515.

_____, and C. Fortelius, 1987: High-frequency transient eddies and blocking. *J. Atmos. Sci.*, **44**, 1632-1645.

Holton, J. R., 1981: Dynamics of sudden stratospheric warmings. *Ann. Rev. Earth Plan. Sci.*, **8**, 169-180.

Hoskins, B. J., A.J. Simmons and D.G. Andrews, 1977: Energy dispersion in a barotropic atmosphere. *Quart. J. Roy. Meteor. Soc.*, **103**, 553-567.

_____, and D. Karoly, 1981: The steady linear response of a spherical atmosphere to thermal and orographic forcing. *J. Atmos. Sci.*, **38**, 1179-1196.

_____, I. N. James and G. H. White, 1983: The shape, propagation and mean-flow interaction of large-scale weather systems. *J. Atmos. Sci.*, **40**, 1595-1612.

_____, B.J., M.E. McIntyre and A.W. Robertson, 1985: On the use and significance of isentropic potential vorticity maps. *Quart. J. Roy. Meteor. Soc.*, **111**, 877-946.

_____, and P.D. Sardeshmukh, 1987: A diagnostic study of the dynamics of the northern hemisphere winter of 1985-86. *Quart. J. Roy. Meteor. Soc.*, **113**, 759-778.

Illari, L., and J. C. Marshall, 1983: On the interpretation of eddy fluxes during a blocking episode. *J. Atmos. Sci.*, **40**, 2232-2242.

_____, 1984: A diagnostic study of the potential vorticity in a warm blocking anticyclone. *J. Atmos. Sci.*, **41**, 3518-3526.

Jacqmin, D., and R.S. Lindzen, 1985: The causation and sensitivity of the northern winter planetary waves. *J. Atmos. Sci.*, **42**, 724-745.

Jenne, R.L., 1970: *The NMC Octogonal Grid.* NCAR, Boulder, CO. 14 pp.

Kalnay-Rivas, E., and L. Merkine, 1981: A simple mechansim for blocking. *J. Atmos. Sci.*, **38**, 2077-2091.

Karoly, D.J., and B.J. Hoskins, 1982: Three-dimensional propagation of planetary waves. *J. Meteor. Soc. Jpn.*, **60**, 109-123.

Klein, W.H., 1957: Principal tracks and mean frequencies of cyclones and anticyclones in the Northern Hemisphere. Research paper No. 40, U.S. Weather Bureau, 60 pp.

Kok, C. J., and J. D. Opsteegh, 1985: On the possible causes of anomalies in the seasonal mean circulation pattern during the 1982/83 El Niño event. *J. Atmos. Sci.*, **42**, 677-694.

Lau, N.C. and E.O. Holopainen, 1984: Transient eddy forcing of the time-mean flow as identified by geopotential tendencies. *J. Atmos. Sci.*, **41**, 313-328.

_____, 1988: Variability of the observed midlatitude storm tracks in relation to low-frequency changes in the circulation pattern. *J. Atmos. Sci.*, **45**, 2718-2743.

Lejenäs, H. and Doos, 1987: Behavior of the stationary and travelling planetary-scale waves and blocking, a Norhtern Hemisphere data study. *J. Meteor. Soc. Jpn.*, **65**, 709-725.

Lindzen, R.S., 1986: Stationary planetary waves, blocking, and interannual variability. *Adv. Geophys.*, **29**, 251-273.

Lorenz, E. A., 1956: Empirical orthogonal functions and statistical weather prediction. Sci. Rep. No. 1, *M.I.T. Statistical Forecasting Project*, Contract no. AF19 (604), 49 pp.

MacVean, M.K., 1985: Long-wave growth by baroclinic processes. *J. Atmos. Sci.*, **42**, 1089-1101.

Maddox, R.A., 1980: An objective technique for separating macroscale and mesoscale features in meteorological data. *Mon. Wea. Rev.*, **108**, 1108-1121.

Malanotte-Rizzoli, P., and P. Malguzzi, 1987: Coherent structures in a baroclinic atmosphere. Part II: Block formation and eddy forcing. *J. Atmos. Sci.*, **44**, 2493-2505.

Malguzzi, P. and P. Malanotte-Rizzoli, 1984: Nonlinear stationary Rossby wave on nonuniform zonal winds and atmospheric blocking. Part I: The analytical theory. *J. Atmos. Sci.*, **41**, 2620-2628.

_____, and _____, 1985: Coherent structures in a baroclinic atmosphere. Part II: A truncated model approach. *J. Atmos. Sci.*, **42**, 2463-2472.

McWilliams, J.C., 1980: An application of equivalent modons to atmospheric blocking. *Dyn. Atmos. Ocean*, **5**, 43-66.

Miyakoda, K., G. Hembree, R. Strickler and I. Shulman, 1972: Cumulative results of extended forecast experiments. 1: Model performance for winter cases, *Mon. Wea. Rev.*, **100**, 836-855.

Mullen, S. L., 1986: The local balances of vorticity and heat for blocking anticyclones in a spectral general circulation model. *J. Atmos. Sci.*, **43**, 1406-1441.

_____, 1987: Transient eddy forcing of blocking flows. *J. Atmos. Sci.*, **44**, 3-22.

Nakamura, H., and J.M.Wallace, 1990: Observed changes in baroclinic wave activity during the life cycle of the persistent low-frequency circulation anomalies. To appear in *J. Atmos. Sci.*

Namias, J., 1950: The index cycle and its role in the general circulation. *J. Meteor.*, **7**, 130-139.

_____, 1978: Multiple causes of the North American abnormal winter of 1976-77. *Mon. Wea. Rev.*, **106**, 279-295.

Navarra, A., 1990: Steady linear response to thermal forcing of an anomaly model with an asymmetric climatology. *J. Atmos. Sci.*, **47**, 148-169.

Nielsen, J.W., 1990: Small-scale cyclogenesis during the Genesis of Atlantic Lows Experiment. M.I.T. Dept. of Earth, Atmospheric and Planetary Sciences, Ph.D. thesis.

Nigam, S., and R.S. Lindzen, 1989: Sensitivity of stationary waves to variations in the basic state zonal flow. *J. Atmos. Sci.*, **46**, 1746-1768.

O'Lenic, E. A. and R.E. Livezey, 1989: Relationships between systematic error in medium-range numerical forecasts and some of the principal modes of low-frequency variability of the Northern Hemisphere 700 mb circulation. *Mon. Wea. Rev.*, **117**,1262-1280.

Palmer, T., 1988: Medium and extended range predictability and stability of the Pacific-North American mode. *Quart. J. Roy. Meteor. Soc.* **114**, 691-713.

Petersen, R.A. and J.D. Stackpole, 1989: Overview of the NMC production suite. *Wea. Forecasting*, **4**, 313-322.

Petterssen, S., 1956: Weather Analysis and Forecasting, Vol. 1, McGraw-Hill, 428 pp.

_____, and S. Smebye, 1971: On the development of extratropical cyclones. *Quart. J. Roy. Meteor. Soc.*, **97**, 457-482.

Pfeffer, H., 1981: Wave-mean flow interactions in the atmosphere. *J. Atmos. Sci.*, **38**, 1340-1359.

Pierrehumbert, R.T., 1986: The effect of local baroclinic instability on zonal inhomogeneities of vorticity and temperature. *Adv. Geophys.*, **29**, 165-182.

Plumb, R. A., 1985: On the three-dimensional propagation of stationary waves. *J. Atmos. Sci.*, **42**, 217-229.

_____, 1986: Three-dimensional propagation of transient quasi-geostropic eddies and its relationship with the eddy forcing of the time-mean flow. *J. Atmos. Sci.*, **43**, 1657-1678.

Rex, D.D., 1950a: Blocking action in the middle atmosphere and its effects on regional climate. I: Aerological study of blocking. *Tellus*, **2**, 196-211.

_____, 1950b: Blocking action in the middle troposphere and its effect on regional climate. II: The climatology of blocking action. *Tellus*, **2**, 275-305.

Reinhold, B. B., and R. T. Pierrehumbert, 1982: Dynamics of weather regimes: Quasi-stationary waves and blocking. *Mon. Wea. Rev.*, **110**, 503-534.

Roads, J. O., 1989: Dynamical extended-range forecasts of the lower tropospheric thickness. *Mon. Wea. Rev.*, **117**, 3-28.

Robertson, A.W., and W. Metz, 1989: Three-dimensional linear instability of persistent anomalous large-scale flows. *J. Atmos. Sci.* **46**, 2783-2801.

Sanders, F. and J.R. Gyakum, 1980: Synoptic-dynamic climatology of the "bomb". *Mon. Wea. Rev.*, **108**, 1589-1606.

_____, and L.F. Bosart, 1985: Mesoscale structure in the megalopolitan snowstorm of 11-12 February 1983. Part I: Frontogenetical forcing and symmetric instability. *J. Atmos. Sci.*, **72**, 1050-1061.

_____, 1986: Explosive cyclogenesis in the west-central North Atlantic Ocean, 1981-1984. Part I: Composite structure and mean behavior. *Mon. Wea. Rev.*, **114**, 1781-1794.

Shukla, J., and H. Mintz, 1982: Influence of land-surface evapotranspiration on the earth's climate. *Science*, **215**, 1498-1501.

Shutts, G.J., 1983: The propagation of eddies in diffluent jetstreams: eddy vorticity forcing of 'blocking' flow fields. *Quart. J. Roy. Meteor. Soc.*, **109**, 737-761.

_____, 1986: A case study of eddy forcing during an Atlantic blocking episode. *Adv. Geophys.*, **29**, 135-162.

Simmons, A.J., and B.J. Hoskins, 1976: Baroclinic instability on a sphere: Normal modes of the primitive and quasi-geostrophic equations. *J. Atmos. Sci.*, **33**, 1454-1477.

_____, and _____, 1978: The life cycles of some nonlinear baroclinic waves. *J. Atmos. Sci.*, **35**, 414-432.

_____, 1982: The forcing of planetary wave motion by tropical diabatic heating. *Quart. J. Roy. Meteor. Soc.*, **108**, 503-534.

_____, J.M. Wallace and G.W. Branstator, 1983: Barotropic wave propagation and instability, and atmospheric teleconnection patterns. *J. Atmos. Sci.*, **108**, 503-534.

Smith, P.J. and C.-H. Tsou, 1988: Static stability variations during the development of an intense extratropical cyclone. *Mon. Wea. Rev.*, **116**, 1245-1250.

Sumner, E.J., 1954: A study of blocking in the Atlantic-European sector of the Northern Hemisphere. *Quart. J. Roy. Meteor. Soc.*, **80**, 402-416.

Sutera, A., 1986: Probability density distribution of large-scale atmospheric flow. *Adv. Geophys.*, **29**, 227-249.

Tibaldi, and Moltini, 1988: On the operational predictability of blocking. *The Nature and Prediction of Extratropical Weather Systems*, **2**, ECMWF, 329-371

Tracton, M. S., K. Mo, W. Chen, E. Kalnay, R. Kistler and G. White, 1989: Dynamical extended range forecasting (DERF) at the National Meteorological Center. *Mon. Wea. Rev.*, **117**, 1604-1635.

Trenberth, K.E., 1986: An assessment of the impact of transient eddies on the zonal flow during a block episode using localized Eliassen-Palm flux diagnostics. *J. Atmos. Sci.*, **43**, 2070-2088.

_____ and J.G. Olson, 1988: Evaluation of NMC Global Analyses: 1979-1987. NCAR Technical Note, NCAR/TN-299+STR., Boulder, CO.

Tsou, C.-H. and P.J. Smith, 1990: The role of synoptic/planetary-scale interactions during the development of a blocking anticyclone. *Tellus*, **42**, 174-193.

Verkley, W.T.M., 1990: Modons with uniform absolute vorticity. *J. Atmos. Sci.*, **47**, 727-745.

Wallace, J.M. and D.S. Gutzler, 1981: Teleconnections in the geopotential height field during the Northern Hemisphere winter. *Mon. Wea. Rev.*,**109**, 784-812.

_____, 1987: Low-frequency Dynamics-Observations. *Dynamics of Low-Frequency Phenomena in the Atmosphere. Vol, I: Observations*. NCAR, Boulder CO., 1-75.

_____, G.-H. Lim and M.L. Blackmon, 1988: Relationship between cyclone tracks, anticyclone tracks and baroclinic waveguides. *J. Atmos. Sci.*, **45**,439-462.

Webster, P.J., 1981: Mechanisms determining the atmospheric response to sea surface temperature anomalies. *J. Atmos. Sci.*, **38**, 554-571.

Weickmann K.M., G.R. Lussky and J.E. Kutzback, 1985: Intraseasonal (30-60 day) fluctuations of outgoing longwave radiation and 250 mb streamfunction during norther winter. *Mon. Wea. Rev.*, **113**, 941-961.

White, G.H., 1980: Skewness, kurtosis and exteme values of Northern Hemisphere geopotential heights. *Mon. Wea. Rev.*, **108**, 1446-1455.

White, W.B. and N.E. Clark, 1975: On the development of blocking ridge activity over the central North Pacific. *J. Atmos. Sci.*, **32**, 489-502.

Whittaker, L. M., and J.L.Horn, 1984: Northern Hemisphere extratropical cyclone activity for four mid-season months. *J. Climatol.*, **4**, 297-310.

Young, R.E., and G.L. Villere, 1985: Nonlinear forcing of planerary-scale waves by amplifying unstable baroclinic eddies generated in the troposphere. *J. Atmos. Sci.*, **42**, 1991-1990.

List of Figures

Fig. A2.3 Examples of a bandpass-filtered and a Barnes objective analysis filtered analyses.

Fig. A2.4 Composite 300 mb VSTAT anomalies computed using the Barnes OA spatially filtered analyses for day +6 of the four PA events

Fig A2.5 Composite 300 mb geopotential height tendencies computed using E-vectors formed using spatially-filtered height data during the onset period centered of the four PA events.

Table 4.1. Composite-mean 300 mb VSTAT anomalies in the indicated regions, the significance level that the anomalies are different from zero and the number of cases that had positive, negative and neutral ($< 0.1\sigma$) anomalies in that region. The table lists values for day -6 during the onset and breakdown of each type of persistent anomaly.